Mass Transfer from In-line Slabs

Application to
High-temperature Kiln Drying
of Softwoods Timber Boards

A thesis submitted in
fulfilment of the requirements for
the Degree of Doctor of Philosophy in the
Department of Chemical and Process Engineering

by
Peter Chin Seng KHO

University of Canterbury
Christchurch
New Zealand
1993

Dedicated to the people of New Zealand.
In appreciation of the opportunity
to pursue my higher education here
in this beautiful and friendly country.

Acknowledgments

During the course of this research, I have received assistance, guidance and encouragement from many people.

In particular, I am most grateful to **Professor Roger Keey**, my supervisor, for his encouragement, advice and criticism throughout the course of this research. His tolerance to and understanding of the many difficult situations I have been in is very encouraging. Thanks are also due to **Dr. John Walker**, my associate supervisor, who has patiently introduced me to the intriguing world of wood at the commencement of this research, and for his ever-ready and invaluable advice throughout the programme.

I would also like to thank **Mr. Paul Fuller** for having skilfully modified the experimental kiln for my experiments. His help, advice and encouragement has made my stay in Christchurch very pleasant and enjoyable in many ways.

The technical staff of the Department of Chemical and Process Engineering for providing their expertise in building and modifying the various equipment needed for my research, and in particular, to **Mr. Trevor Berry** for his advice on all the photographic work presented in thesis. To you all, many thanks.

I would also like to thank **Mr. Wayne Miller**, the project coordinator, for his advice and comments on the work done during the course of this research.

I am particularly grateful to the School of Forestry for the use of the experimental kiln and to the Department of Mechanical Engineering for the use of the TSI hot-wire anemometer system. The contributions to the work on turbulence intensity measurements by **Mr. Graham R. Harris** and **Dr. Tim Langrish** are also gratefully acknowledged.

Special thanks are due to **Mrs. Daphne Keey**, for helping my family to settle down, particularly in the first year of our stay in Christchurch.

The financial support from the Forest Research Institute of the Ministry of Forestry, New Zealand without which this research is not possible. For this I am very grateful.

Friends and colleagues for their moral support.

Finally, I would like to thank my wife, **Annie** for her support as a mother to **Marilyn**, **Lionel** and **Hamish**. Her encouragement and patience as a wife have been inestimable. To my parents, brothers and sisters for their support, both morally and financially.

To you all, *terima kasih.*

Table of Contents

Abstract

The transfer of moisture vapour from the surface of a timber board in a kiln stack has been modelled by investigating the sublimation of naphthalene from a coated slab. The variation of local mass-transfer coefficients over a series of in-line, blunt slabs in the streamwise direction similar to that of a timber stack has been obtained over a velocity range of 3 to 7 m s^{-1}. The knowledge of these coefficients will be useful in the design of new kilns for drying specific timbers or in appraising new schedules for existing kilns.

The local mass-transfer coefficients over these boards in the experimental kiln were found to be approximately 60% higher than those predicted from data obtained for a sharp flat-plate at very low turbulence levels. The mass-transfer coefficients varied as the 0.8 power of the velocity, indicating that the transfer was through the turbulent boundary layers. The higher level of free-stream turbulence found in the experimental kiln than those in the wind tunnels used to obtained earlier data agreed with the conclusions of Sugawara *et al.* [1988], who found that the coefficient in the correlation for heat/mass-transfer is dependent on the free-stream turbulence intensity.

Small gaps of up to 1.0 mm wide between the adjacent boards in a layer are inevitable owing to the way boards are arranged to form a stack. Discontinuities in the mass-transfer coefficient profile were observed to occur over these minute gaps as a result of greatly enhanced coefficients in these regions. From flow visualization studies done, a recurring and periodic disturbance, having three distinct phases of motion, was observed to distort constantly the streamlines in the region near to the leading edge of the following board, causing the local mass-transfer coefficients over these regions to be enhanced. Turbulence intensity measurements done by Wu [1989] in a wind tunnel confirmed that turbulence intensity were higher over these gaps than those above the boards. The disturbance had periods of between 0.5 to 1.5 seconds which was in good agreement with the 2 seconds predicted by Langrish *et al.* [1992] from numerical simulation studies, using a κ-ε model of turbulence and computational fluid dynamics (CFD) methods. The corresponding Strouhal number, the dimensionless vortex-shedding frequency in the gap was calculated to be 0.05 at a Reynolds number of approximately 800. Sublimation tests and flow visualization studies confirmed that interlayer flow was not the cause of this enhancement.

Minor board irregularities in timber stacks are the consequence of inaccurate sawing, poor stacking and/or changes in dimensions of the boards (shrinking) during the drying process were found to enhance the coefficients and are favourable for drying permeable boards at high temperatures where external conditions in the kiln are relatively more important.

Surface roughness has relatively insignificant effect on the coefficients, confirming the current practice of machining the boards after drying because of added dimensional stability.

Thinner stickers of 15 mm in thickness can be used to increase kiln capacity as sticker thickness over the range 15 to 25 mm was found to have negligible effect on the local mass-transfer coefficients.

The coefficients of the board 3 metres downstream was found to reach an asymptote value at similar levels, suggesting the possibility of using wider stacks to increase kiln capacity. However, drying may be hindered towards the end of the wide stack where the moisture vapour concentration gradient between the board and the bulk air stream may be approaching zero.

1

Introduction

1.1 Background

Radiata pine (*Pinus radiata*), a native to the Monterey Peninsula of California, was first introduced into New Zealand in the early 1850s. Its prominence in New Zealand is due to the ease of propagation, the fast growth rate of the tree over a wide range of site conditions, relative freedom from diseases and the two periods of high level of planting, one between 1925 and 1936 because afforestation was seen to be necessary to alleviate prospective shortages of native timbers in the 1970s and beyond. It also offered work during the depression. The other period was the direct result of Government incentives between the late 1960s and early 1980s. Today, radiata pine constitutes 89% of the wood in the 1.2 million hectares of plantation forest in New Zealand.

For the year ending 1989, 84% of the 1.9 million cubic meters of sawn timber produced was radiata pine. As the domestic demand for timber is not expected to rise significantly in the future, the volume of wood available for export is expected to increased dramatically, with a three-fold increase over the next ten years. In the processing of sawn timber from log, drying is one of the intermediary processes. To meet the anticipated increase in the volume of wood to be processed, very large volumes of timber will have to be dried rapidly, efficiently and with minimal degrade. This will require an understanding of the drying process.

1.2 The need for drying timber

The moisture content of boards cut from a freshly-felled New Zealand radiata pine tree varies from about 50% in the heartwood to ~~50%~~ 150% and above in the sapwood. In that state,

timber is unsuitable for use within a dwelling and therefore must be dried by some means. Removal of this moisture from timber during the manufacturing process is called seasoning or drying. Correctly dried timber has advantages for both the producers and the end-users in the following ways.

(a) Improved dimensional stability of the wood

All timber, with the exception of those to be used in a marine environment, must be dried below the fibre-saturation point. As this involves the removal of bound water from within the cell walls, wood will shrink. Wood, being a hygroscopic material, alters its moisture content depending on the temperature and relative humidity of the environment. This process of adjusting its moisture content is accompanied by dimensional changes. Thus, if wood can be dried to the moisture content it will ultimately attain in use, and is placed in a reasonably stable environment, further dimensional changes would be minimal. Dressed timber can be cut or turned to exact dimensions.

(b) Enhanced quality

Owing to the consolidation of the cell wall material during the process of drying, dried timber exhibits an improvement in both tensile and compressive strength, rendering it a more suitable building material. Also, properly controlled drying eliminates or reduces the occurrence of warps, checks and splits.

(c) Retarded degeneration of material

As fungi and other organisms will not thrive in wood under 22% moisture content, wood dried below this moisture level will not rot. Fungi-related stains will be minimised if wood is kept dry in use.

(d) Facilitating further treatment

Where chemicals used in either a fire-retardant treatment or preservative treatment (to prevent insect attacks, fungi growth and sapstain), wood must be dried so that the it can be impregnated with ease. Gluing quality of wood is considerably improved at lower moisture contents.

(e) Reduced transportation costs

As shipping and handling costs are based on weight, transporting dried timber will be a direct economic benefit in terms of reduced freight cost.

1.3 Stacking for the kiln

Air, being the drying medium, must be in direct contact with the surface of the boards to facilitate the transfer of heat to and the removal of evaporated moisture from the boards. To achieve this, boards are assembled in horizontal rows or tiers, with each row separated by a number of regularly spaced stickers to form a stack (Figure 1.1).

It is important that supports under the tiers are level, square and not more than 600 mm apart. Stickers should be of uniform thickness and length, and aligned vertically above the supports. The last sticker must be as close as possible to the end of the stack, with the ends and sides of the stacks flushed and vertically aligned. For boards of uneven length, the ends must be supported on stickers. In such a situation, length sorting should be done to ensure a more solid stack, which in turn will reduce moisture content variation and warping [Bester, 1982].

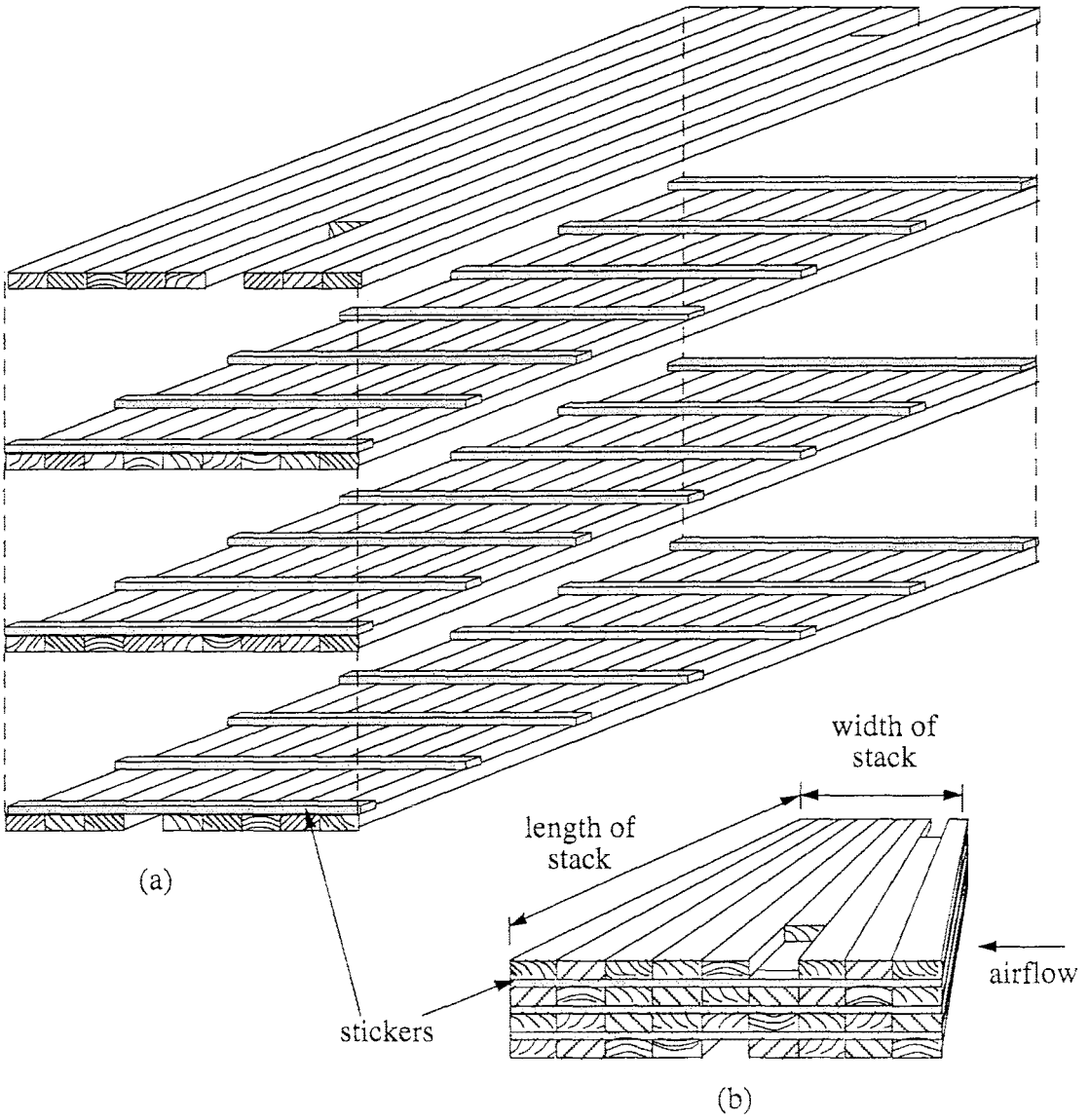

Figure 1.1 (a) Exploded view and (b) isometric view of a small timber stack.

1.4 Development of kiln drying

Air seasoning in the open air is the oldest method of drying timber. The advantage of gentle drying with little or no additional energy to dry the timber boards is offset by the long drying time and hence low throughput. Another disadvantage is the failure of the method to produce dried timber boards with a moisture content low enough for most uses inside buildings. Also, there is virtually no control over the drying environment. Though it is still used for "difficult-to-dry" species, air seasoning is becoming obsolete in recent years owing to the slow and uncontrollable drying process culminating in low throughput and the high cost of holding large inventories.

With an increasing appreciation of wood as a building material, the awareness of the need to conserve non-renewable resources and growing populations in almost every country, the demand for wood is steadily rising. Increased demand has brought about an evolution in kiln drying, which has the definite advantage over air seasoning in that the drying environment can be manipulated to suit a particular species. Thus, shorter drying times, an increased throughput and boards dried to low moisture contents are possible. Kilns can be classified generally by their operating temperature. The two main types are the conventional

kilns and high-temperature kilns. The basic difference between the two is that conventional kilns operate at dry-bulb temperatures below 100°C, whereas high-temperature kilns operate at dry-bulb temperatures above 100°C.

The advantages of high-temperature drying over conventional drying are summarised in Figure 1.2. The annual throughput of a high-temperature kiln is four times that of a conventional kiln of similar size, with a capital cost of only fifty percent more. Generally, high-temperature drying requires about 10% less energy and wood dries 2 to 5 times faster [Rosen, 1981]. Boards can also be dried to a lower final moisture content in a high-temperature kiln than those dried in a conventional kiln. As high-temperature kilns are often used as reconditioning chambers to relieve stress at the end of drying, these alternating extreme environments can cause the kiln and ancillary equipment in the kiln to deteriorate faster. Insulation of the structure in such kilns is of prime importance. If heat loss through the walls is excessive during reconditioning, most of the steam would condense on the cooler wall, leading to inadequate stress relief.

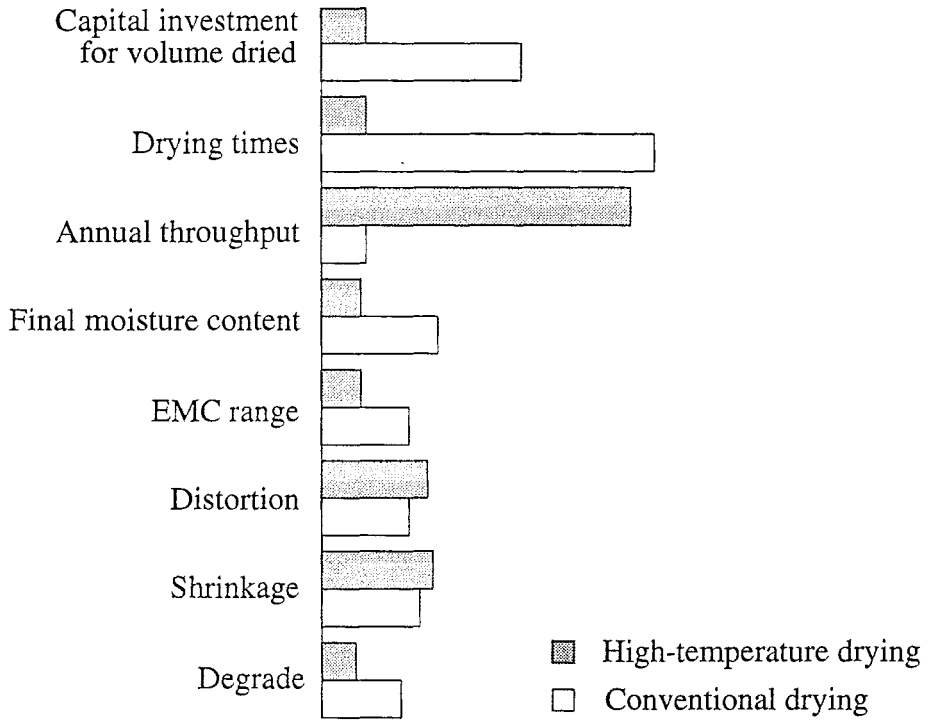

Figure 1.2 Comparison between high-temperature kiln drying against conventional kiln drying [after Williams, 1983].

1.5 Drying processes in wood

Wood is a hygroscopic capillary-porous material [Keey, 1972], with water occurring in three forms : liquid (or free) water in the cell cavities, water vapour in the cell cavities and bound (or hygroscopic) water in the cell walls.

The drying of wood is a critical process in which water is carefully and systematically removed from the wood using empirically determined schedules. It involves a dynamic balance between heat transfer from the bulk air stream to the surface of the wood, surface evaporation from the wood, diffusion of moisture through wood and mass flow of free water (and vapour, if the temperature exceeds the boiling point of water) in the wood.

The drying curve of wood can be divided into three distinct regimes, as shown in Figure 1.3 : a constant-rate period followed by two falling-rate periods [Adesanya *et al.*, 1988], although the constant-rate period may be relatively short or absent.

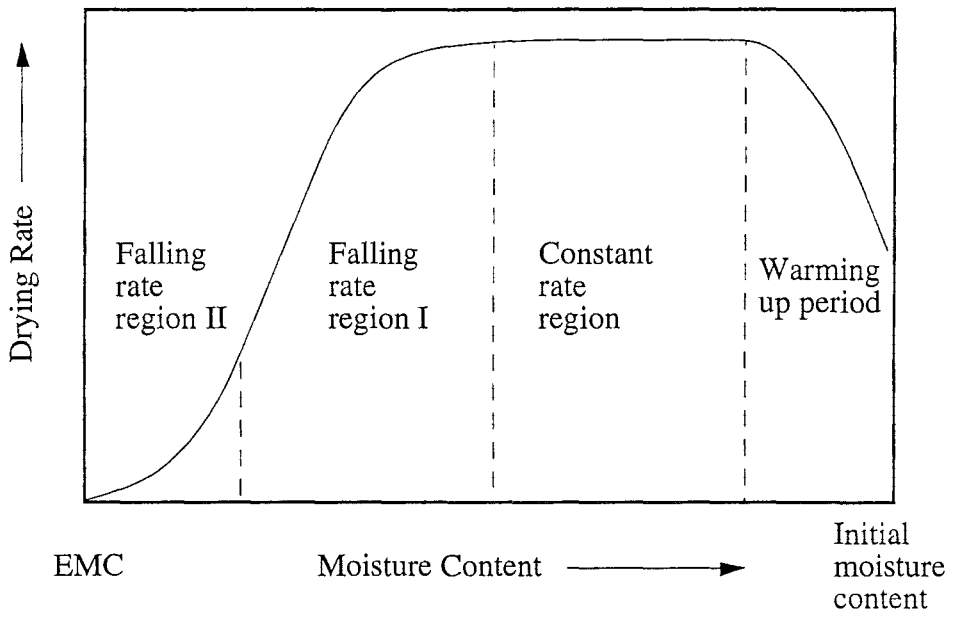

Figure 1.3 Theoretical drying-rate curve for wood.

The constant-rate period, where drying rate is essentially independent of time, is externally controlled by the rate of heat transfer to the wood surface. Moisture evaporates at the surface and mass flow of free water continues to move from the interior to the surface through the capillary structure of the cell cavities and the interconnecting pits as the wood dries. The first falling-rate period, where the change in moisture content is sometimes a linear function of the square root of time, begins when the evaporation front or wet line falls below the fibre-saturation point (fsp) and the region at fibre-saturation point or below is no longer confined to the surface. The evaporation front or wet-line retreats within the wood resulting in a wet core, separated from the surface by a dry zone each on either side. In the zone adjacent to the surface, which is below fibre saturation point, moisture migration will be by bound water diffusion across the cell walls and vapour diffusion across the cell cavities, supplemented by mass flow of vapour through pit pores if the wood is permeable and when the temperature of the drier zone exceeds the boiling point temperature. In the wet zone, moisture migration will be by capillary action in permeable woods [Hart, 1975]. During the first part of the second falling-rate period, the extent of drying is a linear function of the square root of time. This occurs after the evaporation front has receded to the centre of the wood. No more free water remains in the wood and moisture migration takes place solely by bound water diffusion and vapour diffusion, until an equilibrium moisture content (emc) is reached.

In high-temperature drying, Pang [1991] has been able to model the experimental temperature profiles across a heartwood board by assuming that the evaporative front sweeps through the material at the boiling point. Sapwood boards, for which the liquid permeability is greater, appear to have a preceding phase of drying, in which the evaporative front recedes only to within a few tracheid diameters of the surface. This period continues until the menisci becomes disrupted within this surface zone. A comparison of predicted and experimental temperature profiles is shown in Figure 1.4.

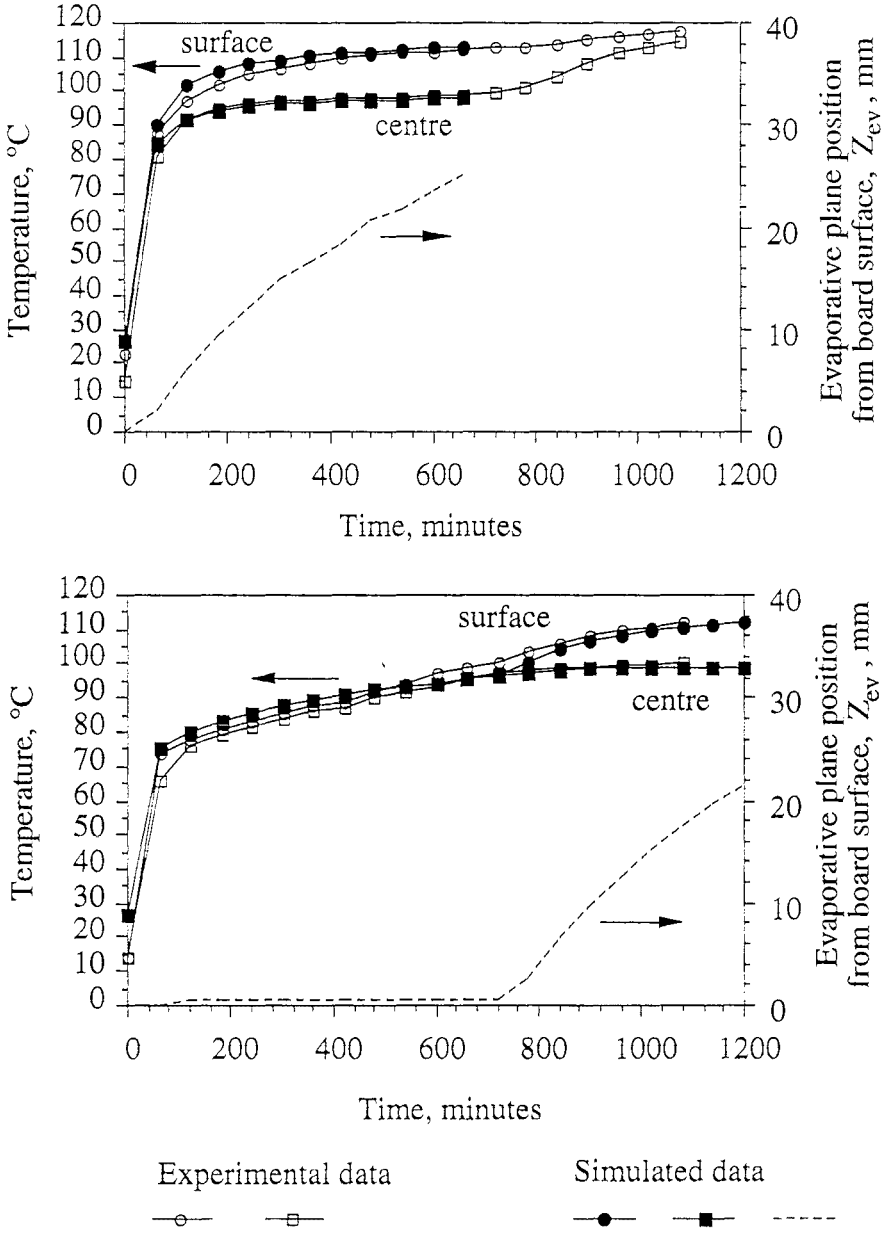

Figure 1.4 Temperature and evaporative plane profiles in the drying of a single Radiata pine board at an air temperature of 120°C for heartwood (top) and sapwood (below). Source : experimental data from Miller [1991] and simulated data from Pang [1991].

1.6 Controllable parameters in a kiln

The process of drying wood involves the removal of moisture from the wood surface as well as its movement from the interior of the wood to the surface. The relative balance between the two determines the significance each of the externally controllable factors, namely heat input, humidity level and air circulation, have upon the drying process. By suitable control of these three interdependent parameters, timber can be dried efficiently and without degrade. The cheapest method to accelerate drying is to reduce the humidity level while the most expensive is to increase the air velocity through the stack [Bachrich, 1980].

1.61 Dry-bulb temperature

Raising the dry-bulb temperature increases the rate of diffusion of either vapour or liquid moisture through the cell wall. For a highly permeable species like radiata pine, this dramatically increases the rate of transfer of moisture from the region above the evaporative front or wet line (i.e. the region below fibre-saturation point where there is no more free water) to the surface of the board into the air stream. Raising the dry-bulb temperature also increases the capacity of the air to absorb more moisture.

Although some softwoods and a few hardwoods have been successfully kiln-dried at dry-bulb temperatures of up to 150°C, research is continuing to explore the possibility of using even higher dry-bulb temperatures (up to 180°C) to reduce drying time further [Tronstad, 1983]. However, the limit to the use of very a high dry-bulb temperature ultimately depends on the properties of the wood to be dried. If high drying stresses induced as a result of increased drying rates exceeded its fracture strain in tension perpendicular to the grain fracture, severe checks are inevitable. Exposure of wood to high temperatures can result in reduction in some of the mechanical properties. In extreme cases, thermal degradation of wood will render the final dried-product useless.

1.62 Humidity

The humidity level in the kiln can be determined from standard hygrometric charts, knowing the dry-bulb and wet-bulb temperatures. The required humidity level in the kiln is maintained by venting a small volume of the humid air leaving the stack to get rid of excess water vapour. This is replaced by drawing in an equivalent amount of ambient air. The air is then heated before it is passed through the stack again. In the event of over-venting, the low humidity level can be compensated by spraying live steam. Increasing the difference between the dry-bulb and wet-bulb temperatures, the wet-bulb depression, increases heat transfer from the air stream to the board and hence the rate of evaporation.

In high-temperature kilns, raising the dry-bulb temperature and increasing the wet-bulb depression are responsible for the increase in drying rates over all periods of drying.

1.63 Air velocity

Air is the normal drying medium in kilns and has two main roles:-

(i) as a heat carrier to supply sufficient heat to the timber, and

(ii) as a moisture carrier to remove moisture (water) and other volatile substances.

Good baffling systems and a uniform minimum air velocity, sufficient to achieve these objectives, will ensure uniform drying and product quality. Attention should be paid to regular stacking arrangements, with uniform stickers to get equal air gaps, to ensure flow uniformity.

For kilns equipped with variable-speed fans, a high air velocity and low temperature can be used initially from green to fibre saturation point and a low air velocity and high temperature can be used from fibre saturation point to the final moisture content. Results from laboratory tests have indicated a reduction of 25% in drying time compared to schedules using non-varying temperature and air velocity, without any appreciable increase in defects [Bachrich, 1980].

For drying thin and highly permeable boards, fan reversals provide an averaging of the drying rates over the stack resulting in more even moisture contents, thus reducing the length of the reconditioning treatment. Only a small number of flow reversals are needed during the drying process to achieve good uniformity in board-to-board moisture contents [Ashworth, 1977].

1.7 Importance of a knowledge of airflow through the stack and of convective mass-transfer coefficients

Until the turn of the century, the design of kilns and development of drying schedules were based solely on experience and trial and error. Formal methods for designing kilns have become a commercial necessity, as these installations have to meet the increasing demand to dry boards quickly with a minimum of degrade and to do this as efficiently as possible under the pressure of escalating energy costs. However, data on the airflow through stacks and how this affects the convective mass-transfer coefficients on the surface of timber boards are not available.

In drying permeable timbers, there is an extensive period in the drying cycle when surface evaporation is the rate-controlling process. The rate at which water evaporates into the air from the surface of the board is dependent on the rate of heat transfer from the bulk air stream to the wood surface. Therefore, external conditions are critical over this period of drying. In the drying of radiata pine at high-temperatures in New Zealand, high wet-bulb depressions are used to achieve rapid heat and mass transfer, hence overall drying time are reduced significantly.

1.8 Previous work done

When a fluid flows along a sharp-edged plate surface which is parallel to the flow, the effect of the surface will be transmitted for some distance into the fluid (Figure 3.1). Initially, the layer of fluid near the plate surface flows in a laminar fashion. Fluid particles moves past one another with exchange between adjacent layers at a molecular level. As the boundary layer develops further along the leading edge, the laminar flow becomes unstable and changes to turbulent flow where bulk flows normal to the flow direction are prevalent, thus greatly enhances the rate of heat and mass transport.

By analogy with the equation for energy conservation in the boundary layer, one finds for the flow over a thin-edged two dimensional surface

$$u\frac{\partial C}{\partial x} + v\frac{\partial C}{\partial y} = D\frac{\partial^2 C}{\partial y^2} \qquad (1.1)$$

Where

u is the velocity component along the surface in the x direction,

v is the velocity component normal to the surface (the y direction),

C is the molar concentration of the vapour in the fluid,

The outer edge of the boundary layer is arbitrary, but the boundary-layer thickness is of order $\left(\frac{\upsilon L}{U_\infty}\right)^{1/2}$, where υ is the kinematic viscosity, L is a characteristic dimension (the swept length for a flat surface) and U_∞ is the bulk stream velocity [Goldstein, 1938]. The developing concentration profile in the boundary layer is assumed to be of the form

$$C = C\left(\frac{y}{(\upsilon x/U_\infty)^{1/2}}\right) \qquad (1.2)$$

where $\frac{x}{U_\infty}$ represents the contact time for the motion over the surface.

This concentration profile leads to an expression for the Sherwood number

$$Sh_x = \frac{Fx}{D} = \frac{x}{(\upsilon x/U_\infty)^{1/2}}\ \phi(Sc) \qquad (1.3)$$

Where

$\phi(Sc)$ is a function of the Schmidt number, normally taken to be proportional to $Sc^{1/3}$.

When the flow becomes turbulent, the dependence on Reynolds number becomes greater :

$$Sh_x = \frac{Fx}{D} = \frac{x}{(\upsilon x/U_\infty)^{n}}\ \phi(Sc) \qquad (1.4)$$

with $\frac{2}{3} < n < 1$.

For a laminar flow over a sharp-edged plate, local mass-transfer coefficients along the plate is given by [Welty, 1978]

$$Sh_x = 0.332\ Re_x^{1/2}\ Sc^{1/3} \qquad (1.5)$$

but should flow be turbulent, then

$$Sh_x = 0.0288\ Re_x^{4/5}\ Sc^{1/3} \qquad (1.6)$$

where

$Re_x = \frac{Lu}{\upsilon_A}$ is the Reynolds number,

$Sc = \frac{\upsilon_A}{D_{NA}}$ is the Schmidt number,

$Sh_x = \frac{k_c L}{D_{NA}}$ is the local Sherwood number,

L is the distance from the leading edge, m,

u is the bulk air velocity through sticker spacing, m s^{-1} and,

υ_A is the kinematic viscosity, $m^2\ s^{-1}$.

However, for flow past a blunt solid body such as a board, the fluid has to alter its flow path to flow over the solid. Danckwerts and Anolick [1962] found that the enhanced mass transfer was due to the formation of a stationary eddy at some distance away from the leading edge. Very high mass transfer rates were observed, particularly at the point of reattachment.

Sørensen [1969] continued these studies for slabs of thickness 1 to 16 mm and over a velocity range of 1.25 to 10.0 m s^{-1}. He found that the mass-transfer coefficients are dependent on the air velocity, the distance from the leading edge and the thickness of the slabs. The results also indicate that mass-transfer coefficients are independent of the Reynolds number based on the thickness of the board, Re_b and follow the expressions for sharp-edged plate if Re_b is less than 245.

$$Sh_x\ Sc^{-1/3} = 0.407\ Re_L^{1/2} \qquad (1.7)$$

For Re_b values greater than 245, a stationary eddy is formed just behind the leading edge and a laminar boundary layer develops from the point of reattachment. Under these conditions,

$$Sh_x\, Sc^{-1/3} = 0.152\, Re_b^{0.179}\, Re_L\, [Re_L - 49.8\, Re_b^{0.61}]^{-0.5} \qquad (1.8)$$

The correlation 1.8 gave values 22% higher than that for sharp-edged plates given by Equation 1.5. While Sørensen attributed the higher values to systematic error, turbulence intensity was also mentioned as a possible cause although no measurements were taken to verify this.

Miller [1973] investigated further the local mass-transfer coefficients over a single slat and an array of in-line slats. For runs using a single isolated slat of 8 mm thickness with an air velocity of 5 m s^{-1}, the mass-transfer coefficient profile similar to that reported by Sørensen was observed. However, the corresponding coefficients were found to be slightly higher. Again, no measurements of turbulence intensity were taken although the author suggested that this might have been the cause. By varying the distance between the slats in the array from 0 to 33 mm, his results showed that the mass-transfer coefficients along the slat are independent of the slat spacing. The mass-transfer coefficient profile for such an arrangement failed to show any sign of a stationary eddy forming, indicating flow for a slat in an array after the first is somewhat different.

Bayley and Turner [1971] found that heat transfer over a turbine blade doubled when the turbulence intensity was increased from 0.45% to 5.9%. The effect of turbulence intensity were further investigated by Sugawara *et al.* [1988]. Their results indicated that the local mass-transfer coefficients for a thin smooth-edged plate increased very rapidly for free-stream intensity levels up to 7%, after which the coefficients started to level off to a value 55% higher than the corresponding Nusselt values obtained for the lowest free-stream intensity level of 0.37%. The authors agreed with Schlichting [1968] that an increased in the free-stream turbulence would culminate in the earlier development of the turbulent boundary layer in the flow.

Wiedeman *et al.* [1989] measured the velocity and turbulence intensity at 11 positions in the 20 mm gap between the two timber layers, 20 mm inside the stack over a 2-minute period. High levels of turbulence were observed to occur at 2.3 and 17.8 mm from the surface of the lower board, which supported the results obtained by Danckwerts and Anolick [1962], Sørensen [1969] and Miller [1973] that an eddy was forming just behind the leading edge of the board. Wu [1989] investigated the effect of a 5 mm-wide gap between the boards on the turbulence intensity at 1, 2 and 3 mm above the surface of a 4-board wide stack in a wind tunnel. He found that the turbulence intensity above the gaps was consistently higher than those over the adjacent boards although no appreciable pressure drop was observed.

Drying of a timber board involves convective heat transfer to the surface and mass transfer of the moisture vapour away into the bulk air stream. These transport processes are related through the so-called Reynolds analogy. For fluids with Prandtl number (Pr) = 1, boundary conditions are identical and similarity exists between momentum and heat transfer. Thus for flow over a flat plate, the dimensionless statement of Reynolds analogy is;

$$Nu_x = \tfrac{1}{2}\, C_f \cdot Re_x \qquad (1.9)$$

where

C_f is dimensionless skin friction coefficient and is equal to $\dfrac{\tau_w}{\rho \cdot u^2/2}$.

Based on this analogy the experimental measurements of local values of heat-transfer coefficients for flow through a stack of timber [Viktorin, 1965] could be correlated in mass-transfer terms as

$$Sh_x\, Sc^{-1/3} = 0.0288\, Re_b^{0.8} \qquad (1.10)$$

which implies fully developed turbulent flow. This overview illustrates that, although transport processes about a flat surface are well known, there is little work concerned with transfer processes about in-line slabs, and almost none for transfer in kilns. The influence of minor irregularities in stacking arrangements and roughness is unknown.

Ashworth [1977] suggests that the equation for turbulent flow in circular ducts, namely

$$Sh_x\, Sc^{-1/3} = 0.023\, Re_D^{0.8} \qquad (1.11)$$

should apply to timber kilns, (if the appropriate hydraulic diameters is taken to define Re_D) but account has to be made for the entrance effect at the inlet face of the stack. He quotes a length of 20 hydraulic diameters for the extent of the entrance region where enhanced transfer takes place. This suggests that for 100 × 25 mm thick boards spaced at 25 mm, with stickers at 600 mm apart, such an entrance region will extend for about 1 m into the stack.

Empirical studies of the influence of airspeed on drying rates of single boards suggest that the influence of turbulence becomes significant at higher air velocities [Kollman and Schneider, 1961] (Table 1.1). Other workers find $0.64 < n < 0.69$ [Ogura and Ohnuma, 1955].

Velocity / v, m s^{-1}	Index / n
3 - 5	0.50
5 - 7	0.53
7 - 9	0.575
9 - 13	0.60

Table 1.1 Drying rate as a function of air velocity ($N \propto v^n$).

1.9 Objectives of this work

The aim of this work is to gather an extensive set of data of the mass-transfer coefficients in a stack similar to that used in a commercial high-temperature kiln. The study includes analysing the air-flow patterns through a timber stack and the influence air velocity has on the convective mass-transfer coefficient on the surface of the boards. Effects of minor board irregularities caused by inaccurate sawing, stacking and shrinking of the timber boards on the mass-transfer coefficients are also examined. Turbulence measurements in the plenum space of the kiln are also measured to provide data for a flow simulation as a basis for estimating mass-transfer coefficients.

The layout of this thesis is as follows :

Chapter 2 covers the flow visualisation method used to investigate flow patterns around timber boards in a stack placed in a wind tunnel. Photographs of these patterns for the various configurations are presented in this chapter.

Measurements of turbulence intensity levels in a kiln and wind tunnel are presented in **Chapter 3**. These are used in the numerical simulation method in Chapter 4. The hardware used and the method of measuring the intensity levels is also outlined.

Chapter 4 summarises the numerical work to predict the convective mass-transfer coefficients over similar arrays from calculated values of the skin friction. The simulation includes time-independent and time-dependent flows

The method of gathering local mass-transfer coefficients using the naphthalene sublimation technique is discussed in **Chapter 5**. Graphical results of these experimental runs are also presented.

A comparison of the experimental results and existing work is made in **Chapter 6**. The results of the flow visualization studies and intensity level measurements are also discussed to explain the experimental results obtained in Chapter 5. The results of the numerical simulation for both time-independent and time-dependent flows are also discussed.

Conclusions and suggestions for further work are given in **Chapter 7**.

2

Flow visualization

2.1 Background

In high-temperature kiln drying of *Pinus Radiata*, the dry-bulb temperature is set at a level above the boiling point of water. Under such drying conditions, there are two ways in which water moves from the wet-line to the surface; the first is by the faster hydrodynamic flow of vapour through the unaspirated pits between tracheids, and the second is by the slower diffusion of bound water through the cell walls. Luikov [1966] quotes Sergovsky's data on the apparent moisture diffusivity of coniferous species in the tangential direction. Over the range of moisture content from 10 to 30% the apparent moisture diffusivity increases fourfold as the temperature is raised from 50°C to 100°C. In a study to determine the feasibility of using high temperatures of up to 180°C to dry wood, Basilico *et al.* [1990] concluded that drying thick boards and "difficult-to-dry" species in very harsh external conditions would induce severe surface checks. Therefore, external conditions in high-temperature kilns are relatively more important. In particular, the air motion between the boards will determine the extent of external convection of moisture.

While there is some work done to examine the development of flow and mass transfer in closed cavities owing to the great interest in selective chemical etching of thin solid film in the fabrication of microelectronic devices in the electronic industry, there has been almost no work done to examine the effect of a gap on the mass transfer downstream of the gap. Collaborative work with Lee [1990], under my supervision, was done to elucidate the flow patterns over an array of boards in a series of exploratory experiments. These flow visualization studies were carried out in the wind tunnel in the Department. Our preliminary results revealed the formation of a periodic disturbance forming in the gap. This Chapter is

a development of these preliminary studies, which included an improvement to the method of producing the smoke and photographing the motion.

2.2 Experimental set-up and procedure

While the smoke produced by the generator used in the flow visualization studies done by Lee [1990] was adequate for single-frame photography, the rapidly declining quality and quantity of smoke produced was found to be insufficient for continuous multiple-frames photography. The decline in the quality and quantity of smoke produced was caused by the accumulation of organic condensates in the galvanised pipe section of the generator. The pipe section of the generator was replaced with a glass section in the present studies, primarily to ease the removal of the accumulated condensates. Being able to see through the glass also assisted in the control of smoke production.

The smoke generator (Figure 2.1) was constructed from a 220 mm-long glass tube of 50 mm diameter in which 8 pieces of mosquito coil were burnt under controlled conditions to give a dense and continuous supply of smoke. The airflow through the generator was controlled by manipulating both the pressure and the regulating valves to ensure that the supply of smoke was dense and continuous. That smoke was injected into the tunnel at the same velocity as that of the air in the tunnel to minimise the dispersion rate of the smoke trail. The smoke was introduced into the tunnel through a 6 mm copper tube as a compromise between an adequate rate of smoke injection and minimising the obstruction to the airflow.

As it was very difficult to modify the kiln for flow visualization studies, a wind tunnel (Figure 2.2) in the Department was used instead. The air for the tunnel was supplied by the Rootes blower through a settling chamber 0.840 m high, 0.740 m wide and 0.510 m long which damped out the fluctuations of the air supply. It was then forced through the contraction section and finally the straw-filled section to further reduce the level of turbulence of the air. The working section of the tunnel is 3.30 m long and has a cross-section of 0.340 m high by 0.225 m wide. The tunnel has clear Perspex sides to enable the smoke patterns to be illuminated and photographed.

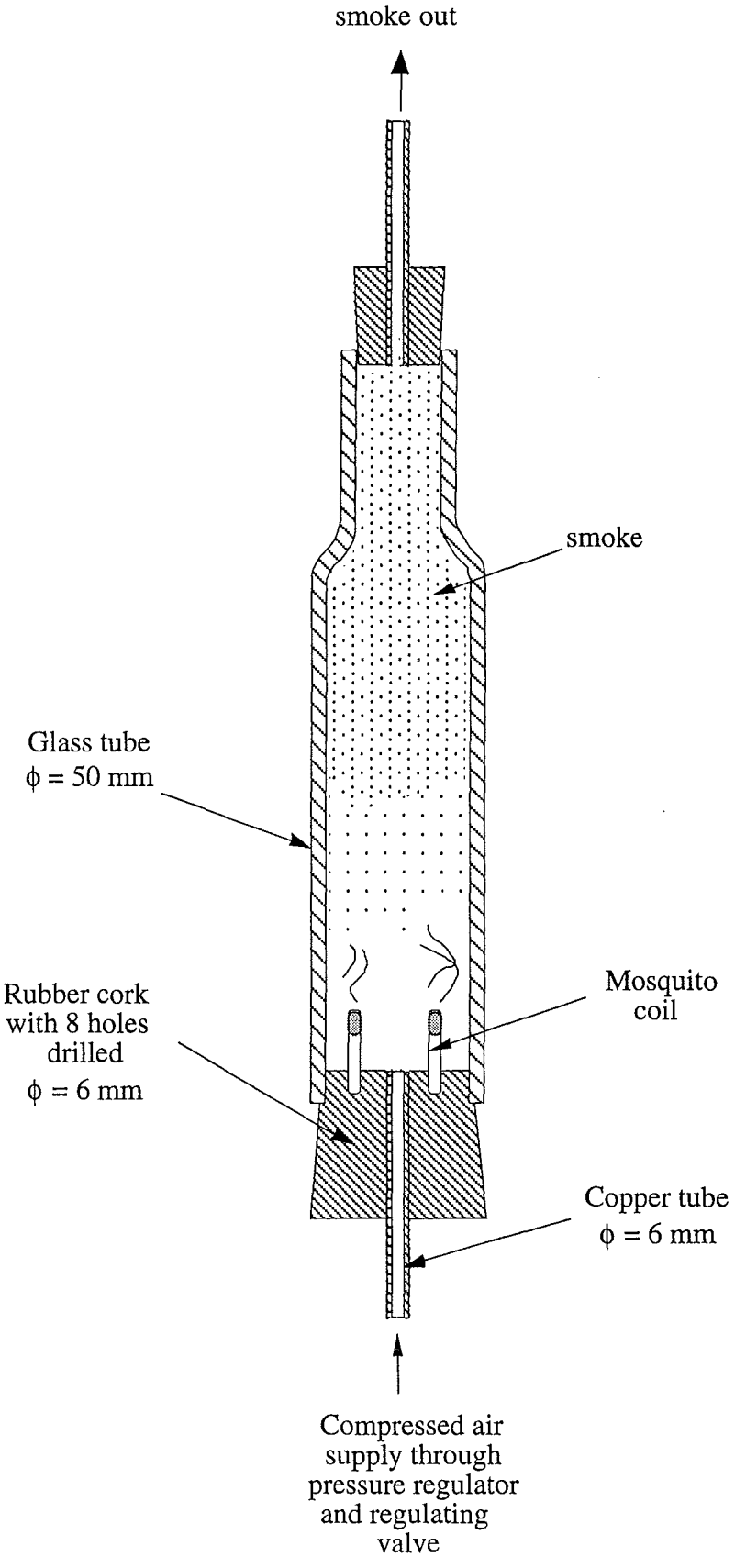

Figure 2.1 The smoke generator.

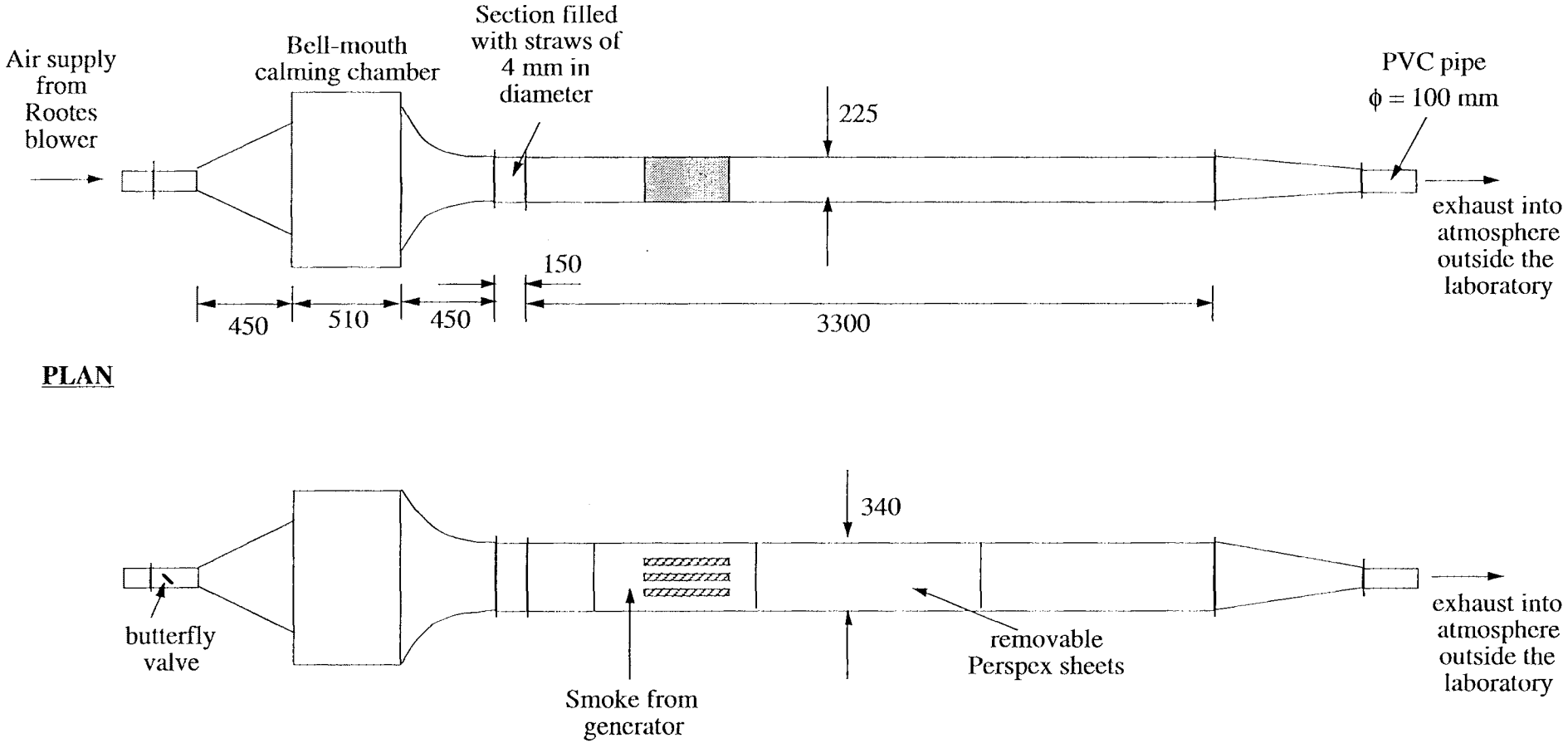

Figure 2.2 Schematic layout of the wind tunnel for flow visualization studies

Prior to the flow visualization studies, 5 velocity and turbulence intensity measurements in the traverse direction were taken along the length of the tunnel to determine its flow characteristics. The velocity was generally found to decrease from the top of the tunnel while the turbulence intensity appeared to attain a minimum value at the centre of the tunnel (Table 2.1) along the length of the tunnel. Attempts to rectify the velocity profile by using finer mesh screen were futile and the centre line between the test boards of the dummy stack was fixed at 190 mm from the top of the tunnel for the flow visualisation studies. Thus, the incident velocity would then vary between about 1.6 and 1.8 m s^{-1} at the lower velocity tested over the zone to be occupied by the boards.

Position from top of tunnel, mm	Velocity, m s^{-1}	Turbulence intensity, %	Velocity, m s^{-1}	Turbulence intensity, %
60	2.2	9.7	3.9	11.1
100	2.0	9.4	3.5	11.7
160	1.7	7.5	2.8	10.0
220	1.6	10.3	2.7	11.5
260	1.6	12.0	2.6	15.2

Table 2.1 Velocity and turbulence intensity at 360 mm from the mesh screen of the wind tunnel (no stack).

Two methods of recording the flow patterns were used. A Nikon FE2 camera, fitted with a Zoom-NIKKOR 35-105 mm lens and a Nikon PK-13 Auto Extension Ring was used to take single frame photographs. A Nikon motor drive (MD 12) was attached to the camera to take continuous frames at the rate of 3.4 frames per second. The exposure was 1/60th of a second at f4. The images were captured on Ilford HP5 Plus black and white film, developed to an effective ASA rating of 800. A Bolex movie camera (H16 SBM)with the aperture set at f2.8 was used to take the images of the motion on Kodak Tri-X Reversal black and white film at the rate of 48 frames per second. From counting the number of the frames between the repeated motion, the periodicity of the eddy formed in the gap was determined.

Illumination and stacking arrangements are shown in Figure 2.3. The smoke particles were made visible by the use of concentrated beams of light from two slide projectors. Glass slabs of the same dimensions were used in the layers above and below the test layer to permit the intense light beam through to the test layer to illuminate the smoke particles. To enhance the visibility of the smoke particles, all other slabs were also painted black. The slabs were slotted in along the grooves of the black Perspex sheet on one side of the tunnel. Each end of the other slabs was held in position by three pins pushed through the tiny holes drilled in the Perspex wall of the tunnel.

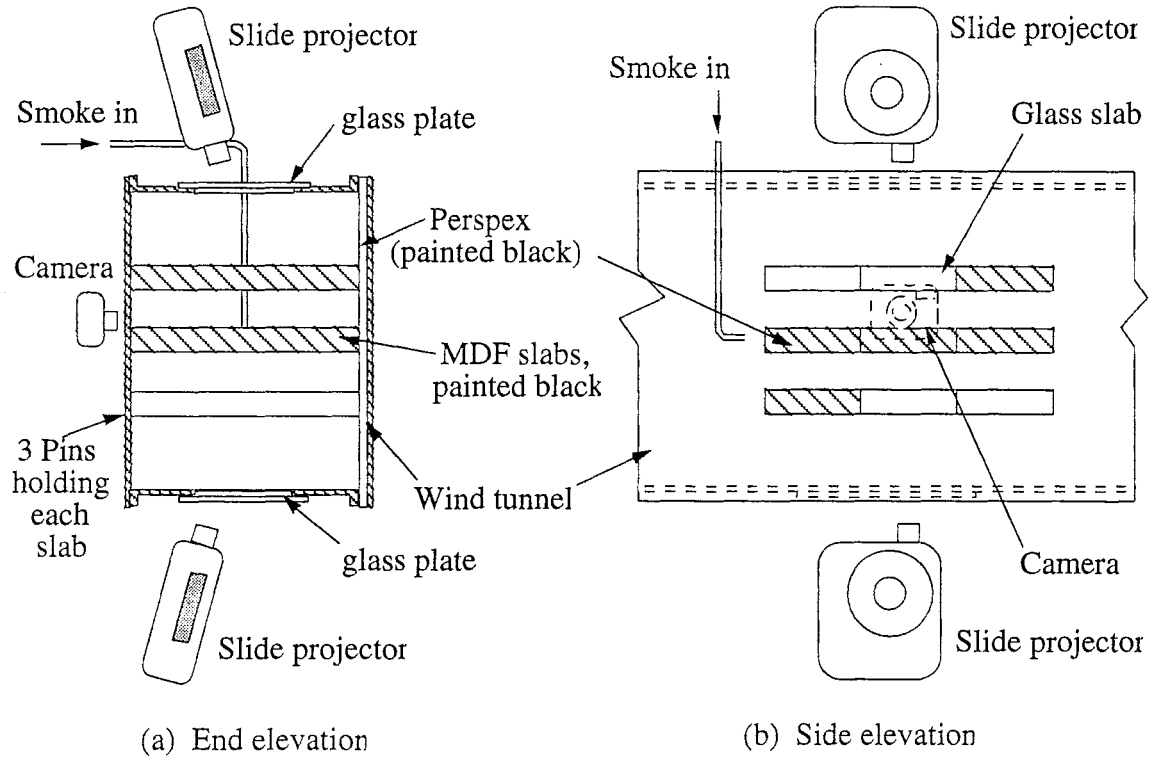

Figure 2.3 Illumination and stacking arrangements. (a) End elevation and (b) side elevation of the wind tunnel.

In flow visualisation, the development of flow over blunt bodies can be best followed if the smoke trails are not dispersed too rapidly. This is usually achieved by injecting smoke into an airstream where flow is laminar. As the airflow through the stack in the experiments carried in the experimental kiln was turbulent, the airflow through the stack in the wind tunnel had to be scaled down to lower air velocities in order to reduce the smoke dispersion so that it could be easily photographed. Dynamic similarity of flow over the board is preserved by keeping the Reynolds number based on flow over the gap size the same.

$$Re_{Kiln} = Re_{wind\ tunnel} \tag{2.1}$$

$$\frac{u_{Kiln}\, d_{gap\ kiln}}{\upsilon_A} = \frac{u_{wind\ tunnel}\, d_{gap\ wind\ tunnel}}{\upsilon_A} \tag{2.2}$$

$$d_{gap\ wind\ tunnel} = \frac{u_{Kiln}\, d_{gap\ kiln}}{u_{wind\ tunnel}} \tag{2.3}$$

This work investigated the effect of an adjacent gap width of 2, 5 and 10 mm on airflow patterns over an airflow range of 0.3 to 0.6 m s^{-1}. From the relation in Equation 2.3, these values corresponded to actual gap widths of 0.2, 0.5 and 1.0 mm and an air velocity range of 3 to 6 m s^{-1}. Closed gaps were similarly investigated over the same airflow range to elucidate the effects of interlayer flow on the airflow over these gaps. Flow visualization studies were also carried out for flow over the first board and for adjacent boards of unequal thickness in a timber stack.

2.3 Results and discussion

2.31 Effect of gaps between adjacent boards

Photographs of the flow visualization studies done to look at the effects of an adjacent gap between two adjacent boards in a stack are shown in Plates 1 and 2. Three distinct consecutive and recurring flow patterns were evident in these two plates. The sequence of events was as follows; the streamlines above the gap were drawn into the gap to form an eddy. As the eddy was formed, it moved in a circular pattern in the clockwise direction down into the gap This was then followed by the expulsion of the eddy into the airstream through a narrow region close to the leading edge of the following board. In this process, the deformed eddy uplifted the streamlines above this region. These periodic disturbances to the streamlines near to the leading edge of the board following the gap have caused the turbulence intensity levels in that region to increase. The gaps investigated corresponded to adjacent board gaps between 0.2 to 1.0 mm in width and over an airflow range of 3 to 6 m s^{-1}. These repeated patterns of eddy formation, circulation and deformation would exist in the proximity of these minute gaps in each layer of boards in a timber stack which are inevitable owing to the way the boards are arranged.

This study was extended to investigate if the above phenomenon was caused by interlayer flow. Closed gaps or slots of the same size were machined at the centre of a board and placed in the wind tunnel under the same experimental conditions.

Photographs taken of the study are shown in Plates 3, 4 and 5. It was observed that the three distinct consecutive and recurring phases were also formed in the vicinity of these closed gaps, confirming that these periodic disturbances were not the result of interlayer flow.

It was also observed that the periodic formation, circulation and deformation of eddies were also formed alternately on the other leading edge of the board, similar to that of the alternate vortex shedding found behind blunt bodies.

The effect of the minute gaps between adjacent boards in an array on Strouhal number, the dimensionless vortex-shedding frequency appears not to have been investigated. From counting the number of frames between the recurring motion taken with the Bolex movie camera, these sequence of eddy movements in the 5 mm-wide gap was found to last between 0.5 to 1.5 seconds at an airflow of 0.5 m s^{-1}. This corresponded to a Strouhal number of 0.05 and a Reynolds number of approximately 800, both of these dimensionless numbers were based on the thickness of the board.

2.32 Effect of differences in board thickness

The airflow patterns over boards of different thickness, a consequence of differential shrinking of the boards during the dying process or inaccurate sawing were also investigated. The top photograph in Plate 6 shows the development of the airflow as it approached a board 3 mm higher (thicker). This board thickness difference represented an actual board height difference of only 0.3 mm. The streamlines appeared to be leaving the region near to the leading edge of the board in the air stream and also through the gap into the air stream in the layer below the gap at the same time. However, no eddies were seen. This could be attributed to the lack of geometrical symmetry as the bottom surface of the boards were in-line and flushed. No stationary eddies were seen as the Reynolds number based on the thickness of the board was less than 245 [Sørensen, 1969].

The airflow patterns for flow over a board 3 mm lower is shown in the middle photograph in Plate 6. A distinct stagnant region was observed to form over the first 40 mm of the

board, corresponding to a distance of 4 mm in an actual board. The streamlines thereafter were "impinging" at a slight angle into the surface.

2.33 Flow over the first board

The flow over the first board is shown in the bottom of Plate 6. A stationary eddy was observed to formed at the leading edge of the board. The Reynolds number based on the thickness of the board, Re_b was calculated to be 800 which exceeded the critical value of 245 found by Sørensen [1969] for a stationary eddy to be formed immediately downstream of the leading edge.

2.4 Conclusions

Flow between the adjacent board layers in a timber stack is turbulent but the flow differs from that through a rectangular smooth duct in that the inevitably small gaps between adjacent boards in a layer of a timber stack was found to induce the formation of recurring disturbances in them. These disturbances cause the distortion of the streamlines in the vicinity near to the leading edge of the board following the gap, raising the levels of turbulence in these region.

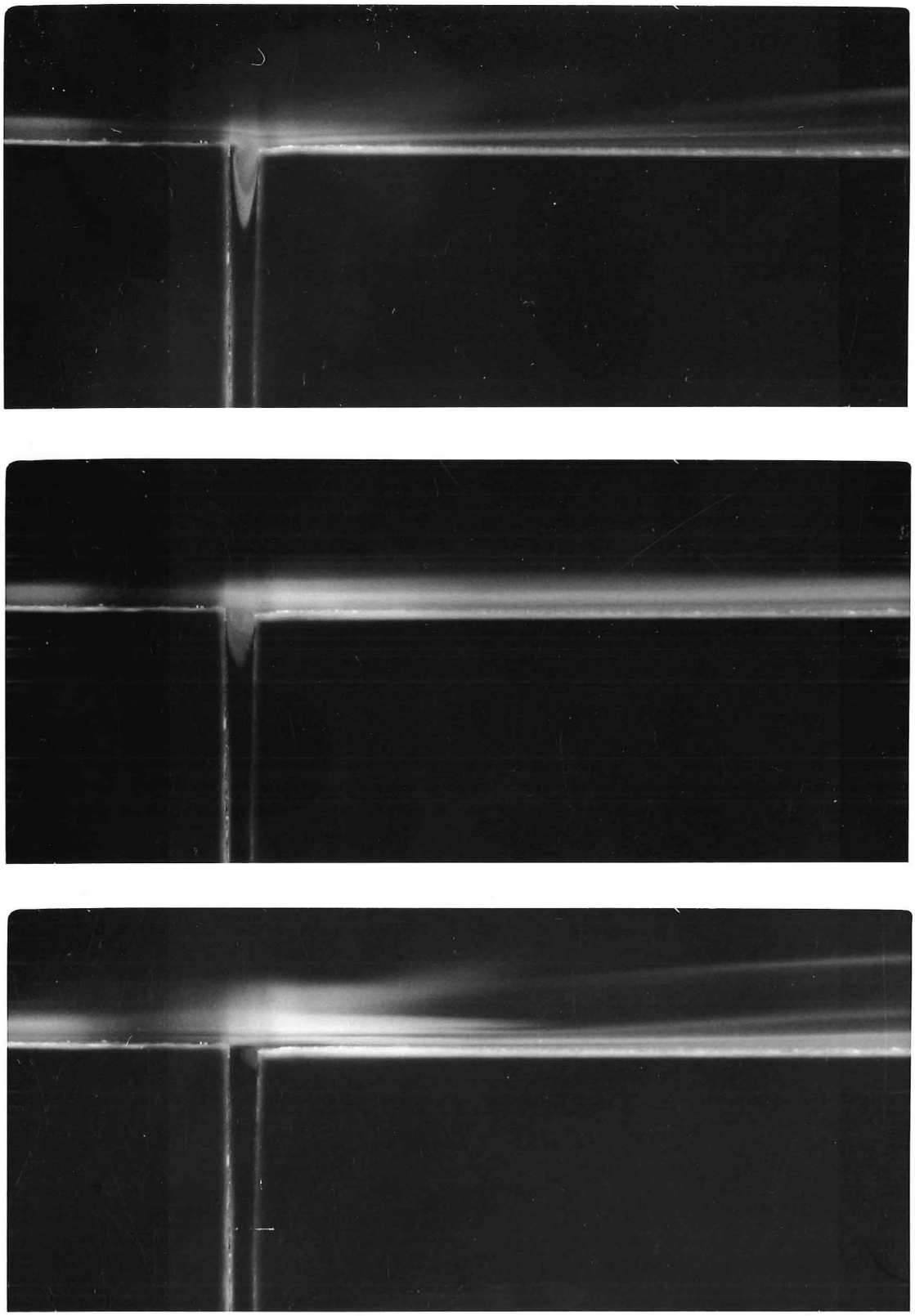

Plate 1 The development of successive eddies in an open gap of 2 mm wide at 0.6 m s^{-1}. (top) the formation of the eddy, (middle) the eddy moving into the main air stream and (bottom) the deformation of the eddy along the surface of the board. Taken on Ilford HP5 Plus film, developed to an effective ASA rating of 800, using a Nikon FE2 camera fitted with a Zoom-NIKKOR 35-105 mm lens and a Nikon PK-13 Auto Extension Ring. The exposure was 1/60 of a second at f4.

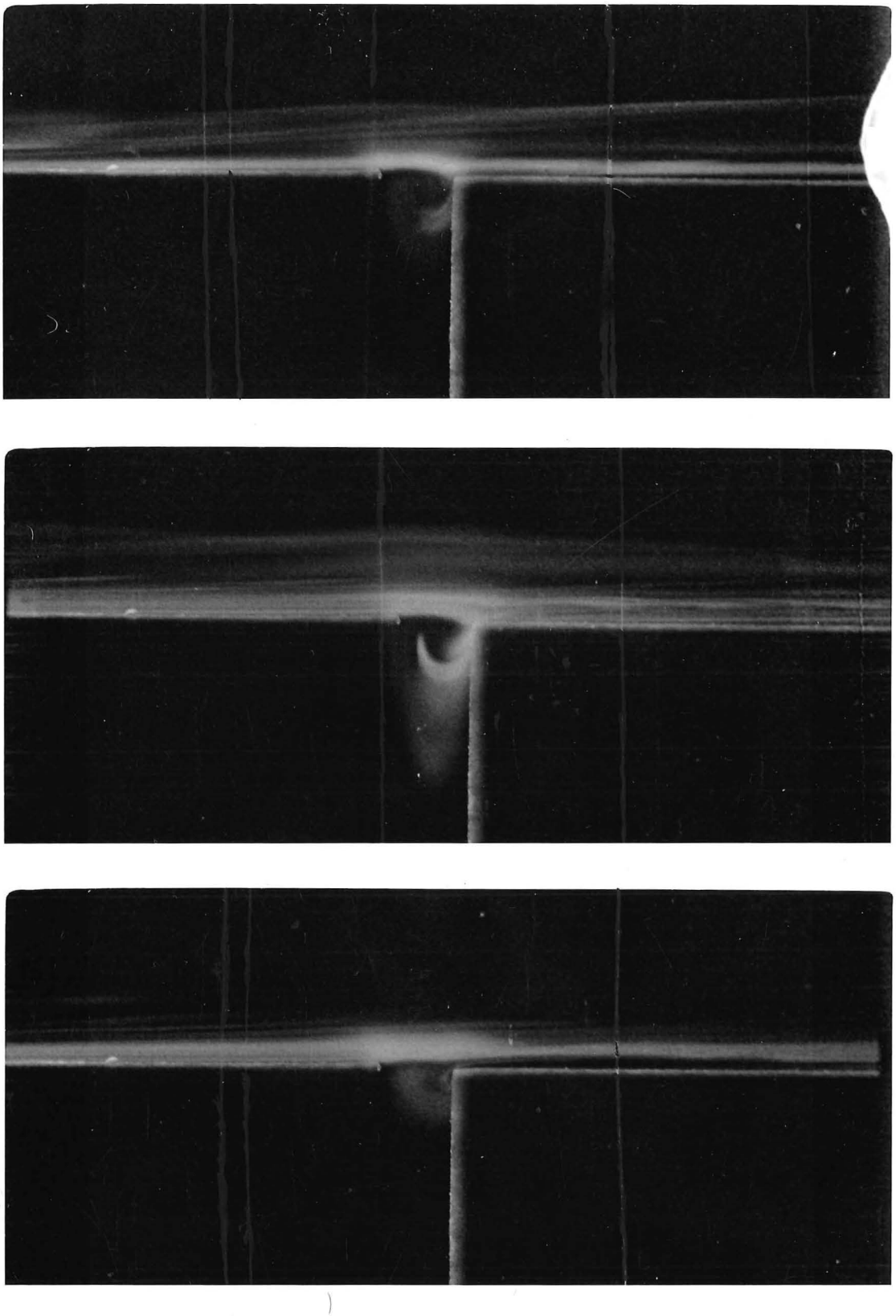

Plate 2 The development of successive eddies in an open gap of 5 mm wide at 0.5 m s^{-1}. (top) the formation of the eddy, (middle) the eddy moving into the main air stream and (bottom) the deformation of the eddy along the surface of the board. Taken on Kodak Tri-X Reversal black and white film at the rate of 48 frames per second, using a Bolex movie camera at f2.8.

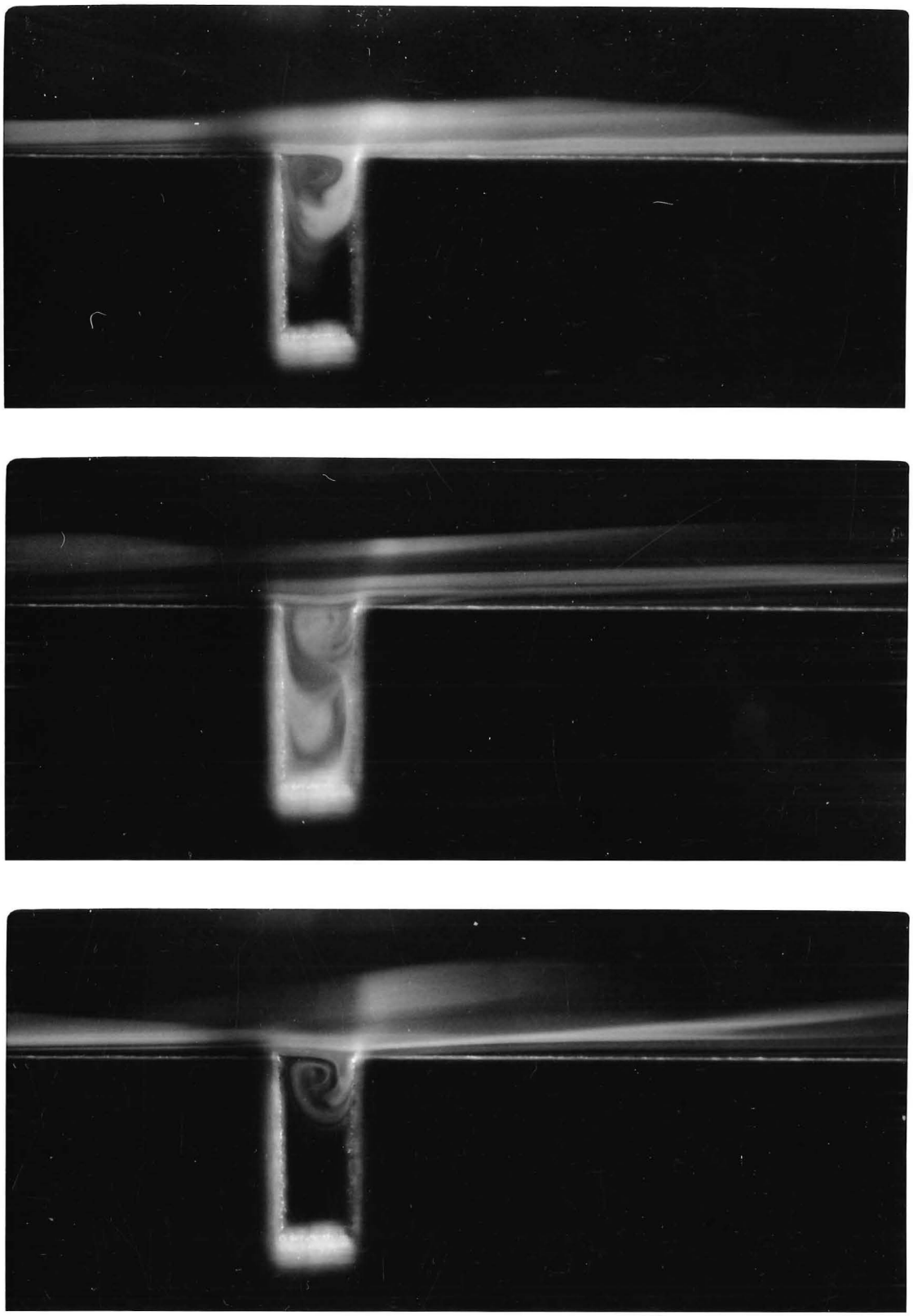

Plate 3 The development of successive eddies in a closed gap of 5 mm wide at 0.3 m s^{-1}. (top) the formation of the eddy, (middle) the eddy moving into the main air stream and (bottom) the deformation of the eddy along the surface of the board. Taken on Ilford HP5 Plus film, developed to an effective ASA rating of 800, using a Nikon FE2 camera fitted with a Zoom-NIKKOR 35-105 mm lens and a Nikon PK-13 Auto Extension Ring. The exposure was 1/60 of a second at f4.

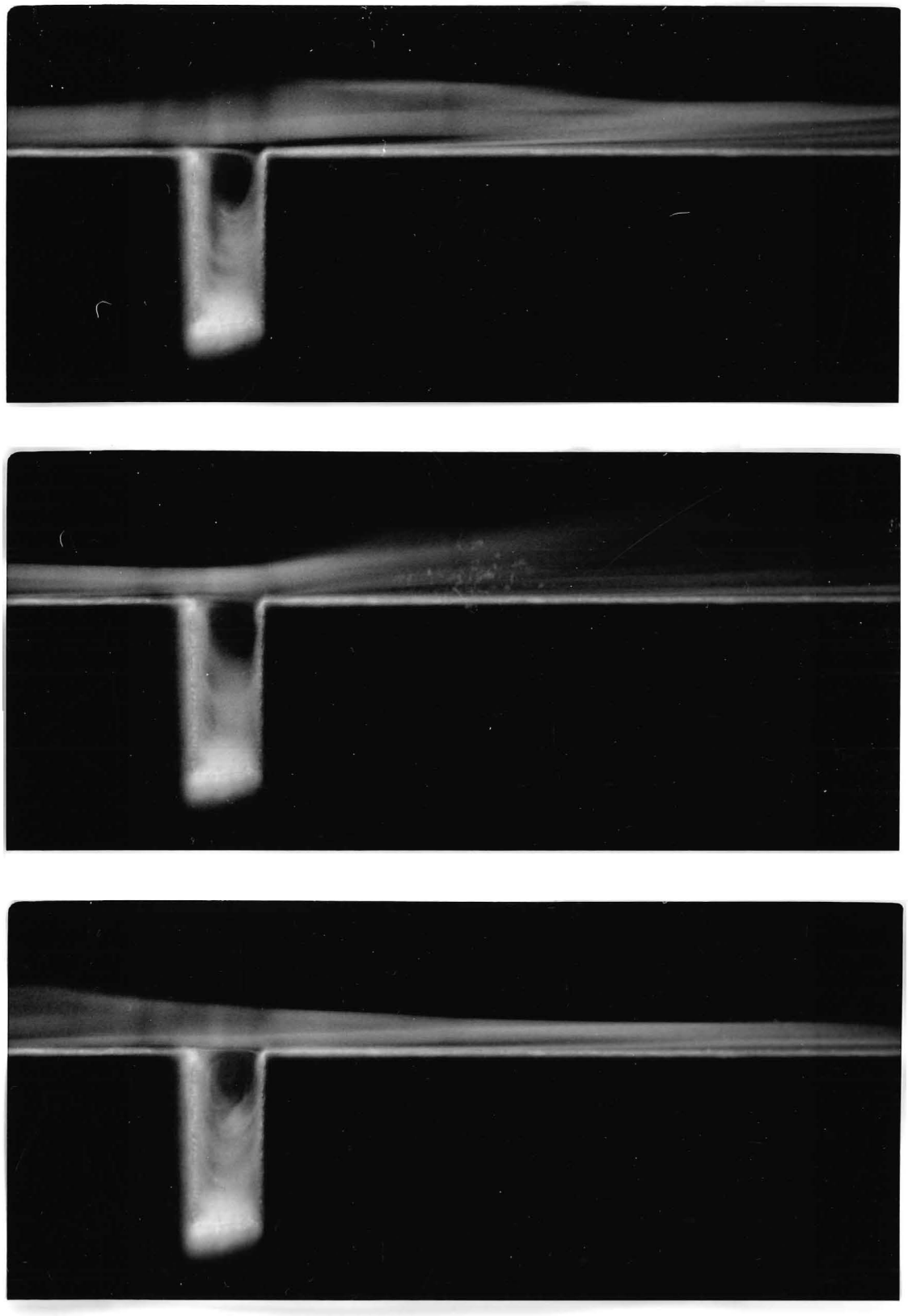

Plate 4 The development of successive eddies in a closed gap of 5 mm wide at 0.5 m s^{-1}. (top) the formation of the eddy, (middle) the eddy moving into the main air stream and (bottom) the deformation of the eddy along the surface of the board. Taken continuously at the rate of 3.4 frames per second on Ilford HP5 Plus film, developed to an effective ASA rating of 800, using a Nikon FE2 camera fitted with a Zoom-NIKKOR 35-105 mm lens and a Nikon PK-13 Auto Extension Ring. The exposure was 1/60 of a second at f4.

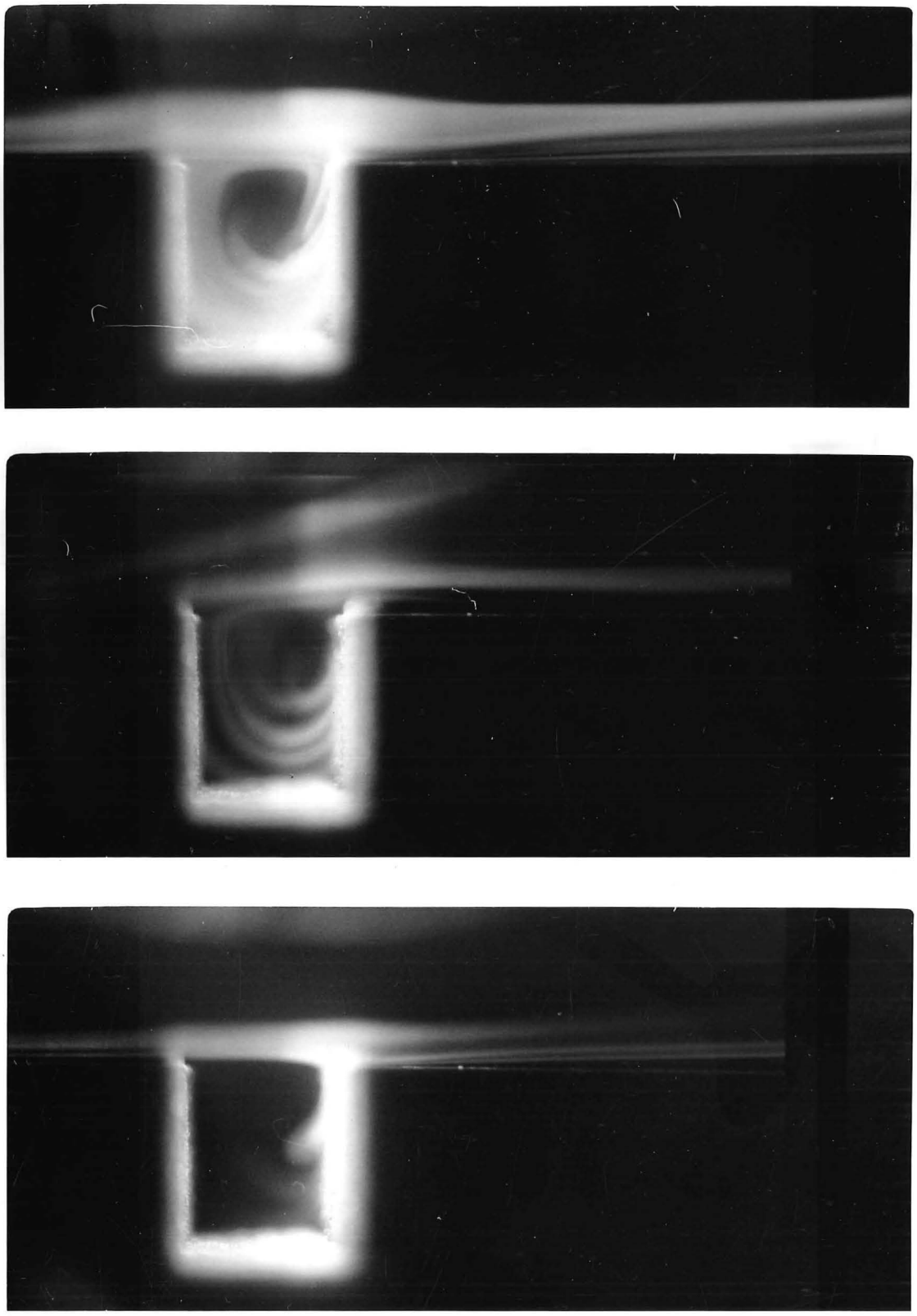

Plate 5 The development of successive eddies in a closed gap of 10 mm wide at 0.6 m s^{-1}. (top) the formation of the eddy, (middle) the eddy moving into the main air stream and (bottom) the deformation of the eddy along the surface of the board. Taken on Ilford HP5 Plus film, developed to an effective ASA rating of 800, using a Nikon FE2 camera fitted with a Zoom-NIKKOR 35-105 mm lens and a Nikon PK-13 Auto Extension Ring. The exposure was 1/60 of a second at f4.

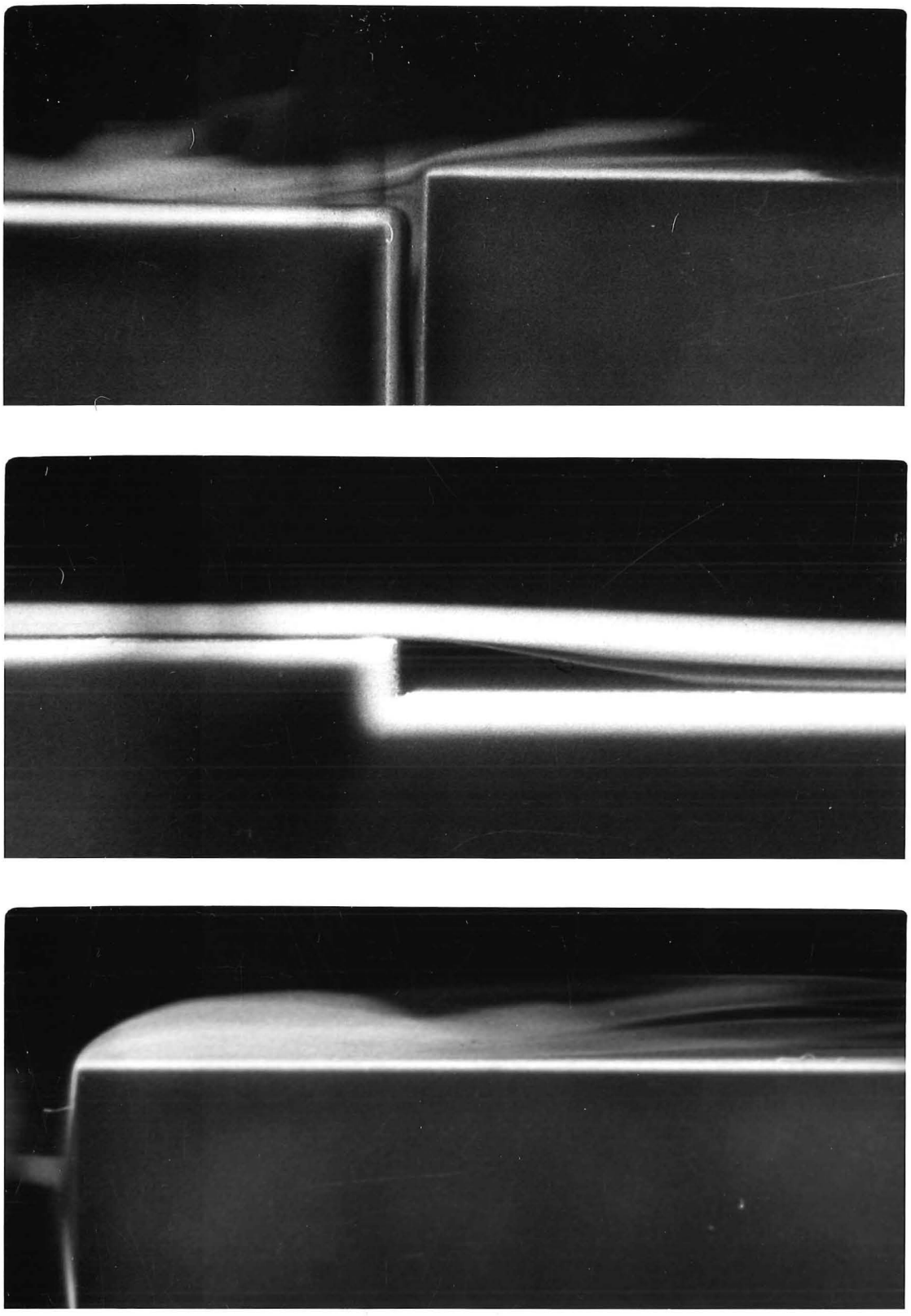

Plate 6 The effect of minor board irregularities on the air flow patterns.
Airflow approaching (top) a board thicker by 3 mm, (middle) a board thinner by 3 mm and (bottom) the first board. Taken on Ilford HP5 Plus film, developed to an effective ASA rating of 800, using a Nikon FE2 camera fitted with a Zoom-NIKKOR 35-105 mm lens and a Nikon PK-13 Auto Extension Ring. The exposure was 1/60 of a second at f4.

3

Turbulence intensity measurements

3.1 Background

Air is the normal drying medium in timber kilns. It has two principal roles; first, as a heat carrier to supply sufficient energy to evaporate the water and other volatile substances in the wood and second, as a moisture carrier to remove the evaporated vapours. When air flows over a timber board, a stationary eddy develops immediately downstream of the leading edge if the Reynolds number based on the thickness of the board, Re_b, exceeds 245 [Sørensen, 1969]. A boundary layer, through which heat and mass transport occurs, then forms downstream of this eddy on the surface of the board (Figure 3.1). As such, any changes made to the characteristics of this boundary layer will affect heat and mass transfer between the bulk air stream and the surface of the board.

The external parameters which affect the characteristics of the boundary layer of a fully developed flow over geometrically-similar bodies are free-stream turbulence intensity and the surface roughness. While the qualitative effect of free-stream turbulence intensity on Nusselt number for blunt bodies (spheres and circular cylinders) and sharp-edged flat plates has been well investigated [Schlichting, 1968 and Blair, 1983], very little research has been done to obtain quantitative expressions for such blunt bodies. Bayley and Turner [1971], in their investigation of heat transfer over a turbine blade, found that the heat transfer coefficients doubled when the turbulence intensity was increased from 0.45% to 5.9%. To demonstrate the quantitative effect of free-stream turbulence on the local heat-transfer coefficients, Sugawara *et al.* [1988] systematically performed experiments on a thin smooth-edged flat plate by varying the free-stream turbulence intensity. They found that the local heat-transfer coefficients increased very rapidly for intensity levels up to around 7%, after

which the coefficients started to level off to a value 55% higher than the corresponding Nusselt values obtained for the lowest free-stream turbulence intensity of 0.37%.

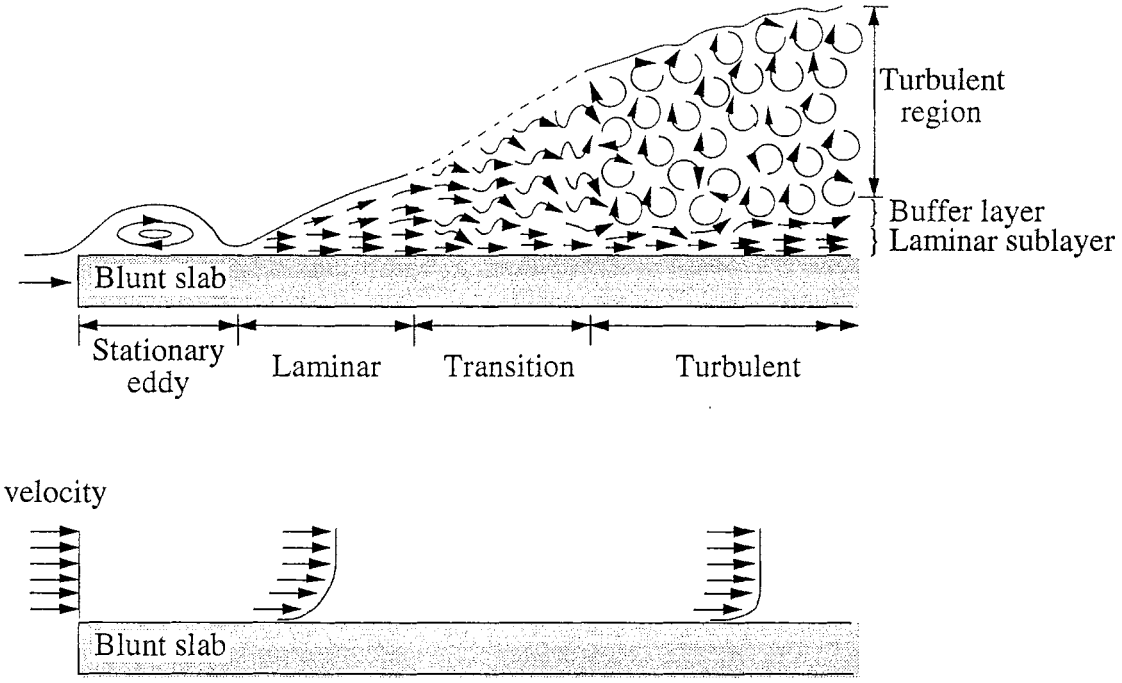

Figure 3.1 Velocity boundary layer development on a blunt slab.

Both Sugawara *et al.* [1988] and Schlichting [1968] have similarly concluded that an increased in the free-stream turbulence intensity would decrease the critical Reynolds number, $Re_{crit.}$, culminating in the earlier development of the turbulent boundary layer in the flow. While the Nusselt number was found to be independent of free-stream turbulence in the laminar boundary layer, small increments in turbulence intensity levels in the presence of a moderate pressure gradient in the flow was found to cause large increments in the Nusselt number in the turbulent boundary layer. Free-stream turbulence under such conditions is thought to intensify the turbulence in the boundary layer of a fully developed flow, causing both the turbulent boundary layer to thicken and the laminar sublayer to retreat, resulting in enhanced heat transport.

There is very little work which has been done to investigate the effect of free-stream turbulence on heat/mass transport for a geometry corresponding to that of a timber stack in a drying kiln. Wiedeman *et al.* [1989], in measuring the velocity and turbulence intensity at 11 positions in the 20 mm gap between the two timber layers over a 2-minute period. He found the levels of turbulence peaked at around 2.3 and 17.8 mm from the surface of the lower board, 20 mm inside the stack. This confirmed the results obtained by Danckwerts and Anolick [1962], Sørensen [1969] and Miller [1973] that an eddy was forming just behind the leading edge of the board. In investigating the effect of a 5 mm-wide gap between the boards, Wu [1989] measured the turbulence intensity at 1, 2 and 3 mm above the surface of a 4-board wide stack in a wind tunnel. He observed that turbulence intensity above the gaps were consistently higher than those over the adjacent boards although no appreciable pressure drop was observed. His results indicated that intensity levels decrease with gap position in the direction of flow. However, both papers did not measure the intensity levels prior to entry to the stack.

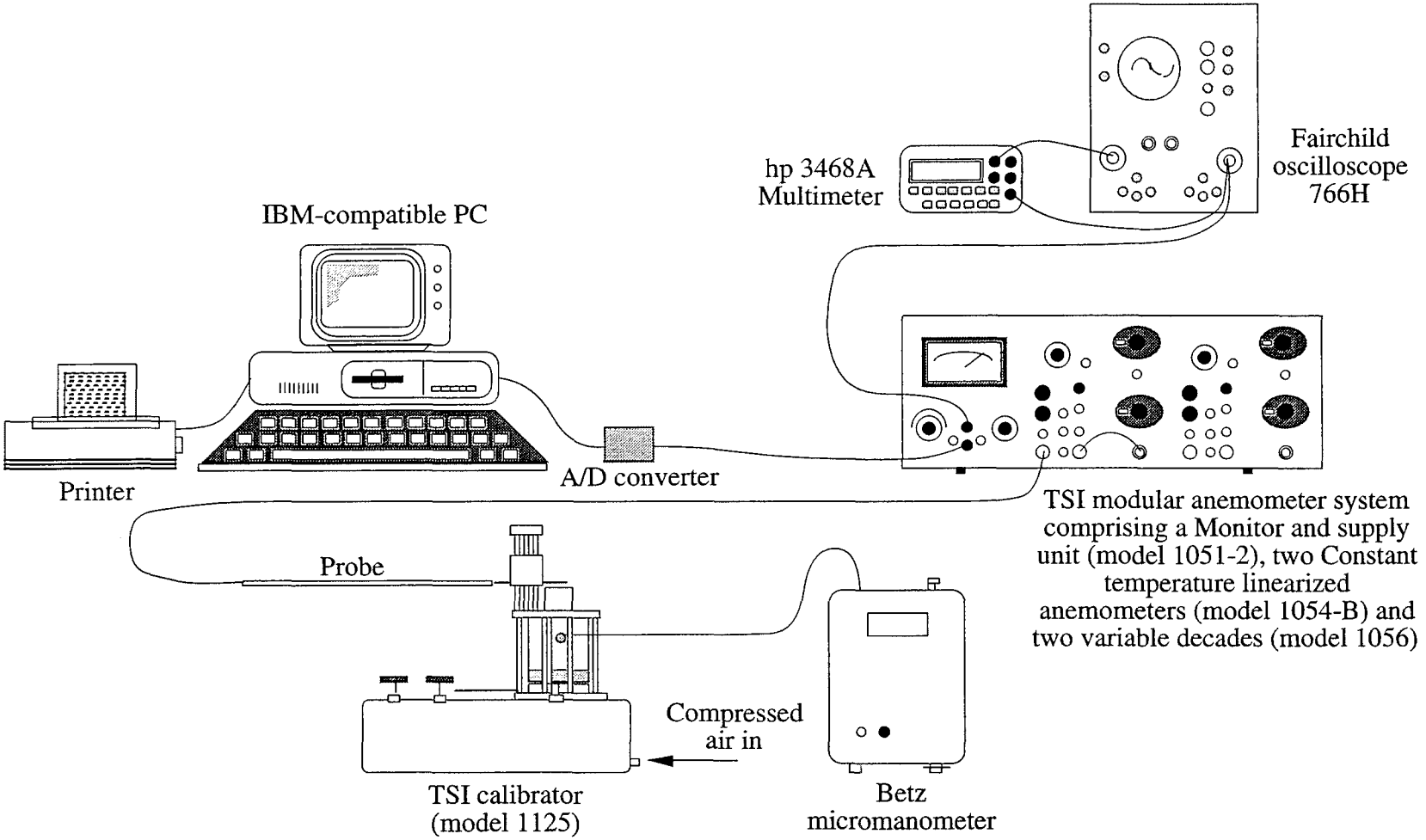

Figure 3.2 Schematic layout of TSI modular anemometer system and ancillary equipment

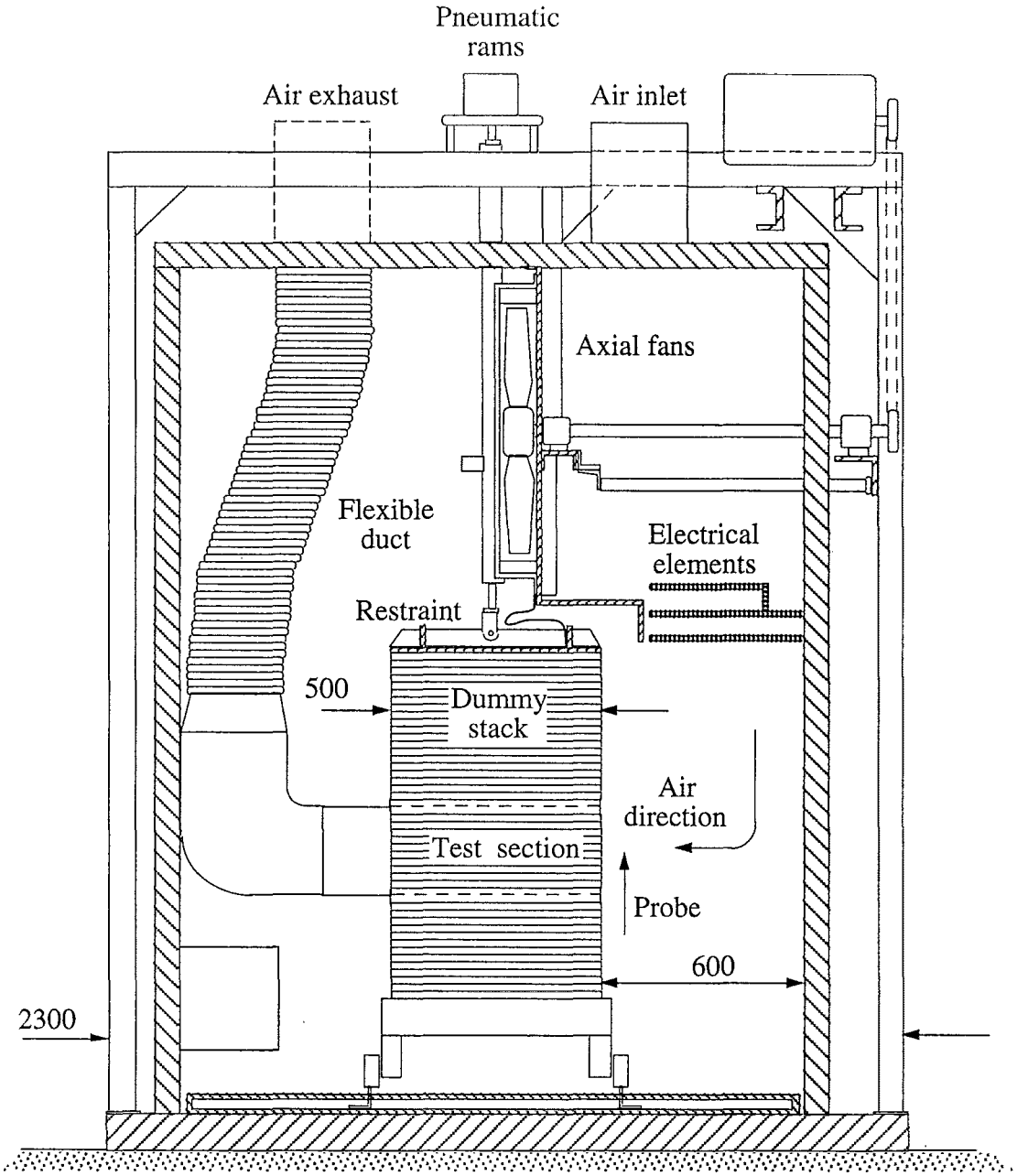

Figure 3.3a Probe location in the experimental kiln.

Most of the earlier experimental work on heat/mass transfer did not indicate the level of free-stream turbulence in their wind tunnels although most authors concluded that the free-stream turbulence on convective heat/mass transport is significant. Turbulence levels in these tunnels could be as low as 0.01% [Schlichting, 1968]. This chapter outlines the method used to measure the free-stream turbulence intensity prior to entry to the stack in both the experimental timber kiln and the wind tunnel. These values are also used in the next chapter as input parameters for the Computational Fluid Dynamics (CFD) software developed by Langrish [1992] to predict the convective mass-transfer coefficients over timber boards from calculated values of skin friction.

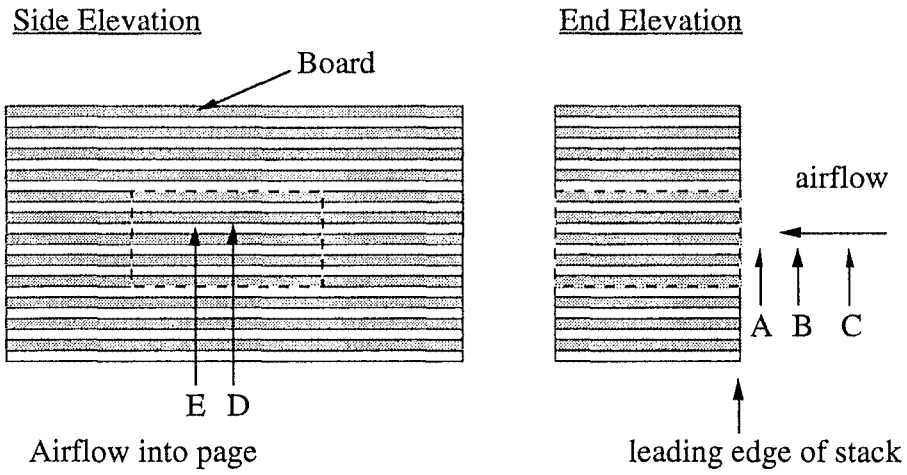

Probe positions
A - 5 mm to leading edge
B - 50 mm to leading edge
C - 100 mm to leading edge
D - Centre of test stack
E - 100 mm to the left of D

Figure 3.3b Position of the probe in the experimental kiln.

3.2 Method

The Thermo-System Inc. (TSI) modular anemometer system, comprising a monitor and supply unit (model 1051-2), two constant temperature linearized anemometers (model 1054 B), two variable decades (model 1056) and a 10μm diameter platinum-rhodium hot-wire DISA probe was used for measuring the velocity and turbulence levels in the experimental kiln and the wind tunnel. To ease the setting of reference voltages during the calibration process, a digital voltmeter and an oscilloscope were connected in parallel to the output of the anemometer. The printer, connected to the output of the anemometer via the computer and analog-to-digital converter, provided print-outs of all the data if required. The schematic layout of the anemometer and ancillary equipment used is shown in Figure 3.2.

For all the average velocity and turbulence intensity data gathered to be meaningful, the anemometer must be able to maintain its calibration over the period the measurements are taken. However, the hot-wire sensor is notoriously troublesome in this respect. Owing to its small size it can easily pick up small contaminants from the fluid stream in which it is placed. This will affect the performance of the sensor, rendering the calibration invalid. All data subsequently collected will be affected. To reduce this effect in the present studies, the sensor used was cleaned by briskly agitating it in pure ethanol solution before every run.

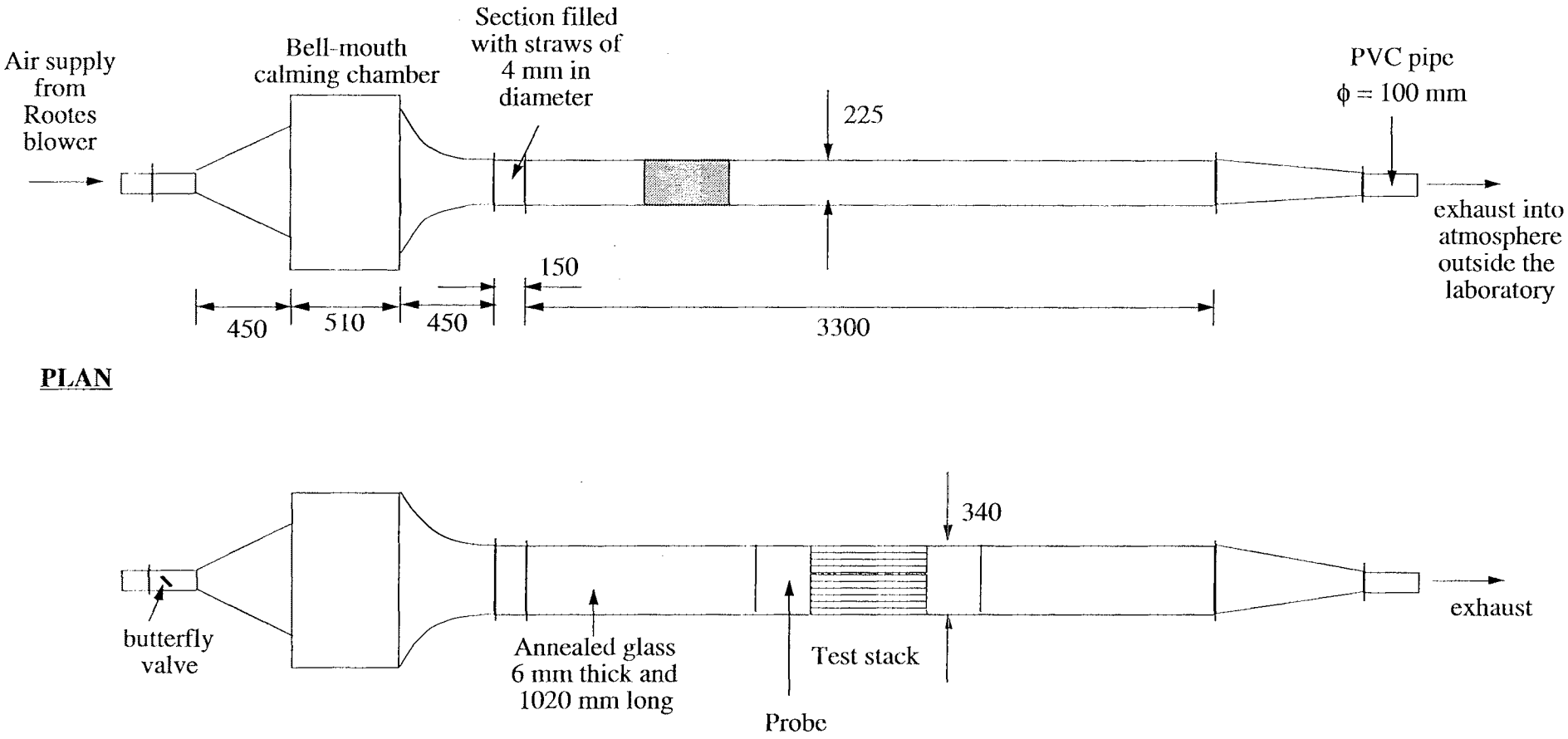

Figure 3.3 c Probe position in the wind tunnel.

Prior to each run, the anemometer has to be calibrated for the specific type of sensor used. This process involved shorting the probe support and setting the combined internal resistance of the anemometer and the probe cable to zero. With the DISA probe firmly inserted in the probe support, the resistance of the platinum-rhodium hot-wire sensor was determined. The operating resistance of the probe was set at a level 80% higher than that of the sensor resistance. The anemometer was then set to give a linear output, and the probe was placed in the nozzle region of the TSI calibrator (model 1125). By varying the air velocity through the nozzle, the voltage signals generated were picked up by the IBM-compatible personal computer via an analog-to-digital converter. A software was then used to determine the best-fit straight line between the values of the voltage signal and the air velocity. The pressure drop across the nozzle of the calibrator was measured using a Betz micromanometer. Ambient air temperature and atmospheric pressure were also noted for every calibration.

After the anemometer was calibrated, the probe was placed in position. A thousand samples at 500 Hz were collected at each position. Using the information obtained earlier in the calibration process the same software was then used to convert the voltage signals gathered to average velocity and turbulence levels. The procedure for calibrating and using the anemometer is appended in A5.

Stack arrangements

The stacking arrangements in the kiln and the wind tunnel in the present study were identical to that used in the sublimation tests described in Chapter 5. The 25 mm thick boards were separated by 25 mm thick stickers. Both arrangements are shown in Figures 3.3a, 3.3b and 3.3c.

For kiln runs the probe was placed in the plenum space at 5, 50 and 100 mm to the leading edge of the test stack, along the centreline of the test stack in the streamwise direction (Figures 3.3a and 3.3b). A further set of measurements were taken at 100 mm to the left of this probe position. Air velocity through the stack was also varied over the range 3-7 ms^{-1}, the same level as that used in the sublimation tests. Measurements further into the stack or at the outlet of the box containing the test section were not taken because of the difficulty of access and the interference that the probe support would have caused to the airflow pattern.

Measurements of turbulence intensity levels along the centreline of the stack in the direction of airflow were only taken at 20 and 90 mm to the leading edge of the test stack owing to the way the wind tunnel was constructed. The air velocity through the stack was 5 m s^{-1}.

3.3 Results

The initial results from the measurements taken in the kiln were found to be inconsistent and were not used. The discrepancies were eventually traced to two possible sources; the unsteady pressure of the compressed air supply during calibration and the drifting of the linear zero voltage during the data acquisition process.

The pressure of the compressed air supply was found to dwindle rapidly at high flowrates. Depending on the state of the compressor, it was observed that the pressure drop across the calibrator could drop by as much as 3 mm at a pressure drop of 12 mm water across the nozzle. This drop corresponded to a 14% decrease in air velocity. To reduce the effect of this fluctuating air supply, higher flowrate calibration points were done first when the compressor was at the highest pressure. While this method of calibration improved the accuracy of the measurements, the discrepancies were still too large for the readings to be accepted. This was eventually traced to a small but highly significant drift in the linear zero voltage, caused by the detaching and reattaching of the sensor on to the probe support. This had to be done in order to position it through the sampling port at the side of the kiln. It was observed that the linear zero, initially set at +0.03 volts drifted to as high as +0.06 volts after

the measurements were taken. Results of later runs, done without detaching the sensor by using a longer lead, were consistent to within experimental errors. These intensity levels are summarised in Table 3.1. Each data based on the average of ten readings.

Position	Run	Velocity		
		3 m s^{-1}	5 m s^{-1}	7 m s^{-1}
C at centre of stack, D	1	16.1	18.6	22.0
C at centre of stack, D	2	14.8	20.1	23.9
C at centre of stack, D	3	14.5	19.8	23.3
C at centre of stack, E	4	16.9	19.0	24.5
B at centre of stack, D	1	13.2	15.4	19.4
B at centre of stack, D	2	15.7	16.8	21.0
B at centre of stack, E	3	15.3	18.1	20.7
A at centre of stack, D	1	9.0	10.1	11.7
A at centre of stack, D	2	9.0	9.8	11.4
A at centre of stack, E	3	8.5	10.2	11.7

Table 3.1 Turbulence intensity levels for all the runs in the plenum space of the experimental kiln.

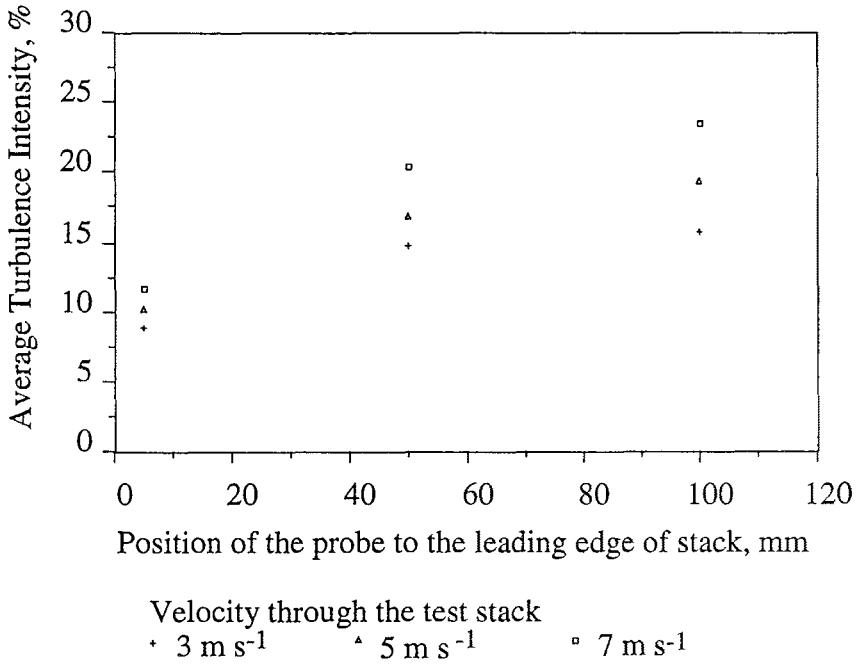

Figure 3.4 Average intensity level in the plenum space of the experimental kiln.

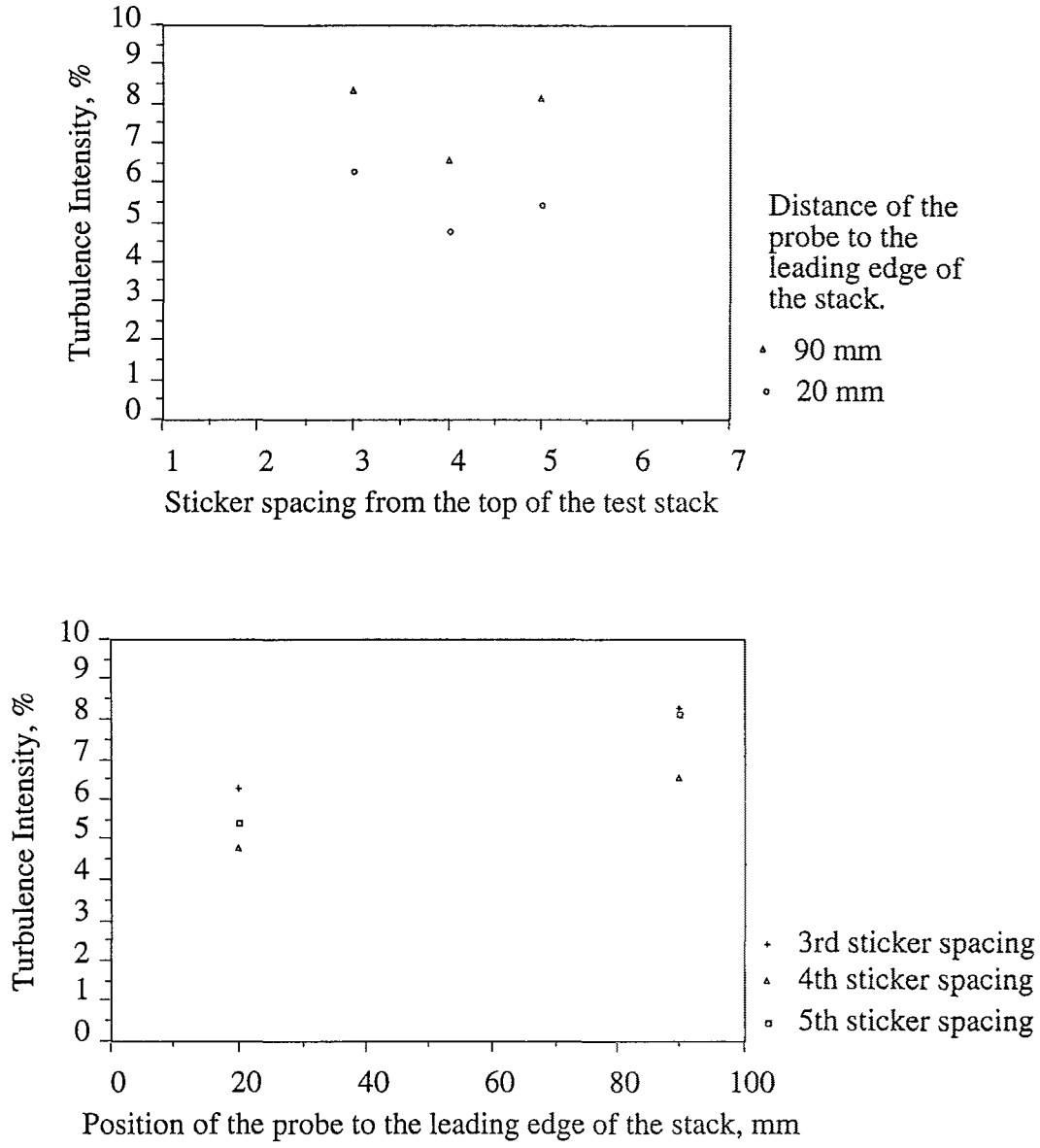

Figure 3.5 Turbulence intensity levels for all the runs (above) and the average intensity levels (below) in the wind tunnel at 5 m s^{-1}.

3.4 Discussion

Figure 3.4 shows the actual and the average turbulence intensity levels for ten runs in the plenum space of the experimental kiln over an airflow range of 3 - 7 m s^{-1}. The turbulence levels were of the order 15.6% - 23.4% at 100 mm to the leading edge of the test stack, decreasing to 8.8% - 11.6% at 5 mm. These levels were much higher than the levels thought to prevail in the wind tunnels in which earlier correlations were derived [Schlichting, 1968].

Figure 3.5 shows the free-stream turbulence levels at the third, fourth and fifth sticker spacing of the test stack in the wind tunnel. At 90 mm to the leading edge of the test stack, these levels were 6.5% - 8.3%, decreasing to 4.8% - 6.3% at 20 mm for an air velocity of 5 m s^{-1} through the stack. These intensity levels are lower than that in the plenum space of the experimental kiln.

As the level of free-stream turbulence decreases in the streamwise direction for flow along a flat plate, the choice of a representative value to define the turbulence level is difficult. Ideally, the free-stream turbulence level at the onset of the transition region should be used, as turbulence only affects heat/mass transfer in the transition and turbulent regimes. However, this was not done in this study owing to the difficulty of access in the stack and the undesirable interference that the probe holder would have caused to the airflow pattern. Free-stream turbulence near to the leading edge of the slab was only measured to give an indication of the levels at the transition regime. As the above measurements were made in the vicinity near to leading edge of the stack, no decisive conclusion could be made with regard to the effect of free-stream turbulence on heat/mass transfer. The blunt edge of the slab, while causing the formation of a stationary eddy, could have raised the level of free-stream turbulence at the onset of the transition regime in the flow.

4

Numerical simulation

4.1 Introduction

The design of kilns and drying schedules requires the knowledge of convective heat- and mass-transfer coefficients. This is often not readily available. To obtain it experimentally can be very costly and time-consuming. Hence there is considerable interest in been able to predict the mass-transfer coefficients over the surface of the boards in an array similar to that in a timber kiln.

In this chapter, airflow patterns around an array of in-line boards in a timber stack were numerically simulated by a colleague, Dr. T.A.G. Langrish, for both time-independent and time-dependent flows, using the data obtained by me and reported in Chapter 3. From calculated values of skin friction, mass-transfer coefficients were predicted using the Reynolds and Chilton-Colburn analogies. This work is included here as a basis for understanding the experimental determination of the mass-transfer coefficients which is the core of this thesis. It validates many of the surprising observations which are discussed in the other chapters of this thesis.

The procedure used is the same as that outlined by Patankar [1980] to predict the horizontal and vertical velocity in a two-dimensional flow, bounded by wall . Flow through the stack was assumed to be incompressible and isothermal. The five variables solved in the simulation were :

u : the average horizontal velocity,

v : the average vertical velocity,

k : the turbulence kinetic energy (per unit mass),

ε : the rate of dissipation of turbulent kinetic energy, and

p : the static pressure.

The time-averaged Navier-Stokes equations for conservation of total mass and conservation of momentum in both the horizontal and vertical directions, and one equation each for the variables k and ε were solved in the simulation. Although the Reynolds number for the flow based on the spacing between board rows (25 mm) was only just turbulent (5000) at the lowest velocity studied (3 m s^{-1}), the high-Reynolds form of the k - ε model of Launder and Spalding [1974] was used here to simplify the simulation. The standard constants for general free turbulent flows, used in the k - ε model were also taken from Launder and Spalding [1974]. The treatment of convection and diffusion (of any property) followed the hybrid scheme described by Patankar [1980].

4.2 Mathematical Formulation

For time-independent flows, a general form for the governing equations including the equation of continuity is given below in Equation 4.1.

$$\frac{\partial(\rho \cdot u \cdot \phi)}{\partial x} + \frac{\partial(\rho \cdot v \cdot \phi)}{\partial y} = \frac{\partial}{\partial x}\left(\Gamma_\phi \frac{\partial \phi}{\partial x}\right) + \frac{\partial}{\partial y}\left(\Gamma_\phi \frac{\partial \phi}{\partial y}\right) + S_\phi \qquad (4.1)$$

where

ϕ is the dependent variable of interest (for example, horizontal velocity),

Γ_ϕ is the transfer coefficient associated with ϕ,

S_ϕ is the source term,

ρ is the density of the fluid.

In the above generalised form, all the terms in the governing equations other than those in the 'convection' and 'diffusion' terms are collected in the source term, S_ϕ. The terms Γ_ϕ and S_ϕ for each of the dependent variables are shown in Table 4.1, in which the generation of turbulence kinetic energy, G is calculated from

$$G = \mu_T \left[\left(\frac{\partial u}{\partial y} + \frac{\partial v}{\partial x} \right)^2 + 2 \left\{ \left(\frac{\partial u}{\partial x} \right)^2 + \left(\frac{\partial v}{\partial y} \right)^2 \right\} \right] \qquad (4.2)$$

The constants, C_μ, C_1, C_2, σ_k and σ_ε in Table 4.1 are taken from the values recommended by Launder and Spalding [1974] for general free turbulent flows. These values are summarised in Table 4.2. In this model, the turbulent viscosity μ_T, is described in terms of measurable flow quantities, and related to the turbulence kinetic energy, k and to the dissipation rate of turbulence kinetic energy, ε by the equation,

$$\mu_T = C_\mu \frac{\rho \cdot k^2}{\varepsilon} \qquad (4.3)$$

Equation	ϕ	Γ_ϕ	S_ϕ
Continuity	1	0	0
x-momentum	u	$\mu_L + \mu_T$	$-\left(\frac{\partial p}{\partial x}\right) + \frac{\partial}{\partial x}\left\{(\mu_L + \mu_T)\left(\frac{\partial u}{\partial x}\right)\right\} + \frac{\partial}{\partial y}\left\{(\mu_L + \mu_T)\left(\frac{\partial v}{\partial x}\right)\right\}$
y-momentum	v	$\mu_L + \mu_T$	$-\left(\frac{\partial p}{\partial y}\right) + \frac{\partial}{\partial x}\left\{(\mu_L + \mu_T)\left(\frac{\partial u}{\partial y}\right)\right\} + \frac{\partial}{\partial y}\left\{(\mu_L + \mu_T)\left(\frac{\partial v}{\partial y}\right)\right\}$
Turbulence kinetic energy	k	$\mu_L + \frac{\mu_T}{\sigma_k}$	$G - \rho \cdot \varepsilon$
Dissipation rate of turbulence kinetic energy	ε	$\mu_L + \frac{\mu_T}{\sigma_\varepsilon}$	$C_1\left(\frac{\rho \cdot \varepsilon}{k}\right)G - C_2\left(\frac{\rho \cdot \varepsilon^2}{k}\right)$

Table 4.1 Equations solved in the numerical simulation.

C_μ	C_1	C_2	σ_k	σ_ε
0.09	1.43	1.92	1.0	0.9

Table 4.2 Constants used in the turbulence model.

To take into account the time-dependent nature of the flow, another term is included on the left hand side of the general conservation equation of Equation 4.1 to give :

$$\frac{\partial}{\partial t}(\rho \cdot \phi) + \frac{\partial(\rho \cdot u \cdot \phi)}{\partial x} + \frac{\partial(\rho \cdot v \cdot \phi)}{\partial y} = \frac{\partial}{\partial x}\left(\Gamma_\phi \frac{\partial \phi}{\partial x}\right) + \frac{\partial}{\partial y}\left(\Gamma_\phi \frac{\partial \phi}{\partial y}\right) + S_\phi \quad (4.4)$$

where

t is the time.

Time steps of 0.1 s have been used in this time-dependent simulation. The grid size used (236 steps in the streamwise direction and 33 steps vertically) was sufficiently fine so that halving the distance between grid lines changed the velocities at any point by less than 5%. The interfacial mass-transfer coefficients have been predicted from wall shear stresses using the Chilton-Colburn analogy between mass and momentum transfer.

The equations have been solved in the order known as the SIMPLE (Semi-Implicit Pressure-Linked Equations) scheme [Patankar, 1980]. In this scheme, the pressure field is guessed first, and the momentum equations are solved to give the velocity field. The velocity field is then corrected so that it satisfies continuity (conservation of mass) and the pressure field is recalculated. The momentum equations are solved again, and this procedure is repeated until conservation of both mass and momentum are satisfied throughout the flowfield within preset tolerances. For each control cell within the finite-difference grid, a residual is defined for each variable as the absolute value of the difference between inflow and outflow. These residuals are then summed over the whole field, and convergence is considered to be achieved when the total residual for each variable is less than an absolute value of 10^{-6}. Taking the continuity equation (total mass) as an example, a total residual of 10^{-6} would imply a mass balance discrepancy over the whole grid of 10^{-6} kg per metre depth of the flowfield. By comparison, the grid was 100 mm high and 775 mm long, so a one metre depth of field has a volume of 0.0775 m^3, and this is approximately 0.09 kg of air at ambient temperature and pressure. Therefore, a total residual of 10^{-6} kg implies a discrepancy of less than 0.001% in the mass balance.

These non-linear equations are proned to diverge even when a solution exists. Changes in the values of the dependent variables from iteration to iteration are been slowed down by using the Wegstein under-relaxation factor (h), defined below as :-

$$\phi_{new} = h \cdot \phi^{*}_{new} + (1 - h) \cdot \phi_{old} \qquad (4.5)$$

where the subscripts old and new refer to the values of the dependent variables (ϕ) from the previous iteration and the current one respectively, and the superscript * refers to the value which would be produced in the current iteration if no under-relaxation were used. The under-relaxation factors were taken as 0.1 for all variables. At least 800 iterations were used in each simulation trial.

The turbulence energy per unit mass at the inlet, k_{inlet} was related to the turbulence intensity at the face of the grid (100 mm in front of the stack) by the following equation:-

$$k_{inlet} = (u \cdot I)^2 \qquad (4.6)$$

where

I is the intensity of turbulence at the inlet.

The value of the energy dissipation rate of the face of the grid (ε_{inlet}) was fitted to the variation of the turbulence intensity which was measured in front of the stack. This procedure is described in the Section 4.31.

The Navier-Stokes equations have been modified for cells near the wall to reduce the amount of grid refinement needed for a grid-independent solution. These equations are obtained by assuming a linear variation of turbulent viscosity with distance from the wall. The universal velocity profile is assumed to apply close to the wall:-

$$u^+ = y^+ \qquad \text{for } y^+ \le 11.225 \qquad (4.7)$$

$$u^+ = \frac{1}{\kappa} \ln (E \cdot y^+) \qquad \text{for } y^+ \ge 11.225 \qquad (4.8)$$

where

y^+ is the dimensionless distance from the wall,

u^+ is the dimensionless velocity,

κ and E are constants.

The Colburn analogy between mass and momentum transfer was used to relate the wall shear stresses to the mass-transfer coefficients, so that:-

$$Sh_x \cdot Sc^{1/3} = \frac{C_f}{2} \tag{4.9}$$

$$C_f = \frac{\tau_w}{\rho \cdot u^2/2} \tag{4.10}$$

where

C_f is the skin friction coefficient, and

u is the free-stream velocity.

The dimensionless distance to the wall is:-

$$y^+ = y_p \frac{\rho \cdot C_\mu^{1/2} \cdot k_p^{1/2}}{\mu} \tag{4.11}$$

where

y_p is the distance of the near-wall grid point from the wall.

k_p is the value of k for the grid point, is calculated from a regular balance over a control volume near the wall, with diffusion of energy to the wall being set to zero as described by Launder & Spalding [1974].

From the value of y^+ calculated in Equation 4.11, the value of u^+ can be calculated from Equations 4.7 or 4.8. This enables the velocity at the near-wall grid point, u_p, to be calculated. Also, if the logarithmic velocity profile is assumed to apply in the near-wall region, uniform shear stress prevails in the region between the near-wall grid point and the wall and generation and dissipation of energy are in balance there. Then the wall shear stress, τ_w, may be calculated from the equation:-

$$\tau_w = \rho \cdot C_\mu^{1/2} \cdot k_p \tag{4.12}$$

Thus the true velocity u_p can be calculated from u^+ using the conventional definition for the skin-friction velocity, as follows:-

$$u_p = u^+ \sqrt{\frac{\tau_w}{\rho}} \tag{4.13}$$

The spacing between the (vertical) grid lines which subdivided them (in the direction of the air flow) was chosen as 0.2 mm. Away from the gaps the spacing between grid lines in the direction of the airflow was gradually expanded up to 2 mm and then up to 20 mm away from the boards. This resulted in 236 grid lines in the direction of the airflow. A finer grid would have resulted in an impractically large number of grid lines.

We are interested in the mass transfer process at the surface of the boards, so the spacing of the finite-difference grid near to the wall (perpendicular to the air flow) is of great importance. The vertical spacing between the wall and the adjacent grid lines was such that the grid line lay in the log-law region of the turbulent boundary layer. This implied a dimensionless distance from the wall, y^+, greater than about 50. A typical resulting grid is shown in Figure 4.1.

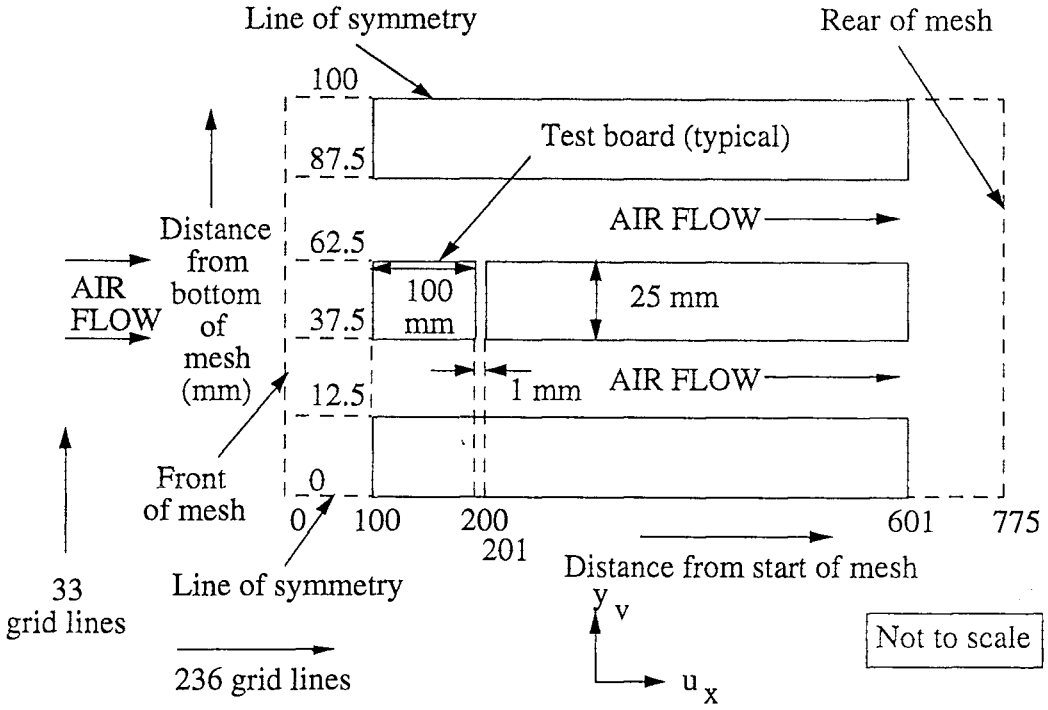

Figure 4.1 Layout of a typical flow situation.

4.3 Results

4.31 Inlet Turbulence Measurements

Figure 4.2 shows both the measured values of turbulence intensity with distance from the front of the stack from Chapter 3 and that predicted by numerical simulation. The turbulence intensities varied significantly with the air velocity. The numerical simulation similarly predicted decreasing intensity with decreasing distance from the stack. The measured turbulence intensity at a distance of 100 mm from the stack was used to calculate values of k_{inlet}, the turbulence energy per unit mass at the face of the grid. Values of the energy dissipation rate were adjusted at the face of the grid to give the continuous curves shown in Figure 4.2 so that the maximum discrepancy between the predicted profiles of turbulence intensity and the measured values (shown as points in Figure 4.2) was minimised. The fitted values of the turbulence energy and the energy dissipation rate are summarised in Table 4.3.

Air velocity between boards ($m\ s^{-1}$)	k_{inlet} Turbulence energy at the front of grid ($m^2\ s^{-2}$)	ε_{inlet} Energy dissipation rate at front of grid ($m^2\ s^{-3}$)
3	0.0547	0.841
5	0.234	7.45
7	0.671	36.2

Table 4.3 Summary of the fitted values of the turbulence energy and the energy dissipation rate at the front of the grid.

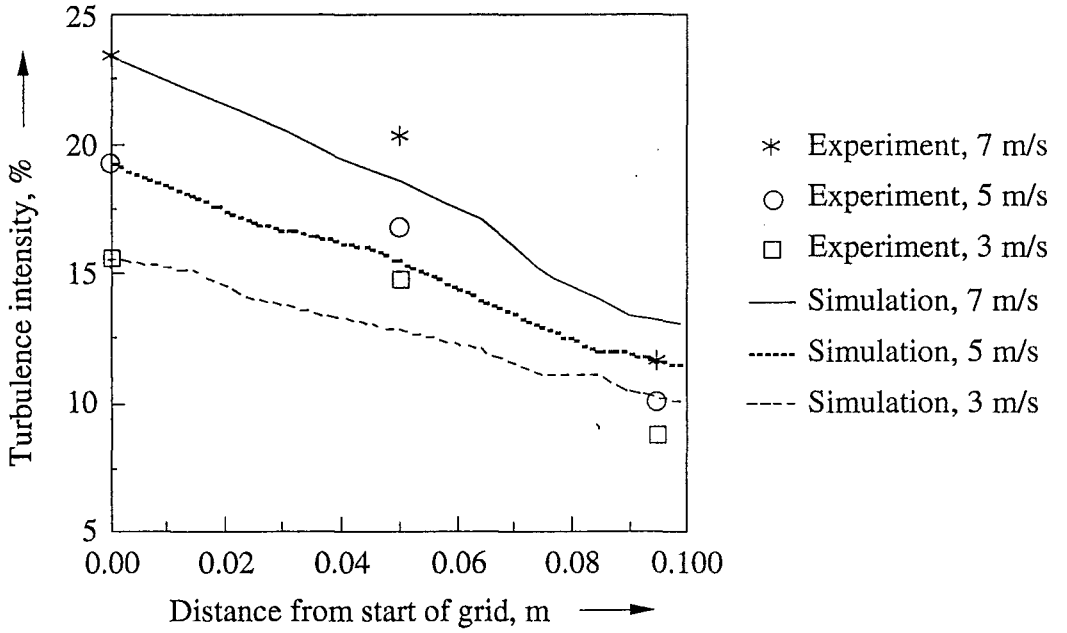

Figure 4.2 Variation of the turbulence intensity with distance from the face of the grid and the air velocity.

Arnaud *et al.* [1991] have simulated the flow patterns around the front and rear of the timber stacks. They calculated a value for the turbulence kinetic energy near the start of the stack of around 0.7 $m^2\ s^{-2}$ at an air velocity of 6 $m\ s^{-1}$, which is similar to the value in Table 4.3 of 0.67 $m^2\ s^{-2}$ at an air velocity of 7 $m\ s^{-1}$. However, they do not state what values for the turbulence parameters they used at the inlet of their simulation, which appears to be just after the air circulation fan. A feature of the qualitative agreement between this work and Arnaud *et al.*. [1991] is our finding of a virtually flat velocity profile in the vicinity of our test section and the maps of velocity vectors given by Arnaud *et al.* [1991]. which predict that the flow is only significantly curved in the area of the top boards in the stack. The values of

the energy dissipation rate given in Table 3 are consistent with a length scale of turbulence (l) of 0.01 m, according to the following equation for non-swirling flow [Gosman, 1978]:-

$$\varepsilon_{inlet} = \frac{k_{inlet}^{3/2}}{1.52l} \qquad (4.14)$$

4.32 Flow Patterns

The simulation predicted the flow in the gap to be periodic with a frequency of 0.5 hertz. This agrees with the time found by counting the number of frames between recurring motions in Chapter 2. The calculated period is not sensitive to the size of the time step used in discretizing Equation 4.4, providing that the size of the time step is less than or equal to 0.1 s. Plots of the computed streamfunctions around the gaps are shown in Figure 4.3.

The sequence of events is:-

1. There is a slow circulation in the gap. The streamlines outside the gap show no large effects due to the slow circulation.

2. The circulation in the gap speeds up. The streamlines drawn into the gap and push away from the leading edge of the board on the downstream side. The increasing speed of circulation is shown by the streamlines becoming more closely spaced, with one closed streamfunction contour in the gap in Figure 4.3b, while there are two fully-closed streamfunction contours shown in Figure 4.3d.

3. The circulation zone speeds up further, pushing the streamlines away from the gap. The streamlines are directed down at the following board.

4. Eventually the main body of the flow pushes the circulation zone back into the gap. The speed of the circulation zone slows down and we return to the original situation (slow circulation in the gap).

Although the generation and dissipation of eddies in the gaps is predicted, the results of the simulation do not show all the features observed experimentally such as the outward movement of the eddies from the gap and their movement along the board surface. However, a significant feature is the substantial amount of momentum exchange between the gaps and the bulk of the airflow.

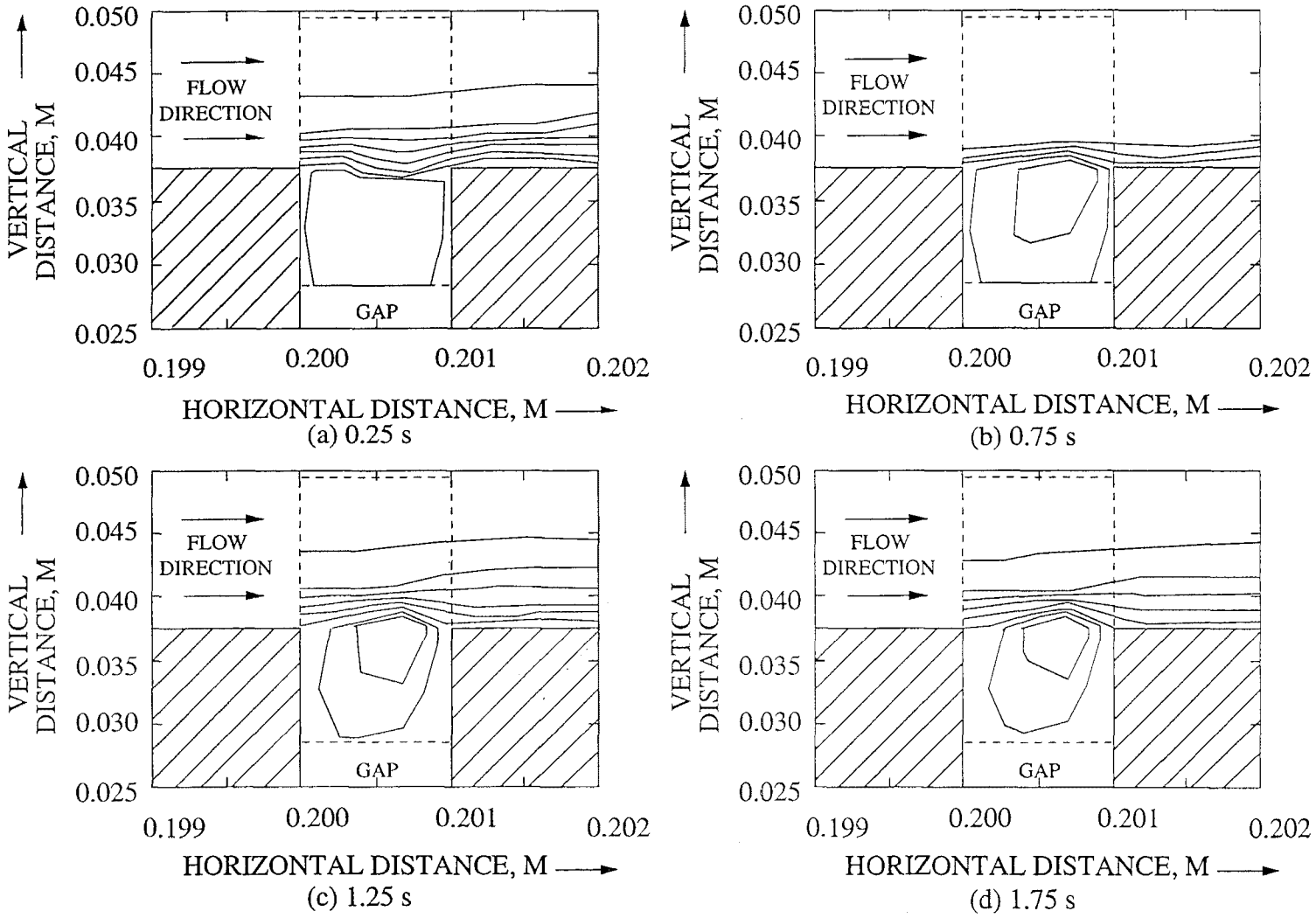

Figure 4.3 Streamfunctions plots around the gap between two boards, from the numerical simulation (distances are relative to the bottom left-hand corner of the grid in Figure 4.1)

4.33 Mass-transfer Coefficients

Figures 4.4, 4.5 and 4.6 shows the comparison between the predictions of the numerical simulation for time-dependent and time-independent flows for velocities of 3, 5 and 7 m s^{-1}. As the flow patterns and therefore the mass-transfer coefficients are predicted to vary with time, time-averaged values of the predicted mass-transfer coefficients are used for time-dependent simulation. The mass-transfer coefficients were averaged over a much longer period of 200 s than the period of the flow oscillations of 2 s. This is to even out the variations in the mass-transfer coefficients caused by the fluctuating velocity (Figure 4.3).

The distinctive feature in Figures 4.4 to 4.6 is that the numerical simulation for time-dependent flows predicted profound enhancement of mass-transfer coefficients near to the leading edges than that predicted for time-independent flows. Results of the time-dependent simulation also showed that there is a greater variation in magnitude of the coefficients along the surface of each board than that of the prediction from time-independent simulation.

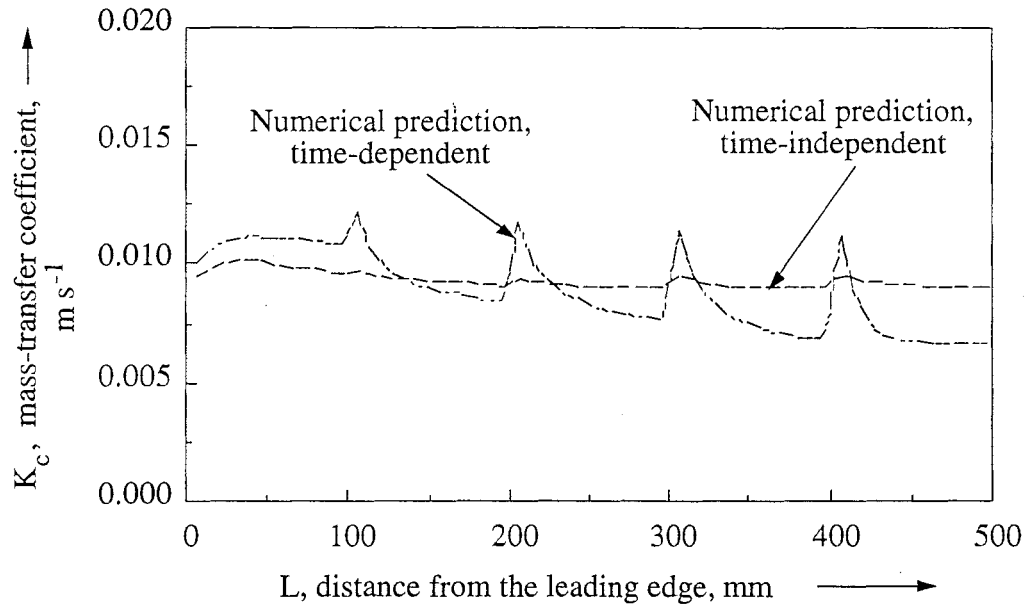

Figure 4.4 Numerically predicted mass-transfer coefficient profiles for both time-dependent and time-independent flows for an air velocity of 3 m s^{-1}.

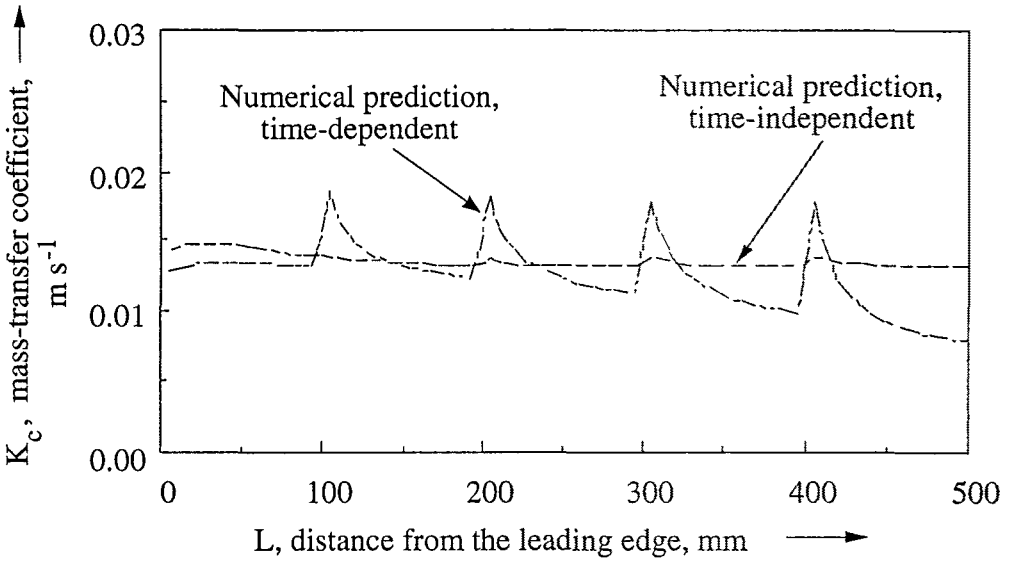

Figure 4.5 Numerically predicted mass-transfer coefficient profiles for both time-dependent and time-independent flows for an air velocity of 5 m s^{-1}.

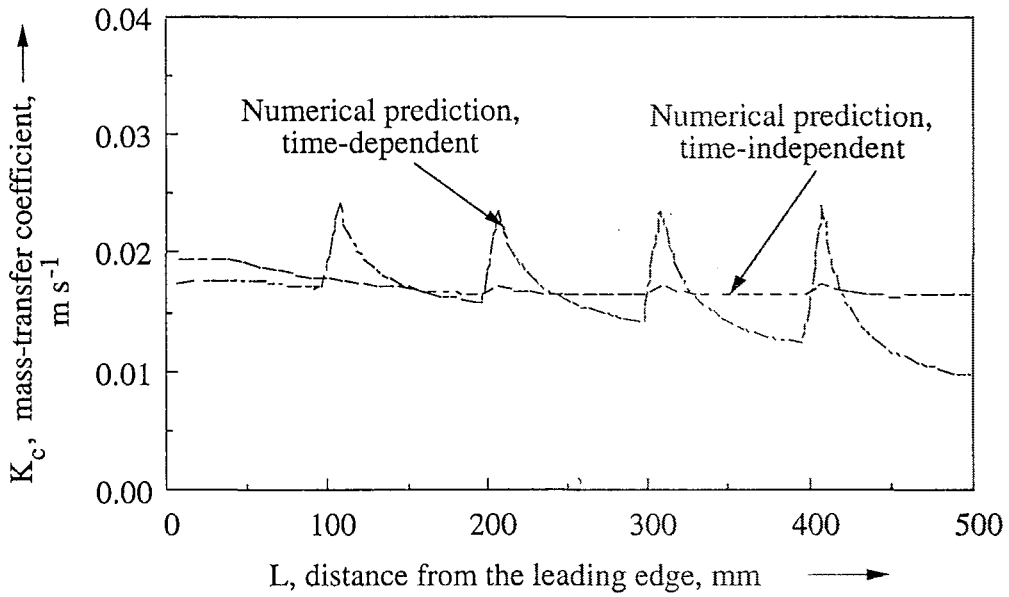

Figure 4.6 Numerically predicted mass-transfer coefficient profiles for both time-dependent and time-independent flows for an air velocity of 7 m s^{-1}.

5

Convective mass-transfer coefficients

5.1 Introduction

Timber boards have been successfully kiln dried since the last century despite the fact that virtually no experimental work had been done prior to the 1970's to obtain quantitative expressions for the heat- and mass-transfer coefficients at the surface of blunt-edged slabs for an array with a geometry similar to that used in stacking timber in kilns. This trial-and-error approach (often complemented by useful experience) to the design of timber kilns and to the development of drying schedules is no longer tolerable. The search for more precise information about the drying process in wood is motivated by economic and environmental considerations, by the desire to decrease drying time, by the need to produce quality-acceptable timber boards efficiently and by the advent of cheaper computer control.

The earliest work in this field was done by Sørensen [1969], who investigated the variation of local mass-transfer coefficients with velocity and thickness on a single isolated slab. Miller [1973] then extended this work to an array but had limited data. Both these experiments were performed in wind tunnels. Sparrow *et al.* [1982] systematically measured the average mass-transfer coefficients of arrays of square modules, 26.7 mm in size with a spacing of 6.7 mm between the modules, along one wall of a flat rectangular duct. Recently, Sugawara *et al.* [1988] examined the influence of free-stream turbulence on heat transfer from a 378 mm-long, 1.32 mm-thick smooth-edged flat plate, again in a wind tunnel.

The present series of experiments was done to extend the scope of the above work, and to investigate the effects of minor board irregularities (consequence of inaccurate sawing, poor stacking and drying shrinkages) in timber stacks on the mass-transfer coefficients. Effects

of both varying air velocity through the stack and of the distance from the leading edge on the local mass-transfer coefficients at the surface of a standard 100 mm-wide board of varying thickness were examined. As throughput in a kiln is dependent on the stacking, various sticker thicknesses were also used to look at the effect it had on the mass-transfer coefficient profiles . The sublimation tests were carried out in a 2550 × 2300 × 2800 mm industrial-type kiln in the Wood Technology Laboratory, School of Forestry, and the 3.3-metre long wind tunnel in the Department of Chemical and Process Engineering, both located at the University of Canterbury.

5.2 Theory

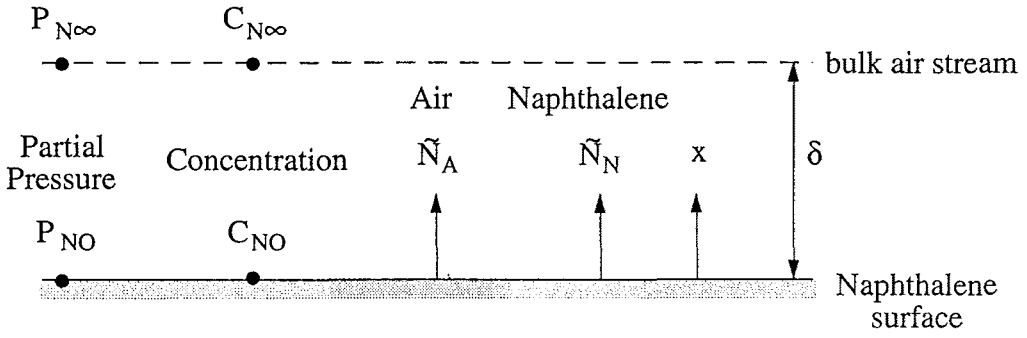

Figure 5.1 Naphthalene vapour diffusion in air.

The rate at which naphthalene vapour moves relative to air from the surface is given by Fick's law, namely

$$J_N = - D_{NA} \frac{d\, C_N}{d\, x} \tag{5.1}$$

where

C_N is the molar concentration of naphthalene vapour, mol m^{-3},

D_{NA} is the diffusion coefficient of naphthalene in air, $m^2\ s^{-1}$,

J_N is the diffusion flux of naphthalene vapour, mol $m^{-2}\ s^{-1}$, and

x is the distance from the naphthalene surface, m.

The moisture-transfer flux from the fixed naphthalene surface to the bulk air stream is given by

$$\tilde{N}_N = J_N + \frac{C_N \left\{ \tilde{N}_A + \tilde{N}_N \right\}}{C} \tag{5.2}$$

where

$\left\{ \tilde{N}_A + \tilde{N}_N \right\}$ is the total flux,

$\frac{C_N}{C}$ is the mole fraction of naphthalene vapour in the air, and

C is the mean molar concentration.

Rearranging, we have

C is the mean molar concentration.

Rearranging, we have

$$\bar{N}_N = \frac{J_N + C_N \bar{N}_A / C}{1 - C_N/C} \tag{5.3}$$

In our case, where the transport of vapour is at right angles to the naphthalene surface, $\bar{N}_A$ can be assumed to be negligible, thus, we get

$$\bar{N}_N = \frac{J_N}{1 - C_N/C} \tag{5.4}$$

Substituting Equation (5.1) into (5.4) yields

$$\bar{N}_N = \frac{- D_{NA}}{\{1 - C_N/C\}} \frac{d\, C_N}{d\, x} \tag{5.5}$$

In our situation a relatively small quantity of naphthalene vapour sublimes into the once-through bulk air stream under atmospheric conditions, and ideal gas properties can be assumed, hence Equation (5.5) can be re-written in terms of mole fractions, $\frac{C_N}{C}$.

$$\bar{N}_N = \frac{- C\, D_{NA}}{\{1 - C_N/C\}} \frac{d\, C_N/C}{d\, x} \tag{5.6}$$

Integrating molar concentration, C_N with respect to x between limits in Figure 5.1 gives

$$\bar{N}_N = \frac{C\, D_{NA}}{\delta} \ln \frac{\{1 - C_{N\infty}/C\}}{\{1 - C_{NO}/C\}} \tag{5.7}$$

which can be re-written as

$$\bar{N}_N = F \ln \frac{\{1 - C_{N\infty}/C\}}{\{1 - C_{NO}/C\}} \tag{5.8}$$

where

C is mean molar concentration of naphthalene vapour, mol m^{-3},

C_{NO} is the molar concentration of naphthalene vapour at the surface of the coating, mol m^{-3},

$C_{N\infty}$ is the molar concentration of naphthalene vapour in bulk air stream, mol m^{-3},

$F = \frac{C\, D_{NA}}{\delta}$, is the mass-transfer coefficient, mol m^{-2} s^{-1},

$\bar{N}_N$ is the molar naphthalene vapour flux, mol m^{-2} s^{-1}, and

δ is the boundary layer thickness, m.

On substituting pressure for molar concentration using the Ideal Gas Law, as shown below,

$$PV = nRT$$

$$P = \frac{n}{V}RT$$

$$= CRT$$

$$F = \frac{\bar{N}_N}{\ln \dfrac{\{1 - P_{N\infty}/P\}}{\{1 - P_{NO}/P\}}} \qquad (5.9)$$

where

P is the total pressure, Pa ,

P_{NO} is the vapour pressure of naphthalene at the sublimating surface, Pa , and

$P_{N\infty}$ is the vapour pressure of naphthalene in bulk air stream, Pa.

The vapour pressure of naphthalene in the bulk air stream is insignificant , i.e. $P_{N\infty} \rightarrow 0$, thus we obtain

$$F = \frac{\bar{N}_N}{\ln \left\{\dfrac{1}{1 - P_{NO}/P}\right\}} \qquad (5.10)$$

Now $\bar{N}_N = \dfrac{N_N}{M_N}$

but $N_N = \rho_N \dfrac{db}{dt}$

where

$\dfrac{db}{dt}$ denotes the infinitesimal change in the thickness of naphthalene coating with time, m s^{-1} ,

M_N is the molar mass of naphthalene, kg mol^{-1},

N_N is the sublimation rate of naphthalene vapour per unit exposed surface, kg m^{-2} s^{-1} and,

ρ_N is the density of naphthalene, kg m^{-3}.

hence $\bar{N}_N = \dfrac{\rho_N}{M_N} \dfrac{db}{dt}$

Therefore for subliming Δb metres of naphthalene over a duration of Δt seconds, we have

$$\bar{N}_N = \frac{\rho_N}{M_N} \frac{\Delta b}{\Delta t}$$

On substituting this in Equation 5.10, gives

$$F = \frac{\frac{\rho_N}{M_N}\frac{\Delta b}{\Delta t}}{\ln\left\{\frac{P}{P - P_{NO}}\right\}} \tag{5.11}$$

Rearranging the above equation gives

$$F = \frac{\rho_N \Delta b}{M_N \Delta t \ln\left\{\frac{P}{P - P_{NO}}\right\}} \tag{5.12}$$

Similarly, an equivalent K-type mass-transfer coefficient can be derived to give

$$K_c = \frac{\rho_N R T}{M_N P_{NO}}\left[\frac{\Delta b}{\Delta t}\right] \tag{5.13}$$

where

K_c is the mass-transfer coefficient, m s^{-1},

R is the universal gas constant, J mol^{-1} K^{-1} and,

T is the absolute temperature, K.

Where a gas flows over an isothermal sharp-edged flat-plate, the local mass-transfer coefficient falls exponentially with distance across the plate as the boundary layer develops and thickens. Should this boundary layer be fully developed and laminar then the local Sherwood number is given by [Incropera and DeWitt, 1990]

$$Sh_x = 0.332\ Re_x^{1/2}\ Sc^{1/3} \tag{5.14}$$

but should it be turbulent , then

$$Sh_x = 0.0288\ Re_x^{4/5}\ Sc^{1/3} \tag{5.15}$$

where

L_Δ is the distance from the position of the maximum local mass-transfer coefficient, m,

$Sc = \frac{\upsilon_A}{D_{NA}}$ is the Schmidt number,

$Re_x = \frac{L_\Delta u}{\upsilon_A}$ is the Reynolds number,

$Sh_x = \frac{K_c L_\Delta}{D_{NA}}$ is the local Sherwood number,

u is the bulk air velocity through sticker spacing, m s^{-1} and,

υ_A is the kinematic viscosity, m^2 s^{-1}.

From suitable plots, the Reynolds number dependency can be determined. This should give an indication of the type of boundary layer that forms downstream of the eddy in a timber stack.

The effect of blunt leading edge on mass transfer from a grid-packing was first investigated in detail by Danckwerts and Anolick [1962], using the naphthalene sublimation method. They found that a stationary eddy was formed near to the leading edge, causing very high mass transfer rates at the point of reattachment. A laminar boundary layer is formed after the point of reattachment.

The effects of air velocity and thickness of truncated slabs on mass transfer were further studied by Sørenson [1969]. He observed that the mass-transfer coefficient depended not only on air velocity and distance from the leading edge but also on the thickness of the slab. He concluded that if Re_b (Reynolds number based on the thickness of the slab, b) is less than 245, the mass transfer coefficients are independent of Re_b and follow the sharp-edged plate correlation. If Re_b is greater than 245, the mass transfer coefficients are dependent on Re_b. The boundary layer formed after the point of reattachment was found to be laminar.

$$Re_b < 245,\ j_d = 0.407\ Re_x^{-1/2} \tag{5.16}$$

and

$$Re_b > 245,\ j_d = 0.152\ Re_b^{0.179}[\ Re_x - 49.8\ Re_b^{0.61}]^{-0.5} \tag{5.17}$$

where

$$j_d = \left(\frac{K_c}{u}\right) Sc^{2/3} \tag{5.18}$$

Mass-transfer coefficients from Equation 5.16 are found to be 22.5% higher in magnitude than those obtained from the sharp-edged plate correlation of Equation 5.14.

Using Sørenson's plot [1969] of $\log \bar{j}_{d(o,z)}$ against Re_x for different values of $\frac{L}{b}$, the mean mass-transfer coefficient, $\bar{K}_c$ for subliming a coating of naphthalene from the surface of a board of 100 mm wide by 25 mm thick, in an air velocity of 5 m s^{-1} at 41°C can be estimated as shown below. The kinematic viscosity of air is 1.68×10^{-5} m^2 s^{-1} and the Schmidt number for the naphthalene-air system is 2.55.

$$Re_x = \frac{u \cdot L}{\nu} = \frac{5 \cdot 0.1}{1.68 \times 10^{-5}} = 29762 \approx 30000$$

$$\frac{L}{b} = \frac{0.1}{0.025} = 4$$

From Sørenson's plot [1969], $\bar{j}_{d(o,z)} = \left(\frac{\bar{K}_c}{u}\right) Sc^{2/3} \approx 8.2 \times 10^{-3}$,

Rearranging to give the mean mass-transfer coefficient, $\bar{K_c}$

$$= \frac{(8.2 \times 10^{-3} \cdot 5)}{1.87} = 2.2 \times 10^{-2} \text{ m s}^{-1}.$$

The corresponding mean mass-transfer coefficient, $\bar{K_c}$ for a sharp-edged plate under similar conditions using Sørenson's results [1969] is

$$\bar{j}_{d(o,z)} = 0.816 \, Re_x^{-1/2} \qquad (5.19)$$

$$\bar{j}_{d(o,z)} = 0.816 \times 30000^{-1/2}$$

$$= 4.7 \times 10^{-3}$$

$$\text{Rearranging to give } \bar{K_c} = \frac{(4.7 \times 10^{-3} \cdot 5)}{1.87} = 1.26 \times 10^{-2} \text{ m s}^{-1}$$

which is approximately 43% lower than the values estimated from blunt slabs. Similarly, for a sharp-edged plate under similar conditions using Equation 5.14, the mean mass-transfer coefficient, $\bar{K_c}$ is 1.03×10^{-2} m s^{-1}. These results clearly demonstrate that the sharp-edged plate correlations cannot be used to derive mass-transfer coefficient data for stacks in a timber kiln.

5.3 Equipment and procedure - experimental kiln and wind tunnel

The naphthalene sublimation technique employed was that used by Danckwerts *et al.* [1962], Sørensen [1969], Miller [1973] and Sparrow *et al.* [1982] to determine the local mass-transfer coefficients, with slight modification.

An aluminium base slab was used which had been milled to give a recess at the centre of the board. The dimensions of this base slab are shown in Figure 5.2. The thickness of this base slab could be increased by bolting a combination of 2, 3, 5 and/or 25 mm-thick aluminium slab(s) of similar dimensions to it. For runs in the kiln, the length of the test slab was 640 mm, whereas a shorter length of 220 mm was used for runs in the wind tunnel.

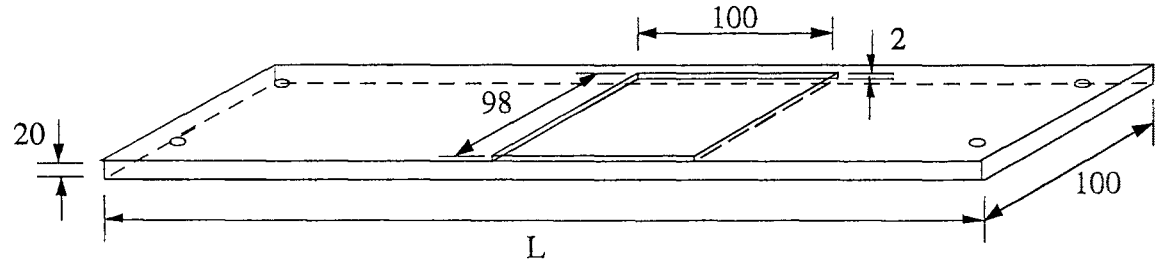

Figure 5.2 Isometric view of the aluminium base slab used in the laboratory kiln (L = 640 mm) and the wind tunnel (L = 220 mm). All dimensions are in mm.

5.31 Preparation of the test board

Prior to casting the naphthalene, the aluminium test slab was preheated to 50°C as this temperature was found to favour the quality of the naphthalene casting [Miller, 1973]. With masking tape firmly placed on both sides of the recess, melted naphthalene of analytical quality was poured into the recess. The masking tape facilitated the easier removal of excess naphthalene and aided the subsequent smoothing process. Upon complete solidification, the naphthalene surface was carefully smoothed with an electric iron, which was set at a temperature slightly higher than the melting point of naphthalene. The melted naphthalene was wiped off immediately with absorbent paper. The masking tape was then removed and this smoothing process repeated until an acceptably level surface corresponding closely to that of the slab itself was obtained. Any residual surface irregularities were kept at a level below 10% of the difference in level between the grid points in the streamwise direction.

The thickness of the naphthalene sublimed during the run was found by taking the difference in the measurements of the height of the casting on the base slab at sixty-five predetermined grid-points from the reference base of a modified face plate before and after a run using a Mitutoyo dial gauge (± 0.005 mm).

Finally, the thickness of the test slab itself was built up to the desired thickness by bolting to it a combination of 2, 3, 5 and/or 25-mm thick, similarly dimensioned aluminium plates before being placed in position in the test section.

5.32 The experimental kiln

The industrial-type kiln used in this experiment has overall dimensions of 2550 × 2300 × 2800 mm, with a capacity of approximately one cubic metre. The kiln was electrically heated by two banks of elements, capable of delivering a total of forty kilowatts. Heating to the kiln was controlled by the two temperature controllers and the four temperature sensors, comprising a dry-bulb and a wet-bulb sensor each on either side of the kiln.

By varying the frequency of the two axial fans, the air velocity through the stack could be set at the desired level. Baffles were put around the base of the trolley and the edges of the dummy stack to prevent by-passing of the heated air.

Ambient air was drawn into the kiln through the inlet duct and through an opening on the left side of the modified door system by the two axial fans (Figures 5.3a and 5.3b). This air was then forced through the two banks of heaters where the air was heated to and maintained at 41.0 ± 0.5°C throughout the run. Air passing through the dummy stack was re-circulated in the kiln whereas that passing through the test section was vented through the flexible duct to the atmosphere. With such a set up, naphthalene vapour pressure (and concentration) in the bulk air stream can be assumed to be zero, thus simplifying the calculation to obtain the value of local mass-transfer coefficients. Otherwise, recycling the air would have involved the complicated and tedious routine of sampling the bulk air stream to determine the naphthalene vapour pressure.

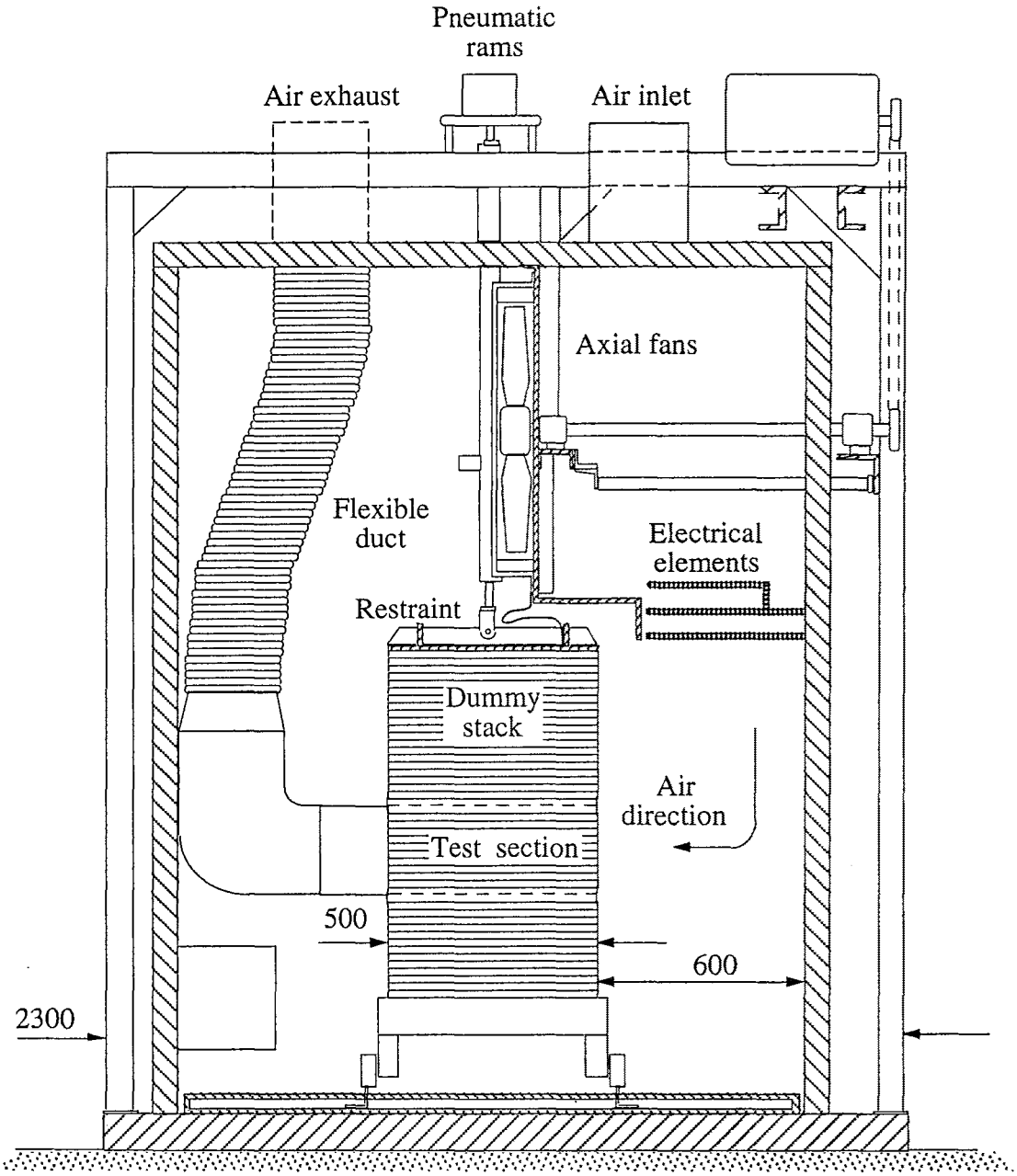

Figure 5.3a End elevation of the experimental kiln.

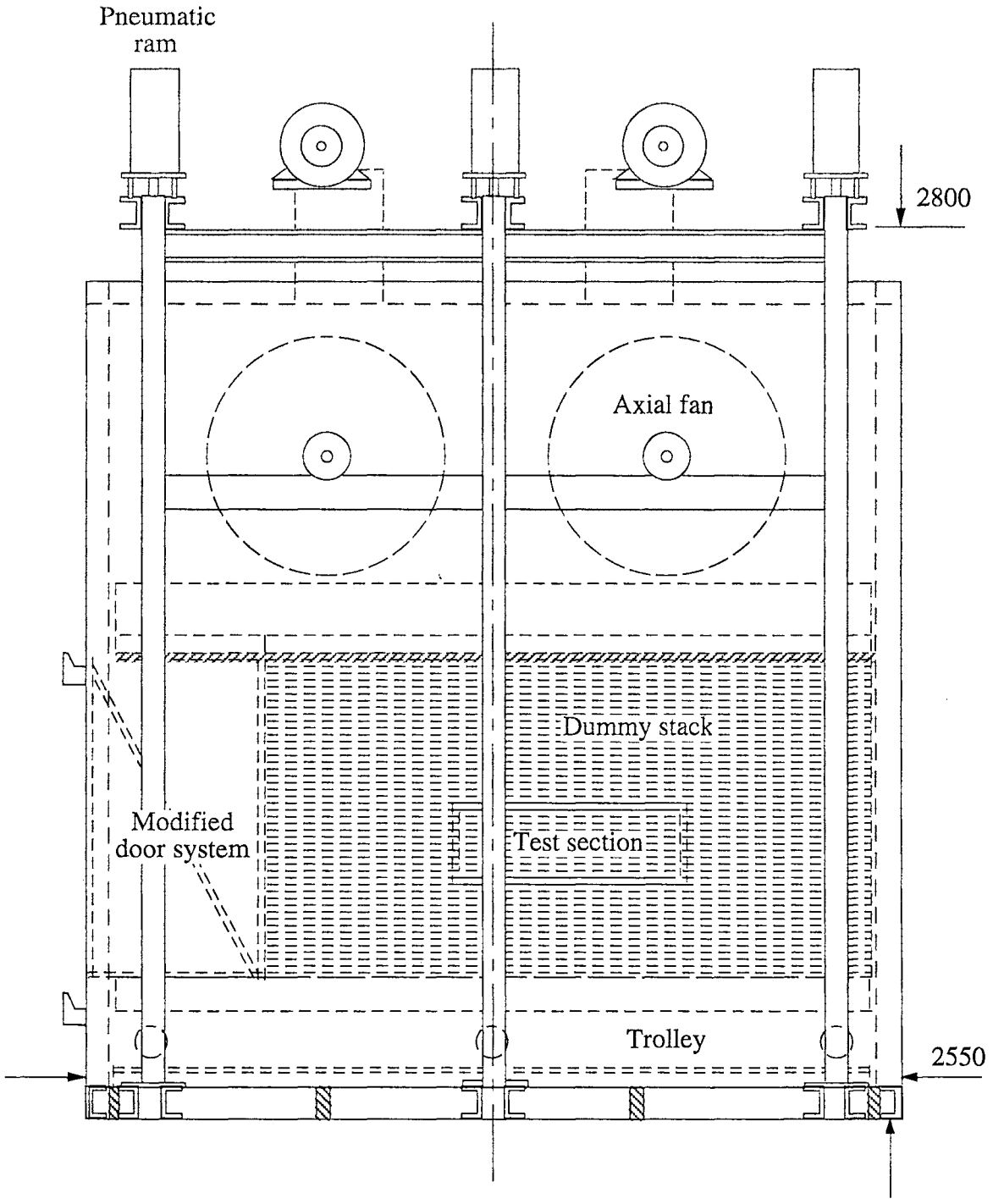

Figure 5.3b Side elevation of the experimental kiln.

The dummy stack was made from 100 × 25 mm rough sawn radiata pine boards and held down firmly by the restraint, which is connected to three pneumatically-controlled rams. The outer edges of the dummy stack were blocked off symmetrically about the centre of the test board to get the maximum air velocity of 7 m s^{-1} required for the experiment. The plenum space on the windward side of the stack was about 600 mm.

The centrally located test section comprised layers of medium density fibreboard which had dimensions of 640 × 500 mm, except in the test layer which had to be re-cut to accommodate the test slab (Figure 5.4). Each board was separated by two stickers which

were securely nailed to it at 600 mm apart. The board with the sticker could then be easily stacked on top of each other on a sliding base, thus forming parallel "ducts" through which air flows. This design allowed the test slab to be removed from and inserted in the test position with ease, enabling the thickness of the naphthalene coating to be measured within a minute of retrieval.

The downstream of the test section was connected to a rectangular duct of similar cross-sectional area, which was moulded to a circular duct in order to fit the existing ducting system of the kiln. The exhaust air containing naphthalene vapours was vented to the atmosphere outside the laboratory.

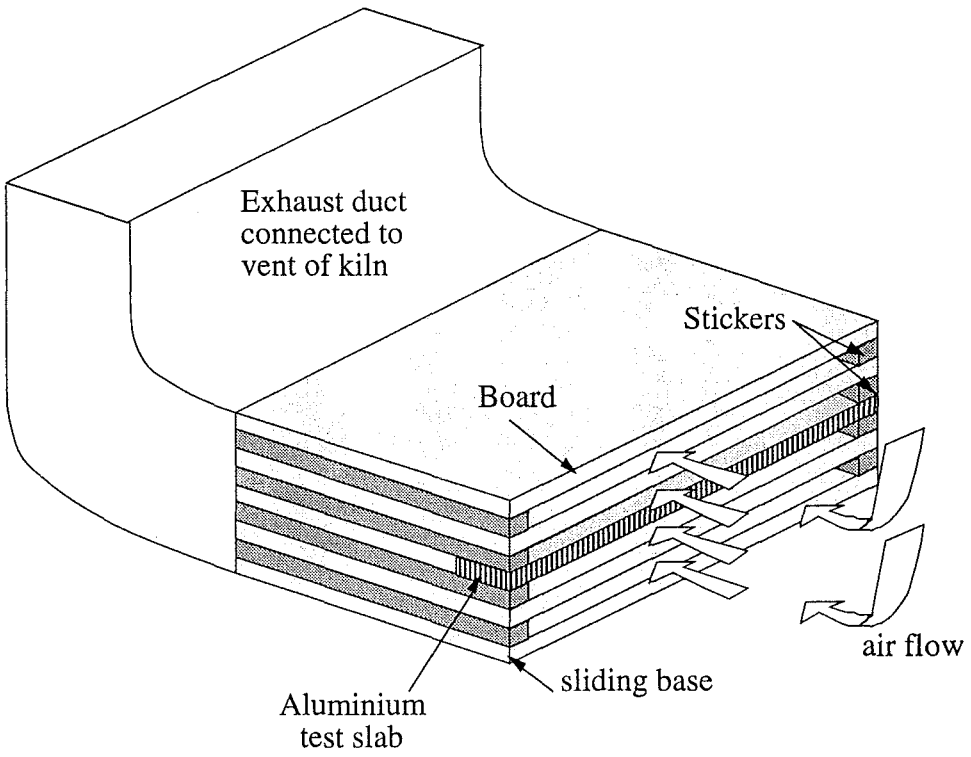

Figure 5.4 Isometric view of the test section in the experimental kiln.

The kiln was switched on for at least an hour before every run was performed. Once steady state was achieved, the profile of the precast naphthalene slab was measured before being inserted in the desired position in the stack. At the end of a run, the test slab was retrieved and the surface of the naphthalene re-measured at the same predetermined grid-points. Pressure readings and temperature of the kiln were noted at the beginning, middle and the end of a run. The average of these three values was used in the calculation.

The effect of the changing surface of the naphthalene coating was first investigated. This was done by placing a test slab in the test layer in an air flow of 5 m s^{-1}. The surface profile of the naphthalene coating was obtained every hour for four hours and results are presented in Section 5.41.

Runs were performed using different air velocities (3, 5 and 7 m s^{-1}) and for different board positions as shown in Appendix A1. The duration of the sublimation tests at 7 m s^{-1} was reduced from 120 to 90 minutes in order to ensure a similar sublimation thickness to other runs at lower air velocities.

5.33 The wind tunnel

Similar runs were performed in the 3.3-metre long wind tunnel (Figure 3.3c) in the Department. Here the object was to examine the effect of turbulence intensity and stack width on the local mass-transfer coefficients. Air was supplied to the tunnel by a Rootes blower through a butterfly valve into the test section before been vented into the atmosphere. Prior to the start of the experiment, the Rootes blower was switched on for an hour to attain steady-state operating conditions. The velocity of the air through the stack was maintained at 5 m s^{-1}. Casting procedure and stack arrangements were similar to that used for runs in the kiln. However, the time for each run had been extended to 5 hours, again for the purpose of achieving the same sublimation thickness.

5.4 Results

Runs were repeated at least three times to ensure consistency in results and to rule out erroneous readings due to a shift in the reference base, resulting from an accidental knock on the dial-gauge measuring system in between runs. This shift in the reference base, a problem in preliminary runs, was eliminated by using the face plate of a lathe as a reference surface. The results of subsequent runs were reproducible and were within the limits of the experimental errors. Three different velocities (3, 5 and 7 m s^{-1}) were used for runs done in the kiln whereas only one velocity (5 m s^{-1}) was used for runs performed in the wind tunnel. Only a selection of the results are shown in this Section. The remaining results are appended in Appendix A3. Raw data for all runs can be found in the floppy disks attached. The variation of mass-transfer coefficient with distance is likely to be more certain than the absolute value. In the calculation of mass-transfer coefficient, the diffusion coefficient of naphthalene into air is assumed to be dependent on temperature and pressure only.

For all the runs performed, the diminution of thickness of the naphthalene casting ranged from 0.10 mm to 0.70 mm for the velocity and time range used.

5.41 Effect of changing naphthalene surface

Preliminary experiments explored the effect of the changing surface of the naphthalene casting with time. This involved subliming a naphthalene-coated test slab in an air stream of 5 m s^{-1} in the kiln for four hours, and mapping the surface profile every hour. After the third hour, the range of the thickness of naphthalene lost during sublimation was from 0.34 mm to 0.98 mm. The results, shown in Figure 5.5, revealed that the changing level of the naphthalene surface had no effect on the subsequent surface profile until the third hour of sublimation. By the fourth hour it was apparent that the sublimated level of the naphthalene casting was beginning to affect the subsequent subliming profile. These results formed the basis for determining the duration of the runs in which the thickness lost was confined to the levels corresponding to "after two-hours profile".

Sublimation losses from the time when the run was terminated to end of the surface mapping session was found to be negligible when compared to the actual thickness of naphthalene lost.

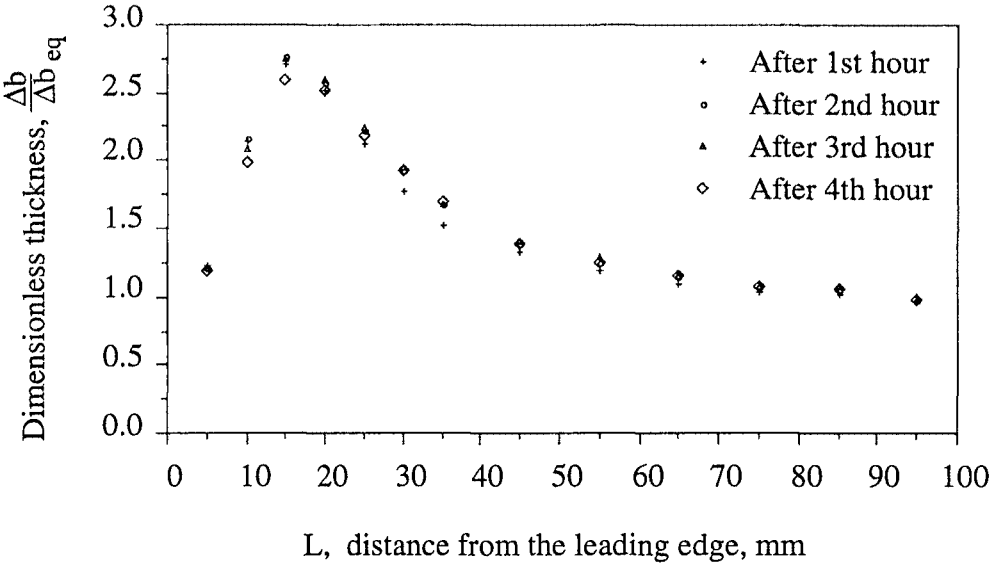

Figure 5.5 Sublimation profile as a function of time elapsed for the first board in the test layer at 5 m s^{-1}.

5.42 Mass-transfer coefficients as a function of distance from the leading edge in an aligned stack for 3, 5 and 7 m s^{-1}

Using Equation 5.12, thicknesses of naphthalene lost during sublimation in the kiln were converted to F-type mass-transfer coefficients, and the results for the various configurations are presented in this Section.

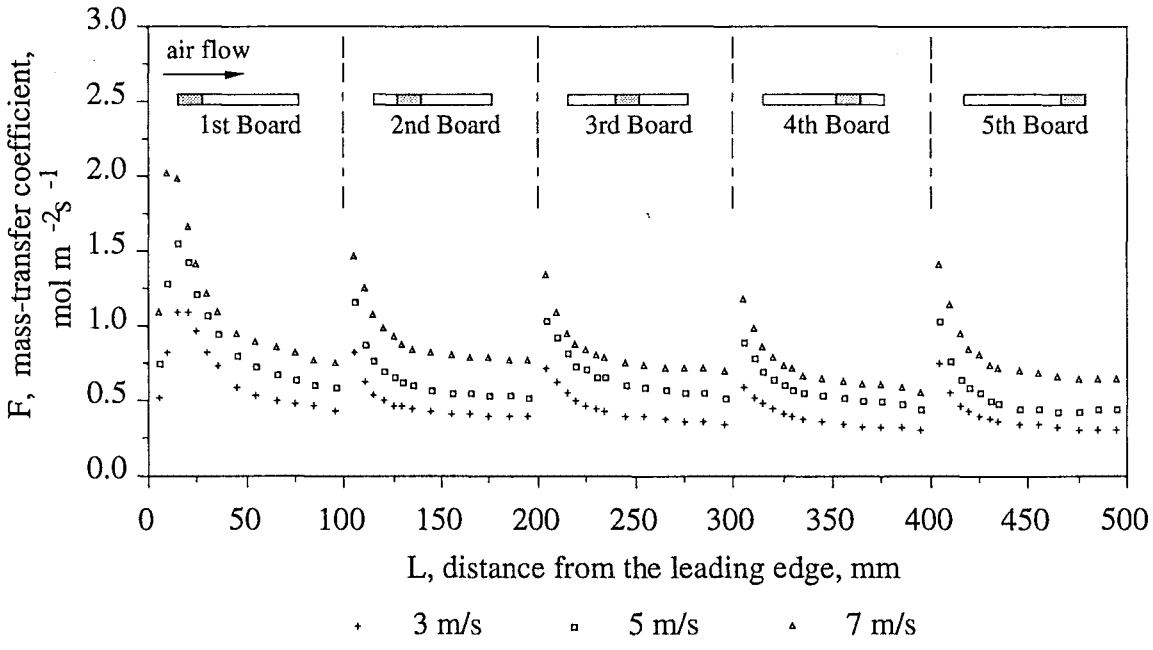

Figure 5.6 Local mass-transfer coefficient, F, as function of the distance from the leading edge, L, for an aligned stack made up of 25 mm-thick boards separated by 25 mm-thick for 3, 5 and 7 m s^{-1}.

Figure 5.6 shows the plot of F, the local mass-transfer coefficient as a function of L, the distance from the leading edge for an aligned stack for 3, 5 and 7 m s^{-1}. Both the test slab and the dummy medium density fibreboards in the test section were 25 mm thick, were separated by two 25 mm-thick stickers. Gaps of 0.5 to 1.0 mm were present between the edges of the test slab and the adjacent dummy boards. The results plotted above were from a series of runs where the test slab was progressively placed in each of the five different positions along the test layer of the stack in the streamwise direction.

The prominent features in Figure 5.6 are the existence of a characteristic maximum, some distance downstream of the leading edge of the leading board and the distinct discontinuities in the mass-transfer coefficient profile over the corresponding small gaps that existed between the adjacent closely-butted boards in the stack.

The characteristic maximum was only observed in the leading board of the test layer, indicating that flow over the first board was different from that of the subsequent boards.

Small gaps of 0.5 to 1.0 mm between adjacent boards are inevitable in stacked timber as boards shrink and are difficult to butt together exactly. These seemingly small gaps have a very profound effect on the mass-transfer coefficient profiles, causing a distinct discontinuity at each of the corresponding gaps. With the exception of the first board, mass-transfer coefficients over the first 30 mm of each of the 100 mm-wide boards were observed to be greatly enhanced, after which these local coefficients decreased exponentially to an asymptotic value.

The maxima of the boards in the test layer were observed to fall exponentially in the streamwise direction, with the exception of the last board where the mass-transfer profile appeared to be similar in magnitude to that of the second board.

5.43 Effect of sticker thickness

It was found that varying the sticker thickness over the range 15 to 25 mm at 5 m s^{-1} for a perfectly aligned stack had very little effect on the overall mass-transfer coefficient profile, apart from the distance from the leading edge to the position of the maximum, Δ, which was found to increase with sticker thickness (Figure 5.7).

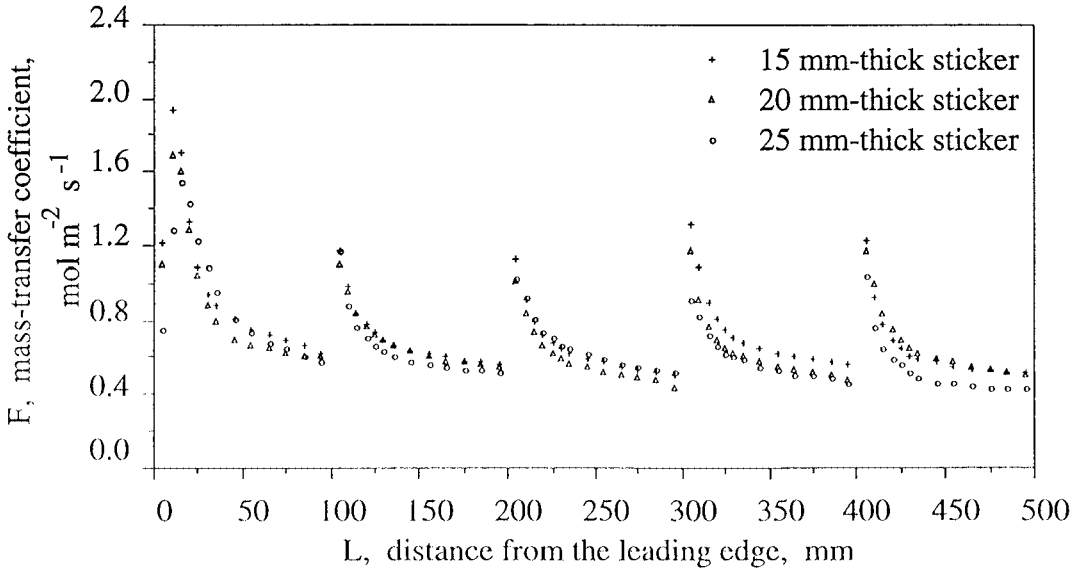

Figure 5.7 Effect of varying sticker thickness on the mass-transfer coefficient at 5 m s^{-1}.

5.44 Effect of board thickness

Figure 5.8 shows the mass-transfer coefficient profiles for 25, 50 and 75 mm-thick boards. With the exception of the distance from the leading edge to the position of the maximum, Δ, being affected, board thickness over the range 25 to 75 mm with 25 mm sticker spacing at 5 m s^{-1} had no clear effect on the profiles .

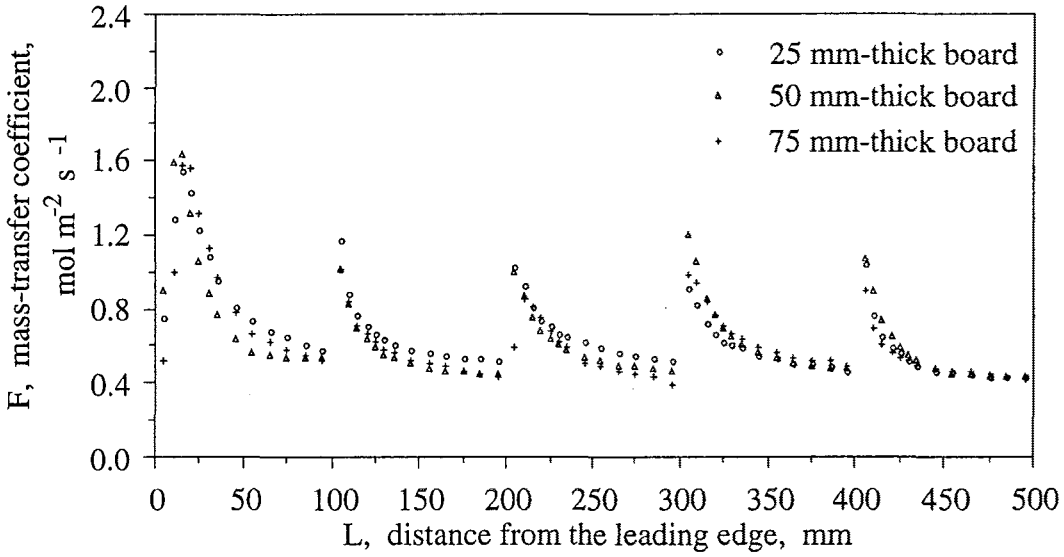

Figure 5.8 Effect of varying board thickness on the mass-transfer coefficient at 5 m s^{-1}.

5.45 Effects of minor board irregularities

Upon reaching fibre-saturation point, wood will shrink if drying is continued. For a softwood species like radiata pine, the only physical effect of further drying will be the reduction of its dimensions provided the drying rate is not excessive which can result in checking of the boards. Owing to the anisotropic properties of wood, the changes in the width and thickness of each board in the stack will vary depending on the way the board is cut and on its final moisture content. This would result in the widening of adjacent board-to-board gaps and a layer of boards with surfaces that would not be level. The following sub-section examines the effect of these board irregularities on the mass-transfer coefficient of the boards in a stack placed in a kiln.

a. Gaps between adjacent boards

Clifton [1985] gives the shrinkage in percentages from green to 12% moisture content of outerwood radiata pine from the central North Island to be 4.0, 3.0 and 0.1 for tangential, radial and longitudinal shrinkage respectively. Depending on the grain orientation in the sawn board, that is, whether it is flat-, mixed- or quarter-sawn, the maximum shrinkage of a 100 mm-wide, perfectly flat-sawn board will be of the order of 4 mm. Taking into account the 1.0 mm gap that exists even in a "closely-butted" timber stack, an adjacent board-to-board gap of 5 mm is common towards the final stages of drying in stacks comprising 100 mm-wide boards. Therefore, the three different size of gaps (configuration J in Appendix A2), a mm gap which was sealed from the underneath with sticky-tape, a mm gap and a 5 mm gap, were used to investigate the effect of varying adjacent board-to-board gaps on the mass-transfer coefficient.

The discontinuities in the mass-transfer coefficient profiles were still very pronounced even though the 1 mm gap was completely sealed from the underneath with sticky tape. Inter-

layer flow was found to be small, as can be inferred from Figure 5.9 where the profiles for the 1 mm gap showed only a marginal increase over that of the profiles for the 1 mm gap which was sealed. However, when the size of gap was increased to 5 mm, the coefficients were increased by up to 30% above its 1 mm-gap values over the first 25 mm of the 100 mm-wide board. Similar results were obtained for the 3 m s^{-1} and 7 m s^{-1} runs are appended in Appendix A3.

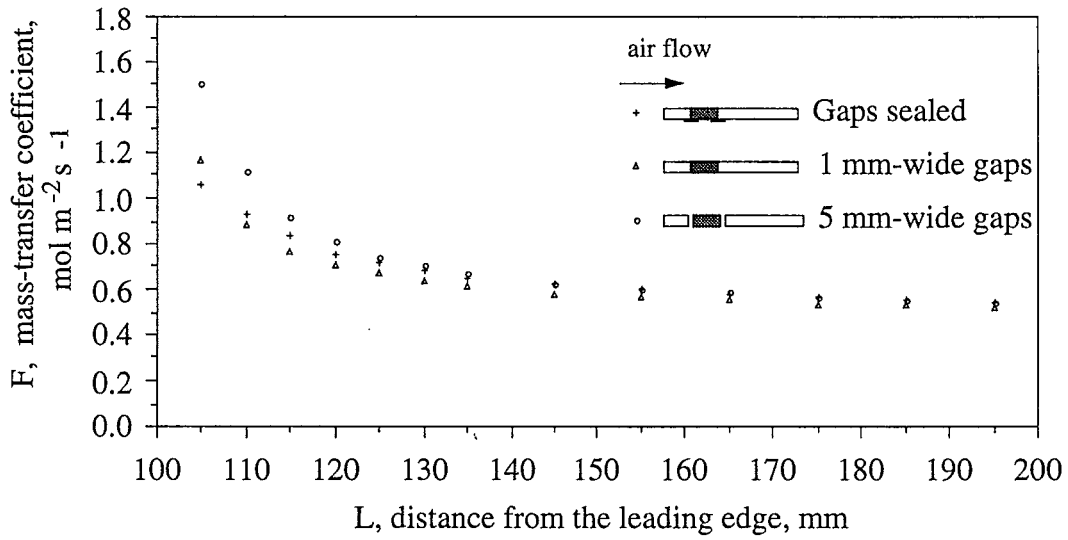

Figure 5.9 Effect of varying adjacent board-to-board gaps on the mass-transfer coefficient of the second board at 5 m s^{-1}

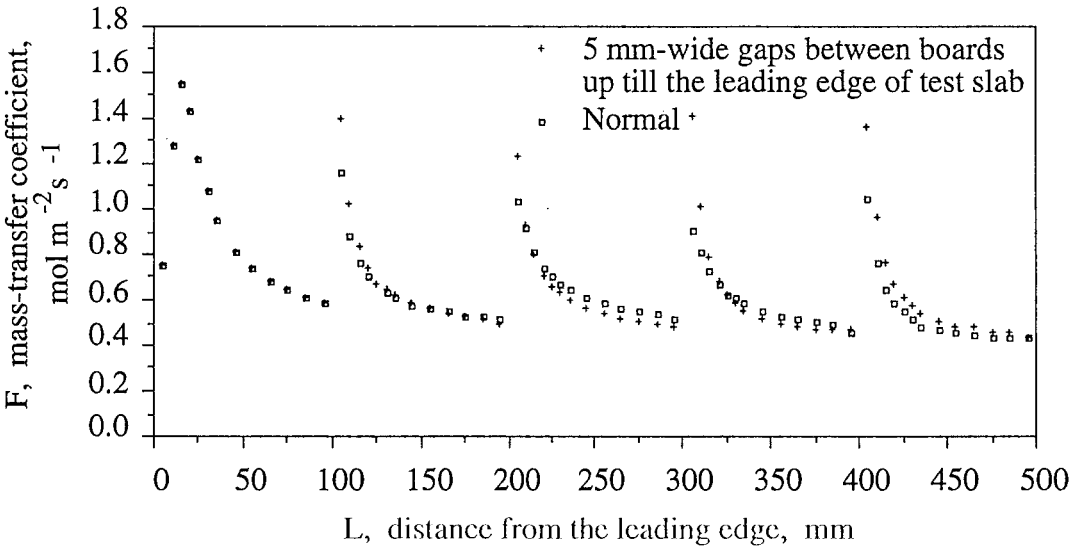

Figure 5.10 Effect of the presence of 5 mm-wide gaps between boards up to the leading edge of the test board on the mass-transfer coefficients at 5 m s^{-1}.

The effect of the 5 mm gap on the mass-transfer coefficients was examined in greater detail. Mass-transfer coefficients profiles for three more configurations (configurations C, D and E in Appendix A2) were plotted in Figures 5.10, 5.11 and 5.12. In this analysis, 5 mm-wide gaps between boards were systematically "introduced" in the test layer; in configuration C, with these gaps up to the leading edge of the test board; in configuration D, with these gaps up to the trailing edge of the test board and in configuration E, with these gaps in between all boards.

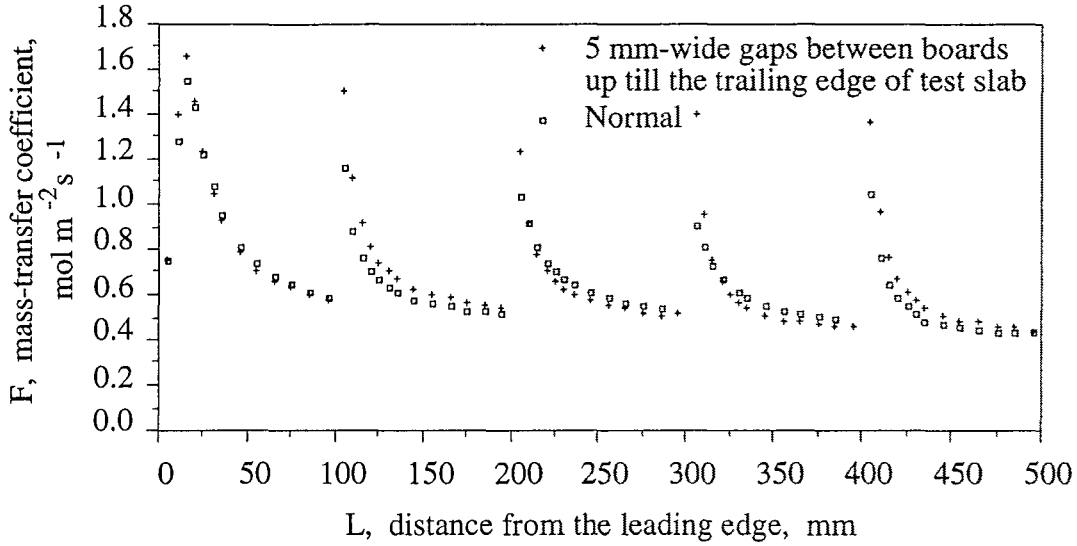

Figure 5.11 Effect of the presence of 5 mm-wide gaps between boards up to the trailing edge of the test board on the mass-transfer coefficients at 5 m s^{-1}.

It was found that the larger 5 mm-wide gap had a greater effect on the initial 20 to 30 mm of the following 100 mm-wide slab in the streamwise direction than on the rear portion of the preceding slab, which were observed to be unaffected by the size of the gaps. These initial enhancements of up to 40% over closely butted boards, decreased in magnitude rapidly in the streamwise direction, but was observed to increase again after the second gap. For the test layer with 5 mm-wide gaps between all boards, the initial enhancements appeared to be unaffected by position. Thus, it can be concluded that gaps between boards as a consequence of shrinkages would not affect mass-transfer significantly for the permeable species. For impermeable species, it may be necessary to even out the differential loss of moisture by switching the airflow direction, if external conditions control the drying process.

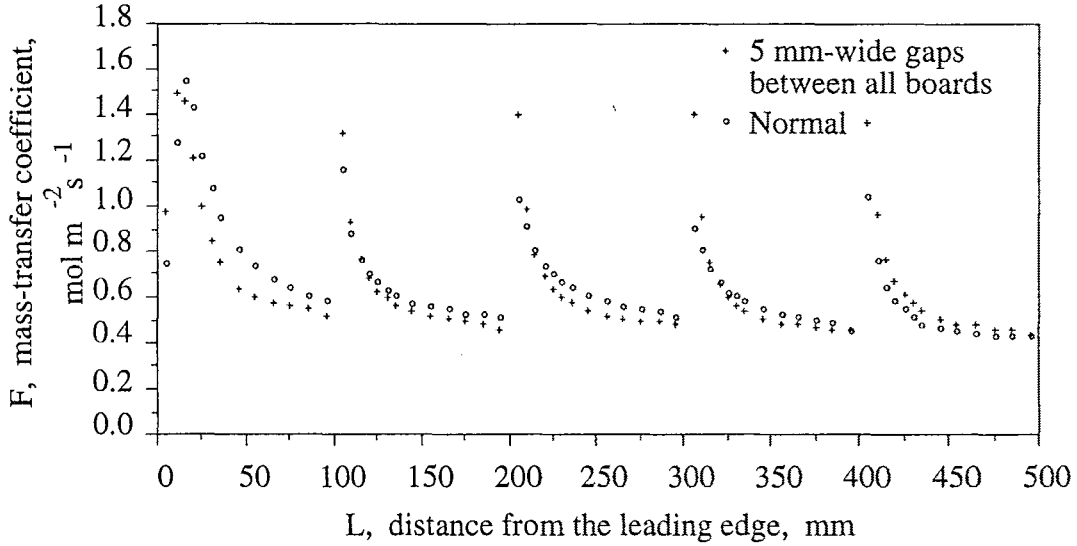

Figure 5.12 Effect of the presence of 5 mm-gaps between all boards in the test layer on the mass-transfer coefficients at 5 m s^{-1}.

b. differences in board thickness

To simulate the effect of a stack which had boards with surfaces that were not level owing to the varying degree of shrinkages in the thickness, a test slab which was 3 mm thinner than that of the adjacent boards was progressively placed in each of the five positions in the layer of the test section of the kiln (Configuration B in Appendix A2).

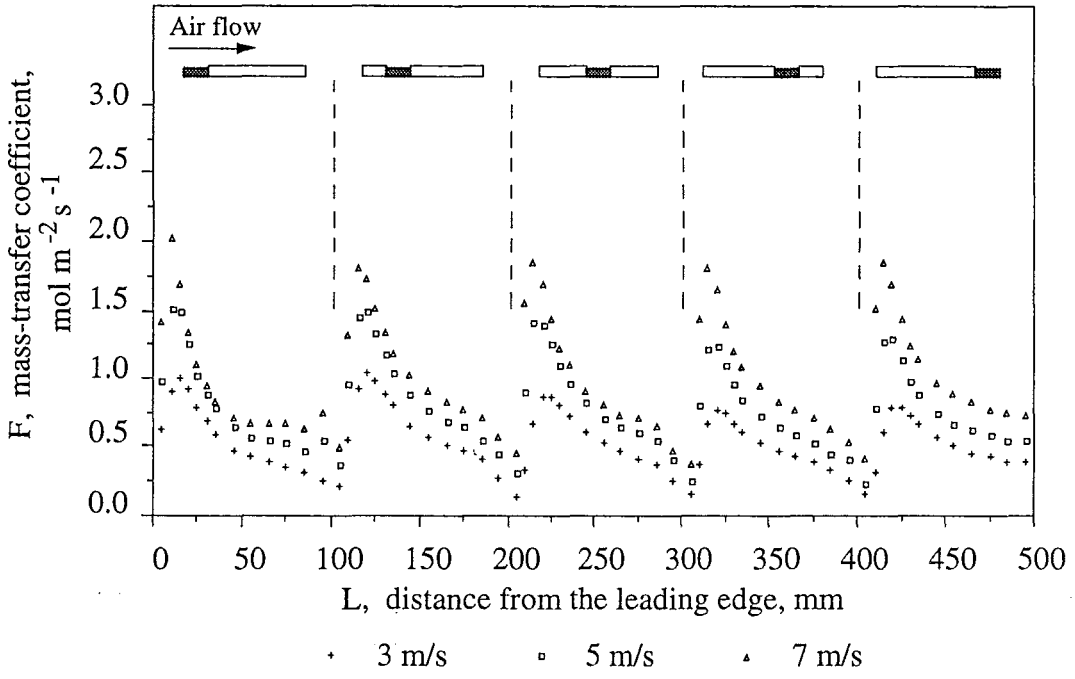

Figure 5.13 Effect of a thinner test slab than the adjacent dummy boards on the mass-transfer coefficient at 5 m s^{-1}

The results generated are plotted in Figure 5.13. A distinct "saw-tooth" like profile revealed that the lower surface of the test slab had a significant effect on mass-transfer mechanism. The presence of a "sharp" maximum at the leading edge of every board indicated the formation of a different recirculating zone from that of an aligned stack. No asymptotic values were seen at the trailing end of each board.

A thinner board placed upstream of the test slab would raise the local mass-transfer coefficients for the first 15 to 30 mm slightly, while a thinner board placed downstream of the test slab had little effect on the coefficients at the rear portion of the board (Figure 5.14). A convex mass-transfer profile was forming in the front portion of the run with a thinner leading board, indicating the embryonic formation of the stationary eddy.

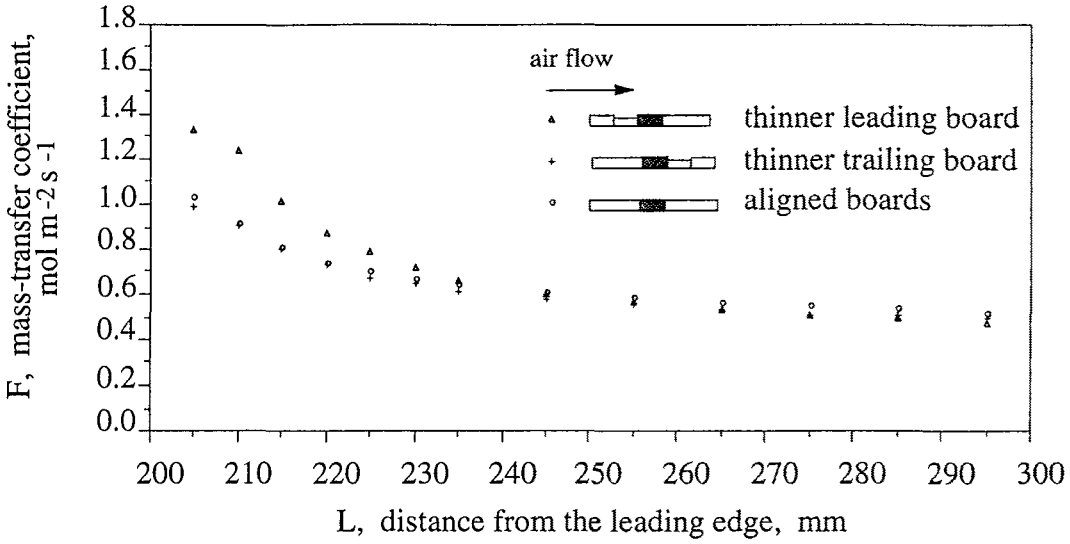

Figure 5.14 Effect of a thinner leading and trailing board on the mass-transfer coefficient at a velocity of 5 m s^{-1}.

5.46 Wind tunnel runs

Exploring the use of wider stacks in large modern kilns is becoming an attractive option. Provided the pressure drop across the stack is not excessive, wider stacks are usually more stable and relatively easier to move around, thereby increasing overall production efficiency. Also a single wider stack that spans the whole width of a modern kiln has the advantage of being aligned, unlike the present practice of having two or more stacks side by side where airflow through the stack could be adversely affected due to misalignment. This can lead to uneven drying and possibly serious degrade. To investigate the effect of wide stacks on the mass-transfer coefficient, runs had to be performed in the wind tunnel in the Department of Chemical and Process Engineering owing to the physical limitations of the experimental kiln. Test runs were done to rule out any possible discrepancies in airflow which may result in a different sublimation profile. Figure 5.15 shows the mass-transfer coefficient profile of a similar five-board stack in an airflow of 5 m s^{-1}.

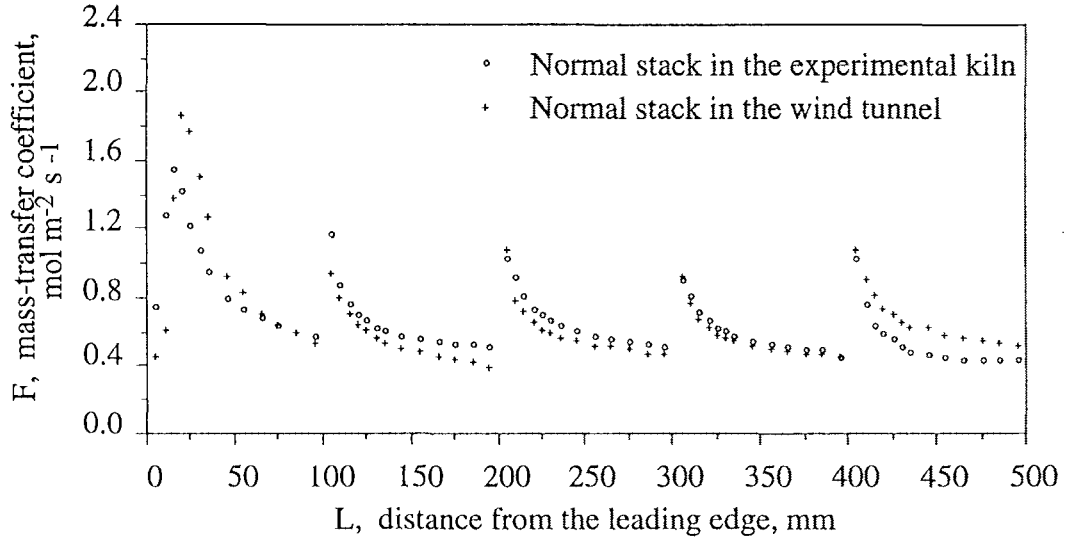

Figure 5.15 Comparison between kiln and wind tunnel runs at 5 m s^{-1}.

The mass-transfer coefficient profile obtained was consistent with that of kiln runs with the exception of the first and the last board. The discrepancy could be due to the way air was introduced into and leaving the stack, which was significantly different from that of the wind tunnel.

a. Wide stack

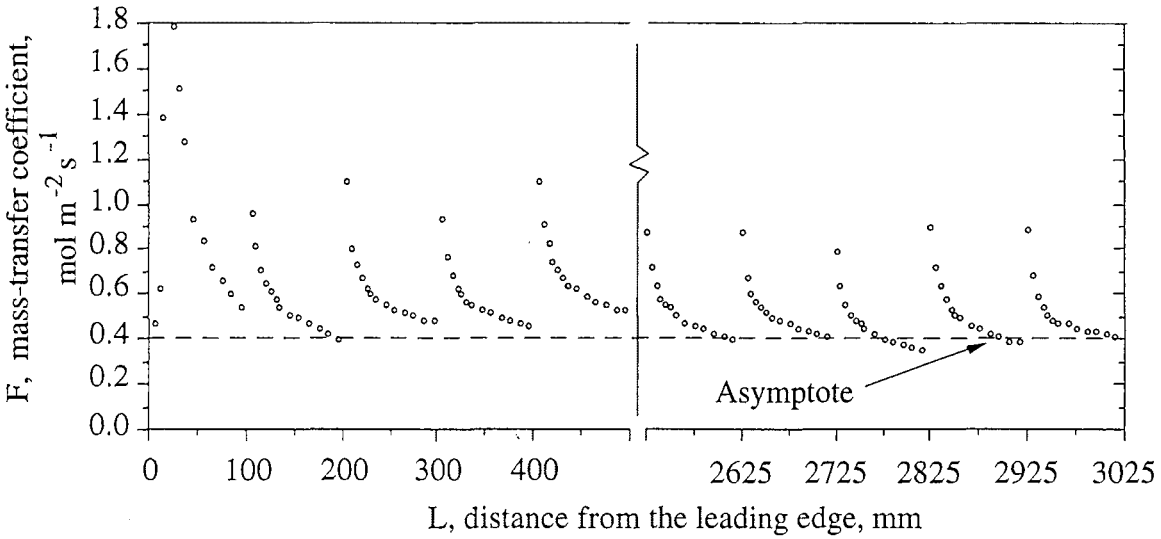

Figure 5.16 Mass-transfer coefficient profiles of a wide stack at 5 m s^{-1}.

Mass-transfer coefficient profiles of a wide stack at 5 m $s^{-1}$are shown in Figure 5.16. The effect of the 1 mm gap between adjacent boards for a wide stack was still very significant, producing similar distinct discontinuities in the mass-transfer profile with greatly enhanced initial values. The mass-transfer coefficient profiles are more consistent at the end of a 3.025 m-wide stack. The initial mass-transfer coefficient values were slightly less, with trailing values of each board tending to an asymptote of 0.4 mol m^{-2} s^{-1} in magnitude. This value is slightly lower than that of the asymptotic value of the first 500 mm.

b. Effect of a slit

Wu [1989], using an optical microscope, found the surface roughness of eighteen kiln-dried boards to have a 0.34 mm peak-to-valley "whisker" over a 1.7 mm diameter field. Assuming that the average thickness of these "whiskers" to be half the peak-to-valley value, we can approximate the surface roughness as slits having an aspect ratio of 2. However, the naphthalene method used in this series was unsuitable to ascertain the effect of surface roughness, the main drawback being the extreme difficulty of measuring accurately the local sublimation loss on the naphthalene coating that had been slit. A modified experiment involving only a single slit in the naphthalene casting (Figure 5.17) was carried out to investigate its effect on the profiles. The slit had an aspect ratio of 2 and was cast half way in the naphthalene coating. The actual surface roughness of sawn timber will be smaller in scale than the dimensions used in these runs. The results obtained were plotted in Figure 5.18.

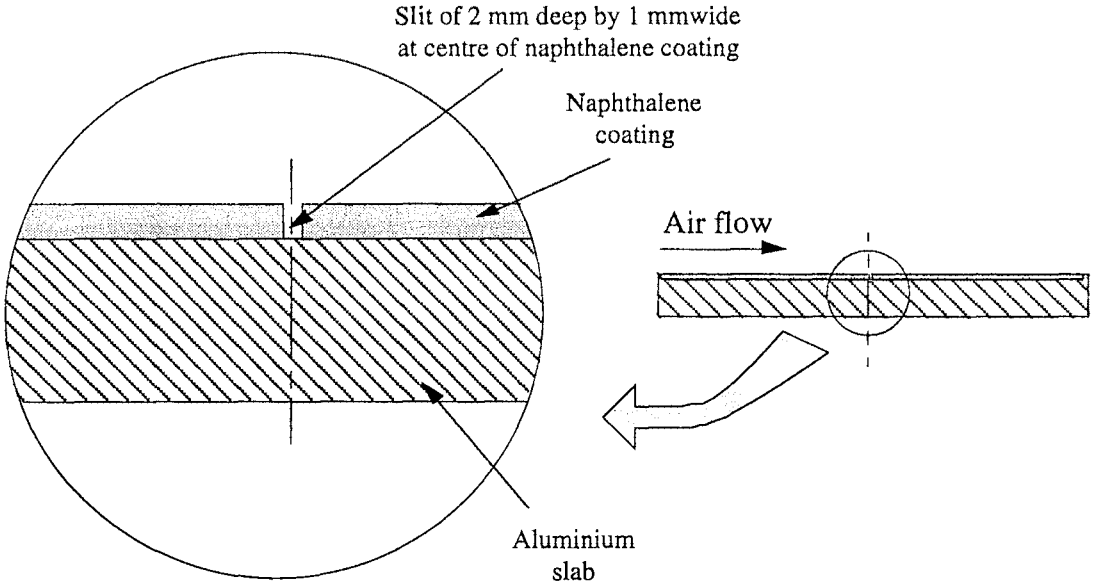

Figure 5.17 Dimensions of the slit in the naphthalene coating

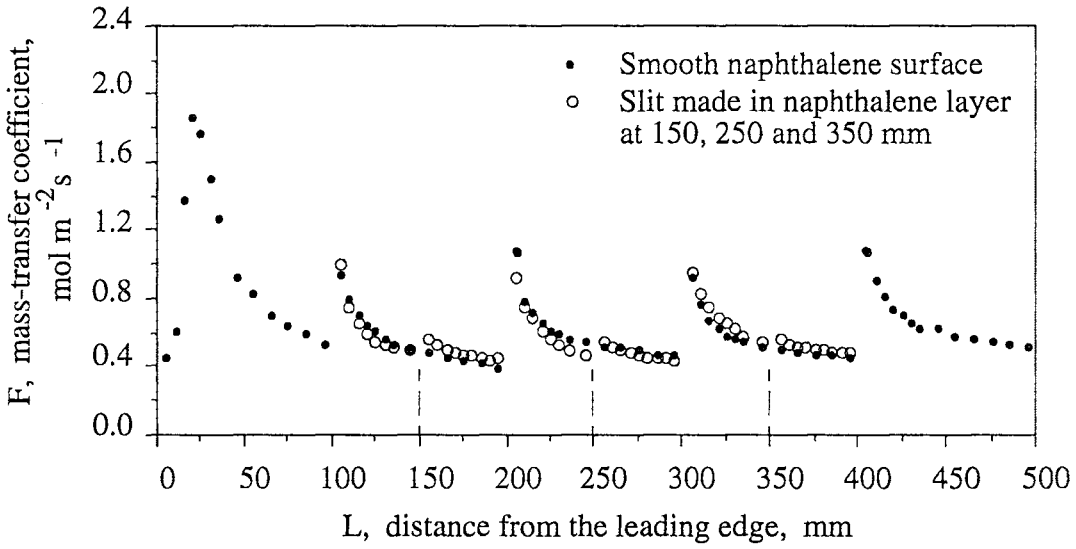

Figure 5.18 Effect of a slit in the naphthalene casting on mass-transfer coefficient at 5 m s^{-1}.

Although a protrusion of this size might be expected to influence the shear force [Coulson and Richardson, 1964] the results plotted in Figure 5.18 demonstrate a slit of the same dimensions does not significantly influence the external mass-transfer rates. However, one can discern a slight enhancement of the mass transfer rates due to the presence of the slit. This results tentatively suggest that surface roughness is not a highly significant factor in influencing the drying rates in the kiln.

6

Discussion

The sublimation work revealed that there is a characteristic maximum in each of the mass-transfer coefficient profile of the leading board for all the velocities investigated (Figure 5.6). This maximum, attributed to the formation of a stationary eddy just downstream of the leading edge of the leading board, was also reported by Danckwerts *et al.* [1962], Sørensen [1969] from sublimation tests of a single isolated slab, and Miller [1973] from similar tests of an isolated slat. No reliable correlation could be inferred from the results about the position of the maxima to the geometry of the stack and velocity through the stack as only three different velocities, board thickness and sticker thickness were used in the experiment. However, it was observed as shown in Figure 6.1 that the distance of the maximum from the leading edge decreased from 17.5 mm to 11.5 mm when the velocity was increased from 3 m s^{-1} to 7 m s^{-1} for a normal stack made up of 25 mm-thick boards separated by 25 mm-thick stickers. Decreasing the sticker thickness from 25 mm to 15 mm for a normal stack consisting of 25 mm-thick boards at 5 m s^{-1} caused this position to shift from 15.5 mm to 10.5 mm. For a stack made up of 25 mm-thick stickers at a velocity of 5 m s^{-1}, the maximum initially decreased from 15.5 mm to 13.0 mm when the board thickness was increased from 25 mm to 50 mm, but the maximum increased to 17.0 mm when the board thickness was further increased to 75 mm.

By subliming naphthalene-coated slabs of varying thickness, Sørensen [1969] found that $Re_{b\ crit}$, the critical Reynolds number based on the thickness of the slat, to be 245. The Re_b in all the cases investigated in this work were all greater than this value. The initial convex nature of the profile when there was a thinner leading board in Figure A3.6 in Appendix A3 indicated the embryonic formation of a stationary eddy. The calculated Re_b in this case had a value of 533, which was higher than that found by Sørensen [1969]. This, again, could be affected by the level of free-stream turbulence in the kiln and the flow characteristics prior to entry into the stack for a given geometry, which will be discussed later in this Section.

From Table 6.1, the distance from the leading edge to the position of maximum local mass-transfer coefficient, Δ, generally decreased slightly when minor board irregularities were present. For boards of the same thickness under identical experimental conditions, this effect was similar to that of increasing velocity through the stack.

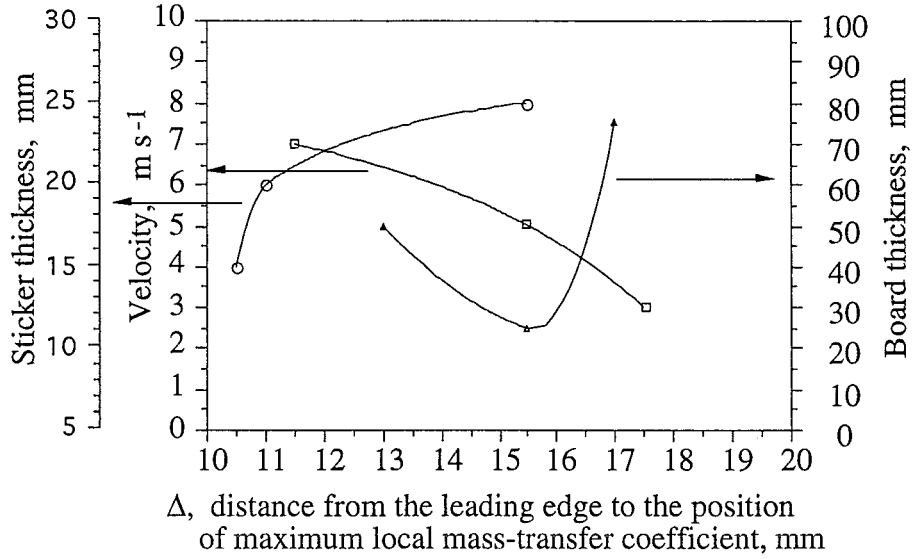

Figure 6.1 The distance from the leading edge to the position of maximum local mass-transfer coefficient, Δ, for the varying sticker and board thickness and air velocities used.

Configuration	Equipment	3 m s^{-1}	5 m s^{-1}	7 m s^{-1}
Run 1	kiln	17.5	15.5	11.5
Run 4	kiln	17.5	15.0	11.0
Run 13	kiln	15.0	12.0	10.0
Run 20	kiln	16.0	11.0	10.0
Run 25	kiln	16.0	11.5	10.0
Run 49	wind tunnel		21.0	

Table 6.1 Effect of minor board irregularities on the distance from the leading edge to the position of maximum local mass-transfer coefficient, Δ. Distances are in mm.

When the runs were performed in the wind tunnel, the position of maximum local mass-transfer coefficient, Δ, was shifted downstream when compared with the position for the kiln tests at the same velocity. As stacking was similar in both cases, this difference must be attributed to the way air was delivered into the stack. In the kiln, air must be entering the stack obliquely near to the entrance of the stack as it was forced down into the plenum space of only 600 mm wide (Figure 3.3a). In the wind tunnel, the airflow entering the stack was parallel to the test layers as air was first forced into the expanding section of the bell-mouth calming chamber before passing through the test stack, which was placed 2 metres downstream of the chamber in the tunnel. This argument was further supported by the fact that the mass-transfer coefficient profiles for the first board in kiln runs were more skewed towards the leading edge than that of the wind-tunnel runs.

This work has found that the flow passages for air in timber stacks, formed as a result of placing stickers between the layers of boards, cannot be treated as continuous ducts. The sublimation experiments showed the minute gaps between the adjacent boards not only

caused discontinuities in the mass-transfer coefficient profiles but also greatly enhanced transfer coefficients occurring over the first 30 mm of each of the 100 mm-wide board for the second and subsequent boards (Figure 5.6). Sparrow *et al.* [1982] used the naphthalene-sublimation method to determine the influence of airflow on the averaged transfer coefficients from 26.7 mm square modules, equally spaced with a 6.7 mm gap between modules, along one side of a flat rectangular duct. Though no clear conclusions could be drawn with regard to the effect of these gaps with respect to position along the flow within a module, it was found that the greatest average enhancement of 40% was found when there was a missing module upstream of the module of interest. The data from Miller [1973], though limited, showed large initial enhancements in the second slat of an arrangement of three aligned but closely-butted slats. Photographs taken from the flow visualization work in Chapter 2 revealed the formation of periodic eddies in these gaps. These minute adjacent board-to-board gaps in an otherwise "continuous" duct, acted as turbulence promoters, enhancing mass transport immediately downstream of these gaps. The discontinuities and enhancements in the transfer coefficient profiles were largely attributed to the increased in momentum transfer (and turbulence intensity) between the air in the gap and that of the bulk air stream as a result of these periodic disturbances to the flow. The contours of the predicted streamfunction around the gaps between the two boards in Figure 4.3 confirmed the formation of these periodic eddies. Discontinuities at these gaps were observed in the mass-transfer coefficient profiles for both time-independent and time-dependent flows. This is in agreement with the results of Wu [1989], who measured the level of turbulence along the flow in a stack made up of 20 mm-thick boards and 20 mm-thick stickers with 4 adjacent board-to-board gaps of 5 mm. Higher levels of turbulence were found to occur over these gaps when compared to the mid-section of the each corresponding board at Re of 5330. The turbulence levels at these gaps were observed to decrease in the streamwise direction with the exception of the last board, which showed slightly higher values than that of the preceding gap. These findings were consistent with the sublimation results of the present study.

Although inter-layer flow between board rows was found to be insignificant, the results as shown in Figure 5.9 confirmed its existence as profiles for the unsealed 1 mm gap showed a marginal increase in the first 10 to 15 mm of the initial portion over that of a similar but sealed gap. This flow between the layers, which appeared to be oscillatory in nature, was also observed in the flow visualisation studies described in Chapter 2. The 5 mm gap was found to raise the mass-transfer coefficient by as much as 40% over the first 20 to 30 mm of the board downstream of this gap. This may be attributed to the relative ease of replacing the volume of air in the space with the air drawn from the other side of the layer of boards as the eddy moved upwards towards into the bulk air stream, causing an increased in momentum exchange.

With the exception of the last board, the best-fit line through the maxima of the mass-transfer coefficient profile of the first 4 boards was found to conform to the general turbulent-flat plate correlation, having a constant of 0.088. This constant is about three times that of the constant (0.0288) in the best-fit line of Equation 5.15 and is about twice that of the constant (0.048) in the best fit line for the experimental data for the five boards. Similar results were observed for other runs. These results (A3.16 and A3.17) are appended in Appendix 3. The presence of these minute gaps between boards enhances the mass transfer at the front portion of every board, causing more uneven drying which could be detrimental to impermeable species causing undesirable added degrade. For a permeable species like radiata pine, provided that its unrestrained shrinkage of the board from green does not exceed its fracture strain in tension, this phenomenon of enhanced drying may be an advantage.

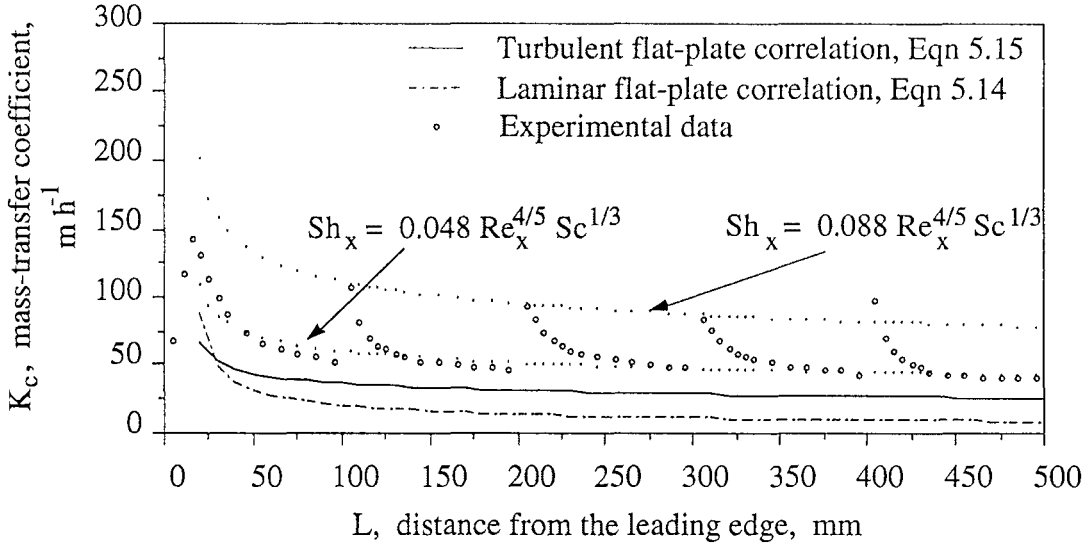

Figure 6.2 Comparison between fitted correlations for 5 m s^{-1} and the flat-plate correlations.

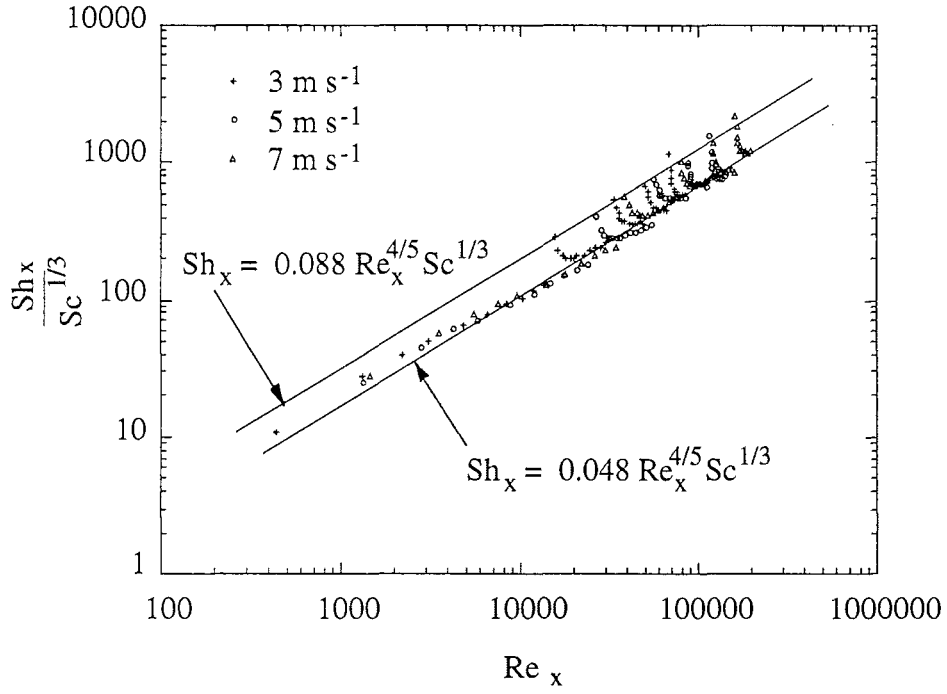

Figure 6.3 Fitted correlation to the experimental data on a log-log plot to determine the nature of the boundary layer developed over the surface of timber boards.

Mass-transfer coefficients found in these experiments were in general considerably higher in magnitude when compared to the laminar and turbulent flat-plate correlations (Figure 6.2). From the log-log plot in Figure 6.3, the best fit line for the experimental data had a slope of 0.8, which confirmed that boundary layer developed after the stationary eddy was turbulent. Based on the fact that the boundary layer was turbulent, it was found that the constant that best fit the data was 0.048, 67% higher than that of the corresponding turbulent flat-plate correlation of Equation 5.15.

F-type mass-transfer coefficients are converted to K-type mass-transfer coefficients using the following relation;

$$K_c = \frac{F\ R\ T\ \ln \dfrac{P}{P - P_{NO}}}{P_{NO}}$$

or are calculated from the raw data collected, using the equation below (see derivation in Section 5.2).

$$K_c = \frac{\rho_N\ R\ T}{M_N\ P_{NO}} \left[\frac{\Delta b}{\Delta t}\right]$$

Position of board	Mean K_c, m h^{-1} (experiment)	Mean K_c, m h^{-1} (Sørensen)
1	81.47	-
2	57.40	40.57
3	59.34	28.98
4	54.38	23.81
5	47.89	20.69

Table 6.2 Mean K-type mass-transfer coefficients for the first 5 boards from the leading edge.

Position of board	Mean K_c, m h^{-1} (experimental)	Mean K_c, m h^{-1} (Sørensen)
5th last	44.50	8.34
4th last	43.98	8.18
3rd last	39.36	8.03
2nd last	43.70	7.88
last	43.14	7.75

Table 6.3 Mean K-type mass-transfer coefficients for the last 5 boards of a wide stack (Configuration M in Appendix A2).

Board-averaged K-type mass-transfer coefficients for the first 5 boards from the leading edge were calculated from values of K_c over the measured range for each board using the trapezoidal rule. Board-averaged K_c values were similarly calculated from K_c values

obtained from Sørensen's empirically-derived mass-transfer correlation (Equation 5.17) over the same range. These values are tabulated in Table 6.2. As Equation 5.17 can only generate K_c values above 45 mm from the leading edge (because of the formation of the stationary eddy), no attempt was made to compare the board-averaged K_c values for the first board. The board-averaged values of K_c from our experiments were found to be higher than those calculated from Sørensen's correlation (Equation. 5.17) for all boards in the stack. The discrepancy between these two values increases with position of the board. This trend is clearly evident as the values in Table 6.3 show hugh discrepancy between the two calculated values for boards near to the trailing edge. Flow channels formed by the stickers in the timber stack cannot be assumed to be continuous, and as such, flat-plate correlations cannot be used.

While most authors agree that the Reynolds number exponent for a fully developed turbulent boundary layer in the flat plate correlation should be 0.8, the averaged constant in their empirically derived flat-plate correlations varied widely with values like 0.0288 [Colburn, 1933], 0.036 [Sørensen, 1969] and a value of 0.048 in this work. Equation 5.15 for the flat-plate correlation must therefore be dependent on other parameters not thought to be significant in those experiments done earlier. These were performed on geometrically similar bodies although the operating conditions under which these experiments were carried out were usually not measured. However, the present results for the sublimation tests in the same kiln by varying sticker thickness over the range 15 to 25 mm and board thickness over the range 25 to 75 mm, and also for an aligned stack in both the kiln and wind tunnel all at the same velocity, demonstrated no significant difference in the mass-transfer profiles. This leads to the conclusion that mass-transfer from the surface of a flat plate is dependent on turbulence levels as these experiments were carried out under similar operating conditions.

Free-stream turbulence is thought to strongly affect the transition from laminar to turbulent flow. When disturbances in the external stream or free-stream turbulence is increased, turbulence in the boundary layer is amplified, resulting in the thickening of the turbulent boundary layer and the thinning of the laminar sublayer, and thus mass transport into the air stream would be enhanced. Earlier studies on a sphere and flat plate [Schlichting, 1968] revealed that as free-stream turbulence decreased, the critical Reynolds number, Re_{crit}, for transition increased rapidly. The only work found in literature that investigated explicitly the effect of free-stream turbulence on flat plate heat transfer was done by Sugawara *et al.* [1988], who investigated the effect of free-stream turbulence on local heat transfer coefficients on a 378 mm-long, 1.32 mm-thick, smooth-edged flat plate in a wind tunnel. The present results were consistent with the experimental findings established by Sugawara *et al.* He found that the coefficients increased rapidly at turbulence levels below 4% but levelled off to a value approximately 55% higher than that obtained for very small free-stream turbulence at turbulence levels above 7-8%. Although the turbulence levels measured at 5 mm prior to entry to the test stack, which comprised 25 mm-thick boards separated by 25 mm-thick stickers in both the kiln and wind-tunnel runs at 5 m s^{-1}, were in the range 9.8 - 10.2% and 8.0 - 9.2% respectively, both mass-transfer coefficient profiles were in good agreement (Figure 5.15) thereby confirming no further enhancements after a free-stream turbulence level of 8%. However, even taking into account of the maximum experimental error of 4% in the present experiments, the enhancement of 67% found in this experiment still appeared to be slightly higher than the value of 55% quoted by Sugawara *et al.* This discrepancy was attributed to the choice of the reference levels for free-stream turbulence. The reference level chosen by Sugawara *et al.* for calculating the enhancements was 0.37% whereas for the flat plate correlation, there was no mention of the magnitude of the level of free-stream turbulence although Schlichting [1968] quoted intensity of turbulence of the order of 0.01% for older wind tunnels. If the empirical Nusselt number found by Sugawara *et al.* is converted to a Sherwood number (Appendix A4), so that percentage increments are then compared on the same basis, the value of the coefficients in both empirically-found Sherwood numbers agree well within the experimental error of 4%. Thus, the higher free-stream turbulence in industrial kilns would undoubtedly increase mass transport considerably. Using the measured values of the intensity level in the plenum space of the

experimental kiln, the predicted asymptotic mass-transfer coefficients for time-independent flows were found to be greater than those calculated from flat-plate correlations. These coefficients were about 15% lower than the experimental values. Enhancements at the leading edge were also predicted but of a smaller magnitude than those measured. When time was taken into account, the enhancements at the leading edge of the boards were well predicted with the exception of the first board which requires improvement in the treatment of the flow near the wall.

The thinner test slab, which had a board surface 3 mm lower than the adjacent dummy boards in the stack, appeared to have large effect on the mass-transfer coefficients as shown in Figure 6.4. The resultant "saw-tooth" profile showed large enhancements over nearly the whole width of the test slab with the exception of the front and rear portions where the mass-transfer coefficients were reduced significantly. Flow visualisation studies in Chapter 2 revealed that the lower board caused the distortion of the airflow resulting in it "obliquely" impinging onto the naphthalene surface some distance away from the leading edge of the lower board. Two stationary eddies, one each at the front and rear, are thought to evolved in the region where mass-transfer coefficients were found to be significantly reduced. This large variation in mass-transfer coefficients over the width of the board will cause large moisture gradient to develop within the thinner board. For boards with a greater tendency (juvenile and reaction wood) to shrink in thickness, this large moisture gradient will result in differential shrinkage causing drying stresses in the board. As the thinner board is no longer under restraint (not in contact with the sticker), board degrade is likely to occur.

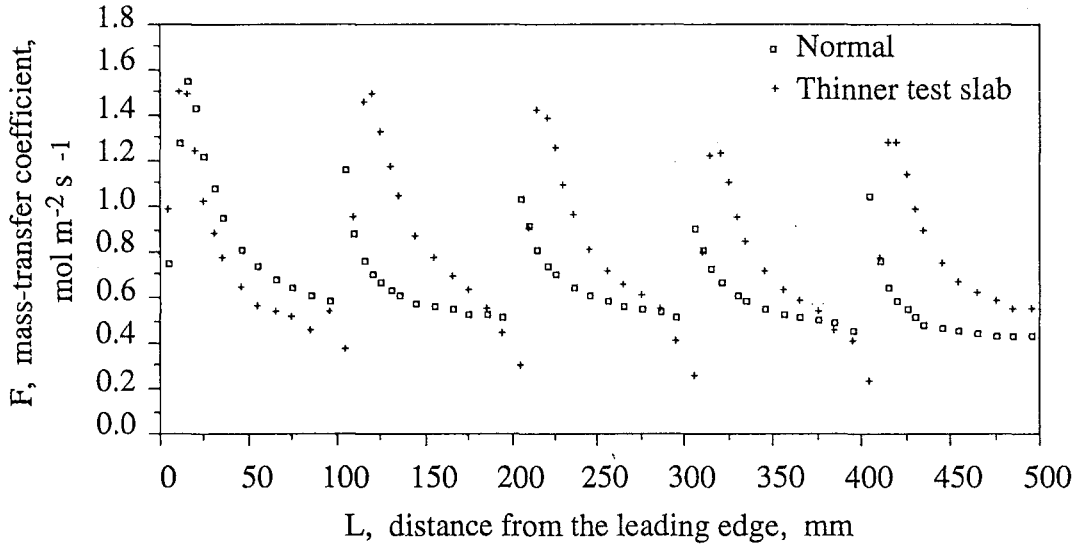

Figure 6.4 Effect of a thinner test slab than the adjacent dummy boards on the mass-transfer coefficient at 5 m s^{-1}

Effects of surface roughness on mass-transfer were found by modifying the experiment where a slit, 1 mm wide by 2 mm deep, was made half way in the naphthalene casting. While the actual surface roughness of sawn timber will be smaller in scale than the dimensions used in these runs, results in Figure 5.18 confirmed that the slit is not significant in affecting mass-transfer in timber kiln. The slit, however, did show some tendencies to cause discontinuities in the profiles.

Mass-transfer coefficients for a 3.025 m-wide stack appeared to have similar initial values and tend to an asymptotic value of 0.4 mol m^{-2} s^{-1} at the trailing end of each board (Figure 5.16). These results demonstrate that the use of wider stacks in kilns would have very little effect on mass transport over the surface of these boards. While the mass-transfer coefficients remain largely unaffected at the trailing edge of the stack, drying may be hindered if the air is saturated.

For all the minor board irregularities considered above, shrinkages in thickness appeared to be the one of most concern. As enhancements were mostly over the central portion of the thinner board, fan reversals would be ineffective as a way to even out the difference in mass-transfer at the two ends of the boards, and degrade may result. Therefore, a charge comprising of different board shrinkages and thicknesses can affect the quality of the dried product considerably.

7

Conclusions and recommendations for further work

The sublimation of naphthalene from a coated plate has been used to simulate the transfer of moisture vapour from the surface of a timber board in a kiln stack. The variation of local mass-transfer coefficients in the streamwise direction over a series of in-line, blunt slabs similar to that of a timber stack has been experimentally obtained over a velocity range of 3 to 7 m s^{-1}. Although the boards were placed closely together in a stack, small gaps of up to 1.0 mm wide between the adjacent boards in a layer were inevitable. From this series of experiment, the minute gaps between adjacent boards were found to have a profound effect on mass transport downstream of the gap. Discontinuities in the mass-transfer coefficient profile were observed to occur over these minute gaps. These were largely due to the coefficients in the region immediately following these gaps being greatly enhanced. The flow visualization studies revealed that a recurring and periodic disturbance was forming in the vicinity of the gap. There were three phases; the periodic formation of the eddy, followed by the clockwise circulation of the eddy down the gap, and finally the expulsion of the eddy distorted the streamlines in the region near to the leading edge of the following board causing the local mass-transfer coefficients over these regions to be enhanced. Thus, empirically-derived flat-plate correlations can not be used to describe transport processes in the drying of timber boards in kilns.

The measured levels of free stream turbulence near to the leading edge of the stack in the plenum space of the experimental kiln were found to be very high (8 to 10% over the velocity range of 3 to 7 m s^{-1}) in comparison to the levels thought to prevail in the wind tunnels in which earlier experiments were performed to obtain earlier data. As there is virtually no information regarding levels of free stream turbulence in a timber kiln, future work could include measuring the turbulence intensity near the leading edge of the whole

stack. This, together with the velocity data acquired, could be used to predict the variation of moisture content along the length of a board and between the first boards of each layer in the stack.

The disturbance over the gap, captured on film using a Bolex movie camera, was observed to form alternately between the two leading edges following the gap. From frame counts of the negatives taken with a the period of the disturbance was in the range of 0.5 to 1.5 seconds which agreed well with the 2 seconds numerically predicted in Chapter 4. The Strouhal number for the minute gap between the boards was calculated to be 0.05 at a Reynolds number of approximately 800. Results of both the sublimation tests and flow visualization studies ruled out interlayer flow to be the cause of the enhancement. Future work could include the determination of the turbulence levels along the flow channels if smaller non intrusive probes or non interfering methods are available for use.

A stationary eddy was formed downstream of the leading edge of the first board in the array for all the runs performed. The maximum local mass-transfer coefficient was found to diminish exponentially in the streamwise direction tending to the same asymptotic value at approximately half way across the board for every board. The mass-transfer coefficients were found to vary as the 0.8 power of the air velocity. The coefficient of 0.048 in the dimensionless transfer correlation was obtained.

Minor board irregularities in timber stacks are the consequence of inaccurate sawing, poor stacking and/or changes in dimensions of the boards (shrinking) during the drying process. These usually result in increases in the width of the adjacent board gaps and/or uneven board surface as a result of different thickness of adjacent boards. The effects of these minor board irregularities on the convective transfer have also been investigated. The results generally indicated that both the adjacent board gaps and the difference in the thickness of the adjacent boards were favourable for drying permeable boards at high temperatures where external conditions in the kiln are relatively more important.

Varying the adjacent board gap from 1 to 5 mm was found to enhance the coefficients by up to 30% over the first 25 mm of the 100 mm-wide board at 5 m s^{-1}.

A thinner leading board has a greater influence over the mass-transfer coefficients in the front portion of the board than that of a thinner trailing board with the same board height difference. Coefficients were enhanced by up to 30% over the first 30 mm for an airflow of 5 m s^{-1}. Greatly enhanced local mass-transfer coefficients for nearly the whole width of the board were also observed where the level of the board was lower (ie. thinner) than the adjacent ones. The exception was the two extremities of the thinner board adjacent to the two thicker boards on both sides where stagnant zones were found to prevail, resulting in lower coefficients. The existence of such stagnant zones was confirmed in the photographs taken in the flow visualization studies taken of such geometry.

Results from sublimation tests of a naphthalene coating with a slit of comparable size to that of the surface roughness of a board confirmed that the surface roughness of 1 mm wide by 2 mm deep has relatively insignificant effect on the coefficients. This demonstrates that there is no advantage to getting smoother sawn surfaces from sawing. The current practice of machining wood after drying has the added advantage of the increased dimensional stability with virtually no consequence to the drying rate at all. Thus, there is also no added advantage in getting smoother sawn surfaces from improved sawing technology.

Flow reversals not only provide an averaging of the coefficients during rate at the extremities of each board but also averages the drying rates. Not many flow reversals are needed during the drying process to achieve good uniformity in board-to-board moisture contents.

Both sticker thickness over the range 15 to 25 mm and board thickness of 25 to 75 mm was found to have negligible effect on the local mass-transfer coefficients, within the scatter of the results. While the use of thinner stickers to increased throughput of the kiln is

advocated, drying may be hindered before reaching the trailing end of the stack as the smaller volume of air passing through the sticker spacing may be fully laden with moisture. While increasing dry-bulb temperature can increased the moisture carrying capacity of the air, there is a limit to the temperature one can use because of the detrimental effect temperature can have on strength of the timber.

The option of having wider stacks is attractive in terms of increased kiln capacity. While the coefficients of the board 3 metres downstream remained very favourable at similar levels, drying may not proceed as the moisture concentration gradient between the board and the bulk air stream towards the end the wide stack may be approaching zero as the air will pick up moisture along the sticker spacing.

To dry wood successfully at high temperatures, there must be a dynamic balance between the moisture evaporation from the surface, the diffusion of moisture through the cell wall and mass flow of vapour through the inter-connecting pits. As this project only examines the effects of the external conditions and geometry on local mass-transfer coefficients, further work to determine the wood properties of the *Pinus radiata* is necessary to elucidate the flow of moisture internally at high temperatures. The modelling of the drying process in *Pinus radiata* board at high temperatures can then proceed.

Nomenclature

Roman

b	thickness of naphthalene sublimed	m
	or thickness of test slab	m
C	molar concentration of the vapour in the fluid	mol m^{-3}
C_1	constant in turbulence model, Table 4.1	-
C_2	constant in turbulence model, Table 4.1	-
C_f	skin friction coefficient, Equation 4.9	-
C_μ	constant in turbulence model, Equation 4.3	-
C_N	molar concentration of naphthalene vapour in air	mol m^{-3}
C_{NO}	molar concentration of naphthalene vapour at the surface of coating	mol m^{-3}
$C_{N\infty}$	molar concentration of naphthalene vapour in the bulk air stream	mol m^{-3}
d	gap between adjacent boards	m
D	diffusion coefficient	m^2 s^{-1}
D_{NA}	diffusion coefficient of naphthalene in air	m^2 s^{-1}
E	constant in wall model, Equation 4.8	-
F	mass-transfer coefficient, = $(CD_{NA}) / \delta$	mol m^{-2} s^{-1}
f	vortex-shedding frequency	s^{-1}
G	generation of turbulence kinetic energy, Equation 4.2	kg m^{-1} s^{-3}
h	under-relaxation factor, Equation 4.5	-
I	turbulence intensity	%
j_d	local j_d-factor, = $(K_c . Sc^{2/3})/U_\infty$	-
$\bar{j}_{d(o,z)}$	mean value of local j_d from 0 to Z	-
J_N	diffusion flux of naphthalene vapour	mol m^{-2} s^{-1}
k	turbulence kinetic energy per unit mass	m^2 s^{-2}
K_c	mass-transfer coefficient	m s^{-1}
k_p	turbulence kinetic energy per unit mass at the near-wall grid point	m^2 s^{-2}
L	distance from the leading edge	m
	or characteristic dimension	m
L_Δ	distance from position of maximum local mass-transfer coefficient	m
M_N	molar mass of naphthalene	kg mol^{-1}

n	number of moles	mol
N_N	sublimation rate of naphthalene vapour per unit exposed surface	kg m^{-2} s^{-1}
$\tilde{N}_A$	molar air flux	mol m^{-2} s^{-1}
$\tilde{N}_N$	molar naphthalene vapour flux	mol m^{-2} s^{-1}
	or distance from the naphthalene surface	m
p, P	pressure, total pressure	N m^{-2} or Pa
P_{NO}	vapour pressure of naphthalene at the sublimating surface	N m^{-2} or Pa
$P_{N\infty}$	vapour pressure of naphthalene in bulk air stream	N m^{-2} or Pa
R	universal gas constant	J mol^{-1} K^{-1}
S_ϕ	source term, Equation 4.1	-
t	time	s
T	absolute temperature	K
u	air velocity through sticker spacing	m s^{-1}
u'	root-mean-square of the fluctuating component of velocity	m s^{-1}
U_∞	bulk stream velocity	m s^{-1}
u^+	dimensionless velocity	-
u_p	velocity at the near-wall grid point	m s^{-1}
v	vertical component of velocity	m s^{-1}
V	volume	m^3
x	horizontal distance	m
y	normal distance from wall	m
y^+	dimensionless distance from the wall	-
y_p	normal distance of the near-wall grid point from the wall	m
y_r	height of the roughness element	m
y_r^+	dimensionless height of the roughness element	-

Subscript

A	air
b	base on thickness of the board
N	naphthalene
NA	naphthalene to air
N∞	naphthalene at bulk air stream
NO	naphthalene at the surface of coating
x	base on the distance from the position of the maximum local mass-transfer coefficient.

Greek

δ	boundary layer thickness	m
	or distance of the bulk air stream to naphthalene surface	m
ε	dissipation rate of turbulence kinetic energy	$m^2 s^{-3}$
ϕ	diameter	m
ϕ	general variable, Equation 4.1	-
ϕ^*_{new}	new value of ϕ produced without under-relaxation	-
ϕ_{new}	new value of ϕ, under-relaxed	-
ϕ_{old}	value of ϕ from last iteration	-
Γ_ϕ	transfer coefficient associated with ϕ, Equation 4.1	-
κ	constant in wall model, Equation 4.8	-
μ	dynamic viscosity	$kg\ m^{-1}\ s^{-1}$
μ_L	laminar viscosity	$kg\ m^{-1}\ s^{-1}$
μ_T	turbulence viscosity	$kg\ m^{-1}\ s^{-1}$
ρ	density of fluid	$kg\ m^{-3}$
ρ_N	density of naphthalene	$kg\ m^{-3}$
σ_ε	constant in turbulence model, Table 4.1	-
σ_k	constant in turbulence model, Table 4.1	-
τ_w	wall shear stress	$N\ m^{-2}$
υ	kinematic viscosity	$m^2\ s^{-1}$
υ_A	kinematic viscosity of air	$m^2\ s^{-1}$
Δ	finite difference	-

Dimensionless numbers

C_f	skin friction coefficient	$\tau_w/(\rho\, u^2/2)$
Re_b	Reynolds number based on b	$(b\, u) / \upsilon_A$
Re_{crit}	critical Reynolds number	$(L_{crit} u) / \upsilon_A$
Re_D	Reynolds number based on D	$(D\, u) / \upsilon_A$
Re_x, Re_L	Reynolds number based on L	$(L_\Delta u) / \upsilon_A$
Sc	Schmidt number	υ_A / D_{NA}
Sh_x	Local Sherwood number	$(K_c L_\Delta)/D_{NA}$
St	Strouhal number	$(f \cdot b)/u$

Constants

$M_N = 0.12816$ kg mol^{-1}

$R = 62.361$ J mol^{-1} K^{-1}

$\rho_N = 1145$ kg m^{-3}

$\upsilon_A = 1.6875$ E -5 m^2 s^{-1}, at 41°C.

References

Adesanya, A., Nanda, A.K. and Beard, J. N., 1988. Drying Rates during high-temperature drying of yellow poplar, *Drying Technology*, Vol 6 No 1, pp. 95-112.

Arnaud, G., Fohr, J-P., Garnier, J-P. and Ricolleau, C., 1991. Study of the Air Flow in a Wood Drier, *Drying Technology*, Vol 9, No. 1, pp. 183-200.

Ashworth, J.C. 1977. The Mathematical Simulation of Batch-Drying of Softwood Timber, PhD. Thesis, University of Canterbury, New Zealand.

Bachrich, J.L. 1980. *Dry Kiln Handbook,* H.A. Simons (International) Ltd., Vancouver, Canada.

Bamber, R.K. and Burley, J. 1983. *The Wood Properties of Radiata Pine*, Commonwealth Agricultural Bureaaux, England.

Basilico, C., Genevaux, J.M. and Martin, M. 1990. High Temperature Drying of Wood Semi-Industrial Kiln Experiments, *Drying Technology - An International Journal,* Vol 8 No 4, pp. 751-765 Commonwealth Agricultural Bureaux, England.

Bayley, F.J. and Turner, A.B. 1971. Transpiration cooled turbines, *Proc. Instn. Mech. Engrs.,* 185, pp. 943-951, London.

Bester, A.B. 1982. Practical Drying Techniques to reduce warp, *Proceedings of the Jubilee Symposia*, Mededeling Communication 98(11), pp. 730-740.

Blair, M.F. 1983. Influence of Free-Stream Turbulence on Turbulent Boundary Layer Heat Transfer and Mean Profile Development, Part 1 - Experimental Data, *ASME Journal of Heat Transfer*, Vol 105, pp. 33-40.

Blair, M.F. 1983. Influence of Free-Stream Turbulence on Turbulent Boundary Layer Heat Transfer and Mean Profile Development, Part 2 - Analysis of Results, *ASME Journal of Heat Transfer*, Vol 105, pp. 41-47.

Bradshaw, P. 1971. *An Introduction to Turbulence and its measurement,* Pergamon Press, Oxford, UK.

Bull, M.K, Pickles, J.M., Martin, B.T. and Welsh, M.C. 1989. Vortex Shedding from Rectangular Plates in Tandem, *Proc. Tenth Australasian Fluid Mechanics Conference*, University of Melbourne, Vol. 1, pp. 4.17-4.20.

Clifton, N.C. 1985. *New Zealand Radiata Pine*, New Zealand Forest Service, Wellington.

Colburn, A.P. 1933. *Trans. Instn Chemical Engrs.* Vol 29, 174

Coulson, J.M. and Richardson, J.F. 1964. *Chemical Engineering*, 2nd ed., Pergamon Press, Oxford.

Danckwerts, P.V. and Anolick, C. 1962. Mass-transfer From A Grid Packing To An Air Stream, *Trans. Instn. Chem. Engrs.*, Vol. 40, pp. 203-213.

Davies, J.T. 1972. *Turbulence Phenomena, An Introduction to the Eddy Transfer of Momentum, Mass, and Heat, Particularly at Interfaces*, Academic Press, London.

Edward, W.W. (editor-in-chief). 1929. *International Critical Tables of Numerical Data, Physics, Chemistry And Technology*, McGraw Hill, New York.

Goldstein, S. 1938. *Modern Developments in Fluid Dynamics*, Oxford University Press, U.K.

Gosman, A.D., 1978. Lecture 7: *The Computer Program*, presented as a short course entitled the Prediction of the Performance of Combustion Chambers and Furnaces, Pennsylvania State University, PA, April 19-21.

Hart, C.A. 1975. *The Drying of Wood*, The North Carolina Agricultural Extension Service, Ext. Cir 471.

Incropera, F.P. and DeWitt, D.P. 1990. *Fundamentals of Heat and Mass Transfer*, 3rd Edition, John Wiley and Sons.

Keey, R.B. 1972. *Drying Principles and Practice*, Pergamon Press, Oxford, UK.

Keey, R.B. 1978. *Introduction to Industrial Drying Operations*, Pergamon Press, Oxford, UK.

Kininmonth, J.A. (compiler) 1974. *Proc. Timber Drying in New Zealand*, FRI Symposium No. 17, Forest Research Institute, Rotorua.

Kininmonth, J.A. and Whitehouse L.J. (eds.) 1991. *Properties and Uses of New Zealand Radiata Pine, Vol. 1 - Wood Properties*, New Zealand Ministry of Forestry, Forest Research Institute.

Kollmann, F and Schneider, A. 1961. Effect of flow velocity on the kiln drying of timber in superheated steam. *Kolz Roh und Werkstoff*, Vol 19, 12.

Langrish, T.A.G., Kho, P.C.S., Keey, R.B. and Walker, J.C.F. 1992. Experimental measurement and numerical simulation of local mass-transfer coefficients in timber kilns, *Drying technology*, Vol 10(3), pp. 753-781.

Langrish, T.A.G., Kho, P.C.S., Keey, R.B. and Walker, J.C.F. 1993. Time-dependent flow in arrays of timber boards : Flow visualization, mass-transfer measurements and numerical simulation, *Chem. Eng. Sci.*, Vol. 48(12), pp. 2211-2223.

Launder, B.E. and Spalding, D.B., 1974. The Numerical Computation of Turbulent Flows, *Computer Methods in Applied Mechanics and Engineering*, Vol. 3, pp. 269-289.

Lee, H.S. 1990. Flow Visualization on High-temperature Wood Drying, B.E. Report, University of Canterbury, New Zealand.

Lienhard, J.H. 1980. *A Heat Transfer Textbook*, Prentice-Hall, New Jersey.

Luikov, A.V. 1966. *Heat and Mass Transfer in Capillary-porous Bodies,* Pergamon Press, New York.

Mackay, J.F.G. and Oliveira, L.C. 1989. *Kiln Operator's Handbook for Western Canada*, Forintek Canada Corporation, Vancouver.

Merzkirch, W. 1987. *Flow Visualization*, 2nd ed., Academic Press, Orlando, Florida.

Miller, W.R. 1973. Mass-transfer Within Arrays, B.E. Report, University of Canterbury, New Zealand.

Miller, W.R. 1991. Personal communication.

New Zealand Official 1990 Year Book, 94th Edition, pp. 465-474, Department of Statistics, New Zealand.

Ogura, T and Ohnuma, K. 1955. An experimental formula for the evaporation rate of wood moisture at constant drying rate. *J. Jap. Wood Res. Soc.* Vol 1, 1.

Pang, S. 1991. Modelling of High-Temperature Kiln Drying of Pinus Radiata Boards, Research report No. 1, Department of Chemical and Process Engineering, University of Canterbury.

Patankar, S., 1980. *Numerical Heat Transfer and Fluid Flow, Hemisphere*, NY, 197p.

Perry, R.H. and Green, D.W. 1984. *Perry's Chemical Engineers' Handbook*, 6th ed., McGraw Hill, New York.

Petrusma, M. and Gai, S.L. 1989. Investigation into the Wake of Blunt Trailing Edge Aerofoils at low Reynolds Numbers, *Proc. Tenth Australasian Fluid Mechanics Conference*, University of Melbourne, Vol. 2, pp. 13.35-13.38.

Powell, R.W. 1940. Further Experiments on the Evaporation of Water From Saturated Surfaces, *Trans. Instn. Chem. Engrs.*, Vol. 18, pp. 36-55.

Roadman, R.E. and Loehrke, R.I. 1983. Low Reynolds Number Flow Between Interrupted Flat Plates, *ASME Journal of Heat Transfer*, Vol 105, pp. 166-171.

Rosen, H.N. 1981. Drying Processes for the year 2000, *Proc. XVII IUFRO World Congess*, Japan.

Schlichting, H. 1968. *Boundary-Layer Theory*, 7th ed., McGraw Hill, New York.

Scott, C.W. 1960. *Pinus Radiata*, FAO Forestry and Forest Products Studies No. 14, FAO of The United Nations, Rome.

Shepherd, C.B., Hadlock, C., and Brewer, R.C. 1929. Drying Materials in Trays, *Ind. Engng. Chem.*, Vol. 21, pp. 976-980.

Sherwood, T.K. 1938. The Drying of Solids - II, *Ind. Engng. Chem.*, Vol. 30, pp. 388-397.

Siau, J.F. 1984. *Transport Processes in Wood*, Springer-Verlag, Berlin, Heidelberg, New York.

Skaar, C. 1988. *Wood-Water Relations*, Springer-Verlag, Berlin, Heidelberg, New York.

Sørensen, A. 1969. Mass-transfer Coefficients On Truncated Slabs, *Chem. Eng. Sci.*, Vol. 24, pp. 1445-1460, Pergamon Press.

Sparrow, E.M., Niethammer, J.E. and Chaboki, A. 1982. Heat transfer and pressure drop characteristics of arrays of rectangular modules encountered in electronic equipment. Int. J. Heat Mass Transfer 31(1) pp. 961-973. *Boundary-Layer Theory*, 7th ed., McGraw Hill, New York.

Sugawara S., Sato T., Komatsu H and Osaka H. 1988. Effect of free stream turbulence on flat plate heat transfer, *Int. J. Heat Mass Transfer*, Vol. 31, No. 1, pp. 5-12.

Tronstad, S. 1983. Regional Paper, *Wood Drying Working Party (S 5.04-06)* IUFRO Division V Conference, Madison, Wisconsin, USA.

Viktorin, Z. 1965. Rate of drying of a timber pile, *Drevársky Výskum*, 4.

Weast, R.C. (editor-in-chief). 1987. *Handbook of Chemistry and Physics*, 68th ed., CRC Press, Florida.

Welty, J.R. 1978. *Engineering Heat Transfer*, SI Version, John Wiley and Sons, New York.

Wiedeman H.G.R., Nassif, N.M., Gostelow, J.P. 1989. Study of the Airflow Profile inside a Timber Drying Kiln, *Proc. Fourth Australasian Conference on Heat and Mass Transfer* , University of Canterbury, Christchurch, New Zealand.

Williams, D.H. 1983. High-temperature Drying, *Timber Drying News No. 2*, Forest Research Institute, Ministry of Forestry, New Zealand.

Wu, Q. 1989. An Investigation of Some Problems in Drying of Tasmanian Eucalypt Timbers, M.E. Report, University of Tasmania.

Zelenka, R.L. and Loehrke, R.I. 1983. Heat Transfer from Interrupted Plates, *ASME Journal of Heat Transfer*, Vol 105, pp. 173-177.

Appendices

A1 - Experimental runs

KILN RUNS

Three different air velocities; 3 m s^{-1}, 5 m s^{-1} and 7 m s^{-1} were used for each of the runs from 1 to 28. The boards in the test section were 25 mm thick and were separated by stickers, also of 25 mm thick. A gap of 1 mm existed between the test slab and the adjacent dummy boards, while the 5 mm-gaps between the boards were slightly exaggerated for illustration purposes only. Boards depicted lower than the adjacent dummy boards were thinner by 3 mm.

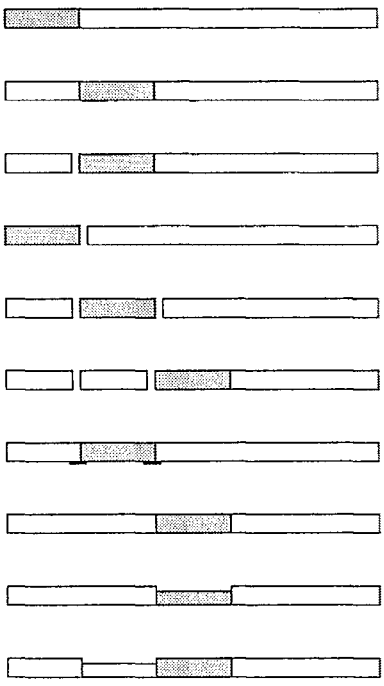

Run 1

Run 2

Run 3

Run 4

Run 5

Run 6/27A

Run 7

Run 8

Run 9

Run 10/19


Run 11/18

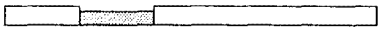
Run 12

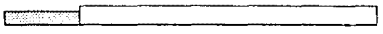
Run 13

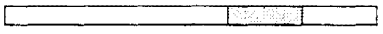
Run 14

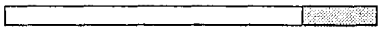
Run 15

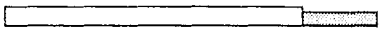
Run 16

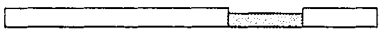
Run 17

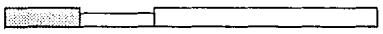
Run 20

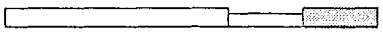
Run 21

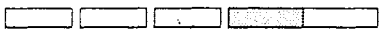
Run 22

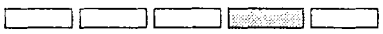
Run 23

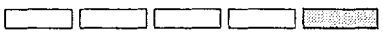
Run 24

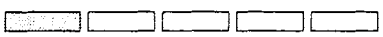
Run 25

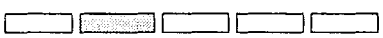
Run 26


Run 27


Run 28

The stack for the following runs 29 to 33 was made up of boards which were 25 mm thick separated by 20 mm-thick stickers. The air flow through the stack was 5 m s^{-1}.

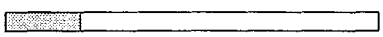
Run 29

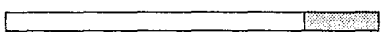
Run 30

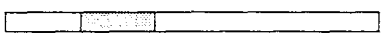
Run 31

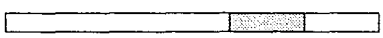
Run 32

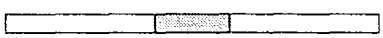
Run 33

The test section for runs 34 to 38 was identical to that of runs 29 to 33 but the thickness of the stickers was further reduced to 15 mm.

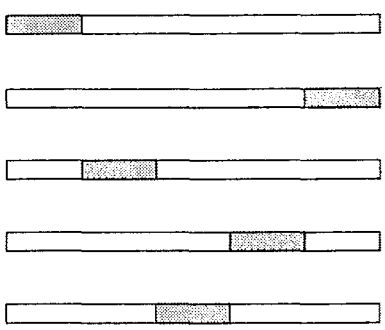

For runs 39 to 43, the test stack was made up of the 50 mm-thick boards separated by 25 mm-thick stickers at 5 m s^{-1}.

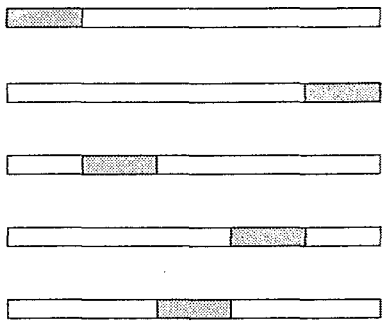

The test section for runs 44 to 48 was identical to that of runs 39 to 43, with the exception of the thickness of the boards which was further increased to 75 mm.

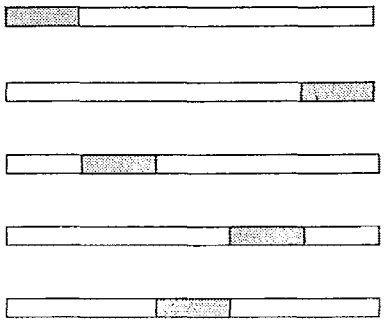

WIND TUNNEL RUNS

Runs 49 to 61 were performed in the wind tunnel in the Department of Chemical and Process Engineering. The stack in the test section was made up of 25 mm-thick boards, separated by 25 mm-thick stickers with the velocity through the stack at 5 m s^{-1}.

Aligned 500 mm-wide stack.

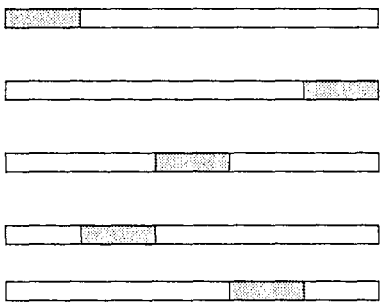

A slit was made in the naphthalene coating at 50 mm from the leading edge of the test slab for runs 54 to 56.

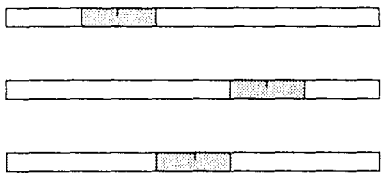

Set up was similar to that of runs 49 to 53 but the "length" of the stack was increased to 3.02 m.

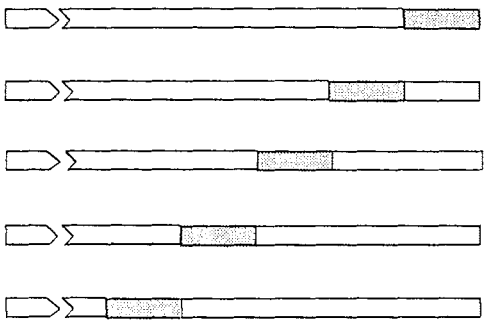

A2 - Grouped configurations

KILN RUNS

The width of the stack in the test section was 500 mm.

Configuration A
Aligned stack

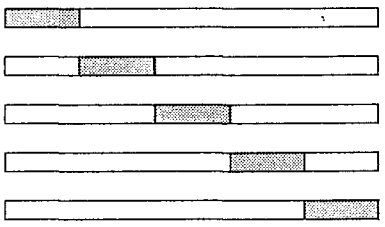

Run 1
Run 2
Run 8
Run 14
Run 15

Configuration B
Thinner test slab than the adjacent dummy boards

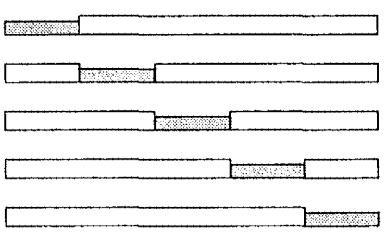

Run 13
Run 12
Run 9
Run 17
Run 16

Configuration C
5 mm-wide gaps between boards up to the leading edge of the test slab

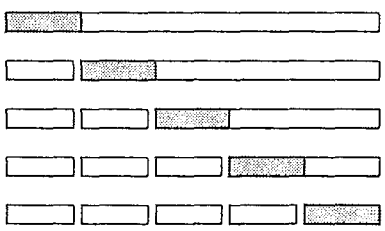

Configuration D
5 mm-wide gaps between boards up to the trailing edge of the test slab

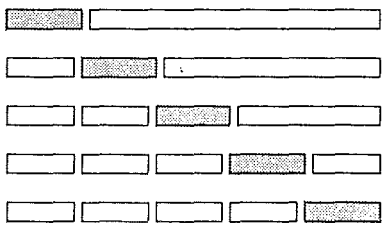

Configuration E
5 mm-wide gaps between all boards

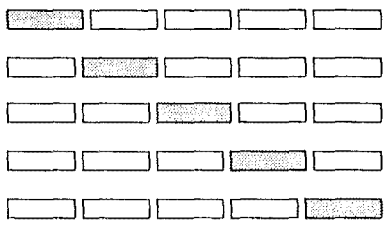

Configuration F
25 mm-thick boards separated by 20 mm-thick stickers

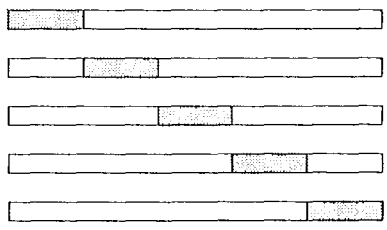

Configuration G
25 mm-thick boards separated by 15 mm-thick stickers

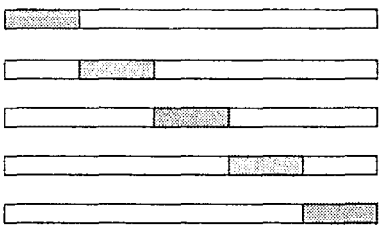

Configuration H
50 mm-thick boards separated by 25 mm-thick stickers

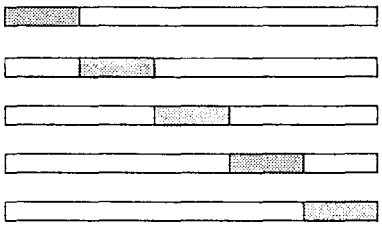

Configuration I
75 mm-thick boards separated by 25 mm-thick stickers

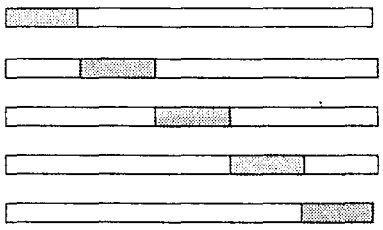

Configuration J
Effect of the size of the gaps between adjacent boards on the mass-transfer coefficients of the second board

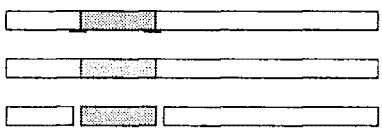

Configuration K
Effect of a thinner leading and trailing board on mass-transfer coefficient of the third board

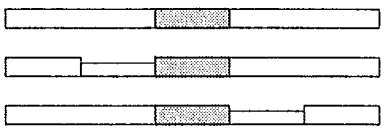

Run 8
Run 10/19
Run 11/18

WIND TUNNEL RUNS

Configuration L
25 mm-thick boards separated by 25 mm-thick stickers for a 500 mm-wide stack

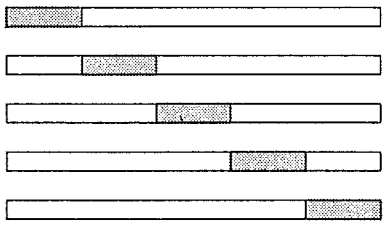

Run 49
Run 52
Run 51
Run 53
Run 50

Configuration M
3.02 m wide stack comprising 25 mm-thick boards separated by 25 mm-thick stickers

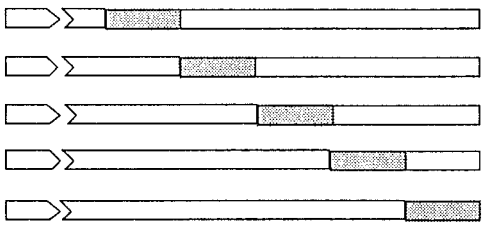

Run 61
Run 60
Run 59
Run 58
Run 57

Configuration N
Effect of a slit in the naphthalene coating on its mass-transfer coefficient for the second, third and fourth slab

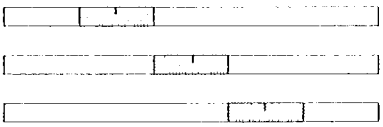

Run 54
Run 56
Run 55

A3 - Other results

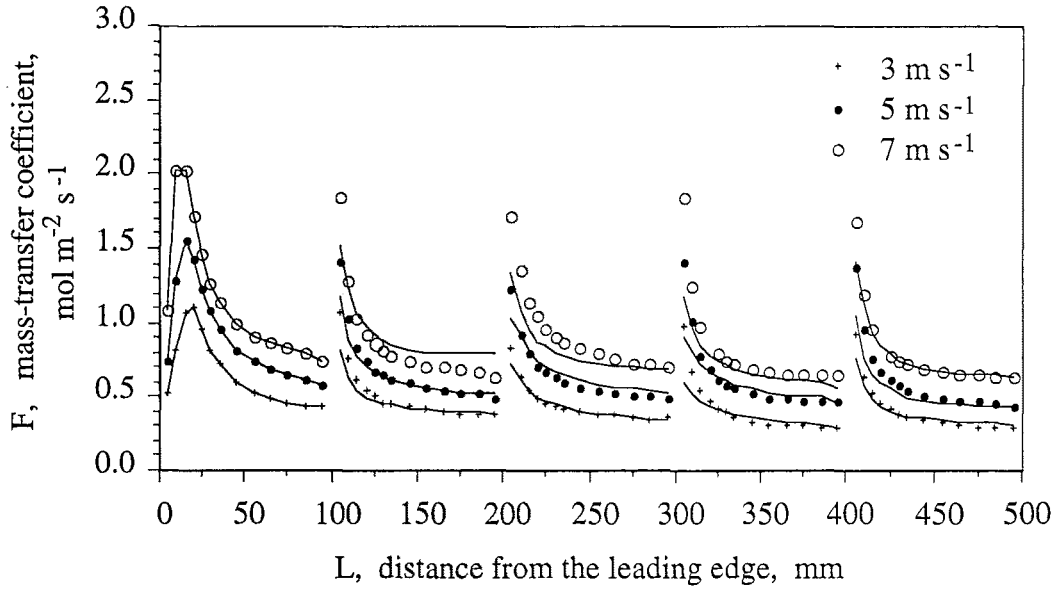

Figure A3.1 Sublimation profiles for a test layer with 5 mm-wide gaps between boards up to the leading edge of the test board for 3, 5 and 7 m s^{-1}. The solid lines represent corresponding profiles for an aligned stack.

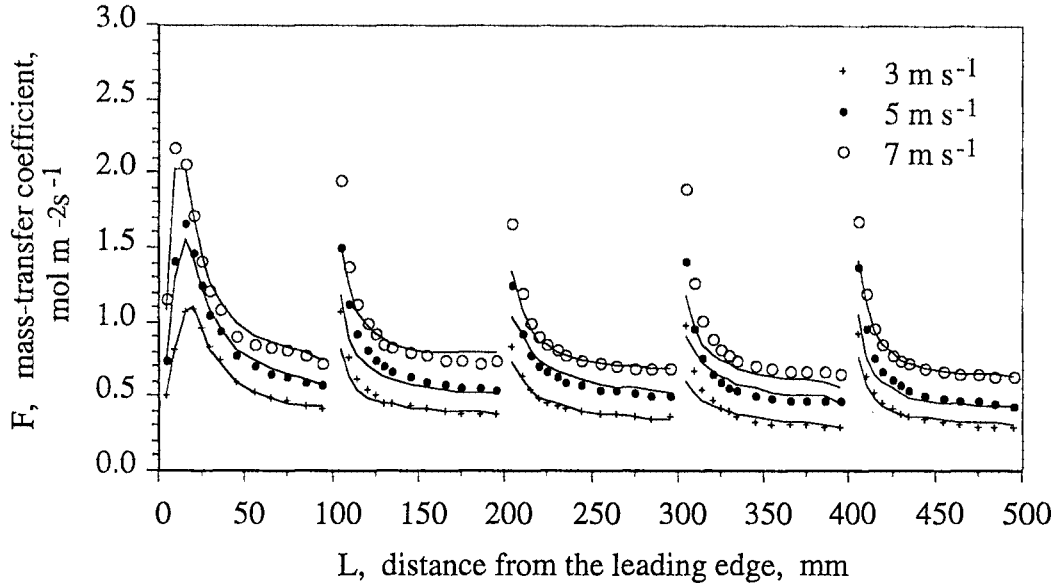

Figure A3.2 Sublimation profiles for a test layer with 5 mm-wide gaps between adjacent boards up to the trailing edge of the test board for 3, 5 and 7 m s^{-1}. The solid lines represent corresponding profiles for an aligned stack.

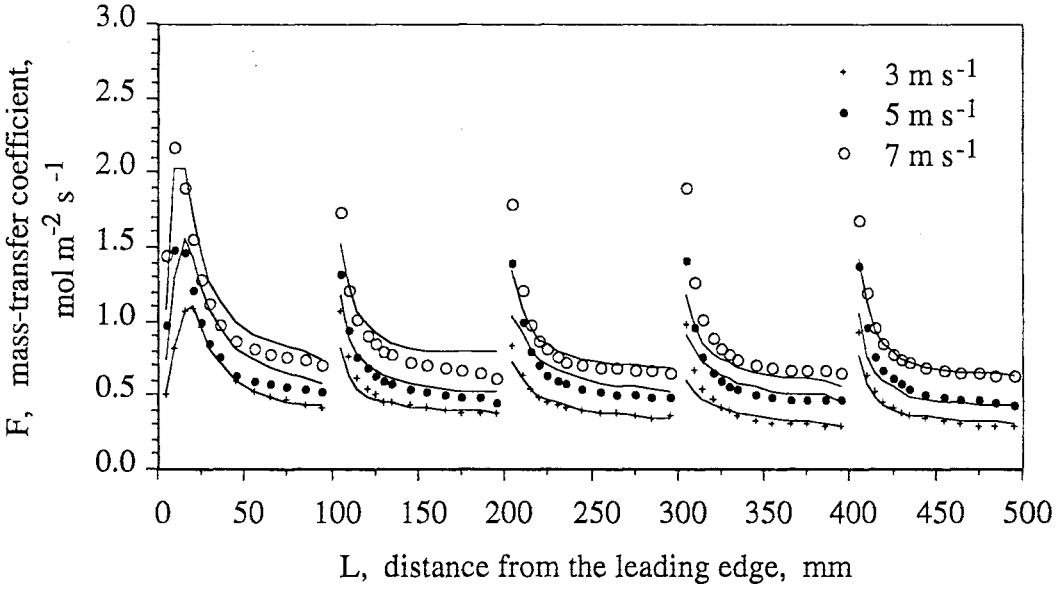

Figure A3.3 Sublimation profiles for a test layer with 5 mm-wide gaps between all adjacent boards for 3, 5 and 7 m s^{-1}. The solid lines represent corresponding profiles for an aligned stack.

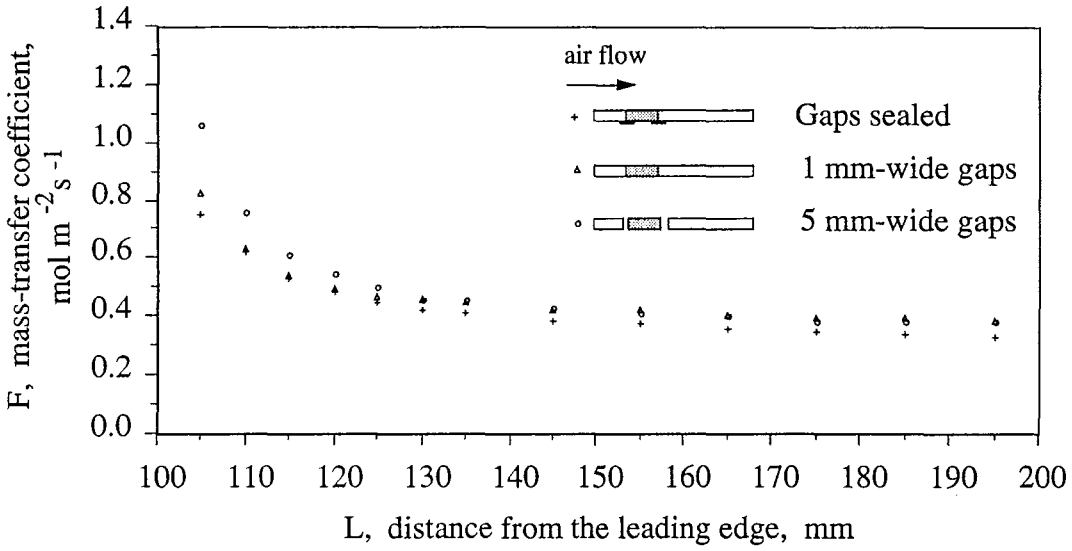

Figure A3.4 Effect of varying adjacent board-to-board gaps on the mass-transfer coefficient of the second board at 3 m s^{-1}

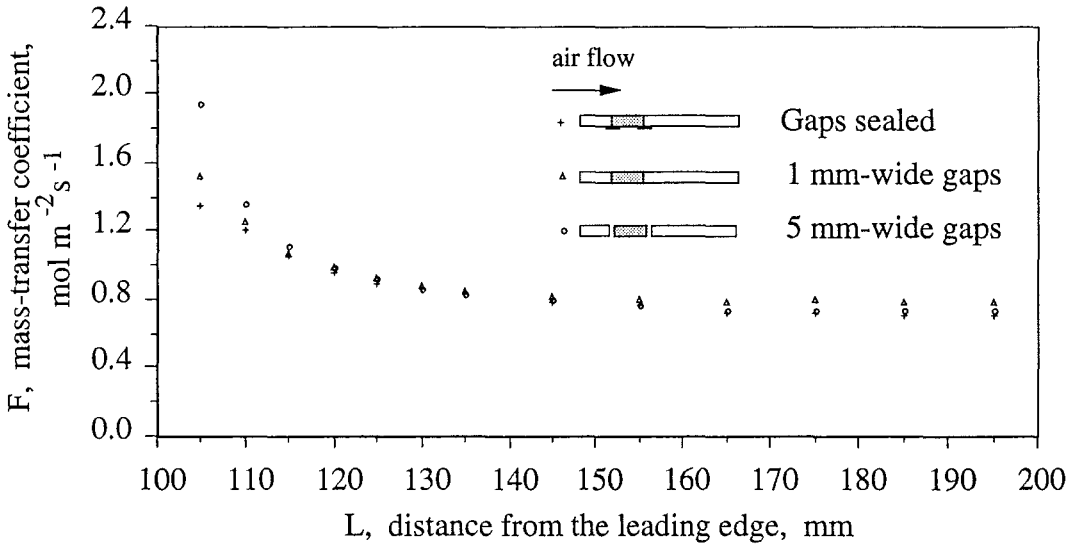

Figure A3.5 Effect of varying adjacent board-to-board gaps on the mass-transfer coefficient of the second board at 7 m s^{-1}

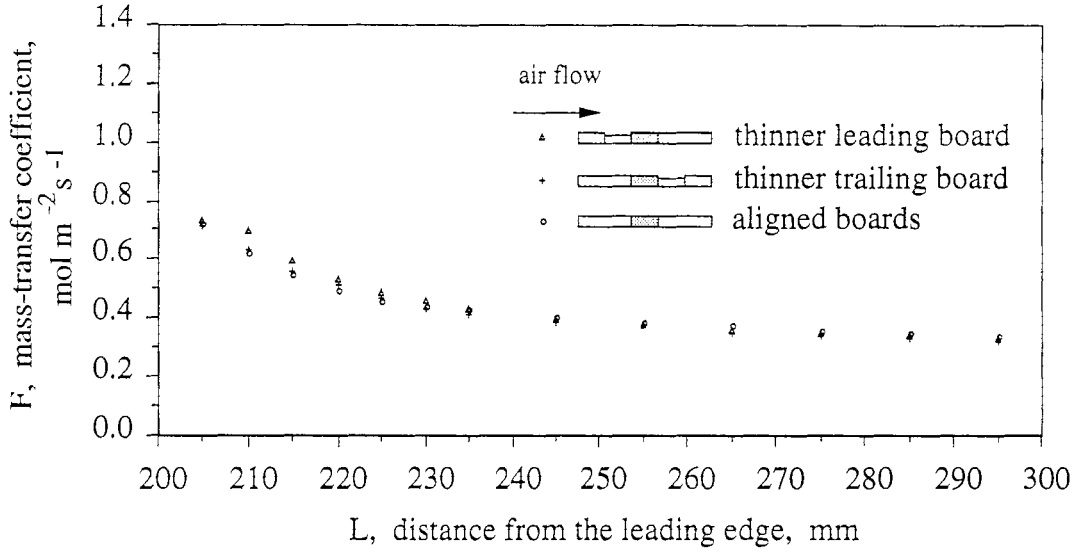

Figure A3.6 Effect of a thinner leading and trailing board on the mass-transfer coefficient of the third board at a velocity of 3 m s^{-1}.

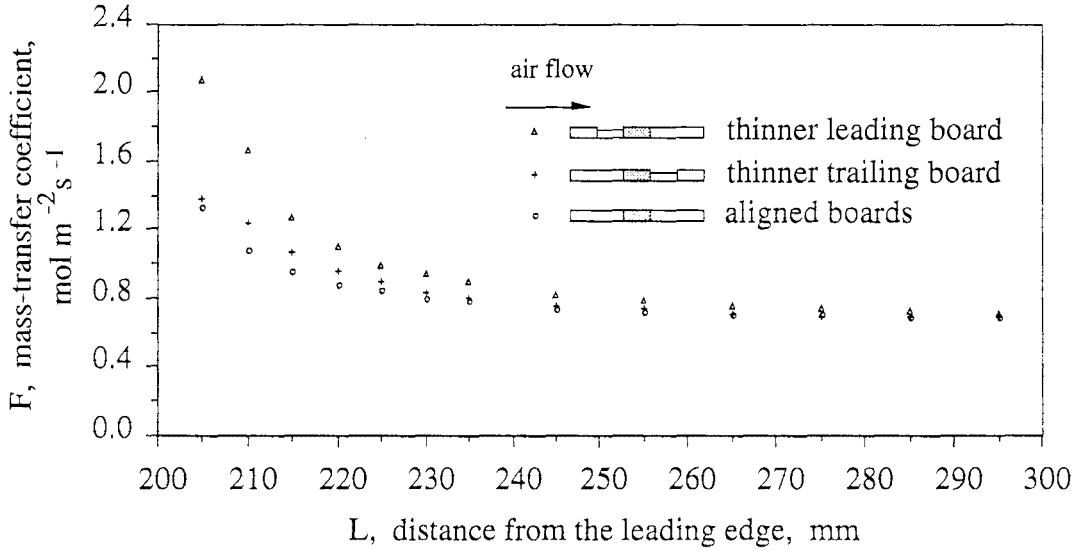

Figure A3.7 Effect of a thinner leading and trailing board on the mass-transfer coefficient of the third board at a velocity of 7 m s^{-1}.

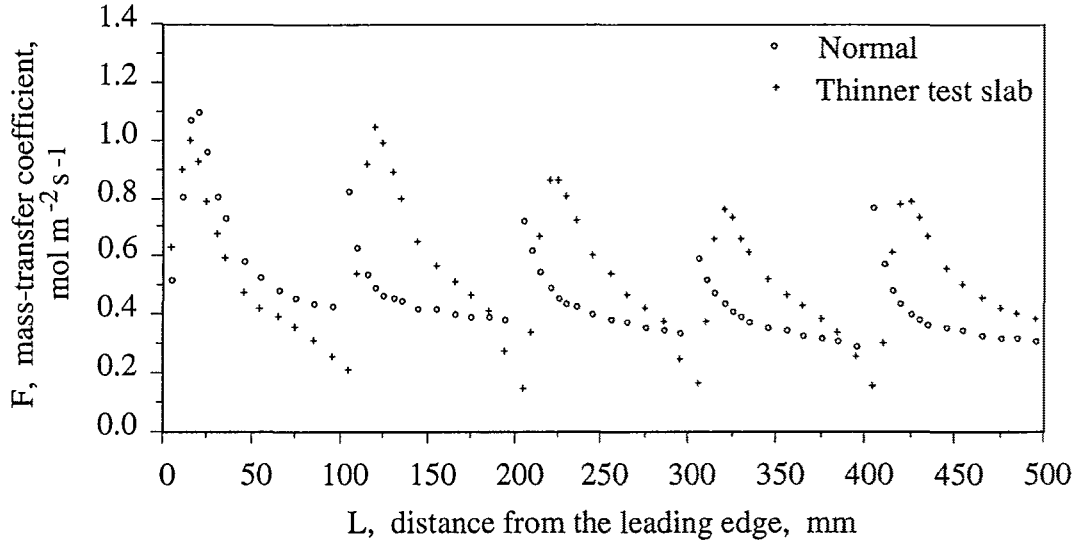

Figure A3.8 Effect of a thinner test slab than the adjacent dummy boards on the mass-transfer coefficient at 3 m s^{-1}

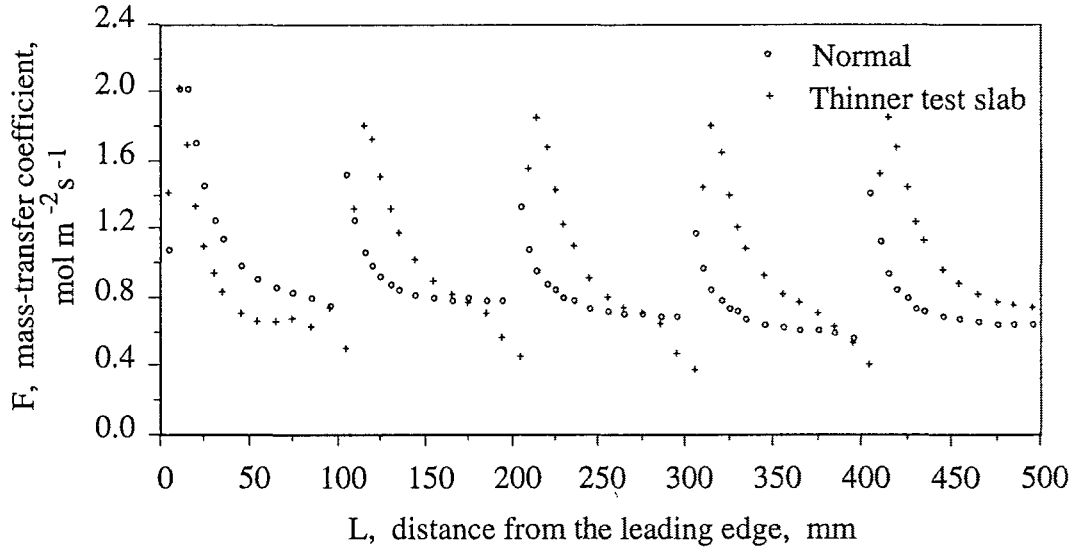

Figure A3.9 Effect of a thinner test slab than the adjacent dummy boards on the mass-transfer coefficient at 7 m s^{-1}

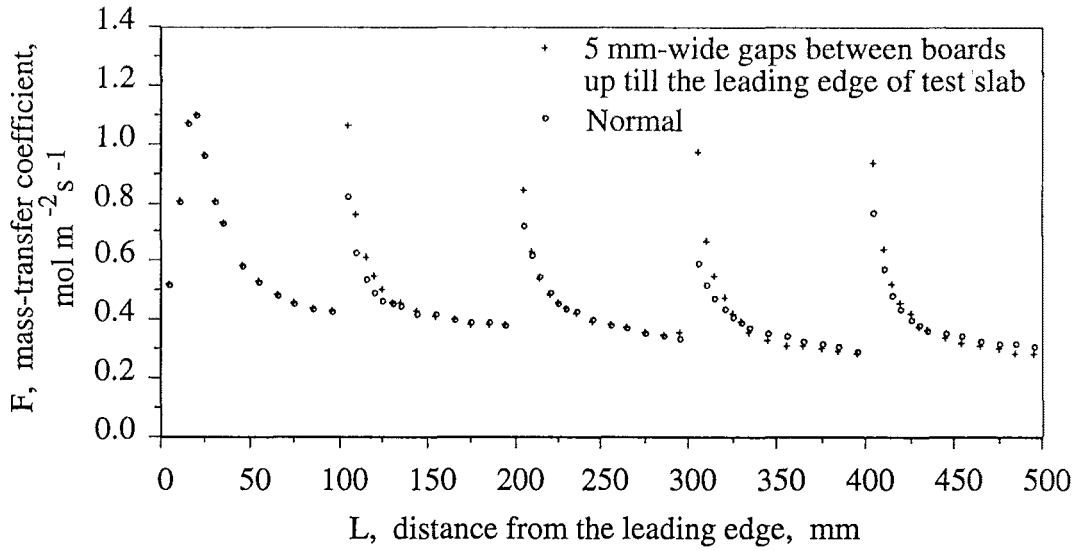

Figure A3.10 Effect of the 5 mm-wide gaps between boards up to the leading edge of the test slab on the mass-transfer coefficients at 3 m s^{-1}.

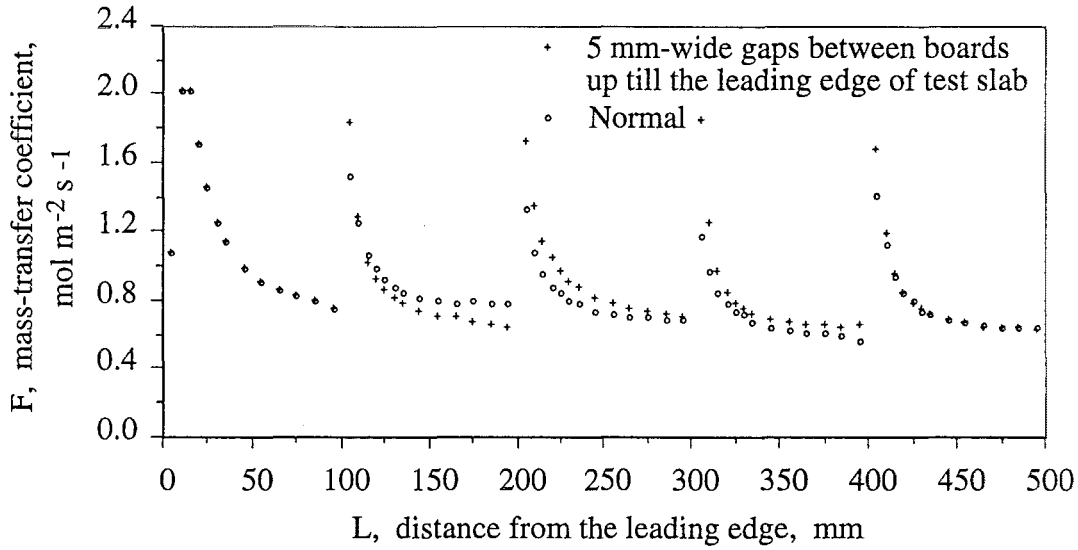

Figure A3.11 Effect of the 5 mm-wide gaps between boards up to the leading edge of the test slab on the mass-transfer coefficients at 7 m s^{-1}.

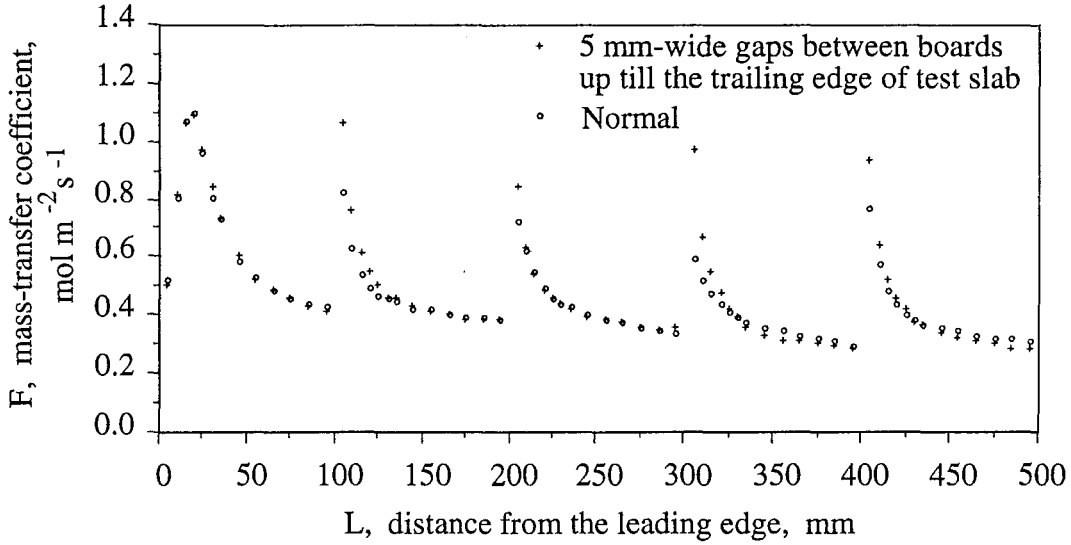

Figure A3.12 Effect of the 5 mm-wide gaps between boards up to the trailing edge of the test slab on the mass-transfer coefficients at 3 m s^{-1}.

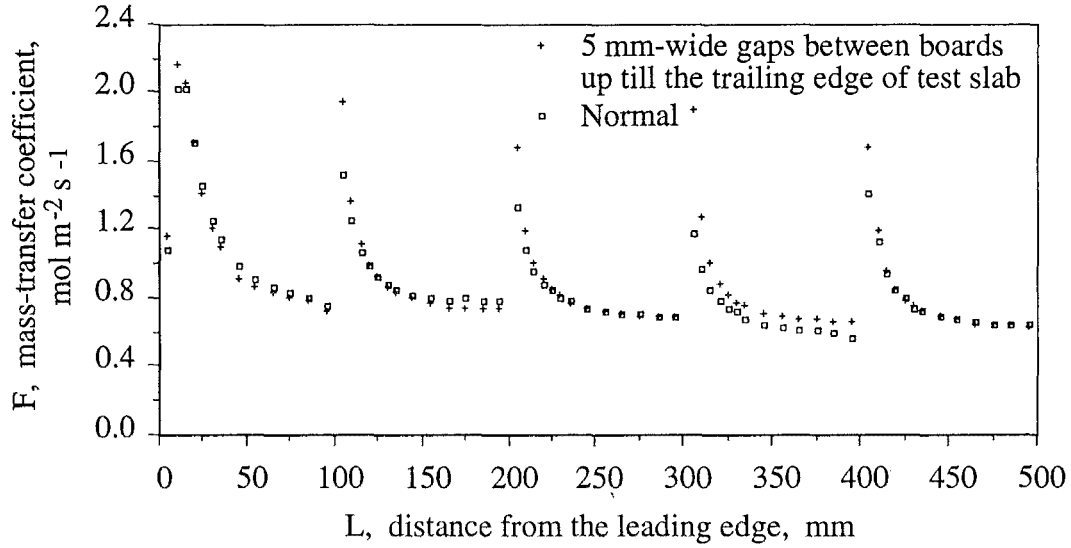

Figure A3.13 Effect of the 5 mm-wide gaps between boards up to the trailing edge of the test slab on the mass-transfer coefficients at 7 m s^{-1}.

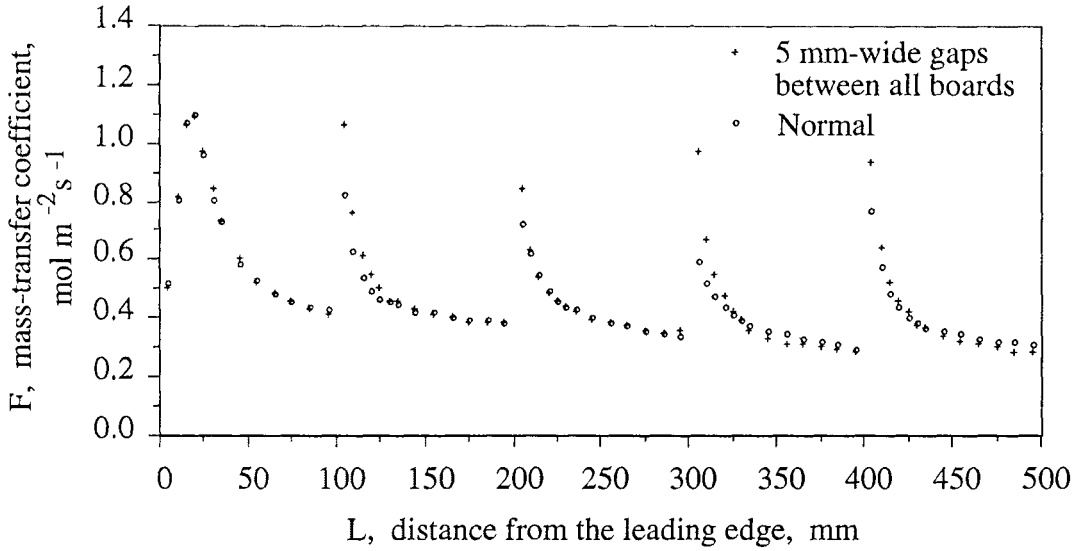

Figure A3.14 Effect of the 5 mm-wide gaps between all boards on the mass-transfer coefficients at 3 m s^{-1}.

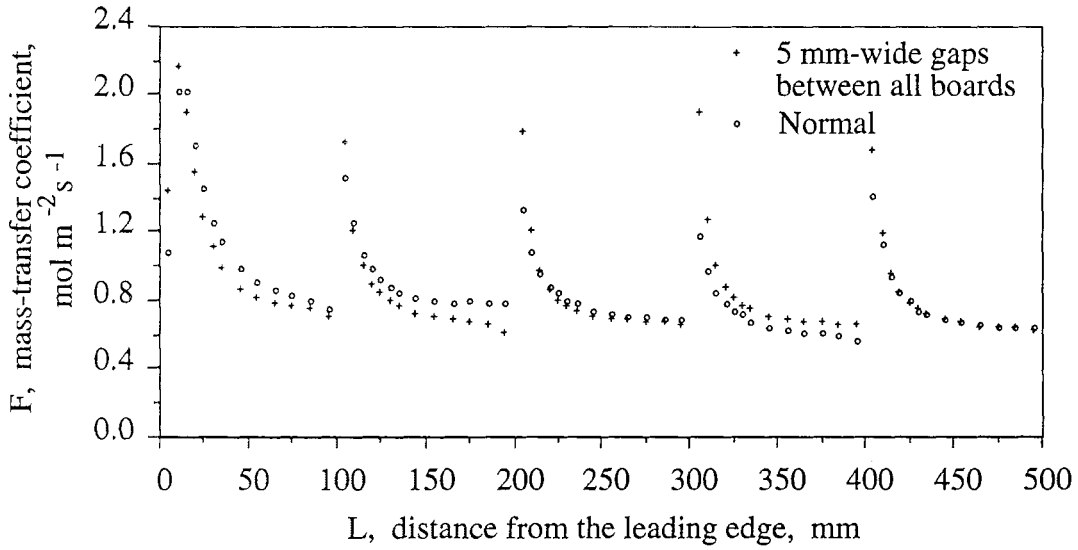

Figure A3.15 Effect of the 5 mm-wide gaps between all boards on the mass-transfer coefficients at 7 m s^{-1}.

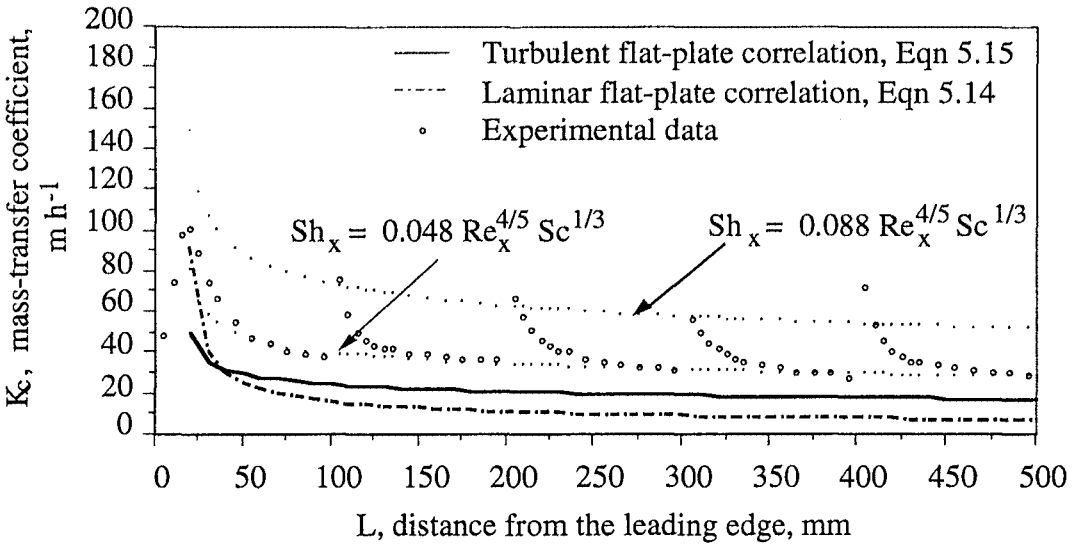

Figure A3.16 Comparison between the empirically-derived correlations and the experimental data for 3 m s^{-1}.

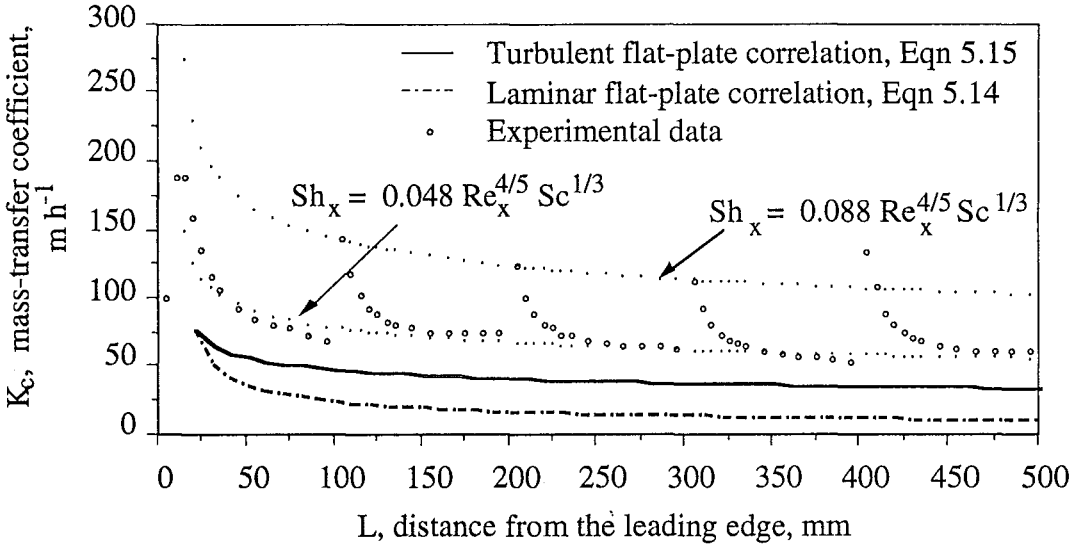

Figure A3.17 Comparison between the empirically-derived correlations and the experimental data for 7 m s^{-1}.

A4 - Comparing the constant in the Sherwood number

According to the heat-mass transfer analogy, Nusselt and Sherwood numbers can be generally expressed in the form as shown below,

$$Nu = f\,(\,Re,\,Pr,\,\chi_i\,)\ \text{and} \qquad (A4.1)$$

$$Sh = f\,(\,Re,\,Pr,\,\chi_i\,) \qquad (A4.2)$$

where

Nu is the local Nusselt number,
Sh is the local Sherwood number,
Re is the Reynolds number,
Pr is the Prandtl number, and
χ_i is the geometrical factor.

In the correlation of heat and mass-transfer data, Equations A4.1 and A4.2 are usually expressed as follows,

$$Nu = Pr^m\, g\,(\,Re,\,\chi_i\,)\ \text{and} \qquad (A4.3)$$

$$Sh = Sc^m\, g\,(\,Re,\,\chi_i\,) \qquad (A4.4)$$

thus,

$$Sh = (Sc/Pr)^m\, Nu \qquad (A4.5)$$

For blunt slabs like timber boards, m can assumed the value of 0.33, Pr = 0.7 for heat transfer in air and Sc = 2.57 for naphthalene diffusion in an air stream, Equation A4.5 reduces to

$$Sh = 1.536\ Nu \qquad (A4.6)$$

Sugawara *et al.* calculated his percentage increments based on his reference Nusselt number at a free-stream turbulence of 0.37%, which he found to be

$$Nu = 0.0194\ Re^{0.8} \qquad (A4.7)$$

and that the Nusselt levels off at 55% above this reference Nusselt number for free-stream turbulence levels exceeding 7-8%, corresponded to

$$Nu = 0.03007\ Re^{0.8} \qquad (A4.8)$$

On converting to Sherwood number, gives Equations A4.9 and A4.10 respectively.

$$Sh = 0.0298\ Re^{0.8} \qquad (A4.9)$$

and

$$Sh = 0.0462\ Re^{0.8} \qquad (A4.10)$$

Our experimentally-derived Sherwood number is,

$$Sh = 0.048\ Re^{0.8} \qquad (A4.11)$$

Thus, within the maximum experimental error of 4%, the constants in Equations A4.10 and A4.11 are fully consistent.

A5 - Instructions for using the TSI anemometer

Procedure for using the TSI modular anemometer system with a DISA probe

These steps are to be followed when using the TSI modular anemometer system with a DISA probe. A schematic diagram of the complete apparatus used for the determination of velocity and turbulence intensity can be found in Figure 3.2 in Chapter 3.

1 Disconnect the analog-to-digital converter lead before switching the computer and anemometer either on or off. Set the anemometer in Standby mode.
(The power surge caused when switching the computer and anemometer either on or off may damage the analog-to-digital converter. As a rule, it is best to connect this lead after switching anemometer on. Disconnect this lead immediately after using the anemometer before switching it off.)

2 Switch on the computer, the TSI modular anemometer (in Standby mode), the digital voltmeter, the oscilloscope, the Betz micromanometer and the calibrator.
(If the anemometer is to be used everyday, it is best to leave the anemometer switched on in Standby mode. Disconnect the analog-to-digital converter lead before switching the computer off.)

3 Remove the hot-wire probe if it is already inserted in the probe support, and again with the anemometer set in the Standby mode.

4 Connect the analog-to-digital converter lead.

5 When the computer is switched on, it should be at MS-DOS. At the C> prompt, type **CD\PCLDAS\BASIC**. Type **GWBasic** after the C> prompt to get into GWBasic. The computer is now ready for either calibrating the anemometer or for gathering velocity and turbulence intensity. (see the following sections for more details.)

6 Insert the shorting probe in the probe support, and set Resistances to zero.

7 Set the Meter Range to 0 - 10 volts Bridge Output.

8 Adjust Ref Set to give a reading of approximately 3 volts. Turn the Meter Range Dial to 0 - 3 volts Bridge Output and use the Ref Set to fine tune the reading to 3 volts if the need arise. The digital voltmeter and oscilloscope can be used to aid this fine tuning process.

9 Push the Res Meas button and adjust the Zero Ohms Pot to take out all needle deflections.

10 Set Decades to a nominal value of 3 ohms.

11 Insert the DISA probe in the probe support.

12 Push the Res Meas button and adjust the Decade Resistance until there is no needle deflection. Use the digital voltmeter and oscilloscope to fine tune this process. This is the resistance of the probe, R.

13 The operating resistance of the probe, R_{op} can then be calculated as shown below

$$R_{op} = R (\alpha + 1), \text{ where } \alpha \text{ is the overheat ratio} = 0.8.$$

14 Set the decades to R_{op}.

15 With the decades set and the hot-wire inserted, turn the anemometer to Run Linear Output.

16 Set Linear Output to 0 - 300 volts.

17 Introduce a step input by blowing directly into the hot-wire to give a zero reading.

18 With no airflow, adjust the Linear Zero to give a nominal reading of 0.030 volts.

At this stage, the anemometer is ready for use. If the anemometer has been calibrated before and the operating conditions have not changed significantly, it can be used for data acquisition straight away.

A - Calibrating the anemometer

19 Zero the Betz micromanometer.

20 Type **Load"HWCALCHE** to load the software for calibrating the anemometer.

21 To run it, type **Run.** A series of questions will be asked on the screen. Type in the following responses (in bold), following the C> prompts,

(a)	Units °C/°F	**C**
(b)	Gas temperature	**x** (in °C)
(c)	Atmospheric pressure	**y** (mm Hg)
(d)	Voltage source	**2**
(e)	Analog-to-digital channel	**0**
(f)	Voltage values	**100 - 200** (max.)

(g)	Frequency $\approx \frac{1}{40}$ of sampling capture rate (see 23 (c) below)	**25** Hz
(h)	Velocity source	**2**
(i)	Pressure source	**1**
(j)	Pressure units	**3**

The software requires a minimum of four readings before it is able to linearise the data. For best results, it is recommended that the pressure drop over the calibrator be increased (or decreased) by a factor of four. Do not take readings beyond calibrated range.

(k)	Print data	**Y**es or **N**o
(l)	Save voltage-velocity data (intercepts in the range of -0.3 to +0.3 are acceptable)	**Y** or **N**
(m)	File name	type a filename
(n)	Save calibration constants	**Y** or **N**
(o)	File name	type a filename
(p)	Probe serial no. (for identification purposes)	type a number
(q)	Room temperature resistance	**R** Ohms
(r)	Operating resistance	$\mathbf{R_{op}}$

You have now calibrated the anemometer. If you wish to stop here, set the anemometer to Standby mode. Disconnect the analog-to-digital lead before parking the harddisk.

To park harddisk, type the following at the C> prompts,
Control C to stop program to return to BASIC.
System to get back into MS-DOS.
CD to get to the root directory.
Park to park harddisk.
Switch off the computer.

B - Using the anemometer for data acquisition

22 Type **Load"HWACQCHE** to load the software for data acquisition using the anemometer.

23 To run it, type **Run**. A series of questions will be asked on the screen. Type in the following responses (in bold), following the C> prompts,

(a)	Calibration information	filename as in 21 (o)
(b)	Hot-wire voltage from	**2**
(c)	Sampling frequency	**1000** Hz
(d)	Analog-to-digital channel number	**0**

(e) Number of samples **500**

(f) Sample at single location? **1**
or at typed position? **2**

The anemometer is now ready for data acquisition. At the end of the session, a number of questions will be asked.

(g) Do you want to print the velocity data? **Yes or No**
If answer is **Y**, the print out will be in the following format

Data	Velocity	Voltage
-	-	-
-	-	-

(h) Do you want to print VBAR, SD, TI and VP? **Yes or No**
If answer is **Y**, the print out will be in the following format

Position	Mean vel.	Std. Dev.	T.I	Mean Voltage
-	-	-	-	-
-	-	-	-	-

(i) Do you want a listing of others? **Yes or No**

(h) Do you want to plot graphics? **Yes or No**

If you have finished using the anemometer, set it to Standby mode. Disconnect the analog-to-digital lead before following these steps to park the harddisk.

Type the following at the C> prompts,
Control C to stop program to return to BASIC.
System to get back into MS-DOS.
CD to get to the root directory.
Park to park harddisk.
Switch off the computer.

RECENT DEVELOPMENTS IN HIGH-TEMPERATURE KILN DRYING OF TIMBER

P.C.S. Kho,
Department of Chemical and Process Engineering, University of Canterbury, Christchurch, New Zealand.

ABSTRACT

Demand for wood and wood products is expected to increase by 28% by the year 2000. With such anticipated increase in timber demand, innovative drying technologies are being explored to produce quality timber products more efficiently. Amongst the promising processes, high-temperature kiln drying is receiving particular attention. This paper discusses some of these developments.

1.0 INTRODUCTION

The consumption of sawn timber in the world is increasing steadily. According to FAO's prediction (Whitehouse, 1988), this is expected to increase by at least 28% from that in 1984 by the year 2000 (figure 1)

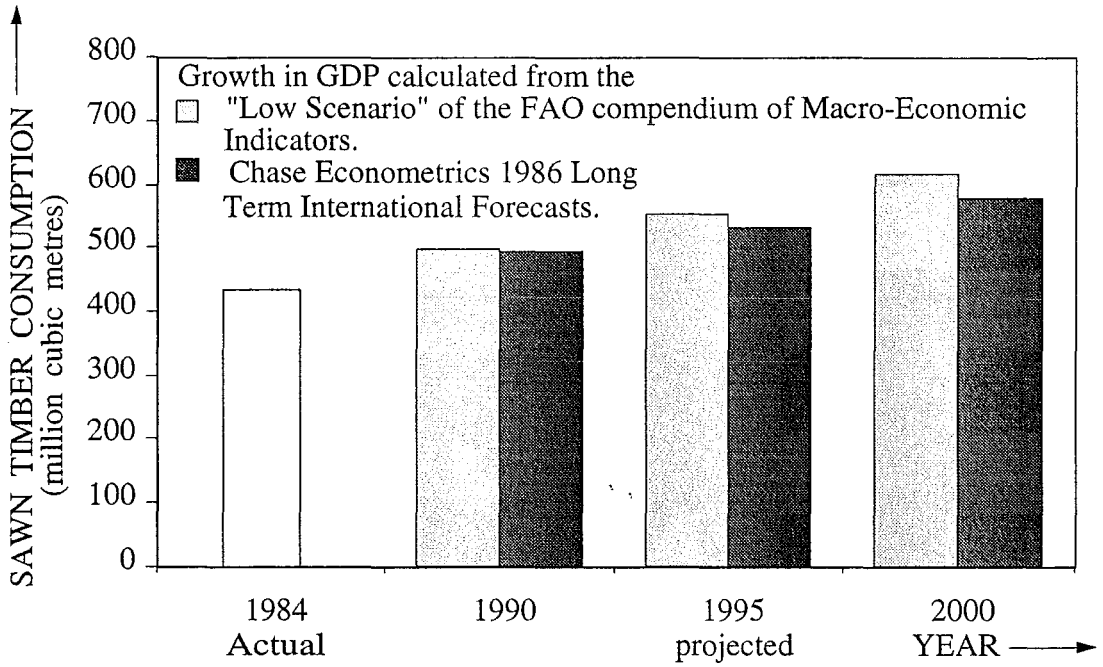

FIGURE 1 FAO projected consumption of sawnwood and sleepers

Drying uses some 40 to 70% of the total energy consumed in processing of sawn timber from the log to the final product (Rosen, 1981). The massive energy requirements and the increasing demand for wood has prompted researchers to develop innovative technology to dry wood more efficiently.

Although conventional kilns will continue to play an important role in wood drying, newly constructed kilns will emphasize energy savings, reduction in drying degrade and decrease in drying time (Simpson, 1983-84). Beside constructional improvements to ensure more uniform drying and better product quality, modifications such as increasing drying temperatures, schedule modifications, computer control of the process and the early detection of failure of wood are likely to be used.

The purpose of this paper is to discuss such developments in high-temperature drying.

1.1 Basic theory

Wood is a hygroscopic capillary-porous material (Keey, 1972), with water occurring in three forms - liquid (or free) water in the cell cavities; water vapour in the cell cavities and bound (or hygroscopic) water in the cell walls.

The drying of wood is a critical process in which water is carefully and systematically removed from the wood using empirically determined schedules. It involves a dynamic balance between heat transfer from the bulk air stream to the surface of the wood, surface evaporation from the wood, diffusion of moisture through wood and mass flow of free water and vapour in the wood.

The drying curve of wood can be divided into three distinct regimes (figure 2) - a constant rate period followed by two falling rate periods (Adesanya et al, 1988).

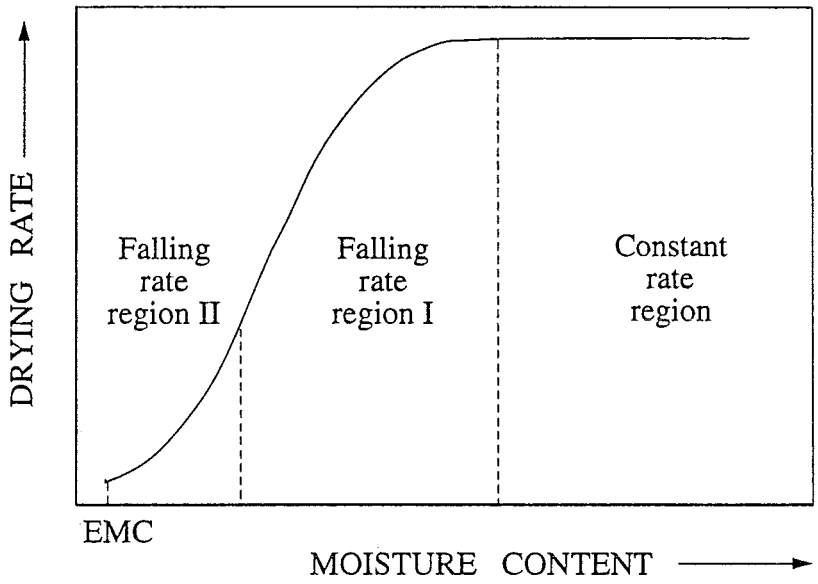

FIGURE 2 Theoretical drying curve for a hygroscopic porous material

The constant rate period, where drying rate is essentially independent of time, is externally controlled by the rate of heat transfer to the wood surface. Moisture evaporates at the surface and mass flow of free water continues to move from the interior to the surface through the capillary structure of the cell cavities and the interconnecting pits as wood dries. The first falling rate period, where the change in moisture content is a linear function of the square root of time, begins when the moisture content of the surface falls below the fibre saturation point (fsp) and the region at fibre-saturation point or below is no longer confined to the surface. The evaporation front or wet-line retreats within the wood resulting in a wet zone sandwiched between two drier zones. In each drier zone adjacent to the surface, which is below fibre saturation point, moisture migration will be by bound water diffusion across the cell walls and vapour diffusion across the cell cavities, supplemented by mass flow of vapour through pit pores if the wood is permeable and when the temperature of the drier zone exceeds the boiling point temperature. In the wet zone, moisture migration will be by capillary action in permeable woods (Hart, 1975). During the first part of the final falling rate period, the extent of drying is a linear function of the square root of time. This occurs after the evaporation front has receded to the centre of the wood. No more free water remains in the wood and moisture migration takes place solely by bound water diffusion and vapour diffusion, until an equilibrium moisture content (emc) is reached.

High-temperature kiln drying, applied for over a century, is a major improvement to traditional kiln drying technology. It reduces drying time by increasing the dry-bulb temperature to above 100°C. Generally, high-temperature drying requires about 10% less

energy and wood dries 2 to 5 times faster (Rosen, 1981). Though high-temperature drying compares favourably to conventional kiln drying (figure 3), associated drying problems such as increased timber warpage, timber discolouration and kiln deterioration have yet to be fully solved.

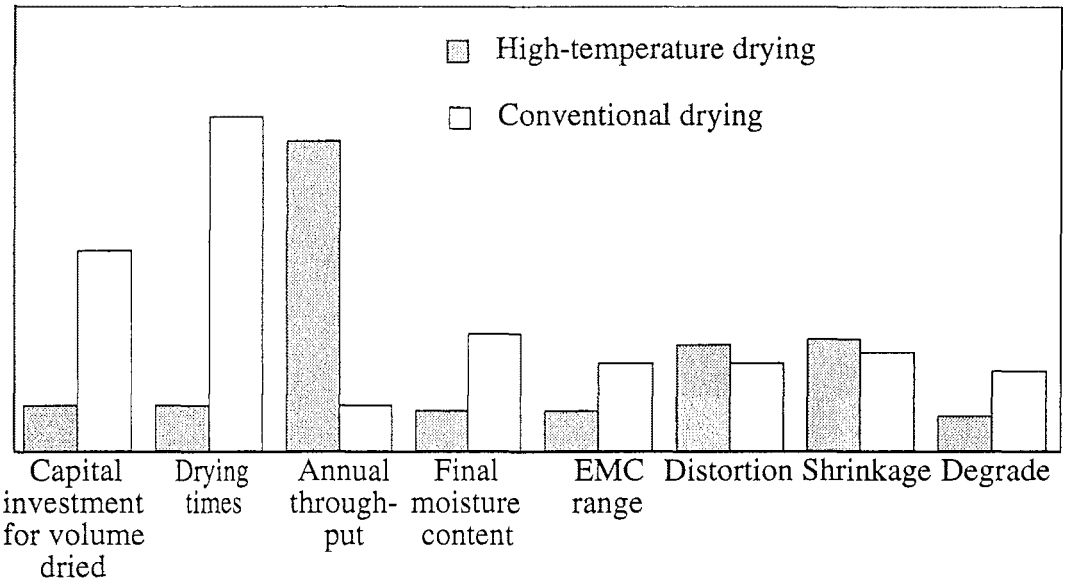

FIGURE 3 High-temperature drying Vs Conventional drying
(Comparisons are approximate only) (After Williams, 1983)

The ever-increasing demand for quality sawn timber and the growing awareness of the need to conserve valuable energy resources have led researchers to modify the kiln structure and evaluate the drying process so as to achieve an improved overall drying efficiency.

2.0 INNOVATIONS IN KILN DRYING

2.1 Kiln conditions

The process of drying wood involves the removal of moisture from the wood surface as well as its movement from the interior of the wood to the surface. The relative balance between the two determines the influence of controllable factors, namely heat input, humidity levels and air circulation, upon the drying process. By suitably controlling these three parameters, timber can be dried efficiently. The cheapest method to accelerate drying is to reduce humidity level while increasing air velocity through the stack is the most expensive (Bachrich, 1980).

2.11 Temperature: Increasing temperature will increase evaporation and the rate of diffusion of either vapour or liquid moisture, and hence decrease drying time over all periods of drying. Though most softwood and some hardwood have been successfully kiln-dried at dry-bulb temperatures of up to 150°C, research is continuing to explore the possibility of using even higher dry-bulb temperatures (up to 180°C) to reduce drying time further (Tronstad, 1983).

2.12 Air circulation: Air is the drying medium in kilns and has two main roles:-
(i) as a heat carrier to supply sufficient heat to the timber, and
(ii) as a moisture carrier to remove moisture (water) and other volatile substances.

Good baffling systems and a uniform minimum air velocity, able to achieve (i) and (ii) above, will ensure more uniform drying and better product quality. Attention should be paid to regular stacking arrangements, with uniform stickers to get equal air gaps.

For kilns equipped with variable-speed fans, a high air velocity and low temperature will be used initially from green to fibre saturation point and a low air velocity and high-temperature is used from fibre saturation point to final moisture content. Results from laboratory tests have indicated a reduction of 25% in drying time compared to schedules using non-varying temperature and air velocity, without any appreciable increase in defects (Bachrich, 1980).

Equal periodic fan reversals will ensure uniform heat and air distribution across the stack. Though this will result in milder overall drying condition, an increased wet-bulb depression will increase drying rate, hence reduce drying time. Not many flow reversals are needed, however, throughout the drying process to achieve near uniformity in board-to-board moisture contents, although frequent reversals (say every 2 hours) are sometimes advocated.

2.13 Development of theory: The theory of kiln drying at low temperatures (dry-bulb temperature less than 100°C) has been well explored by Ashworth (1977). Less is understood about the mechanism of drying at temperatures above 100°C, and such understanding will be needed to provide guide-lines for the optimization of high-temperature schedules.

2.2 Kiln

2.21 Energy source, conservation and recovery

The energy intensive process of drying wood requires about 40 to 70% of the total amount of energy used in processing sawn timber from log to the final product. Thus, any savings of energy in drying would have considerable impact on the overall needs of the timber industry.

A significant change to anticipate is the generation of energy using wood-waste to supplement the energy requirements of the timber industry. Wood-waste fired kilns can be directly heated or heated through heat exchangers (table 1). This cheap way of generating energy from a readily available source has the advantage of getting energy for drying while reducing the problem of waste disposal. In United States alone, utilization of wood-waste for fuel accounts for approximately 40% of the total energy consumed in the timber industry (Rosen, 1981). However, changes in the design of steam boilers, timber handling systems and electrical generation is needed before extensive use of wood-waste can be utilized in this way.

MEDIUM	Heating medium temp. °C	Add. humidity	Heat exchanger	Vent control	Direct fired	Constant bleed to atmosphere	Most suitable for
Woodwaste Direct fired	204	Optional steam or water	No	Yes	Yes	Yes	Medium to High Temp. Low Humidity
Woodwaste fired with heat exchanger	538	Optional steam or water	Yes	Yes	No	No	Medium to High Temp.
Woodwaste fired heat exchanger with heating oil	204 to 260	Optional steam or water	Yes	Yes	No	No	High Temp.

TABLE 1 Methods of heating using woodwaste (After Bachrich, 1980)

Other energy-conservation methods include improvements to the kiln structure to eliminate leaks near doors and vents, and the use of better insulating material and high heat reflecting surface inside the kiln (Bachrich, 1980).

Waste heat from the vent exhausts of high-temperature kiln can be recovered through the use of heat exchangers, to preheat incoming air to the kiln, to supply supplement heat to conventional kilns or to provide heat to dry wood-waste which is to be used as fuel. Considerable savings of 12 to 15% over conventional methods can be achieved (Rosen, 1981).

The concept of using vapour recompression in kiln drying, which is capable of reducing energy demand by as much as 65% of the total energy used in conventional drying, is being explored (Miller, 1977). Experimentation at pilot plant level is necessary to verify its suitability to dry timber.

Drying should cease once the average moisture content of the sawn timber is within the limits specified in standards. Overdrying will result in energy wasted and loss of revenue owing to loss of "saleable" moisture.

2.22 Restraint and stacking
Increased timber warpage due to elevated dry-bulb temperatures can be minimized if stacking is done properly and stack is dried under restraint.

A lightweight stack filleting frame, originating from Australia, consisting of a bar of square section steel (25 mm) with slots attached to align the fillets above the bar and hold the frame in place below the bar can be used to achieve quality stacking in small timber mills (Haslett, 1988).

It is important that supports under the stacks are level, square and not more than 600 mm apart. Stickers should be of uniform thickness and length, and aligned vertically above the supports. The last sticker must be as close as possible to the end of the stack, with the ends and sides of the stacks flush and vertically aligned. For uneven length boards, the ends must be supported on stickers, and where possible, length sorting should be done to ensure a more solid stack, which in turn will reduce moisture content variation and warping (Bester, 1982).

Restraints capable of delivering at least 1000 kg m^{-2} uniformly (Bester, 1982 and Kinimonth and Williams, 1984) over the entire horizontal area of the stack will reduce warping in the first few upper layers of the stack while warping occurring in the rest of the stack will depend almost entirely on the efficiency of the stacking.

2.3 Continuous kilns

The recent success in high-temperature drying of softwood have rekindled the researchers' old dream of a continuous timber dryer, which had been abandoned owing to long drying times under conventional schedules. Continuous kilns have the advantage of being simple in design where maximum volume of timber can be accommodated with minimum fan equipment. Handling is simplified as small amounts of timber are loaded and unloaded continuously (Bachrich, 1980).

The Australian CSIRO has developed a vertical continuous feed kiln (figure 4), that can dry and stress-relieve 42 mm thick radiata pine boards in 16 hours. This kiln has two major advantages over compartment-type kilns, namely, lower operating cost and increased productivity. These are achieved through :-

(i) elimination of tedious manual stacking and unstacking,
(ii) avoidance of the usual handling operations from green to final dried state of the timber,
(iii) reduction in the stock of stickers,
(iv) elimination of stack weights and associated handling equipment,
(v) greater thermal efficiency of the kiln.

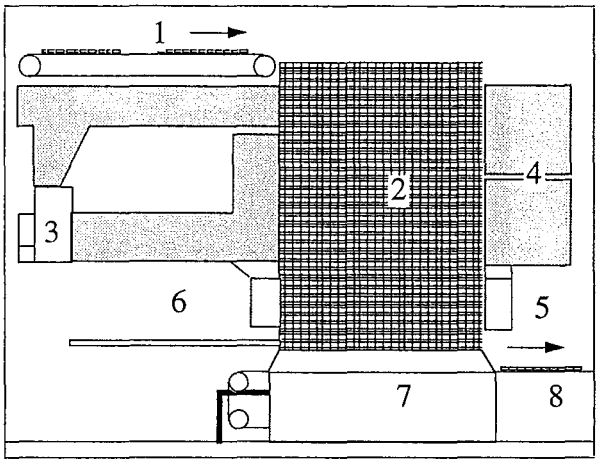

1 Green Timber feed conveyer
2 Timber stack
3 Hot air circulation fans
4 Hot air circulation ducts
5 Steaming compartment
6 Timber unloading tynes
7 Timber unloading table
8 Dry timber discharge

FIGURE 4 The Continuous Timber kiln developed by the Australian CSIRO
(After Christensen and Northway, 1978)

Koch and Wellford (1977) have developed a continuous tunnel dryer to dry 44 mm thick southern pine in the United States. The stack of timber is moved continuously through a zone-controlled tunnel at 132°C with air velocity of 8 ms^{-1} for 8 hours. It is then conditioned for 3 hours at 91°C and cooled for another hour before discharge.

2.4 Control of the drying process

Recent advances in integrated circuits and micro-processor technology have reduced the cost of the electronic components necessary to automate kilns. As such, computer control of dry kilns, is becoming attractive, with the advantages of increased product quality and reduced manpower needed to operate the kiln. Computer control provides continuous regulation of the drying process through feedback of data on wood moisture content and the temperature and humidity inside the kiln.

Process control in timber drying is based on some estimate of the moisture content of the boards. At the present, cumbersome manual sampling procedures or inexact time-based procedures are used. However, for kilns to be successfully automated, continuous on-line moisture content readings are needed. The development of equipment capable of doing this accurately is still being investigated (Simpson, 1983-84). Psychrometers, capable of measuring humidities at dry-bulb temperatures up to 180°C are being developed (Kent and Rosen, 1983-84).

In wood drying, the limiting factor is the development of stresses in the wood that lead to drying defects. Several ways of monitoring these stresses to provide warning signals that drying defects are about to occur have been researched. In this way, one could maximize drying rate while being able to control degrade at the maximum acceptable level.

For example, acoustic emissions from micro-cracks in timber drying can be used as an early warning signal of drying defects. The rate of drying and occurrence of surface cracks are related to the amplitude and number of acoustic emissions (Honeycutt et al., 1985, Masami et al., 1983 and Shigeru et al., 1984). If a reliable correlation between defects and acoustics emissions can be developed, then drying time can be minimized at an acceptable level of degrade.

When wood dries, surface fibres dry and shrink before the interior fibres, resulting in a differential strain between the shell and the core. This can be measured at the edge of a board by using a differential strain gauge developed by Hill (Simpson, 1983-84). As drying progresses, the differential strain increases to a maximum before beginning to decrease again when the core starts to dry and shrink. Its success in controlling the process of drying depends on whether strain data collected can be correlated with the development of drying defects.

The development of dry kiln schedules using the Shrinkage-Strain-Control (S-S-C) method, proposed by Bello and Kubler (1975), is based on the hypothesis that if the unrestrained shrinkage of the wood from green to a certain moisture content exceeds its fracture strain in tension perpendicular to the grain under the same conditions, fracture will occur. The curves relating unrestrained shrinkage to moisture content at different temperatures are superimposed on the curves relating to fracture strain in tension to moisture content at the same temperatures, the intersection should give the limiting conditions for the prevention of surface checking during drying (figure 5). The corrected drying schedule for northern red oak compares well with results based on extensive drying tests of similar boards.

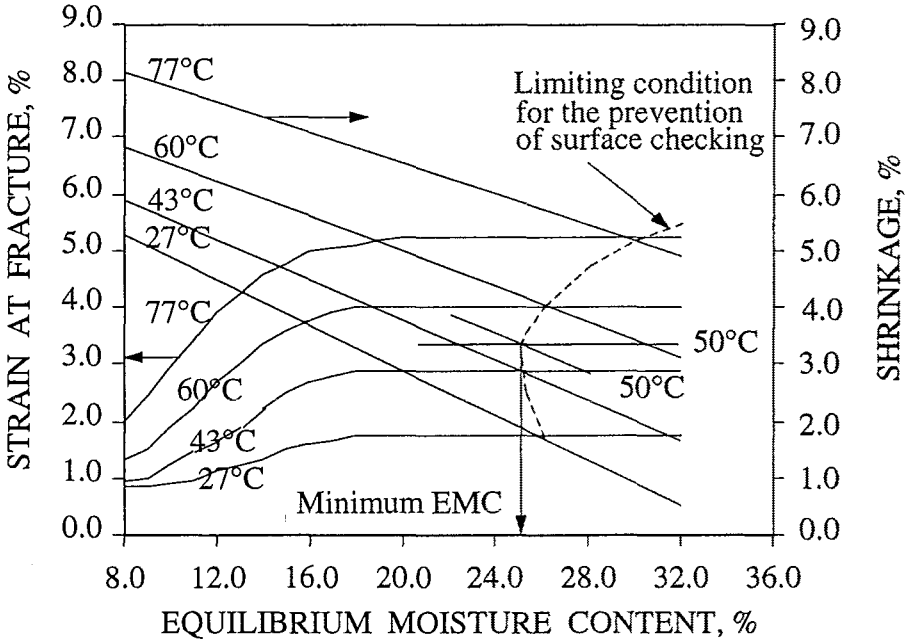

FIGURE 5 Method of determining initial drying conditions for northern red oak (After Bello and Kubler, 1975)

Another method for determining drying times for high-temperature drying is the temperature-drop-across-the-load-method (TDAL) proposed by Wengert (Rosen, 1984). The temperature of the air drops from the leading edge to the trailing edge of the stack as air passes through the stack. The magnitude of this drop is dependent upon the rate of evaporation from the wood surface. Drying is terminated at a specified TDAL, which correlates well with final moisture content.

3.0 CONCLUSION

With recent advances in the micro-chip and high-temperature drying technology, computerized control of high-temperature kiln drying (compartment or continuous) is becoming an attractive option in the future .

Several methods of process control are being investigated. With innovative modifications to kiln arrangements and careful manipulation of the controllable parameters, drying times can be reduced with lower energy demands while still achieving an acceptable level of board degrade. Models of the high-temperature drying process are needed, however, to enable the process to be optimized with regard to energy efficiency and minimizing degrade.

REFERENCES

ADESANYA, B.A., NANDA, A.K. AND BEARD, J.N., Drying Rates during high-temperature drying of yellow poplar, Drying Technology 6(1), 95-112 (1988).

ASHWORTH, J.C., The Mathematical Simulation of the Batch-drying of Softwood Timber, Ph.D. Thesis, University of Canterbury, New Zealand (1977).

BACHRICH, J.L., "Dry Kiln Handbook", H.A. Simons (International) Ltd., Vancouver, B.C., Canada (1980).

BELLO, E.D. AND KUBLER, H., Shrinkage-Strain-Control (S-S-C) - A new approach to the Process of kiln-drying wood, Wood Science 7(3), 191-197 (1975).

BESTER, A.B., Practical Drying Techniques to reduce warp, Paper presented at the Proceedings of the Jubilee Symposia, Mededeling Communication 98 (11), 730-740 (1982).

CHRISTENSEN, F.J. AND NORTHWAY, R.L., Development of the CSIRO Continuous Feed Kiln for Sawn Timber to the commercial evaluation stage, Australian For. Ind. Journal (1978).

HART, C.A., "The Drying of Wood", The North Carolina Agricultural Extension Service, Ext. Cir. 471 (1975).

HASLETT, T., Stack Filleting Frame, Wood Processing Newsletter, Issue No. 4 (1988).

HONEYCUTT, R.M., SKARR, C. AND SIMPSON, W.T., Use of acoustic emissions to control drying rate of red oak, Forest Products Journal 35(1), 48-50 (1985).

KEEY, R.B., "Drying Principles and Practice", Pergamon, Oxford (1972).

KENT, C.A. AND ROSEN, H.N., Measurement of Humidity above Temperature of 100°C with a double-wick Wet Bulb Psychrometer, Drying Technology 1(1), 141-150 (1983-1984).

KININMONTH, J.A. AND WILLIAMS, D.H., High-Temperature drying of radiata pine - New Zealand Experience, Australian Forest Industries 50(5), 45-47 (1984).

KOCH, P. AND WELLFORD, W.L. JR., Continuous Tunnel Kiln Direct-fired With Bark to dry 1.75 Inch Southern Pine in 12 hours, Forest Products Journal 27(5), 39-47 (1977).

MASAMI, N., KAGAWA, Y. AND KATAGIRI, J., Acoustic Emission Generation in the Process of Drying Hardwoods, Journal of the Japan Wood Research Society 29(1), 10-12 (1983).

MILLER, W., Energy Conservation in Timber-Drying Kilns by Vapour Recompression, Forest Products Journal 27(9), 54-58, (1977).

ROSEN, H.N., Theoretical Developments in High-Temperature Drying of Wood, Paper presented at the North American Wood Drying Symposium, Mississippi State, M.S., (1984).

ROSEN, H.N., Drying Processes for the year 2000, Paper presented at the XVII IUFRO World Congress, Japan (1981).

SHIGERU, O., KAINO, K. AND SUZUKI, M., Detection of Lumber Checking during Drying by means of acoustic emission technique (1984).

SIMPSON, W.T., Drying Wood : A review, Drying Technology
2(2), 235-264 (1983-1984)
2(3), 353-368 (1983-1984).

TRONSTAD, S., Regional Report, Paper presented at the Wood Drying Working Party (S 5.04 - 06), IUFRO Division V Conference, Madison, Wisconsin, U.S.A. (!983).

WHITEHOUSE, L.J., editor, Export Prospects For Radiata Pine, FRI Bulletin No.136, Forest Research Institute, Ministry of Forest, New Zealand (1988).

WILLIAMS, D.H., High-temperature Drying, Timber Drying News No 2 Forest Research Institute, Rotorua, New Zealand (1983).

EFFECTS OF MINOR BOARD IRREGULARITIES AND AIR FLOWS ON THE DRYING RATE OF SOFTWOOD TIMBER BOARDS IN KILNS

P.C.S. KHO, R.B. KEEY,
Department of Chemical and Process Engineering,
University of Canterbury, Christchurch, New Zealand.

and

J.C.F. WALKER,
School of Forestry,
University of Canterbury, Christchurch, New Zealand.

ABSTRACT

Local mass-transfer coefficients were experimentally estimated for a 100 X 25 mm truncated aluminium board, placed in a stack within a small industrial-type kiln, for air flows from 3 to 7 m s^{-1} at 41°C by sublimating a coating of naphthalene. The results confirmed the existence of a critical Reynolds number, Re_b, for the formation of a stationary eddy behind a truncated slab. The distance from the leading edge to the position of the maximum local mass-transfer coefficient was found to be proportional to $Re_b^{1/2}$. Variations in the height of adjacent boards in a stack layer enhanced the local mass-transfer coefficients more than variations in the gaps between boards in a stack layer. The variation of the local mass-transfer coefficient with air velocity indicated that transitional boundary-layer flow developed in the stack, which agreed with results in the literature.

INTRODUCTION

Until the turn of the century, commercial timber drying kilns were designed solely on experience and trial and error. Formal methods for designing kilns have become a commercial necessity, as these installations have to meet the increasing demand to dry boards quickly with a minimum of degrade and to do this as efficiently as possible under the pressure of escalating energy costs. However, this requires knowledge of the heat and mass-transfer coefficients on the surface of timber boards for the geometry similar to that for timber stacks in commercial kilns.

To date, there has been very little experimental work to obtain quantitative expressions for the heat and mass-transfer coefficients at the surface of blunt-edged slabs. Sørensen [1969] investigated the variation of local mass-transfer coefficients with velocity and thickness on a single isolated slab. Miller [1973] extended this work to an array. Both these experiments were performed in wind tunnels.

This present series of experiments aims to extend the scope of existing work. We have investigated the effects of both varying air velocity through a stack and of the distance from the leading edge on the local mass-transfer coefficients at the surface of a standard 100 X 25 mm board placed within an array, having a geometry similar to a timber stack in a commercial kiln. The influence of minor board irregularities, a consequence of drying or inaccurate sawing, on the local mass-transfer coefficients is also examined. All drying tests have been carried out in a 2550 X 2300 X 2800 mm industrial-type kiln at the School of Forestry, University of Canterbury, Christchurch, New Zealand.

EXPERIMENTAL APPARATUS AND PROCEDURE

The naphthalene sublimation technique used by Danckwerts and Anolick [1962], Sørensen [1969] and Miller [1973] to determine the local mass-transfer coefficients was employed, with slight modification.

An aluminium slab of dimensions 640 X 100 X 20 mm, with a 100 X 98 X 2 mm recess milled at the centre of the board was used as the test board (fig. 1).

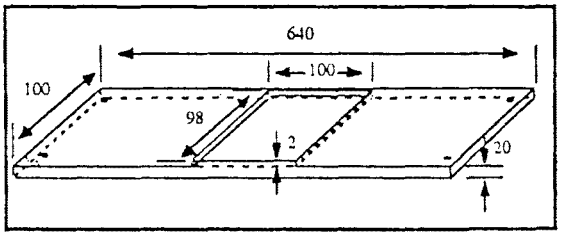

Figure 1 Isometric view of the test board.

Naphthalene crystals of analytical quality were melted slowly before being poured into the recess of the test board, which had been preheated to 50°C. Upon complete solidification, the naphthalene surface was lightly smoothed with an electric iron, which was set at a temperature slightly higher than the melting point of naphthalene. The melted naphthalene was then wiped off immediately with absorbent paper. This smoothing process was repeated until an acceptably level surface was obtained.

The thickness of the test board was then built up to the desired thickness by bolting 2 or 3-mm thick, similarly dimensioned aluminium boards to it.

Changes in the thickness of naphthalene sublimation during the test were measured by a Mitutoyo dial gauge (± 0.005 mm) placed on a modified face plate.

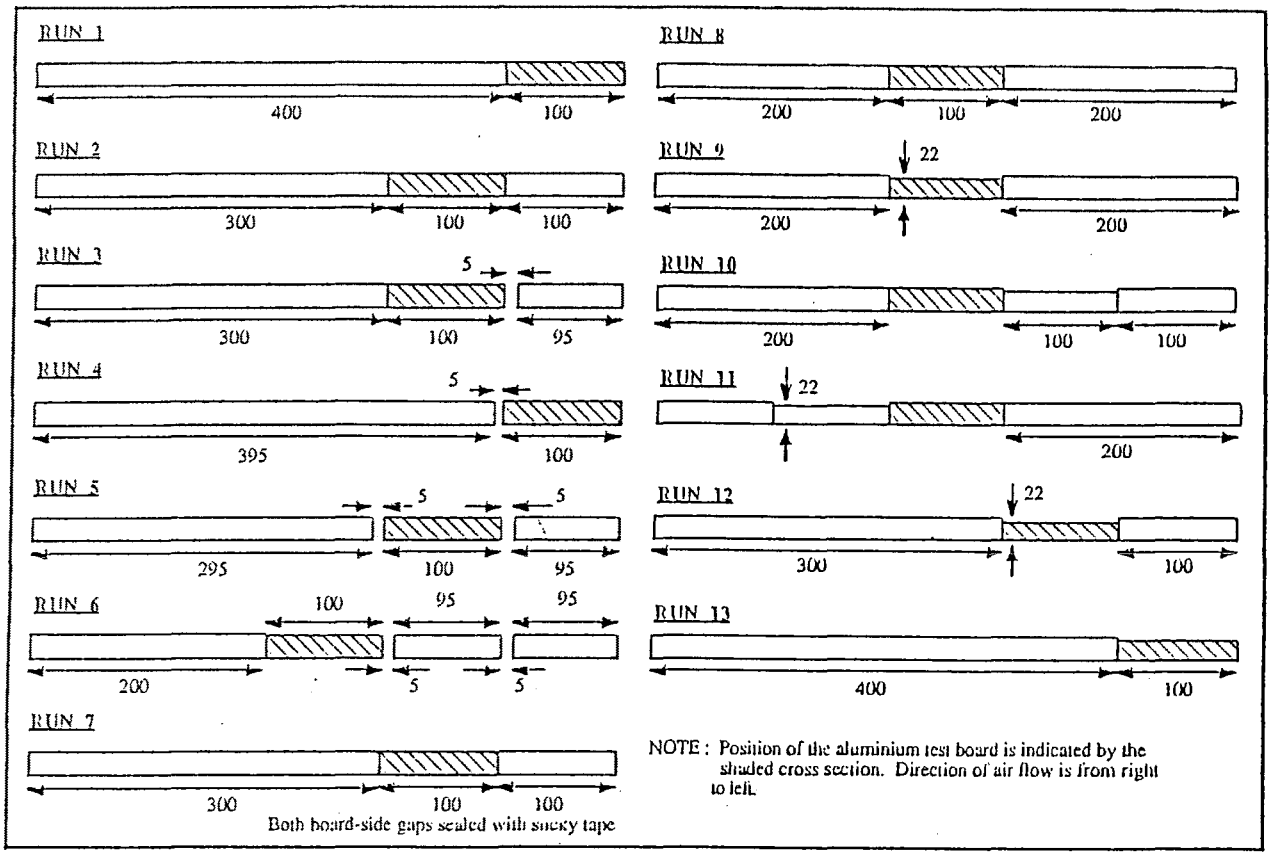

Figure 2 Position of the bolted test board in the drying tests.

A box to contain the bolted test board was connected directly to the exhaust duct of the kiln to get once-through air flow. Inside this box were five sheets of medium density fibreboard, each with dimensions 640 X 500 X 25 mm, except the test layer which had to be recut to accommodate the aluminium board. These layers were separated by two 25 X 25 mm stickers placed at 600 mm apart. This box system allowed retrieval of the aluminium board in less than a minute. The entire kiln was stacked with dry timber boards using the same geometrical configuration. Air was thus recycled through this material until it was vented to the atmosphere through the box containing the aluminium board.

The temperature in the kiln was set at 41 ± 0.5°C. The fan speed was adjusted to give the required air velocity through the sticker gaps. The kiln was switched on for at least an hour before any runs were performed. Once steady state was achieved, the bolted test board was inserted in the desired position in the stack. The pressure reading was noted. To ensure consistency, reproducibility and to minimize errors, each run was repeated three times.

A total of one hundred and fifty runs was carried out. These were performed at three different velocities - 3, 5 and 7 m s^{-1}, and at thirteen different configurations as shown above in figure 2. The duration for sublimation tests for runs at 7 m s^{-1} was reduced from 120 to 90 minutes, to achieve a similar sublimation thickness to other runs at lower air velocities.

THEORY

Fick's Law states that the rate at which a vapour moves relative to air is given by

$$J_N = -D_{NA} \frac{d C_N}{d x}$$

where, in our case,

C_N is the molar concentration of naphthalene, (mol m^{-3});
D_{NA} is the diffusion coefficient of naphthalene in air, (m^2 s^{-1});
J_N is the diffusion flux of naphthalene vapour, (mol m^{-2} s^{-1});
and x is the distance from the naphthalene surface, (m).

Assuming that the density of naphthalene and the diffusion coefficient of naphthalene in air are both constant and that transport of air at right angles to the surface is zero, i.e. $N_A = 0$, we get

$$\tilde{N}_N = F \ln \frac{\left(1 - \frac{C_{N\infty}}{C}\right)}{\left(1 - \frac{C_{No}}{C}\right)}$$

where

C is mean molar concentration of naphthalene vapour, (mol m^{-3});

C_{No} is the molar concentration of naphthalene vapour at the surface of the coating, (mol m^{-3});

$C_{N\infty}$ is the molar concentration of naphthalene vapour in bulk air stream, (mol m^{-3});

$F = (CD_{NA}) / \delta$, is the mass-transfer coefficient, (mol m^{-2} s^{-1});

$\tilde{N}_N$ is the molar naphthalene vapour flux, (mol m^{-2} s^{-1});

and δ is the boundary layer thickness, (m).

On substituting pressure for molar concentration using the Ideal Gas Law, and assuming the vapour pressure of naphthalene in the bulk air stream to be zero, i.e. $P_{N\infty} = 0$, we obtain

$$F = \frac{\rho_N \Delta b}{M_N \Delta t \ln\left[\frac{P}{P - P_{No}}\right]}$$

where

M_N is the molar mass of naphthalene, (kg mol^{-1});

P is the total pressure, (N m^{-2});

P_{No} is the vapour pressure of naphthalene at the sublimating surface, (N m^{-2});

Δt is the time of sublimation, (s);

Δb is the thickness of naphthalene sublimed in the drying test, (m);

and ρ_N is the density of solid naphthalene, (kg m^{-3}).

Similarly, an equivalent K-type mass-transfer coefficient can be derived to give

$$K_c = \frac{\rho_N R T}{1000 M_N P_{No}} \frac{\Delta b}{\Delta t}$$

where

K_c is the mass-transfer coefficient, (m s^{-1});

R is the universal gas constant, (J mol^{-1} K^{-1});

and T is the absolute temperature, (K).

When a gas flows over a blunt-edged plate like a timber board, it is thought an eddy forms behind the leading edge [Sørensen, 1969]. The local mass-transfer coefficient rises rapidly to a maximum, thereafter falling exponentially with distance across the slab as the boundary layer develops and thickens. Should this boundary layer be fully developed and laminar, then the local Sherwood number is given by

$$Sh_x = 0.332 \, Re_x^{1/2} Pr^{1/3}$$

but should it be turbulent, then

$$Sh_x = 0.0288 \, Re_x^{4/5} Pr^{1/3}$$

where

$Pr = \upsilon_A / D_{NA}$ is the Prandtl number;

$Re_x = (L_\Delta u) / \upsilon_A$ is the Reynolds number;

$Sh_x = (k_c L_\Delta) / D_{NA}$ is the local Sherwood number;

υ_A is the kinematic viscosity, (m^2 s^{-1});

L_Δ is the distance from the position of the maximum local mass transfer coefficient, (m);

u is the bulk air velocity through sticker spacing, (m s^{-1}).

By determining the Reynolds number dependency, it was hoped to be able to distinguish the nature of the motion downstream of the eddy.

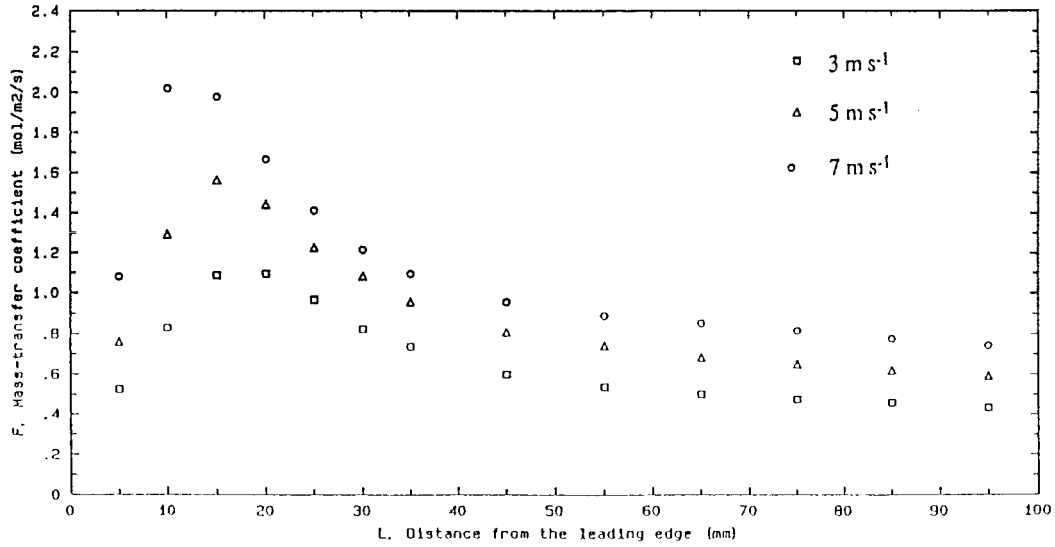

Figure 3 Variation of the local mass-transfer coefficients with distance from the leading edge for the first board of the array for an air velocity of 3 m s^{-1}.

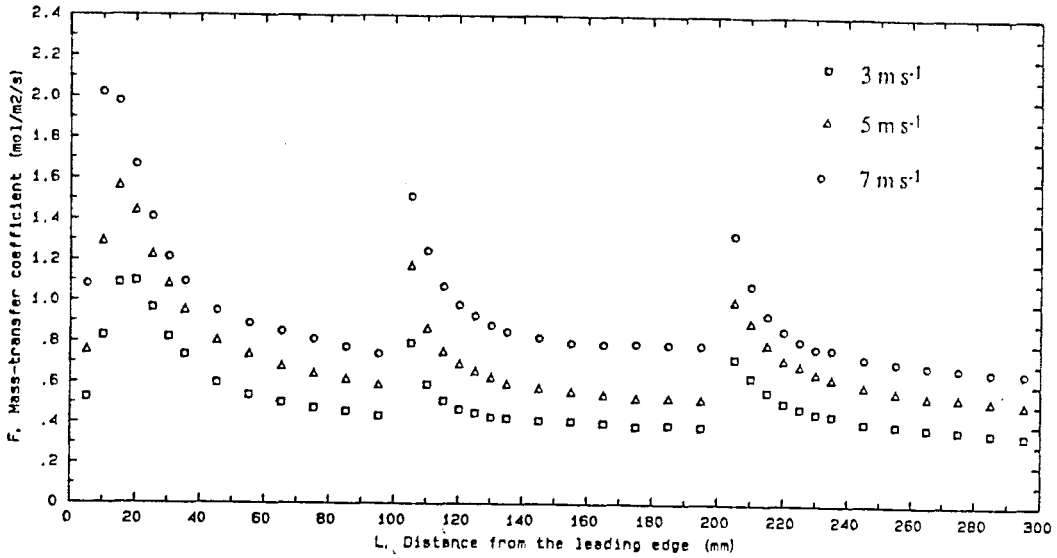

Figure 4 Local mass-transfer coefficient as a function of the distance from the leading edge for the first three boards with normal board-side gaps and uniform board height for an air velocity of 3 m s^{-1}.

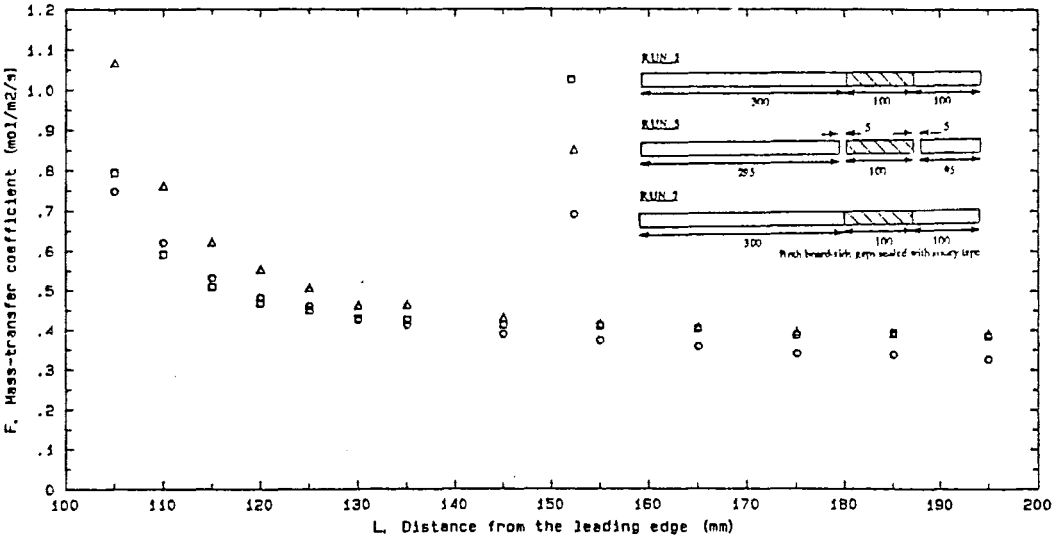

Figure 5 The effect of board-side gaps on the local mass-transfer coefficients for 3 m s^{-1} for the second board

RESULTS AND DISCUSSION

Plots of the local mass-transfer coefficient against the distance from the leading edge for the first board revealed the presence of a maximum local mass-transfer coefficient at some distance from the leading edge (fig. 3). This result followed a similar profile to that obtained by Sørensen [1969] and Miller [1973], confirming the idea that a stationary eddy was formed just behind the leading edge of the board. The distance from the leading edge to the position of the maximum local mass-transfer coefficient, Ω, was found to be

$$\Omega \propto Re_b^{-1/2}$$

whereas for a single isolated truncated slab used by Sørensen, the correlation was

$$\Omega \propto Re_b^{-1/5}$$

This difference might be attributable to a different air flow pattern around the single isolated slab used by Sørensen [1969] in the wind tunnel and that around the array in the kiln as in this series of experiments.

Discontinuities in the local mass-transfer coefficient profiles were observed at the beginning of subsequent boards, which followed similar trends to that obtained by

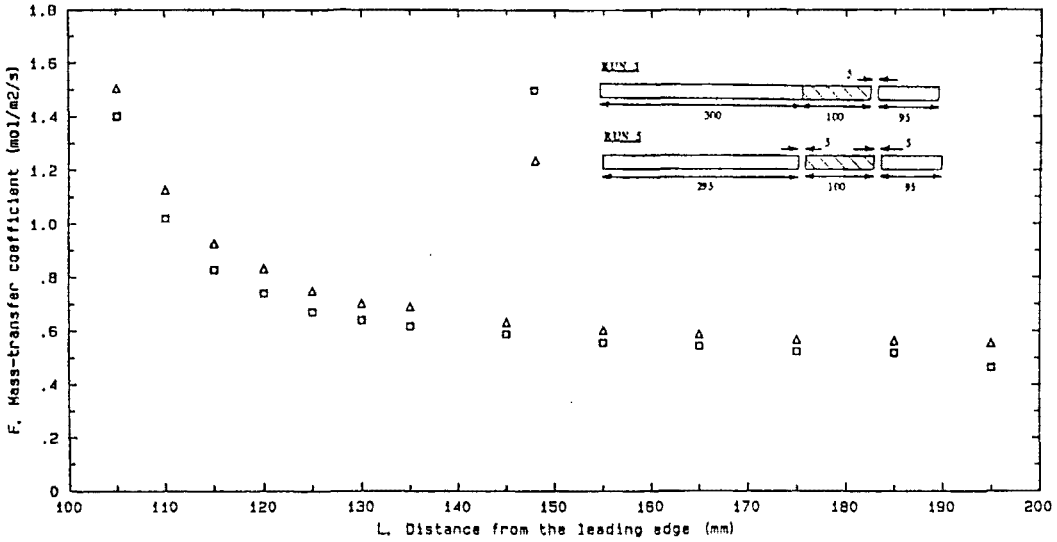

Figure 6 The effect of a 4-mm increased in board-side gap at the trailing edge of the aluminium board at an air velocity of 5 m s^{-1}.

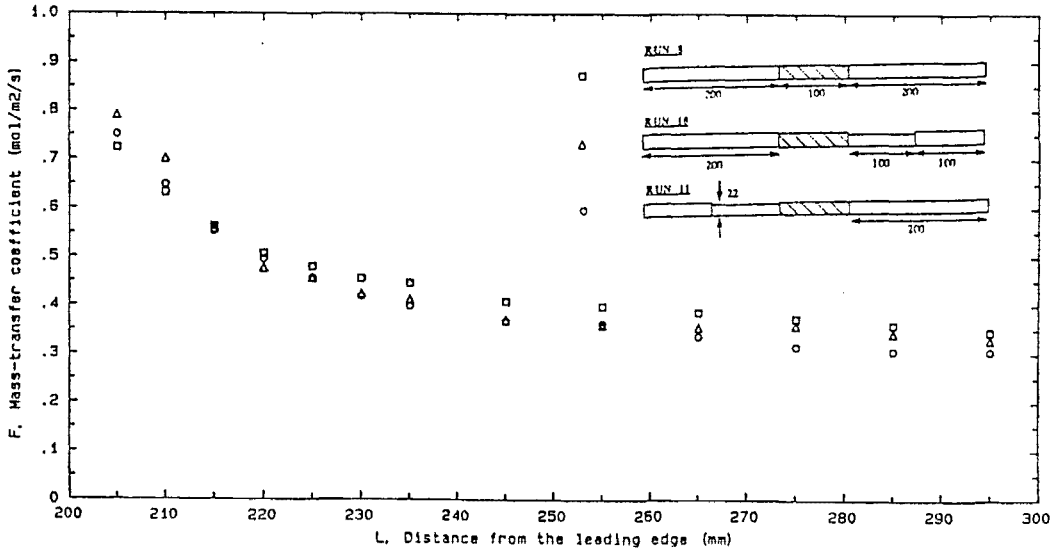

Figure 7 The effect of a thinner leading and a thinner trailing board on the local mass-transfer coefficients on the aluminium board for an air velocity of 3 m s^{-1}.

Sørensen [1969] and Miller [1973] (fig. 4). Values of the mass-transfer coefficient decreased exponentially, reaching an asymptotic value at about the mid-point across the board, with decreasing initial values for each discontinuity across the row. These asymptotic values tend to a similar value for each experimental configuration.

THE EFFECT OF INCREASED BOARD-SIDE GAPS

A discontinuity in the plot of local mass-transfer coefficient against distance from the leading edge was observed even though the board-side gaps were completely sealed with sticky tape (fig. 5). This discontinuity might be due to the small difference in board-top level where the Reynolds number based on board thickness was less than the $Re_{b\ critical}$, the critical value for the formation of a stationary eddy, but large enough to cause that discontinuity.

The 1-mm gap on both sides of the aluminium board enhanced mass-transfer coefficient from 20 to 30 mm onwards across the board, by as much as 17%. Wider gaps of 5-mm on both sides of the aluminium board increased initial mass-transfer coefficients for distances up to 20 to 40

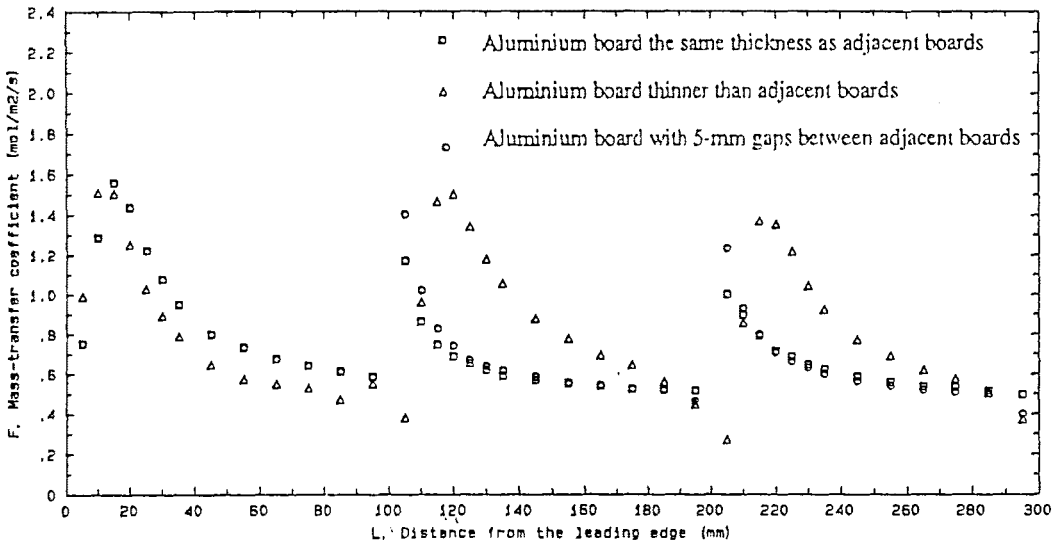

Figure 8 The effect of an increased board-side gap (5 mm) and an increased variation in board thickness (3 mm) on the local mass-transfer coefficients for an air velocity of 5 m s^{-1}.

mm, by as much as 32% depending on bulk air velocity, reaching an asymptotic value similar to that for board-side gaps of 1 mm.

Similar results were obtained when comparing the mass-transfer coefficient profiles of the first board with identical gaps at the trailing edge, indicating consistency in our results.

The influence of an increase in board-side gap at the trailing edge of the aluminium board appeared to enhance mass-transfer coefficients over the whole board, leading a slightly higher aysmptotic value for the board (fig. 6).

THE EFFECT OF VARIATION IN BOARD HEIGHT

Both a thinner leading and a thinner trailing board in the direction of the air flow increased the mass-transfer coefficients on the aluminium board for the first 15 to 30 mm across the board, but lowered them thereafter, the actual values depending on velocity (fig. 7). A thinner leading board increased the mass-transfer coefficients on the aluminium board more than that of a thinner trailing board. An interesting trend - a convex mass-transfer profile was observed in the front portion of the aluminium board - indicated the evolution of a stationary eddy. The calculated value for the critical Reynolds number, Re_b, was 533 at an air velocity of 3 m s^{-1} compared with Sørensen's value of 245.

When a thinner board was placed downstream of the first board in a layer, the mass-transfer coefficient across that thinner board was greatly enhanced (by as much as 100%) except for the region rear the trailing edge of the board, generating a 'saw-tooth'-like mass-transfer coefficient profile (fig. 8). The sharp maxima in the plot implied that the flow pattern of the stationary eddy formed behind each board was different from that formed over boards of uniform thickness.

These results indicate that the board height irregularities are more significant in influencing the local mass-transfer coefficient than are variations in the gaps between the boards.

NATURE OF THE FLOW

The parameter $Sh_x/Pr^{1/3}$ was plotted against Re_x on logarithmic coordinates and slopes were measured. Data from the initial and end portions of the board across the board were excluded due to the disturbance of air flow pattern in these regions, caused by board irregularities.

Table 1 Reynolds number exponent.

Velocity m s^{-1}	Runs 1 and 4	Runs 1, 2 and 8	Runs 1, 3 and 6
3	0.67	0.66	0.64
5	0.66	0.67	0.64
7	0.71	0.68	0.65

The values of these slopes indicated that a transitional boundary layer was developing with increasing turbulence as velocity was increased. These values were in agreement with values obtained by Sørensen (0.69), Powell (0.70) who used a "box" of height 194 mm with varying length, with a surface covered with wet linen, Sherwood (0.64) who dried a 50 X 15 mm pressed sulphite pulp slab and Shepherd *et al.* (0.75), who performed drying tests on a 305 X 305 X 25.4 mm tray, filled with sand and water. All these experiments were conducted in wind tunnels.

CONCLUSION

The measured variation of the mass-transfer coefficient with distance agrees with that obtained by Sørensen and Miller, indicating the existence of a minimum critical Re_b for the development of a stationary eddy. The distance from the leading edge to the position of the maximum local mass-transfer coefficient can be correlated by the relation

$$\Omega \propto Re_b^{1/2}$$

Discontinuities in the mass-transfer coefficient profile were observed with each board, with the maximum local mass-transfer coefficient diminishing exponentially in the streamwise direction reaching an asymptotic value approximately half way across the aluminium board. This value tends to the same value for each successive board. Gaps of 5 mm enhanced the local mass-transfer more when compared with a narrower gap of 1 mm. An increase in the variation in the height of the adjacent boards on either side of the aluminium board will raise the local mass-transfer coefficient of the board. A thinner leading board has a bigger influence on the mass-transfer coefficient on the front portion of the aluminium board than that of a thinner trailing board with the same board height difference. Thereafter, lower values would be observed.

Greatly enhanced local mass-transfer coefficients for nearly the whole width of the board were observed where the level of the aluminium board was lower than the adjacent ones.

The results indicate that both the board-side gaps and the variation in board height are favourable during the first period of drying timber boards, when surface evaporation is rate controlling.

The boundary layer developed over each board was found to be transitional, with a Reynolds number exponent of 0.64 to 0.71.

ACKNOWLEDGEMENTS

The authors wish to thank the Forest Research Institute of the Ministry of Forestry, New Zealand for financially supporting this research project. Travel Grants from the Forest Research,Institute New Zealand, The Royal Society of New Zealand, Wellington (Head Office) and Canterbury Branch, School of Forestry and Department of Chemical and Process Engineering both of the University of Canterbury, and the Canterbury Chemeca Trust for one of the authors, P.C.S. Kho, to attend this conference are also gratefully acknowledged.

NOMENCLATURE

Roman

b	thickness of naphthalene sublimed	m
c	mean molar concentration	mol m^{-3}
C	molar concentration	mol m^{-3}
D	diffusion coefficient	m^2 s^{-1}
F	$= (CD_{NA}) / \delta$, mass-transfer coefficient	mol m^{-2} s^{-1}
J	diffusion flux	mol m^{-2} s^{-1}
K_c	mass-transfer coefficient	m s^{-1}
L_Δ	distance from position of maximum local mass-transfer coefficient	m
M	molar mass	kg mol^{-1}
$\tilde{N}$	molar gaseous flux	mol m^{-2} s^{-1}
P	pressure	N m^{-2}
R	universal gas constant	J mol^{-1} K^{-1}
t	time	s
T	absolute temperature	K
u	air velocity through sticker spacing	m s^{-1}
x	distance from the naphthalene surface	m

Subscript

A	air
b	base on thickness of the board.
N	naphthalene
NA	naphthalene to air
N∞	naphthalene at bulk air stream
No	naphthalene at the surface of coating
x	base on the distance from the position of the maximum local mass-transfer coefficient.

Greek

δ	boundary layer thickness	m
Δ	finite difference	-
ρ	density	kg m^{-3}
υ	kinematic viscosity	m^2 s^{-1}
Ω	distance from the leading edge to the position of maximum local mass-transfer coefficient	m

Dimensionless numbers

Pr	Prandtl number	υ_A / D_{NA}
Re_x	Reynolds number	$(L_\Delta u) / \upsilon_A$
Sh_x	Local Sherwood number	$(k_c L_\Delta)/D_{NA}$

Constants

M_N	= 0.12816 kg mol^{-1}
R	= 62.361 J mol^{-1} K^{-1}
ρ_N	= 1145 kg m^{-3}
υ_A	= 1.6875 E -5 m^2 s^{-1} (at 41°C)

REFERENCES

DANCKWERTS, P.V. and ANOLICK, C., Mass-transfer From A Grid Packing To An Air Stream, Trans. Instn. Chem. Engrs., 40, 203 - 213 (1962).

EDWARD, W.W., Editor-in-chief, "International Critical Tables of Numerical Data, Physics, Chemistry And Technology", McGraw Hill, New York (1929).

KEEY, R.B., "Drying Principles and Practice", Pergamon Press, Oxford (1972).

KEEY, R.B., "Introduction to Industrial Drying Operations", Pergamon Press, Oxford (1978).

MILLER, W.R., Mass-transfer Within Arrays, B.E. Report, University of Canterbury (1973).

PERRY, R.H. and GREEN, D.W., "Perry's Chemical Engineers' Handbook", 6th Edition, McGraw Hill (1984).

POWELL, R.W., Further Experiments on the Evaporation of Water From Saturated Surfaces, Trans. Instn. Chem. Engrs., 18, 36-55 (1940).

SCHLICHTING, H., "Boundary-Layer Theory", 7th Edition, McGraw Hill (1968).

SHEPHERD, C.B., HADLOCK, C., and BREWER, R.C., Drying Materials in Trays, Ind. Engng. Chem., 21, 976-980 (1929).

SHERWOOD, T.K., The Drying of Solids - II, Ind. Engng. Chem., 30, 388-397 (1938).

SØRENSEN, A., Mass-transfer Coefficients On Truncated Slabs, Chemical Engineering Science, 24, 1445 - 1460, Pergamon Press (1969).

WEAST, R.C., Editor-in-chief, "Handbook of Chemistry and Physics", 68th Edition, CRC Press, Florida (1987).

WELTY, J.R., "Engineering Heat Transfer", SI Version, John Wiley and Sons, New York (1978).

THE VARIATION OF LOCAL MASS-TRANSFER COEFFICIENTS IN STREAMWISE DIRECTION OVER A SERIES OF IN-LINE, BLUNT SLABS

P.C.S. KHO[1], R.B. KEEY[1] and J.C.F. WALKER[2]

[1]Department of Chemical and Process Engineering, University of Canterbury, Christchurch, New Zealand
[2]School of Forestry, University of Canterbury, Christchurch, New Zealand

ABSTRACT

As a basis for understanding the transfer of moisture vapour inside a stack of timber boards, local mass-transfer coefficients were determined along a set of blunt slabs 100 mm wide by 640 mm long, placed side by side with each layer being separated by stickers of thickness 15, 20 and 25 mm to form a rectangular 'duct' for the air flow. Three slab thickness were used; 25, 50 and 75 mm and three velocities; 3, 5 and 7 m s^{-1} were employed. The coefficients were estimated by measuring the reduction in the thickness of a naphthalene layer cast over the slab. The influence of the gap between adjacent slabs and small variation in slab thickness were also considered. The presence of a maximum in the mass-transfer coefficient profile for the leading slab and diminishing initial value for the subsequent slabs indicated some flow recirculation and boundary-layer thinning at these small gaps, while the local mass-transfer coefficients fell towards an asymptotic value away from each upstream edge. Variation in height between adjacent boards has a great influence on the coefficients, suggesting that the discontinuities in the mass-transfer profiles are the likely consequences of small height differences. The critical Reynolds number, $Re_{b\,crit}$, for the formation of the stationary eddy is 533.

INTRODUCTION

Green timber must be dried to the required moisture level as specified in the Standards, if it is to be used as a satisfactory product. Although there are many methods of drying timber currently available, kiln drying will continue to be one of the key methods used.

At the present, designing of such kilns and drying schedules is based solely on a trial and error procedure, utilising valuable 'hands-on' experiences, due to the lack of heat and mass-transfer data for slabs corresponding to the geometry used in these kilns. However, with requirement for efficiently-dried quality wood under more intensive conditions and mounting pressure from both escalating energy costs and environmentalists, formal methods of designing kilns and drying schedules are needed, thus requiring precise knowledge of the heat and mass-transfer coefficients over the timber boards in these kilns.

While Sørensen [1969] has explored mass-transfer coefficients about a single slab and Miller [1973] provides limited data on the behaviour of in-line slabs, this paper describes the first work concerned with the local convective mass-transfer in kiln geometries. Investigated is the effect of varying board thickness, sticker thickness and air velocity on the mass-transfer, as well as the influence of irregularities in stacking. Local mass-transfer coefficients are determined by measuring the rate of sublimation of a naphthalene coating on an aluminium test slab.

EXPERIMENTAL EQUIPMENT AND PROCEDURE

The aluminium test slab used had dimensions of 640 x 100 x 20 mm with a centrally machined recess of 100 x 98 x 2 mm on it. Analytical-grade naphthalene crystals were melted slowly before being poured into the recess of the aluminium test slab which was preheated to 50°C. Upon complete solidification, the surface of the naphthalene coating was slowly smoothed in stages with an electric iron, with any melted naphthalene wiped off immediately with absorbent paper, until a reasonably smooth surface was achieved. This aluminium slab was the 'built' up to desired thickness by bolting similarly-dimensioned 2-,3- or 50-mm thick slabs to it. It was then placed in position in the stack in the test section (figure 1) of a 2550 x 2300 x 2800 mm electrically-fired kiln in the School of Forestry, University of Canterbury, and allowed to sublime in the air stream for a pre-determined period of time. Measurements of the level of the naphthalene surface at 65 grid points on the casting before and after the sublimation tests were done using the Mitutoyo dial gauge (± 0.005 mm).

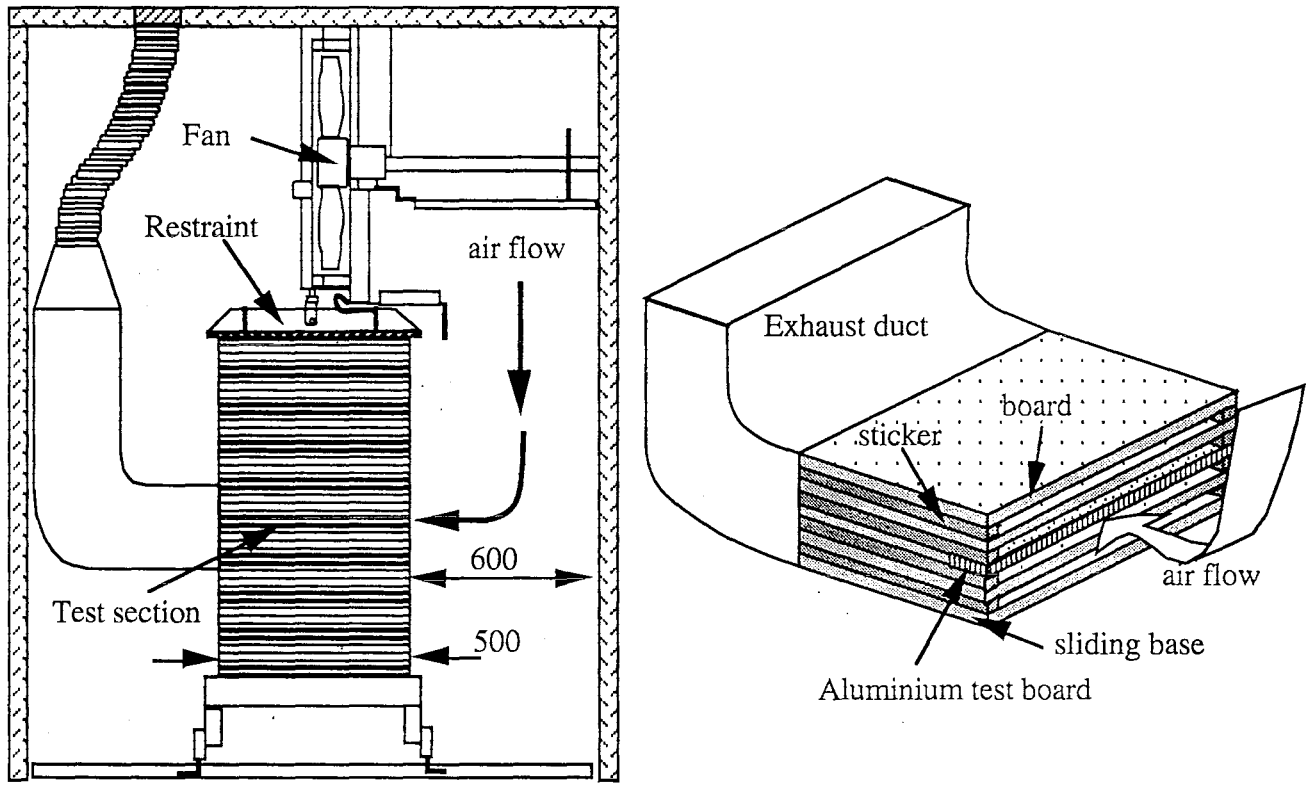

Figure 1 Side elevation of the kiln arrangements and isometric view of the test section

The stack in the test section was made up of layers of medium density fibreboard, which had dimensions of 640 x 500 mm, except the test layer which had to be re-cut to accommodate the test slab. These sheets of boards were separated by two stickers placed at 600 mm apart, forming a 'duct' through which the air flows. This set-up allowed retrieval of the test slab to within a minute. This stack was connected by a ducting system to the vent of the kiln to ensure no recirculation of the air containing naphthalene vapour.

The temperature in the kiln was maintained at 41 ± 0.5°C. The required air velocity was achieved by adjusting the variable-speed fans. Pressure readings were noted.

THEORY

From Fick's law of diffusion, and assuming that the density of naphthalene and the diffusion coefficient of naphthalene vapour in air are both constant and that transport of air at right angles to the surface is zero (i.e. $\tilde{N}_A = 0$), we get

$$\tilde{N}_N = F \ln \frac{[1 - C_{N\infty}/C]}{[1 - C_{NO}/C]} \quad (1)$$

On substituting pressure for molar concentration using the Ideal Gas Law, and assuming the vapour pressure of naphthalene in the bulk air stream to be zero, i.e. $P_{N\infty} = 0$, we obtain the mass-transfer coefficient in terms of the diminution of the naphthalene coating $\Delta b/\Delta t$:

$$F = \frac{\rho_N \Delta b}{M_N \Delta t \ \ln P/(P - P_{NO})} \quad (2)$$

Similarly, an equivalent K-type mass-transfer coefficient can be derived to give

$$K_c = \frac{\rho_N R T}{1000 M_N P_{NO}} \frac{\Delta b}{\Delta t} \quad (3)$$

When a gas flows over a blunt-edged plate like a timber board, it is thought an eddy forms behind the leading edge as Danckwerts and Anolick [1962] have found in their experiments. The local mass-transfer coefficient rises rapidly to a maximum, thereafter falling exponentially with distance across the slab as the boundary layer develops and thickens. Should this boundary layer be fully developed and laminar, then the local Sherwood number is given by

$$Sh_x = 0.332 \ Re_x^{1/2} Sc^{1/3} \quad (4)$$

but should it be turbulent, then

$$Sh_x = 0.0288 \ Re_x^{4/5} \ Sc^{1/3} \quad (5)$$

By determining the Reynolds number dependency, it was hoped to be able to distinguish the nature of the motion downstream of any eddy which might form.

RESULTS AND DISCUSSION

Over four hundred runs were performed using the different combinations of air velocities (3, 5 and 7 m s^{-1}), sticker thickness (15, 20 and 25 mm), board thickness (25, 50 and 75 mm) and gaps of 5 mm and height difference of 3 mm between adjacent boards.

In figure 2, where the local mass-transfer coefficient, F, was plotted as a function of the distance from the leading edge, L, for 3, 5 and 7 m s^{-1}, the striking feature about the profiles was the presence of a characteristic maxima in the leading board of the test layer, similar to that observed by Danckwerts and Anolick [1962] and Sørensen [1969] for an isolated slab. No reliable correlation could be found between the position of these maxima, the geometry of the stack and air velocity owing to the lack of data points. However, it was observed that the maximum decreased from 16.8 mm to 10.6 mm when velocity was increased from 3 m s^{-1} to 7 m s^{-1} for a stack of 25 mm-thick boards, separated by 25 mm-thick stickers. Decreasing sticker thickness from 25 mm to 15 mm for a stack consisting of 25 mm-thick boards at 5 m s^{-1} decreased this position from 11.3 mm to 10.2 mm, while increasing the board thickness from 25 mm to 75 mm, separated by 25 mm-thick stickers, increased this maximum from 11.3 mm to 16.8 mm at 5 m s^{-1}.

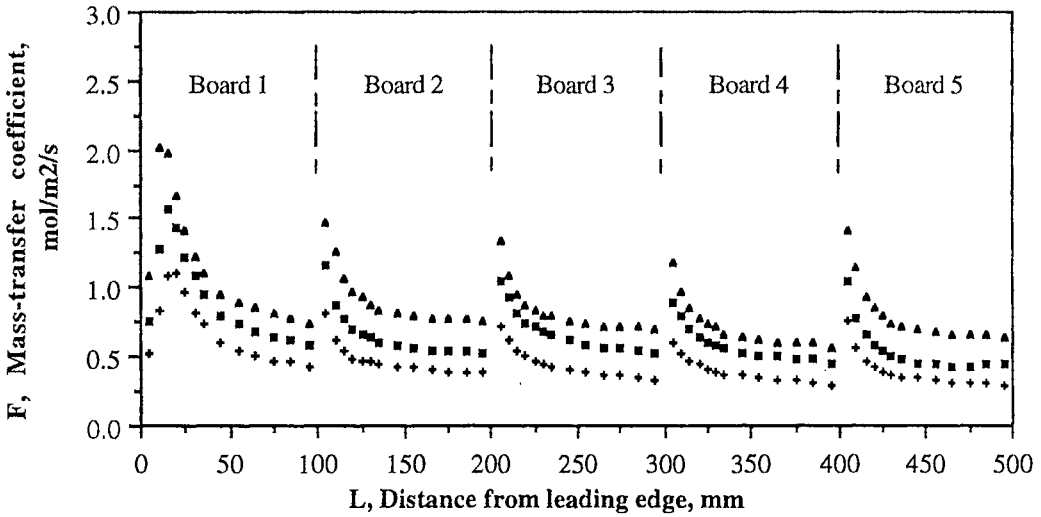

Figure 2 Local mass-transfer coefficient, F, as a function of the distance from the leading edge, L, for a stack made up of 25 mm-thick boards separated by 25 mm-thick stickers with normal adjacent board-gaps of 0.5 to 1.0 mm.

• 3 m/s ▪ 5 m/s ▲ 7 m/s

The small gaps of 0.5 to 1.0 mm between the test board and the dummy boards in the test layer produced discontinuities on the mass-transfer profiles at these positions. Mass-transfer coefficients for the front portion of these boards were enhanced considerably, when compared to those at a flat surface, with these initial values decreasing exponentially in the direction of the air flow, except for the last board which had somewhat higher values. The mass-transfer coefficients of each board also decreased exponentially and tended to a limiting value at about half way across each board. Wu [1989], in his wind-tunnel experiments, has found that turbulence levels measured at 1 mm above a board surface for the first three gaps in the direction of air flow decreased from 24% to 13%,.with the last (fourth) gap at a higher level of 17% level, with no appreciable increase in pressure drop for the 5-mm gap between adjacent boards. He attributed this increase to a vertical air circulation in the gap between the adjacent boards.

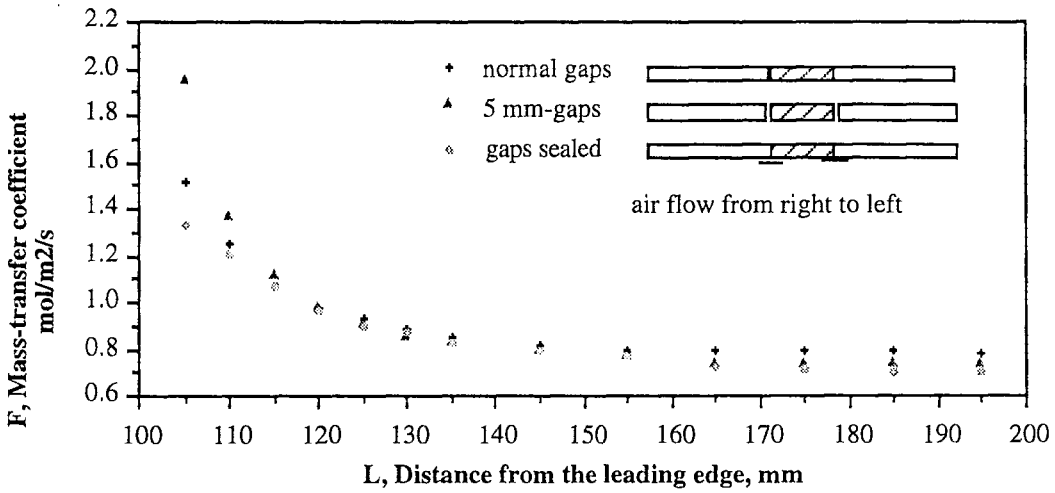

Figure 3 Effect of adjacent board-gaps on the mass-transfer coefficients for the second board at 7 m/s

The gaps on either side of the second board in the test layer were varied to investigate the influence of these gaps on the local mass-transfer coefficients (figure 3). The run with gaps sealed with sticky tape from the underneath still exhibited the initial enhancement of coefficients and the

discontinuities of the mass-transfer profiles. A small difference in the level of adjacent boards, disturbing the air flow at that region around the gap, may be the explanation to the existence of these discontinuities and enhancements. Sørensen [1969] concluded that if the Reynolds number based on the board thickness, Re_b exceeded 245, a stationary eddy would be formed. If the same rule holds for the configuration used in our experiment, the critical thickness for the formation of the eddy will be
0.8 mm for 5 m s^{-1}, implying that any height difference between adjacent boards less than 0.8 mm will disturb the air flow significantly. There no significant change in the mass-transfer coefficient profile for runs with gaps sealed and that with a normal gap, whereas the initial enhancement in the run with 5 mm gaps on both side of the test board could be attributed to the presence of a slight increase in board-height difference.

When the test board was lower by 3 mm than all the adjacent dummy boards, a 'saw-tooth' like profile shown in figure 4 was observed. With the exception of the first and the last board, the first and last ten millimetres of all boards had smaller mass-transfer coefficients, suggesting the existence of a stagnant zone. However, over the rest of the board, mass-transfer coefficients were enhanced considerably.

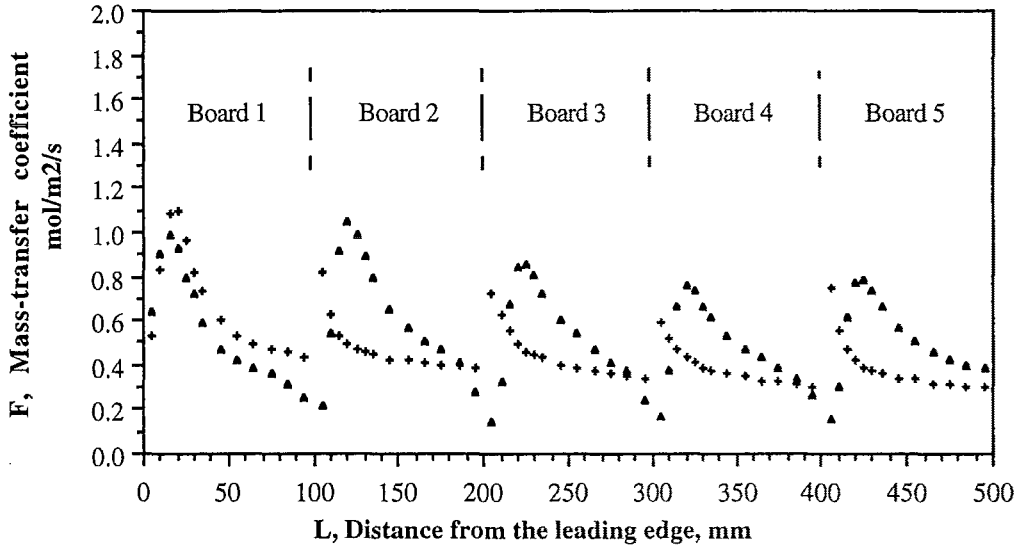

Figure 4 Effect of a lower considered board at 3 m/s
+ normal ▲ lower considered board

With a thinner leading board upstream, the local mass-transfer coefficients for the first 15 to 30 mm on the considered board was slightly increased, whereas a trailing thinner board downstream had little effect on the coefficients at the rear portion of the board (figure 5), depending on velocity. A convex mass-transfer profile was forming in the front portion of the run with a thinner leading board, indicating the formation of the stationary eddy. The calculated critical Reynolds number,
$Re_{b\,crit}$, for eddy formation due to board-height differences was 533 for an air velocity of 3 m s^{-1} and a normal gap between the boards. Sørensen's tests indicated a value of 245 for laminar flow conditions.

Varying board thickness over the range 25 to 75 mm with 25 mm sticker spacing at 5 m s^{-1} appeared to have no clear effect on the mass-transfer coefficient profiles. It was also observed that sticker thickness over the range 15 to 25 mm at 5 m s^{-1} have a negligible influence on the mass-transfer coefficients. However, the position of the maximum mass-transfer coefficient at the leading board of the test layer was affected slightly.

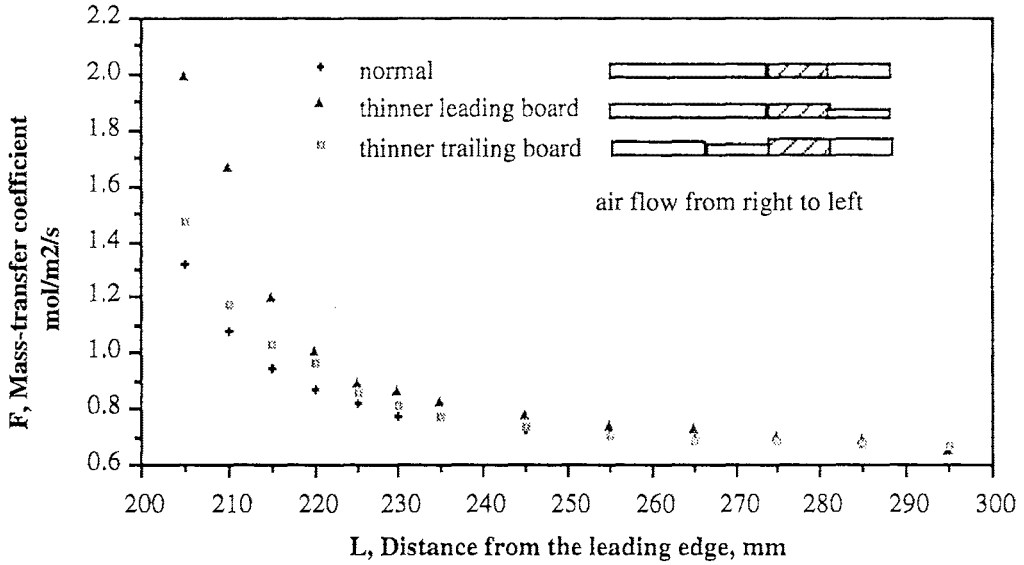

Figure 5 Effect of a leading and trailing thinner board on the mass-transfer coefficients of the third board at 7 m/s

FITTING THE DATA TO THE FLAT-PLATE CORRELATION

The parameter $Sh_x/Sc^{1/3}$ was plotted against Re_x on a logarithmic scale. Data from the initial and the end portion of the boards were excluded due to possible flow disturbances caused by board irregularities. The average value of the slope was 0.75, indicating a transitional boundary-layer was formed after the eddying. This value was comparable to the values obtained by Sørensen (0.69), Powell (0.70) who used a "box" of height 194 mm with varying length, with a surface covered with wet linen, Sherwood (0.64) who dried a 50 x 15 mm pressed sulphite pulp slab and Shepherd *et al.* (0.75), who performed drying tests on a 305 x 305 x 25.4 mm tray, filled with sand and water. All these experiments were conducted in wind tunnels.

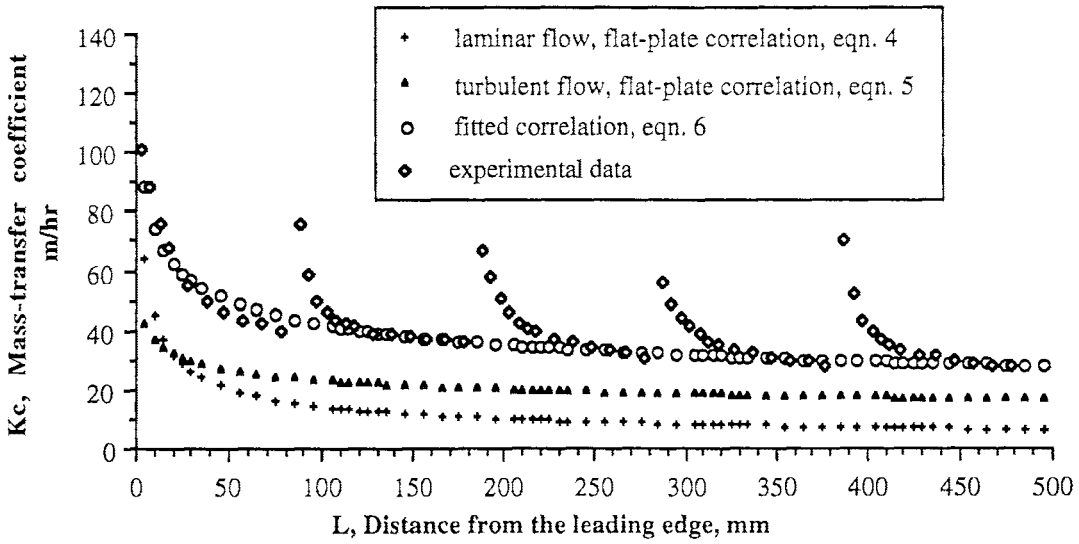

Figure 6 Comparison of experimental data to the flat-plate correlation

The constant in the flat-plate correlation was the found by plotting $Sh_x/Sc^{1/3}$ against $Re_x^{3/4}$, and was found to be 0.084, giving the following correlation

$$Sh_x = 0.084\ Re_x^{3/4}\ Sc^{1/3} \qquad (6)$$

The above correlation was plotted in figure 6, with both the flat-plate correlation for both laminar and turbulent boundary-layer flow for comparison. The constant in the above correlation obtained this way was three times that of the constant in the flat-plate correlation for turbulent flow.

CONCLUSIONS

The measured variation of local mass-transfer coefficients indicated the presence of a characteristic maximum at the leading board of the stack. The position of this maximum was slightly dependent on the geometry of the stack and air velocity.

Discontinuities in the mass-transfer coefficient profile over the boards were observed at each gap between adjacent boards, with the local mass-transfer coefficient diminishing exponentially in the streamwise direction, reaching an asymptotic value given by equation (6), approximately half-way across the board. The initial value of each board also decreased exponentially except for the last board where the initial value was similar to that of the second board. This discontinuity in the profile and enhancement in mass transfer is probably due to the small difference in height between adjacent boards.

The critical Reynolds number, $Re_{b\,crit}$, for the formation of a stationary eddy in such a geometry is 533 under the flow conditions and geometry investigated.

Sticker thickness over the range 15 to 25 mm and board thickness of 25 to 75 mm have negligible effect on the mass-transfer coefficients, within the scatter of the results.

The boundary layer developed over each board was found to be transitional, the mass-transfer correlation having an average Reynolds number exponent of 0.75, with a coefficient of 0.084. The average mass-transfer rate is about three times greater than the rate from a flat-plate of similar extent under the same flow conditions. Even though the stacked boards form an apparent continuous duct, the discontinuities between adjacent boards are sufficient to enhance the overall mass transfer greatly.

ACKNOWLEDGEMENT

Financial support from the Forest Research Institute of the Ministry of Forestry, New Zealand for this research project is gratefully acknowledged.

NOMENCLATURE

Roman

b	thickness of the naphthalene coating sublimed	m
C	molar concentration or mean molar concentration	mol m^{-3}
D	diffusion coefficient	$m^2\ s^{-1}$
F	$= (CD_{NA}) / \delta$, mass-transfer coefficient	mol $m^{-2}\ s^{-1}$
K_c	mass-transfer coefficient	m s^{-1}
L	distance from the leading edge	m
M	molar mass	kg mol^{-1}
$\tilde{N}$	molar gaseous flux	mol $m^{-2}\ s^{-1}$
P	pressure	N m^{-2}
R	universal gas constant	J $mol^{-1}\ K^{-1}$
t	time	s
T	absolute temperature	K

u	air velocity through the sticker spacing	$m\ s^{-1}$

Subscript

b	based on thickness of the board
N	naphthalene
NA	naphthalene to air
N∞	naphthalene at bulk air stream
NO	naphthalene at the surface of coating
x	based on the distance from the position of the maximum local mass-transfer coefficient

Greek

δ	boundary-layer thickness	m
Δ	finite difference	-
ρ	density	$kg\ m^{-3}$
υ	kinematic viscosity	$m^2\ s^{-1}$

Dimensionless numbers

Re_x	Reynolds number	$(L_x u) / \upsilon_A$
Sc	Schmidt number	υ_A / D_{NA}
Sh_x	Local Sherwood number	$(k_c L_x)/D_{NA}$

Constants

M_N = 0.12816 $kg\ mol^{-1}$
R = 62.361 $J\ mol^{-1}\ K^{-1}$
ρ_N = 1145 $kg\ m^{-3}$
υ_A = 1.6875 E -5 $m^2\ s^{-1}$ (at 41°C)

REFERENCES

DANCKWERTS, P.V. and ANOLICK, C., Mass-transfer From A Grid Packing To An Air Stream, Trans. Instn. Chem. Engrs., 40, 203 - 213 (1962).

EDWARD, W.W., Editor-in-chief, "International Critical Tables of Numerical Data, Physics, Chemistry And Technology", McGraw Hill, New York (1929).

KEEY, R.B., "Drying Principles and Practice", Pergamon Press, Oxford (1972).

KEEY, R.B., "Introduction to Industrial Drying Operations", Pergamon Press, Oxford (1978).

MILLER, W.R., Mass-transfer Within Arrays, B.E. Report, University of Canterbury (1973).

PERRY, R.H. and GREEN, D.W., "Perry's Chemical Engineers' Handbook", 6th Edition, McGraw Hill (1984).

POWELL, R.W., Further Experiments on the Evaporation of Water From Saturated Surfaces, Trans. Instn. Chem. Engrs., 18, 36-55 (1940).

SCHLICHTING, H., "Boundary-Layer Theory", 7th Edition, McGraw Hill (1968).

SHEPHERD, C.B., HADLOCK, C., and BREWER, R.C., Drying Materials in Trays, Ind. Engng. Chem., 21, 976-980 (1929).

SHERWOOD, T.K., The Drying of Solids - II, Ind. Engng. Chem., 30, 388-397 (1938).

SØRENSEN, A., Mass-transfer Coefficients On Truncated Slabs, Chemical Engineering Science, 24, 1445 - 1460, Pergamon Press (1969).

WEAST, R.C., Editor-in-chief, "Handbook of Chemistry and Physics", 68th Edition, CRC Press, Florida (1987).

WELTY, J.R., "Engineering Heat Transfer", SI Version, John Wiley and Sons, New York (1978).

WU, Q., An Investigation of Some Problems in Drying of Tasmanian Eucalypt Timbers, M.E. Report, University of Tasmania (1989).

EXPERIMENTAL MEASUREMENT AND NUMERICAL SIMULATION OF LOCAL MASS-TRANSFER COEFFICIENTS IN TIMBER KILNS

T.A.G. LANGRISH[1], P.C.S. KHO[1], R.B. KEEY[1],
J.C.F. WALKER[2]

[1] Department of Chemical and Process Engineering, University of Canterbury, Christchurch 1, New Zealand.
[2] School of Forestry, University of Canterbury, Christchurch 1, New Zealand.

ABSTRACT

A comparison has been made between measurements of mass-transfer coefficients inside a timber drying kiln and a numerical simulation of the air flow pattern in an array of boards. This solved the two-dimensional Navier-Stokes equations on a finite difference grid. The experimental results showed that the small gaps between boards, which are inevitable in practice, caused large enhancements in the mass-transfer coefficients near the leading edge of the boards. The asymptotic values of these coefficients were always greater than those predicted from flat plate correlations. The simulation also predicted enhancements in the mass-transfer coefficients at the leading edge, but of smaller magnitude than those measured. The asymptotic values were predicted within 15%. The simulation predicted that the increase over the flat plate correlations was due to the generation of turbulence by the gaps between boards.

Key Words and Phrases : mass transfer; timber stack; mathematical model; turbulence.

INTRODUCTION

Recently, there has been a strong tendency towards the use of drying conditions in kilns drying softwood boards where the air temperature is above 100°C. This is known as high-temperature drying of timber (lumber). The principal benefit of using these conditions is to reduce the drying time. It is important to have information about the external mass-transfer coefficients above the boards in order to design and analyse the performance of these kilns.

The traditional correlations for mass transfer over flat plates have been measured using an air jet issuing from a smoothly converging nozzle in parallel with the flat evaporating surface (Ranz and Dickson, 1965). For example, where a laminar boundary layer is developing across a plate, the correlation for mass transfer is given by (Schlichting, 1960):-

$$Sh_x = 0.332\ Re_x^{1/2}\ Sc^{1/3} \qquad (1)$$

where

$Sc = \upsilon_A/D_{AB}$ is the Schmidt number;

$Re_X = (x.u)/\upsilon$ is the local Reynolds number;

$Sh_x = (K.x)/D_{AB}$ is the local Sherwood number;

K is the local mass-transfer coefficient, (m s^{-1});

υ is the kinematic viscosity of air, (m^2 s^{-1});

x is the distance from the leading edge of the slab, (m);

u is the bulk velocity above the plate, (m s^{-1}).

D_{AB} is the diffusivity of the solute through air, (m^2 s^{-1}).

If the boundary layer above the plate is turbulent, then from Schlichting (1960):-

$$Sh_x = 0.0288\ Re_x^{4/5}\ Sc^{1/3} \qquad (2)$$

It is possible that the turbulence intensity influences both the magnitude and the streamwise variation of the mass-transfer coefficient. The turbulence intensity (I) may be defined as follows:-

$$I = \frac{u'}{u} \times 100\ (\%) \qquad (3)$$

where u' is the root mean square of the fluctuating component of velocity and u is the mean velocity. As an illustration of the importance of the turbulence intensity in influencing transfer coefficients, Bayley and Turner (1971) measured a doubling of the heat-transfer coefficients over a turbine blade when the intensity of turbulence was increased from 0.45% to 5.9%. Most existing correlations are based on turbulence produced by jets, where the turbulence intensities can be as low as 1% (Polat *et al..*, 1990), and these may not be valid for the higher turbulence intensities found in the rectangular channels of kiln stacks. Typical values of the turbulence intensity in channels range from 2 - 12% (Bird, Stewart and Lightfoot, 1960).

The results of Sparrow, Niethammer and Chaboki (1982) are interesting in this respect. They measured mass-transfer coefficients from naphthalene sublimation rates in arrays of modules placed along one wall of a rectangular duct. The modules, 27 mm square, were arranged in rows with 6.3 mm between modules. The highest Sherwood number was observed in the first row, but the Sherwood number reached a limiting value after five rows. The important feature of their results is that the Sherwood numbers in the asymptotic region were considerably above those which would be predicted from flat plate correlations. Although the authors did not comment on this, it is possible that the turbulence-inducing effects of the gaps between modules were responsible for the enhancement in the asymptotic heat-transfer coefficients over the flat plate correlations.

To date, there has been very little experimental work to obtain quantitative expressions for the heat and mass-transfer coefficients at the surface of blunt-edged slabs. Sørenson (1969) has investigated the variation of local mass-transfer coefficients with velocity and thickness on a single isolated slab. Miller (1973) extended this work to an array. Both these experiments were performed in wind tunnels.

Kho, Keey and Walker (1989) have investigated the effects of minor board irregularities (a consequence of inaccurate sawing of timber) and varying air velocities on the variation of the local mass-transfer coefficients with distance from the leading edge of the boards inside an array. The geometry of this array was similar to a timber stack inside a timber kiln. Here we report preliminary results of a comparison of the experimental results for the effects of gaps between the boards in the direction of the airflow with the predictions of a numerical simulation of the airflow inside the array.

NUMERICAL SIMULATION

The numerical simulation followed the procedure outlined by Patankar (1980) for predicting the horizontal and vertical velocities in a two-dimensional flow which is bounded by walls or which may be assumed to be incompressible and isothermal. The simulation solved for five variables:-

- u : the average horizontal velocity;
- v : the average vertical velocity;
- k : the turbulence kinetic energy (per unit mass);
- ε : the rate of dissipation of turbulent kinetic energy;
- p : the static pressure.

The simulation solved the continuity equation, the momentum equation in the horizontal and vertical directions, and one equation each for the variables k and ε. The high Reynolds number form of the k - ε model of Launder and Spalding (1974) was used. The treatment of convection and diffusion (of any property) followed the hybrid scheme described by Patankar (1980).

Mathematical Formulation

A general form for the governing equations including the equation of continuity is:-

$$\frac{\partial(\rho u\phi)}{\partial x} + \frac{\partial(\rho v\phi)}{\partial y} = \frac{\partial}{\partial x}\left(\Gamma_\phi \frac{\partial \phi}{\partial x}\right) + \frac{\partial}{\partial y}\left(\Gamma_\phi \frac{\partial \phi}{\partial y}\right) + S_\phi \qquad (4)$$

where ϕ is the dependent variable of interest (for example, horizontal velocity). In order to express the governing equation of a particular variable in the above generalised form, the terms other than those in the 'convection' and 'diffusion' terms are collected in the source term, S_ϕ. The terms Γ_ϕ and S_ϕ are shown in Table 1, in which the generation of turbulence kinetic energy is calculated from

$$G = \mu_T\left[\left(\frac{\partial u}{\partial y} + \frac{\partial v}{\partial x}\right)^2 + 2\left\{\left(\frac{\partial u}{\partial x}\right)^2 + \left(\frac{\partial v}{\partial y}\right)^2\right\}\right] \qquad (5)$$

The constants, C_μ, C_1, C_2, σ_k and σ_ε in Table 1 are taken from the values recommended by Launder and Spalding (1974) for general free turbulent flows. These values are summarized in Table 2. In this model, the turbulent viscosity μ_T, is described in terms of measurable flow quantities, and related to the turbulence kinetic energy k and to the dissipation rate of turbulence kinetic energy ε by the equation,

$$\mu_T = C_\mu \frac{\rho k^2}{\varepsilon} \qquad (6)$$

Equation	ϕ	Γ_ϕ	S_ϕ
Continuity	1	0	0
x-momentum	u	$\mu_L + \mu_T$	$-\left(\frac{\partial p}{\partial x}\right) + \frac{\partial}{\partial x}\left\{(\mu_L + \mu_T)\left(\frac{\partial u}{\partial x}\right)\right\} + \frac{\partial}{\partial y}\left\{(\mu_L + \mu_T)\left(\frac{\partial v}{\partial x}\right)\right\}$
y-momentum	v	$\mu_L + \mu_T$	$-\left(\frac{\partial p}{\partial y}\right) + \frac{\partial}{\partial x}\left\{(\mu_L + \mu_T)\left(\frac{\partial u}{\partial y}\right)\right\} + \frac{\partial}{\partial y}\left\{(\mu_L + \mu_T)\left(\frac{\partial v}{\partial y}\right)\right\}$
Turbulence kinetic energy	k	$\mu_L + \frac{\mu_T}{\sigma_k}$	$G - \rho \cdot \varepsilon$
Dissipation rate of turbulence kinetic energy	ε	$\mu_L + \frac{\mu_T}{\sigma_\varepsilon}$	$C_1\left(\frac{\rho \cdot \varepsilon}{k}\right)G - C_2\left(\frac{\rho \cdot \varepsilon^2}{k}\right)$

TABLE 1 Equations solved in the numerical simulation.

C_μ	0.09	C_1	1.43	C_2	1.92
σ_k	1.0	σ_ε	0.9		

TABLE 2 Constants used in the turbulence model.

Solution Procedure

The equations which we solve are non-linear and prone to diverge even when a solution exists, so we slow down the changes in the values of the dependent variables from iteration to iteration. This is termed under-relaxation, and we can define under-relaxation factors (f) by:-

$$\phi_{new} = f \cdot \phi^*_{new} + (1 - f) \cdot \phi_{old} \qquad (7)$$

where the subscripts old and new refer to the values of the dependent variables from the previous iteration and the current one respectively, and the superscript * refers to the value which would be produced in the current iteration if no under-relaxation were used. The

under-relaxation factors were taken as 0.1 for all variables. At least 800 iterations were used in each simulation trial.

Inlet Conditions

The turbulence energy per unit mass was related to the turbulence intensity at the face of the grid (100 mm in front of the stack) by the following equation:-

$$k_{inlet} = (uI)^2 \tag{8}$$

where I is the intensity of turbulence at the inlet. The value of the energy dissipation rate of the face of the grid (ε_{inlet}) was fitted to the variation of the turbulence intensity which was measured in front of the stack. This procedure is described in the section reporting the results from the turbulence intensities measured at the inlet.

Wall Conditions

The equations are modified for cells near the wall. These equations are obtained by assuming a linear variation of turbulent viscosity with distance from the wall. The principle is that the universal velocity profile is assumed to apply close to the wall:-

$$u^+ = y^+ \qquad \text{for } y^+ \leq 11.225 \tag{9}$$

$$u^+ = \frac{1}{\kappa} \ln (Ey^+) \qquad \text{for } y^+ \geq 11.225 \tag{10}$$

where y^+ is the dimensionless distance from the wall, u^+ is the dimensionless velocity, and κ and E are constants. The Colburn analogy between mass and momentum transfer was used to relate the wall shear stresses to the mass-transfer coefficients, so that:-

$$Sh_x \cdot Sc^{1/3} = \frac{C_f}{2} \tag{11}$$

$$C_f = \frac{\tau_w}{\rho u^2/2} \tag{12}$$

where C_f is the skin friction coefficient and u is the free-stream velocity. From Launder and Spalding (1974), the dimensionless distance to the wall is:-

$$y^+ = y_p \frac{\rho C_\mu^{1/2} k_p^{1/2}}{\mu} \tag{13}$$

where y_p is the distance of the near-wall grid point from the wall. The quantity k_p, the value of k for the grid point, is calculated from a regular balance over a control volume near the wall, with diffusion of energy to the wall being set to zero as described by Launder & Spalding (1974). From the value of y^+ calculated in equation (13), the value of u^+ can be calculated from equations (9) or (10). This enables the velocity at the near-wall grid point, u_p, to be calculated. Also, if the logarithmic velocity profile is assumed to apply in the near-wall region, uniform shear stress prevails in the region between the near-wall grid point and

the wall and generation and dissipation of energy are in balance there. Then the wall shear stress may be calculated from the equation:-

$$\tau_w = \rho C_\mu^{1/2} k_p \quad (14)$$

This enables the factor C_f to be calculated in equation (12).

Grid Layout

The experimental results which we are simulating (Kho *et al.*., 1989) show that relatively small gaps (1 mm) between boards have a large effect on the mass-transfer coefficient. This suggests that we need to resolve the gaps by including a number of grid lines to subdivide the gaps. The spacing between the (vertical) grid lines which subdivided them (in the direction of the air flow) was chosen as 0.2 mm. Away from the gaps the spacing between grid lines in the direction of the airflow was gradually expanded up to 2 mm and then up to 20 mm away from the boards. This resulted in 236 grid lines in the direction of the airflow. A finer grid would have resulted in an impractically large number of grid lines.

We are interested in the mass transfer process at the surface of the boards, so the spacing of the finite-difference grid near to the wall (perpendicular to the air flow) is of great importance. The vertical spacing between the wall and the adjacent grid lines was such that the grid line lay in the log-law region of the turbulent boundary layer. This implied a dimensionless distance from the wall, y^+, greater than about 50. A typical resulting grid is shown in Figure 1.

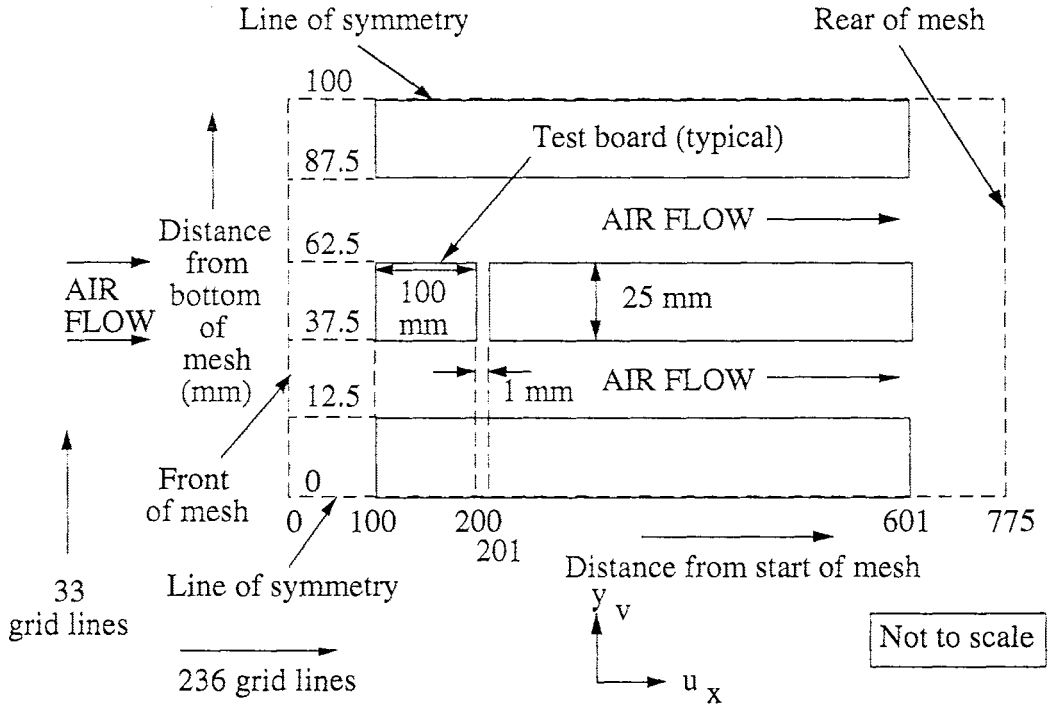

FIGURE 1 Layout of a typical flow situation.

EXPERIMENTAL APPARATUS AND PROCEDURE

Mass-transfer Coefficients

As reported by Kho *et al.*. (1989), all experiments were carried out in a 2.55 × 2.3 × 2.8 m industrial type kiln at the School of Forestry, University of Canterbury, Christchurch, New Zealand. A side elevation of the kiln arrangements and an isometric view of the test section are shown in Figure 2. Local mass-transfer coefficients were determined using a slight modification of the naphthalene sublimation technique used by Danckwerts and Anolick (1962), Sørenson (1969) and Miller (1973). An aluminium slab of dimensions 640 × 100 × 20 mm, with a 100 × 98 × 2 mm recess milled at the centre of the board was used as the test board (Figure 3).

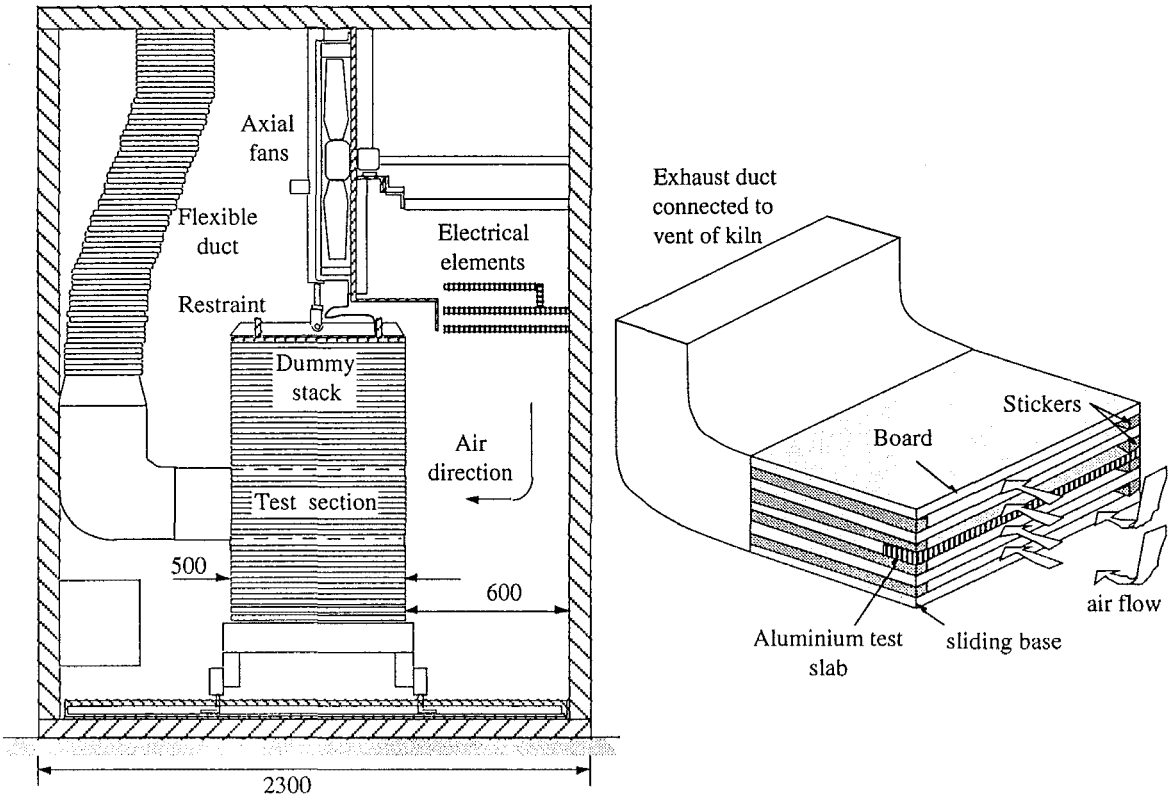

FIGURE 2: Side elevation of the kiln arrangements and an isometric view of the test section.

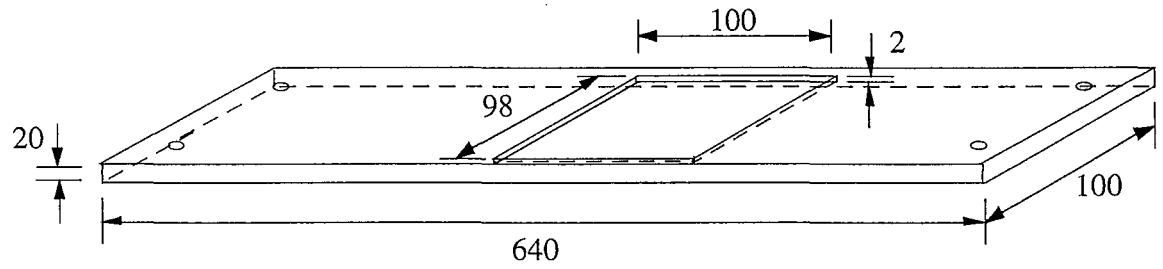

FIGURE 3: Isometric view of the test board.

Naphthalene crystals of analytical quality were melted slowly before being poured into the recess of the test board, which had been preheated to 50°C. Upon complete solidification, the naphthalene surface was lightly smoothed with an electric iron, which was set at a temperature slightly higher than the melting point of naphthalene. The melted naphthalene was then wiped off immediately with absorbent paper. This smoothing process was repeated until a visually level surface was obtained. Any minor residual irregularities are negligibly small compared with the diameter of the dial gauge head (3 mm).

The thickness of the test board was then built up to the desired thickness by bolting 2 or 3 mm thick aluminium boards of a similar dimension to the test board. Changes in the thickness of naphthalene sublimed during the test were measured by a Mitutoyo dial gauge (±0.005 mm) placed on a modified face plate. The resolution of the dial gauge (± 0.005mm) is 4% of the minimum thickness of naphthalene sublimed in any experiment, so the uncertainty in the measured mass-transfer coefficients is of this order.

A box to contain the bolted test board was connected directly to the exhaust duct of the kiln to give once-through air flow. Inside this box were five sheets of medium density fibreboard, each with dimensions 640 × 500 × 25 mm, except the test layer which had to be recut to accommodate the aluminium board. These layers were separated by two 25 × 25 mm stickers placed 600 mm apart. This box system allowed retrieval of the aluminium board in less than a minute. The entire kiln was stacked with dry timber boards using the same geometrical configuration. Air was thus recycled through this material until it was vented to the atmosphere through the box containing the aluminium board.

The temperature in the kiln was set at 41 ± 0.5°C. The fan speed was adjusted to give the required air velocity through the sticker gaps. The kiln was switched on for at least an hour before any runs were performed. Once steady state was achieved, the bolted test board was inserted in the desired position in the stack. To ensure consistency, reproducibility and to minimize errors, each run was repeated three times. Trials were performed at three different velocities - 3, 5 and 7 m s^{-1}. The duration for sublimation tests for runs at 7 m s^{-1} was reduced from 120 to 90 minutes to achieve a similar sublimation thickness to other runs at lower air velocities.

A mass-transfer coefficient can be found from the results of the sublimation experiments (Kho *et al.*., 1989) as :-

$$K = \frac{\rho_N . R . T}{1000 . M_N . p_{No}} \cdot \frac{\Delta b}{\Delta t} \qquad (15)$$

where

ρ_N is the density of solid naphthalene, (kg m^{-3});

R is the universal gas constant, (8.314 J mol^{-1} K^{-1});

T is the absolute temperature, (K);

M_N is the molar mass of naphthalene, (kg mol^{-1});

p_{No} is the vapour pressure of naphthalene at the subliming surface, (Pa);

Δb is the thickness of naphthalene sublimed in the test,(m);

Δt is the time of sublimation, (s).

Turbulence Intensities

Turbulence intensity measurements were performed using a Thermo-Systems Inc. (T.S.I.) hot-wire anemometer. This consisted of a monitor and supply unit (Model 1051-2), a constant temperature linearized anemometer (Model 1054-B), a variable decade (Model 1056) and a 10μm diameter platinum-rhodium wire probe on a DISA Ltd. probe support. The wire was cleaned after every run by agitating it in an ethanol solution. Prior to each run, the anemometer was calibrated using a T.S.I. calibrator, which consisted of a compressed air supply, pressure reduction valves, a calming chamber with a series of wire meshes, and a calibrated, rounded entry nozzle. The pressure drop across the nozzle was measured using a Betz micromanometer. The anemometer voltages were monitored on an IBM-compatible personal computer with an analogue-to-digital converter. The computer recorded 1000 samples at 500 Hz for every run.

Five to ten readings were taken for each run at the centre of the stack at the 13^{th} fillet spacing from the top of the stack at predetermined positions. These were 100 mm, 50 mm and 5 mm in front of the stack, between the fillets. Measurements further into the stack or at the outlet of the box containing the test section were not taken because of the difficulty of access and the interference that the probe holder would have caused to the airflow pattern.

RESULTS AND DISCUSSION

Inlet Turbulence Measurements

The variation in the turbulence intensity with distance from the front of the stack was measured with a hot wire anemometer. This is shown in Figure 4. The turbulence intensities varied significantly with the air velocity but the velocity and turbulence intensity profiles 100 mm in the front of the stack were flat within experimental error. The intensity decreased with decreasing distance from the stack and this was also predicted by the numerical simulation. The turbulence intensity at a distance of 100 mm from the stack was used together with equation (8) to give values of k_{inlet}, the turbulence energy at the face of the grid. We adjusted values of the energy dissipation rate at the face of the grid to give the continous curves shown in Figure 4 so that the maximum discrepancy between the predicted profiles of turbulence intensity and the measured values (shown as points in Figure 4) was minimised. The fitted values of the turbulence energy and the energy dissipation rate are summarized in Table 3.

Air velocity between boards ($m\ s^{-1}$)	k_{inlet} Turbulence energy at the front of grid ($m^2\ s^{-2}$)	ε_{inlet} Energy dissipation rate at front of grid ($m^2\ s^{-3}$)
3	0.0547	0.841
5	0.234	7.45
7	0.671	36.2

TABLE 3: Summary of the fitted values of the turbulence energy and the energy dissipation rate at the front of the grid.

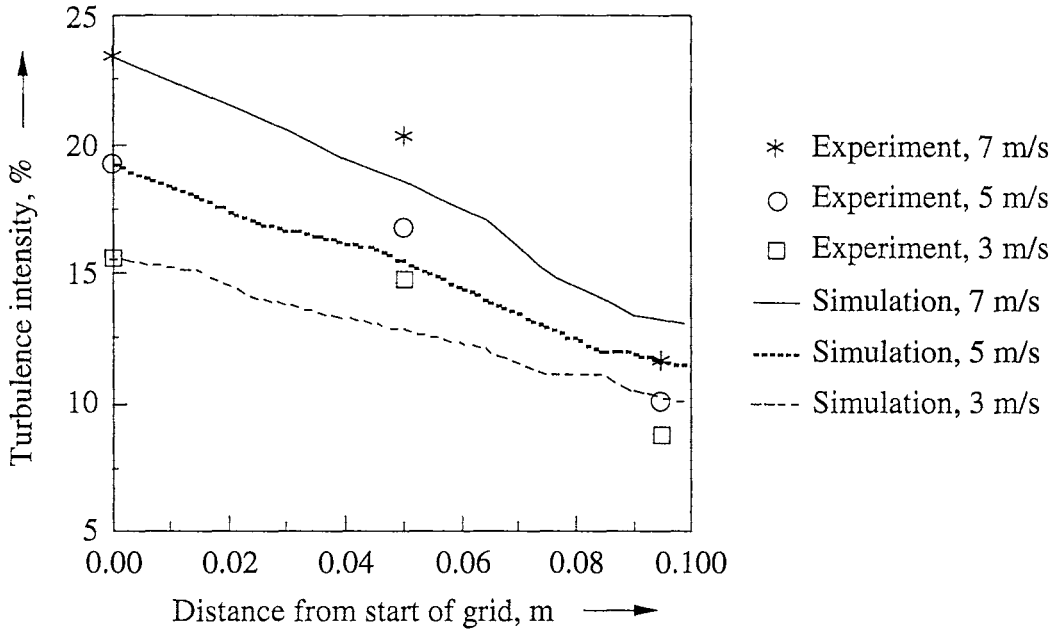

FIGURE 4: Variation of the turbulence intensity with distance from the face of the grid and the air velocity.

Arnaud, Fohr, Garnier and Ricolleau (1991) have simulated the flow patterns around the front and rear of the timber stacks. They calculated a value for the turbulence kinetic energy near the start of the stack of around 0.7 $m^2 s^{-2}$ at an air velocity of 6 m s^{-1}, which is similar to the value in Table 3 of 0.67 $m^2 s^{-2}$ at an air velocity of 7 m s^{-1}. However, they do not state what values for the turbulence parameters they used at the inlet of their simulation, which appears to be just after the air circulation fan. A feature of the qualitative agreement between this work and Arnaud *et al.*. (1991) is our finding of a virtually flat velocity profile in the vicinity of our test section and the maps of velocity vectors given by Arnaud *et al.* (1991). which predict that the flow is only significantly curved in the area of the top boards in the stack. The values of the energy dissipation rate given in Table 3 are consistent with a length scale of turbulence (l) of 0.01 m, according to the following equation for non-swirling flow (Gosman, 1978):-

$$\varepsilon_{inlet} = \frac{k_{inlet}^{3/2}}{1.52l} \qquad (16)$$

Mass-transfer Coefficients

Figure 5 shows the variation of the mass-transfer coefficient with distance as predicted by the numerical simulation at the velocities (between the boards) of 3, 5 and 7 m s^{-1} respectively. The inlet values of the turbulence kinetic energy and the energy dissipiation rate reported in the previous section were used in the simulations. Figures 6, 7 and 8 show comparisons (for velocities 3, 5 and 7 m s^{-1} respectively) with the measured mass-transfer coefficients and theoretical correlations for mass transfer above flat plates, treating the distance from the leading edge of the first board as the appropriate distance in equations (1) and (2). Inspection of Figures 6 to 8 shows that the numerical simulation describes the trends in the experimental mass-transfer coefficients well, but underestimates the magnitudes of the enhancements considerably. It does predict the asymptotic values of the mass-transfer coefficients (far from the leading edges of the boards) within 15%, and much better than the empirical correlations for mass-transfer coefficients over the plates.

Explorations with the numerical simulation suggested that these asymptotic values were larger than those over continuous flat plates because of the turbulence-generating effects of the leading edges of the boards. This is an important contribution of this numerical simulation. These results are also consistent with those of Sparrow *et al.*. (1982).

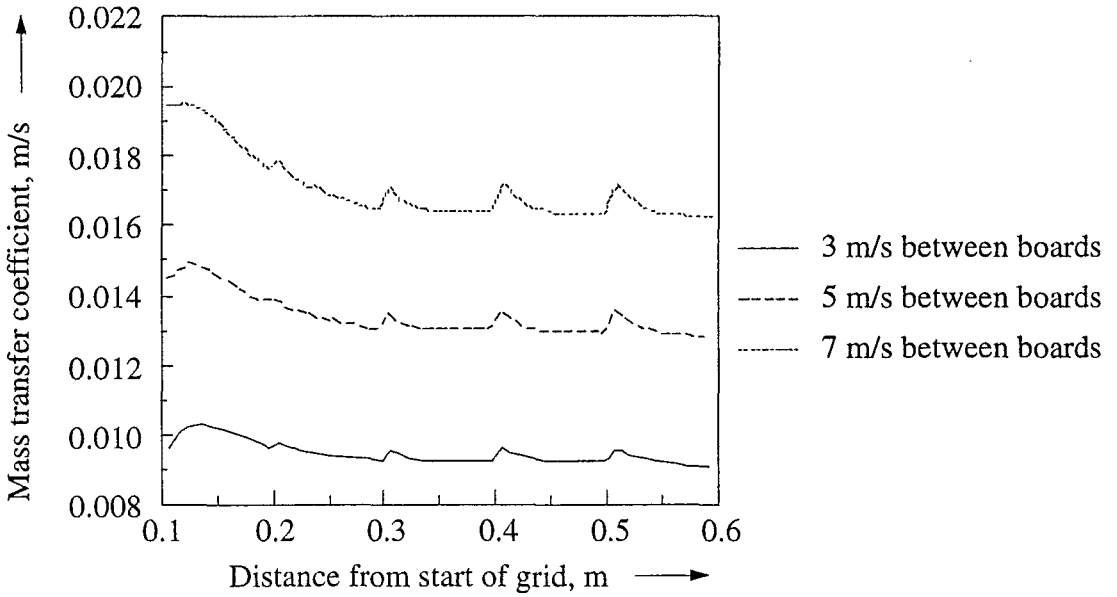

FIGURE 5: Variation of local mass-transfer coefficient with distance predicted by the numerical simulation for uniform board heights and air velocities of 3, 5 and 7 m s^{-1}.

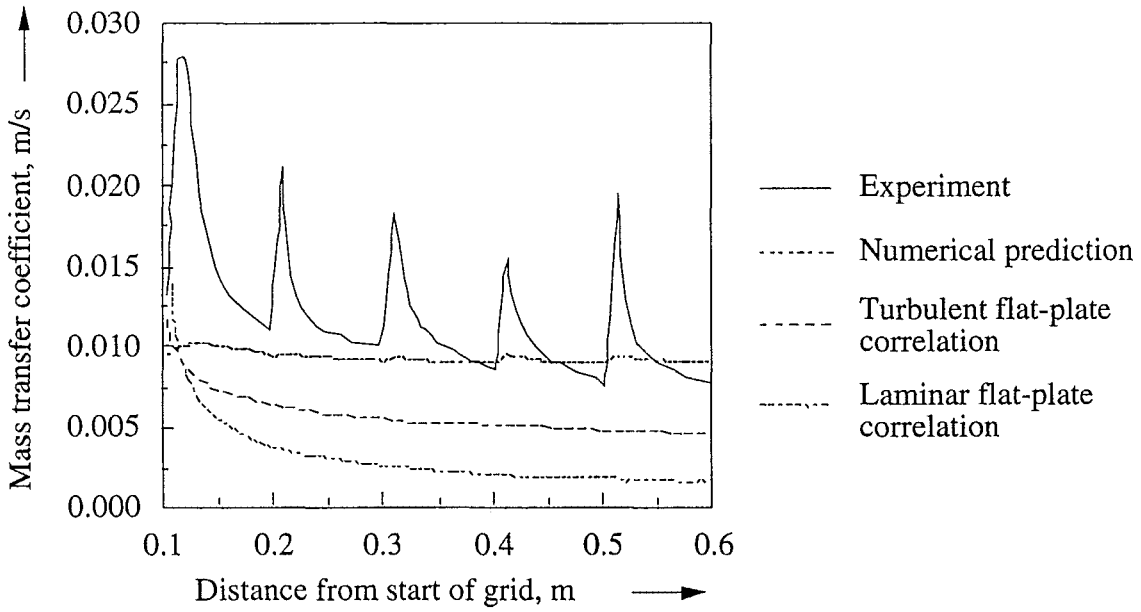

FIGURE 6: Comparison of the predictions of the numerical simulation, the experimental results and empirical correlations for an air velocity of 3 m s^{-1}.

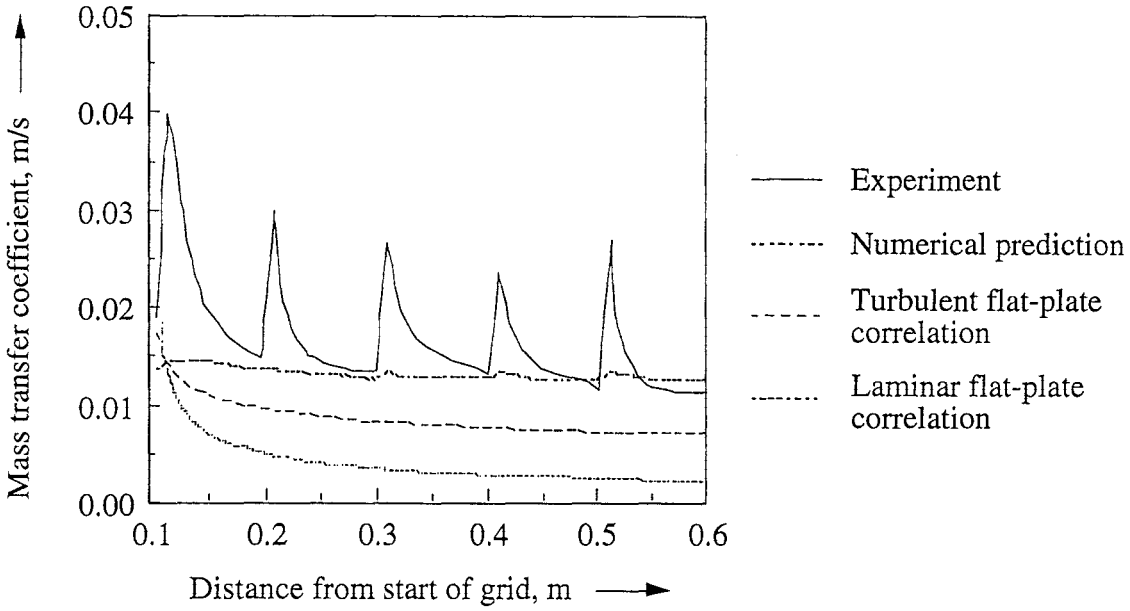

FIGURE 7: Comparison of the predictions of the numerical simulation, the experimental results and empirical correlations for an air velocity of 5 m s^{-1}.

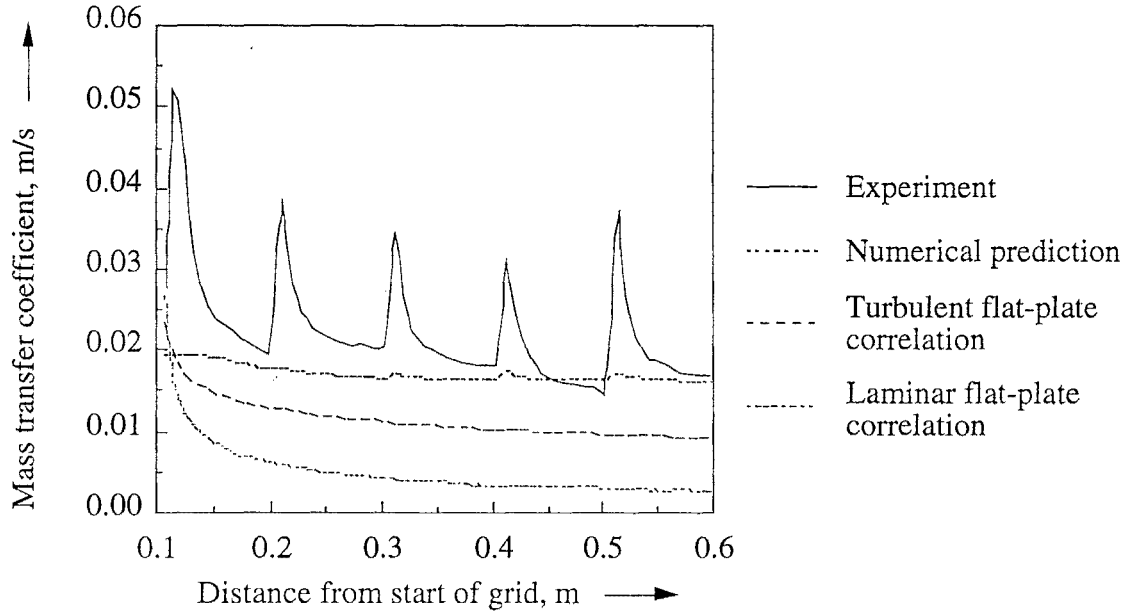

FIGURE 8: Comparison of the predictions of the numerical simulation, the experimental results and empirical correlations for an air velocity of 7 m s^{-1}.

There are a number of possible reasons for the failure of the numerical model to predict the magnitude of the mass transfer enhancements at the leading edges closely.

In the experiments, we used a single subliming board with the other boards in the array being inert. Therefore the boundary conditions around the boards were similar to those for a single plate and different to those in the numerical simulation, where all the boards were assumed to have identical surface conditions. This suggests that the relative variation of the mass-transfer coefficient with distance over each board may be similar to that over a flat

plate. As an illustration, Figure 9 shows what happens in this case for a velocity of 3 m s^{-1}. We estimate the enhancement at the leading edge of each board from the difference between the correlated mass-transfer coefficient (for turbulent flow) at a given distance from the leading edge and the asymptotic value of the correlated coefficient. This predicted enhancement is added to the asymptotic value from the numerical simulation. This procedure is illustrated in Figure 10. This seems to give much closer agreement with the experimental results.

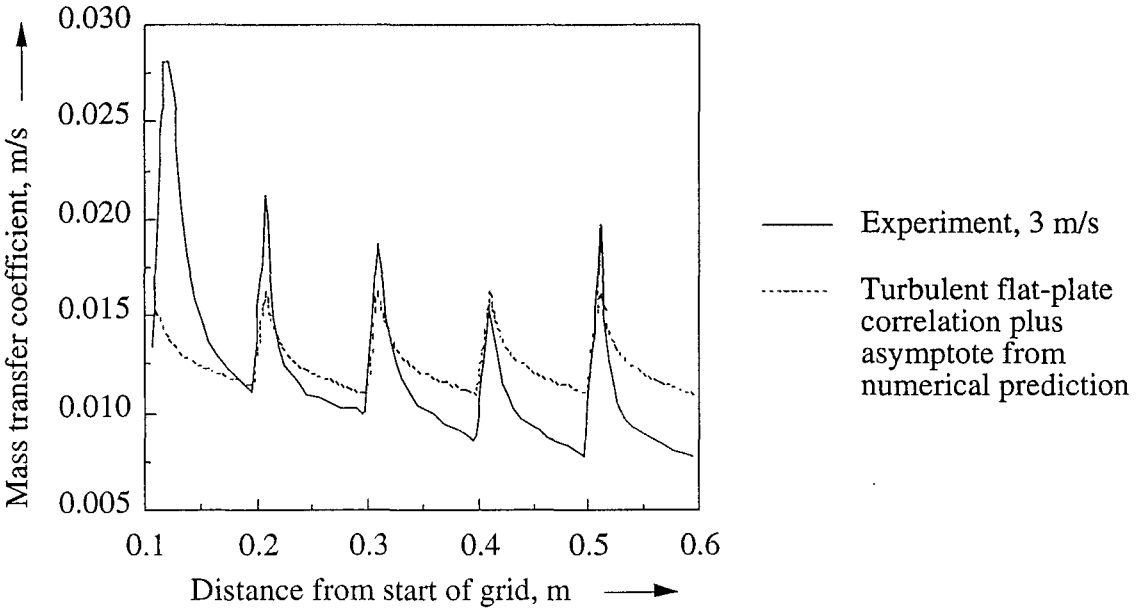

FIGURE 9: The effect of adding the enhancement from the correlation to the asymptotic value from the numerical simulation at a velocity of 3 m s^{-1}.

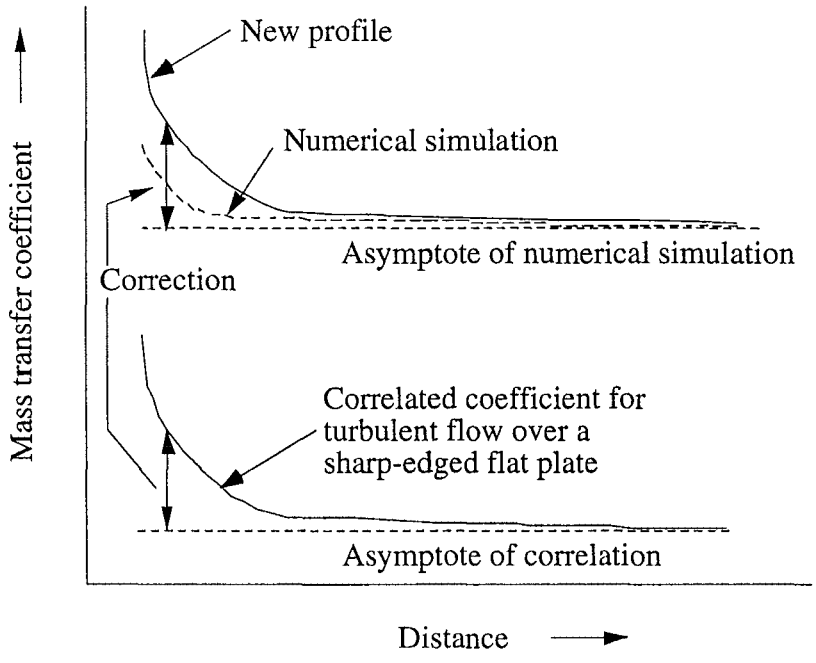

FIGURE 10: Procedure for calculating the new profile in Figure 9.

Another reason for the disagreement between the simulated coefficients and the observed ones may be the time dependency of the flow, as observed by Lee (1990). In flow visualisation experiments in a separate wind tunnel using smoke injection, he found that there were three consecutive and repeated motions of the air flow in the gap, involving the generation of eddies at the gap, outward motion of eddies from the gap and forward motion of deformed eddies along the slab surface. These movements were repeated every 2-3 seconds. The intermittent flow around the gaps may enhance the transfer coefficients near the leading edge considerably. The numerical simulation performed here was time-independent. While the transfer coefficients are implicitly time-averaged by this procedure, it would be more accurate to model the time dependency of the fluid flow pattern before calculating the mass-transfer coefficients. The coefficients would then be averaged.

Also, strictly speaking, at velocities between 3 and 7 m s^{-1} between the boards, the flow should be transitional in nature, so the use of a relatively simple high Reynolds number turbulence model may not be strictly correct. The values of the mass-transfer coefficient predicted by the numerical simulation are likely to be very strongly affected by the choice of wall treatment. It is possible that more sophisticated wall models (as investigated by Polat *et al.*., 1990) may give closer quantitative agreement.

CONCLUSION

The numerical simulation predicts the presence but not the magnitude of the enhancement in the mass-transfer coefficients at the leading edges of the boards. The asymptotic values are predicted within 15%, and this is much closer than predictions from flat plate correlations. The simulation suggests that the gaps between the boards generate additional turbulence over that present with continuous flat plates and this is the cause of the higher coefficients predicted by the numerical simulation. The failure to predict the magnitude of the enhancements may be due to the time dependency of the flow, the inapplicability of the turbulence model or the wall model, or to the boundary conditions in the simulation being different from those in the experiment.

NOMENCLATURE

b	thickness of naphthalene sublimed	m
C_1	constant in turbulence model, Table 1	-
C_2	constant in turbulence model, Table 1	-
C_μ	constant in turbulence model, equation (6)	-
D_{AB}	diffusivity of the solute through air	$m^2\ s^{-1}$
E	constant in wall model, equation (10)	-
f	under-relaxation factor, equation (7)	-
G	generation of turbulence kinetic energy, Table 1	$kg\ m^{-1}\ s^{-3}$
I	turbulence intensity	-
k	turbulence kinetic energy per unit mass	$m^2\ s^{-2}$
K	local mass-transfer coefficient	$m\ s^{-1}$
M_N	molar mass of naphthalene	$kg\ mol^{-1}$
p	static pressure	$N\ m^{-2}$
p_{No}	vapour pressure of naphthalene at the subliming surface	$N\ m^{-2}$
R	universal gas constant	$8.314\ J\ mol^{-1}\ K^{-1}$
S_ϕ	source term in equation (4)	-
t	time	s
T	absolute temperature	K
u	horizontal component of velocity	$m\ s^{-1}$
v	vertical component of velocity	$m\ s^{-1}$
x	distance from the leading edge of the slab	m
y	normal distance from wall	m

Greek

Δ	finite difference	-
ϕ	general variable, equation (4)	-
ε	dissipation rate of turbulence kinetic energy	$m^2\ s^{-3}$
κ	von Karman constant, equation (10)	-
μ	dynamic viscosity	$kg\ m^{-1}\ s^{-1}$
μ_L	laminar viscosity	$kg\ m^{-1}\ s^{-1}$
μ_T	turbulent viscosity	$kg\ m^{-1}\ s^{-1}$
υ	kinematic viscosity	$m^2\ s^{-1}$
Γ_ϕ	transfer coefficient associated with phi, equation (4)	-
ρ	density	$kg\ m^{-3}$
ρ_N	density of solid naphthalene	$kg\ m^{-3}$
σ_k	constant in turbulence model, Table 1	-
σ_ε	constant in turbulence model, Table 1	-
τ_w	wall shear stress	$N\ m^{-2}$

Subscripts

inlet	at inlet of grid
new	new values
old	old values
p	near-wall grid point

Superscripts

+	dimensionless
*	with no under-relaxation
'	instantaneous

Dimensionless numbers

C_f	skin friction coefficient = $\tau_w/(\rho u^2/2)$
Re_x	local Reynolds number = $(x \cdot u)/\upsilon$
Sc	Schmidt number = υ/D_{AB}
Sh_x	local Sherwood number = $(K \cdot x)/D_{AB}$

REFERENCES

Arnaud, G., Fohr, J-P., Garnier, J-P. and Ricolleau, C., 1991. Study of the Air Flow in a Wood Drier, Drying Technology, 9, No. 1, pp. 183-200.

Bayley, F.J. and Turner, A.B., 1971. Transpiration Cooled Turbines, Proc. Instn. Mech. Engrs. (London), 185, pp. 943-951.

Bird, R.B., Stewart, W.E. and Lightfoot, E.N., 1960. Transport Phenomena, J. Wiley, NY, 780 p.

Danckwerts, P.V. and Anolick, C., 1962, Mass transfer From a Grid Packing to an Air Stream, Trans. Instn. Chem. Engrs., 40, pp. 203-213.

Gosman, A.D., 1978. Lecture 7: The Computer Program, presented as a short course entitled the Prediction of the Performance of Combustion Chambers and Furnaces, Pennsylvania State University, PA, April 19-21.

Kho, P.C.S., Keey, R.B. and Walker, J.C.F., 1989. Effects of Minor Board Irregularities and Air Flows on the Drying Rate of Softwood Timber Boards in Kilns, Proc. I.U.F.R.O. Wood Drying Symposium, Seattle, Washington, U.S.A., pp. 150-157.

Launder, B.E. and Spalding, D.B., 1974. The Numerical Computation of Turbulent Flows, Computer Methods in Applied Mechanics and Engineering, 3, pp. 269-289.

Lee, H.S., 1990. Flow Visualisation on High Temperature Wood Drying, B.E. Report, Unviersity of Canterbury, New Zealand, 67 p.

Miller, W.R., 1973. Mass transfer Within Arrays, B.E. Report, University of Canterbury, New Zealand, 22 p.

Patankar, S., 1980. Numerical Heat Transfer and Fluid Flow, Hemisphere, NY, 197p.

Polat, S., Mujumdar, A.S., van Heiningen, A.R.P. and Douglas, W.J.M., 1990. Effect of Near-Wall Modelling on Prediction of Impingement Heat Transfer, Drying Technology, 8, No. 4, pp. 705-730.

Ranz, W.E. and Dickson, P.F., 1965. Mass and Heat Transfer Rates for Large Gradients of Concentration and Temperature, Ind. Eng. Chem. Fundamentals, 4, No. 3, pp. 345-353.

Schlichting, H.L., 1960. Boundary Layer Theory, McGraw-Hill, NY, 748p.

Sørenson, A., 1969. Mass-Transfer Coefficients on Truncated Slabs, Chem. Eng. Sci., 24 pp. 1445-1460.

Sparrow, E.M., Niethammer, J.E. and Chaboki, A., 1982. Heat Transfer and Pressure Drop Characteristics of Arrays of Rectangular Modules Encountered in Electronic Equipment, Int. J. Heat Mass Transfer, 25, No. 7, pp. 961-973.

TIME-DEPENDENT FLOW IN ARRAYS OF TIMBER BOARDS : FLOW VISUALIZATION, MASS-TRANSFER MEASUREMENTS AND NUMERICAL SIMULATION

T.A.G. LANGRISH[1], R.B. KEEY[2], P.C.S KHO[2] AND J.C.F. WALKER[3]

[1] Department of Chemical Engineering, University of Sydney, N.S.W. 2006, Australia.
[2] Department of Chemical and Process Engineering, University of Canterbury, Christchurch 1, New Zealand.
[3] School of Forestry, University of Canterbury, Christchurch 1, New Zealand.

ABSTRACT

A numerical simulation of the airflow patterns around an array of boards in a timber kiln has been modified to include the prediction of time-dependent flows, and the predictions of the simulation have been compared with airflow patterns recorded in a previous flow visualization study and experimental measurements of the mass-transfer coefficients along the boards. The numerical simulation solves the two-dimensional Navier-Stokes equations on a finite-difference grid.

The simulation predicts that the enhancement of the asymptotic values of the mass-transfer coefficients above those predicted by conventional flat-plate correlations is due to the effects of the gaps between the boards in generating additional turbulence throughout the array of boards. The enhancements at the leading edges of the boards are also predicted by the simulation to be consequence of the time-dependent nature of the flow. Periodic oscillations in the flow patterns around the gaps with a period of 1 - 7 s were observed in the flow visualization study, in agreement with the period of 2 s predicted by this simulation. The variation in the experimentally-observed time period may be due to the sensitivity of the vortex-shedding phenomenon to small differences in alignment within the geometry between experiments. The enhancement in the mass-transfer coefficients at the leading edge of the first board is not predicted well, because the treatment of the flow near the wall requires improvement in the simulation.

INTRODUCTION

Increasingly, softwood sawnboards are seasoned in kilns at temperatures above 100°C. Reduction of the drying time is the principal benefit of this technique, which is known as high-temperature drying of timber. Under these conditions, the external convection is relatively more important in determining the drying time than at the lower temperatures traditionally used in kiln seasoning. It is important to have information about the external mass-transfer coefficients along the boards in order to design these newer kilns and analyze their performance.

The importance of the external heat- and mass-transfer process in high-temperature drying of timber can be gauged from the simulation of the drying of spruce under these conditions by Perré and Moyne (1991), who found that all of the unbound water was removed from within the timber after 20 hours for a total drying time of 50 hours. During the removal of unbound water, the external mass-transfer process will control the rate of drying since the internal mass-transfer resistance is very small when unbound water is present. This

suggests that external mass transfer is important for approximately 40% of the total drying time.

As the board temperature increases, so the apparent resistance to moisture movement diminishes. Luikov (1966) quotes Sergovsky's data for the moisture-diffusion coefficient of coniferous species in the tangential direction over a range in moisture content from 10 to 30 percent. For both sapwood and heartwood, the moisture-diffusion coefficient is proportional to the tenth power of the temperature, implying a fourfold increase over the temperature range from 50°C to 100°C. Thus, the external mass transfer is expected to be relatively more dominant in high-temperature drying compared with that at lower temperatures.

Figure 1 shows a typical stacking arrangement, highlighting three dimensions of possible interest. These dimensions are the pitch (typically 500 mm) between stickers, which are pieces of timber separating rows of boards to allow air to flow through the stack, the spacing between rows of boards (between 15 and 25 mm), and gaps between board edges, which are an inevitable result of both imperfect sawing and shrinkage. These gaps are usually of the order of 1 mm. In this paper, we will refer to 'gaps' as the distance between board edges in the streamwise direction and 'spacing' as the distance between rows of boards. A deliberate increase in the gap dimensions would mean a reduction in kiln capacity, since fewer boards would fit inside a stack of a given size.

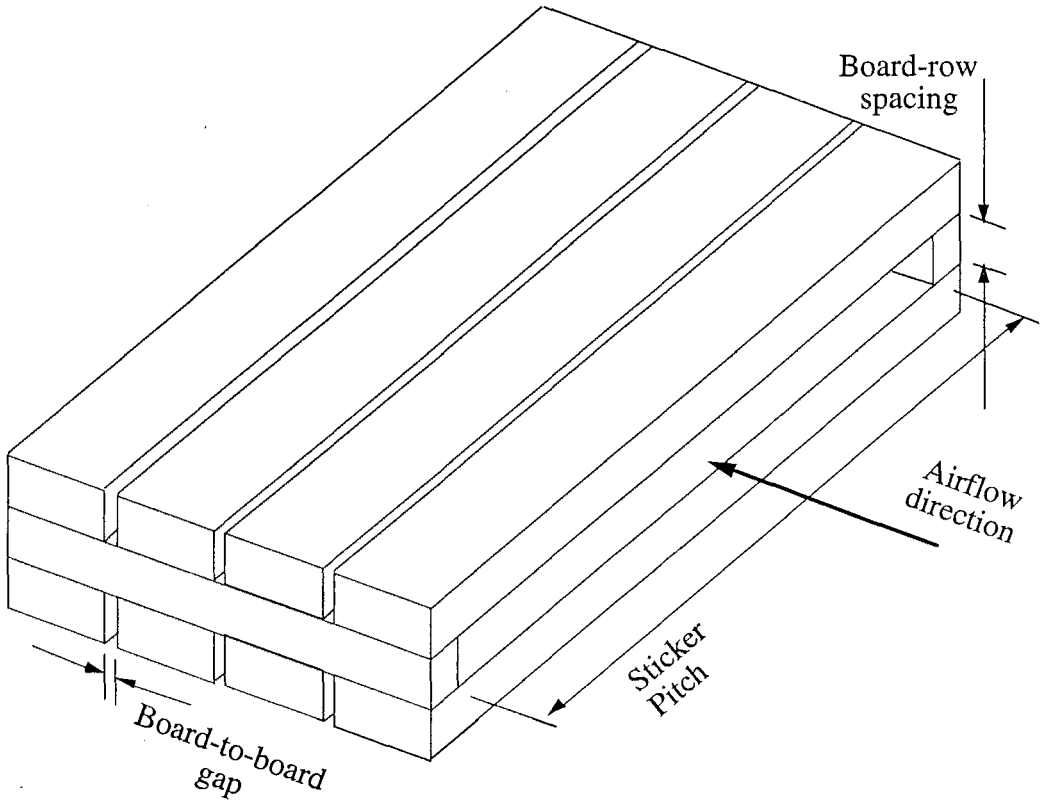

Figure 1 Nomenclature for kiln-stacking arrangements.

The traditional correlations for mass transfer over flat plates have been measured using an air jet issuing from a smoothly converging nozzle in parallel with the flat evaporating surface (Ranz and Dickson, 1965). For example, whenever a laminar boundary layer is developing across a plate, the correlation for mass transfer is given by (Welty *et al.*, 1969):-

$$Sh_x = 0.332\, Re_x^{1/2}\, Sc^{1/3} \qquad (1)$$

where Sh_x is the local Sherwood number (based on the distance from the leading edge), Re_x is the local Reynolds number and Sc is the Schmidt number. If the boundary layer above the plate is turbulent, then from Welty *et al.* (1969):-

$$Sh_x = 0.0288\ Re_x^{4/5}\ Sc^{1/3} \qquad (2)$$

There is considerable experimental evidence that the turbulence intensity, defined as the ratio of the root mean square of the fluctuating component of velocity to the mean velocity, influences both the magnitude and the streamwise variation of the mass-transfer coefficient. The turbulence intensity (I) may be defined as follows:-

$$I = \frac{u'}{u} \times 100\ (\%) \qquad (3)$$

where u' is the root mean square of the fluctuating component of velocity and u is the mean velocity. The importance of the turbulence intensity in influencing transfer coefficients has been shown by Bayley and Turner (1971), who found that increasing the intensity of turbulence from 0.45% to 5.9% doubled the heat-transfer coefficients over a turbine blade. Also, Sugawara *et. al.* (1988) have found that the heat-transfer coefficients from a blunt-edged flat plate increased with the level of free-stream turbulence, rapidly at small turbulence levels and levelling off at a turbulence level of 7 - 8% to coefficients which are about 55% higher than those obtained for very small free-stream turbulence. Most existing correlations for turbulent transfer are based on turbulence produced by jets, where the turbulence intensities may be as low as 1% (Polat *et al.*, 1990). These correlations may not be valid for the higher turbulence intensities found in the rectangular channels of kiln stacks. For the array of slabs studied here, we would expect the turbulence intensities to be even greater than those reported by Bird *et al.* (1960) for channels (2 to 12%).

Mass transfer in arrays of modules placed along one wall of a rectangular duct has been studied experimentally by Sparrow *et al.* (1982). They measured mass-transfer coefficients from naphthalene sublimation rates and related these to heat-transfer coefficients using the Chilton-Colburn analogy. The modules, 27 mm square, were arranged in rows with 6.3 mm between modules. The highest Sherwood number was observed in the first row, but the Sherwood number reached a limiting value after five rows. The important feature of their results is that the Sherwood numbers in the asymptotic region were considerably above those which would be predicted from flat-plate correlations. Although the authors did not comment on this, it is possible that the turbulence-inducing effects of the gaps between modules were responsible for the enhancement in the asymptotic heat-transfer coefficients above those predicted by the flat-plate correlations.

In a kiln, the gaps between boards are typically small (of the order of 1 mm) compared with the spacing between board rows (15-25 mm). The ratio of length scales (about 1:20) is significantly different to the ratio of tube pitch to tube diameter in the shell-side flow path of heat exchangers (of order 1:1). The length-scale ratio in kilns is also different to the ratios of shell diameter to baffle spacing (1:1.5) and baffle height to shell diameter (1:4) as studied by Mackley and co-workers (Mackley and Ni, 1991; Harrison and Mackley, 1992). This difference in geometrical ratios raises doubts that the information gained about the oscillations and vortices generated behind baffles in heat exchangers is directly applicable to the vortices generated in the gaps between boards in timber kilns.

To date, there has been very little experimental work to obtain quantitative expressions for the heat- and mass-transfer coefficients at the surface of blunt-edged slabs. The variation of local mass-transfer coefficients with velocity on a single isolated slab has been investigated by Sørenson (1969). Miller (1973) has extended this work to an array of slabs. Both these experiments were performed in wind tunnels. Kho *et al.* (1989) have investigated the effects of minor board irregularities (a consequence of inaccurate sawing of timber) and varying air velocities on the profile of the local mass-transfer coefficients with distance from the leading edges of the boards in an array inside a timber kiln. The geometry of this array

was similar to a stack of boards, and the air velocity between the boards ranged from 3 m s^{-1} to 7 m s^{-1}.

In a preliminary paper, Langrish *et al.* (1991) have reported a comparison between these measurements and a numerical simulation of the airflow patterns in an array of boards. They solved the two-dimensional Navier-Stokes equations on a finite-difference grid, assuming that the flow was time-independent. The experimental results showed that the small gaps between the boards, which are inevitable in practice, caused large enhancements in the mass-transfer coefficients near the leading edges of the boards. The asymptotic values of these coefficients were always greater than those predicted from flat-plate correlations. The simulation also predicted enhancements in the mass-transfer coefficients at the leading edges, but of smaller magnitude than those measured. The asymptotic values were predicted within 15%. The simulation showed that the measured increase over the values predicted by the flat-plate correlations was due to the generation of turbulence by the gaps between the boards.

However, a visualization study of the flow in the gaps between the boards (Lee, 1990) has found low-frequency oscillations in the flow patterns around the gaps, with a period of 1 - 7 seconds. These oscillations cast doubt over the assumption made by Langrish *et al.* (1991) that the flow patterns in a stack are independent of time. These low-frequency oscillations resembled vortex shedding from bluff bodies. Nakamura *et al.* (1991) have investigated vortex shedding from isolated flat plates with square leading and trailing edges at Reynolds numbers from 1000 - 3000. For chord-to-thickness (c/W) ratios of 3 to 5, the Strouhal number (St), defined as

$$St = \frac{f \cdot W}{u} \tag{4}$$

was virtually constant and equal to 0.6. Here f is the frequency of vortex shedding, W is the thickness of the plate and u is the freestream velocity. The effect of an array of boards on the Strouhal number for vortex shedding does not seem to have been studied, particularly where the gaps between the boards are small as in this investigation.

At the low frequencies seen by Lee (1990), the time-dependency of the flow may be readily incorporated into the numerical simulation reported by Langrish *et al.* (1991), which is based on solving the time-averaged Navier-Stokes equations. This modification will be described here. The flow patterns predicted by this numerical simulation will be compared with those observed experimentally. Finally, the effect of time-dependent flow on the time-averaged mass-transfer coefficients in the numerical simulation will be reported, and the predictions compared with the experimental measurements of Kho *et al.* (1989).

This paper describes the extension of the time-independent model of Langrish et al. (1991) to the consideration of time-dependent flow around boards in stacks of timber within kilns. We demonstrate that there is a significant improvement in the agreement between the predicted and the observed mass-transfer coefficients when time-dependent flow around the boards is taken into account.

NUMERICAL SIMULATION

The numerical simulation followed the procedure outlined by Patankar (1980) for predicting the horizontal and vertical velocities in a two-dimensional flow which is bounded by plane walls. Any three-dimensionality of the flow has been ignored, since the pitch between stickers is typically large (500 mm) compared to the spacing between rows of board (15 - 25 mm). The flow was also assumed to be incompressible and isothermal. The simulation solved for five variables:-

u : the average horizontal velocity (x-direction);
v : the average vertical velocity (y-direction);
k : the turbulence kinetic energy (per unit mass);
ε : the rate of dissipation of turbulence kinetic energy;
P : the static pressure.

The procedure is to solve the time-averaged Navier-Stokes equations for continuity (conservation of total mass) and conservation of momentum in the horizontal and vertical directions, and one equation each for the variables k and ε. The high-Reynolds form of the k - ε model of Launder and Spalding (1974) was used for simplicity, even though the Reynolds number for the flow based on the spacing between board rows (25 mm) was only just turbulent (5000) at the lowest velocity studied (3 m s $^{-1}$). The standard constants for general free turbulent flows, also taken from Launder and Spalding (1974), were used in the k - ε model. The treatment of convection and diffusion (of any property) followed the hybrid scheme described by Patankar (1980).

The basic mathematical formulation of the governing equations has been given by Langrish *et al.* (1991). However, in order to account for the time-dependent nature of the flow, the general form of the governing equations has been modified from the form given by them by including the time-dependent term on the far left of the general conservation equation, as below:-

$$\frac{\partial}{\partial t}(\rho\cdot\phi) + \frac{\partial(\rho\cdot u\cdot\phi)}{\partial x} + \frac{\partial(\rho\cdot v\cdot\phi)}{\partial y} = \frac{\partial}{\partial x}\left(\Gamma_\phi \frac{\partial\phi}{\partial x}\right) + \frac{\partial}{\partial y}\left(\Gamma_\phi \frac{\partial\phi}{\partial y}\right) + S_\phi \qquad (5)$$

Here ϕ is the dependent variable of interest (for example, horizontal velocity), Γ_ϕ is an effective diffusion coefficient and S_ϕ is the source term, which includes all the terms in the governing equations other than those in the 'convection' and 'diffusion' terms. The density of the fluid is ρ and t is time. The terms Γ_ϕ and S_ϕ have been described in detail in Langrish *et al.* (1991) and Polat *et al.* (1991) for each of the dependent variables. The source terms (S_ϕ) and the diffusion coefficients (Γ_ϕ) follow directly from rearranging the Navier-Stokes equations in the form of equation (5), as described in Patankar (1980). For example, in the conservation equation for x-directed momentum, the diffusion coefficient is the effective viscosity and the source term includes the pressure gradient in the x-direction and the gradient of the velocity vector. Equation (5) has been discretized as described in Patankar (1980). Time steps of 0.1 s have been used in this simulation. The grid size used (268 steps in the streamwise direction and 33 steps vertically) was sufficiently fine so that halving the distance between grid lines changed the velocities at any point by less than 5%. The interfacial mass-transfer coefficients have been predicted from wall shear stresses using the Chilton-Colburn analogy between mass and momentum transfer, as described in the discussion of the near-wall flow at the end of this section.

The equations have been solved in the order known as the SIMPLE (Semi-Implicit Pressure-Linked Equations) scheme (Patankar, 1980). In this scheme, the pressure field is guessed

first, and the momentum equations are solved to give the velocity field. The velocity field is then corrected so that it satisfies continuity (conservation of mass) and the pressure field is recalculated. The momentum equations are solved again, and this procedure is repeated until conservation of both mass and momentum are satisfied throughout the flowfield within preset tolerances. For each control cell within the finite-difference grid, a residual is defined for each variable as the absolute value of the difference between inflow and outflow. These residuals are then summed over the whole field, and convergence is considered to be achieved when the total residual for each variable is less than an absolute value of 10^{-6}. Taking the continuity equation (total mass) as an example, a total residual of 10^{-6} would imply a mass balance discrepancy over the whole grid of 10^{-6} kg per metre depth of the flowfield. By comparison, the grid was 100 mm high and 775 mm long, so a one metre depth of field has a volume of 0.0775 m^3, and this is approximately 0.09 kg of air at ambient temperature and pressure. Therefore, a total residual of 10^{-6} kg implies a discrepancy of less than 0.001% in the mass balance.

These equations are all non-linear and prone to diverge even when a solution exists, so the changes in the values of the dependent variables from iteration to iteration have been slowed down by Wegstein under-relaxation. Under-relaxation factors (h) have been defined by:-

$$\phi_{new} = h \cdot \phi^{*}_{new} + (1 - h) \cdot \phi_{old} \qquad (6)$$

where the subscripts *old* and *new* refer to the values of the dependent variable (ϕ) from the previous iteration and the current one respectively, and the superscript * refers to the value which would be produced in the current iteration if no under-relaxation were used. The under-relaxation factors have been taken as 0.1 for all variables. At least 800 iterations have been used in each simulation trial.

The boundary conditions and layout were described in detail in Langrish *et al.* (1991). The inlet conditions were also measured experimentally, and these were also reported in that work. A typical grid layout is shown in Figure 2.

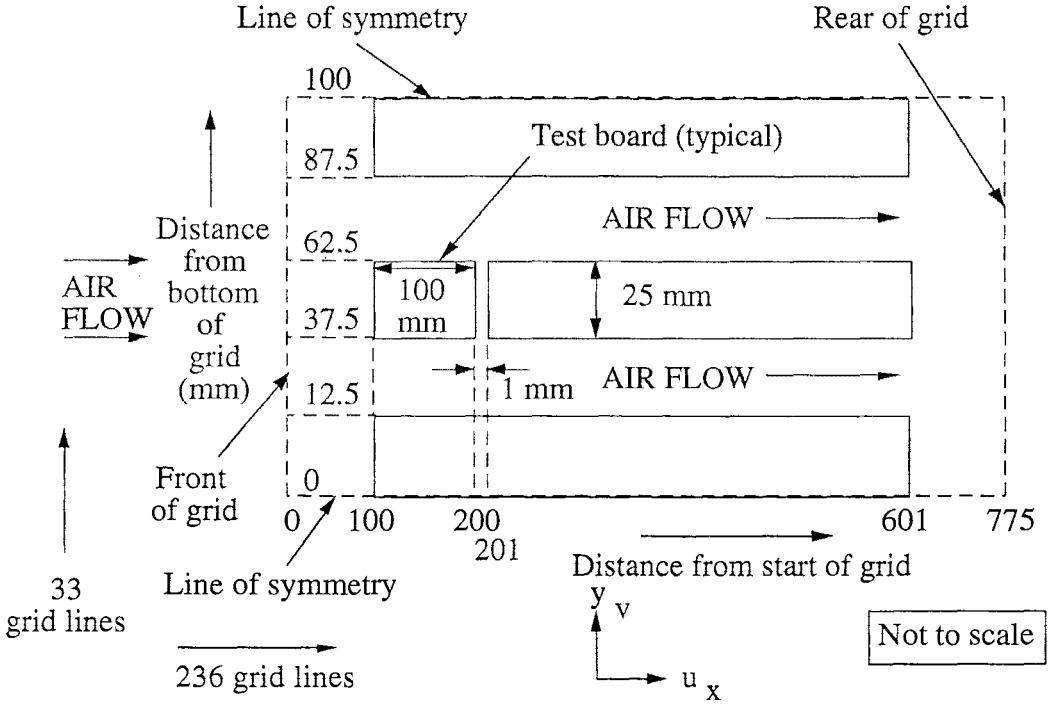

Figure 2 The layout of the flow situation.

For cells near the wall, the Navier-Stokes equations have been modified in order to reduce the amount of grid refinement needed for a grid-independent solution. These equations were obtained by assuming a linear variation of turbulent viscosity with distance from the wall, and the 'universal' velocity profile was assumed to apply close to the wall:-

$$u^+ = y^+ \qquad \text{for } y^+ \leq 11.225 \tag{7}$$

$$u^+ = \frac{1}{K} \ln (Ey^+) \qquad \text{for } y^+ \geq 11.225 \tag{8}$$

Here u^+ is the dimensionless velocity, and K and E are constants. The dimensionless distance to the wall is:-

$$y^+ = y_p \frac{\rho \cdot C_\mu^{1/2} \cdot k_p^{1/2}}{\mu} \tag{9}$$

where y_p is the distance of the near-wall grid point to the wall, μ is the dynamic viscosity of the fluid and C_μ is a constant in the k - ε turbulence model. The quantity k_p, the value of k for the grid point, was calculated from a standard balance over a control volume near the wall, with diffusion of energy to the wall being set to zero. This balance has been described by Launder and Spalding (1974). From the value of y^+ calculated in equation (9), the value of u^+ may be calculated from equations (7) or (8). This enables the velocity at the near-wall grid point, u_p, to be calculated. Also, if the logarithmic velocity profile is assumed to apply in the near-wall region, uniform shear stress prevails in the region between the near-wall grid point and the wall, and generation and dissipation of energy are in balance there. Then the wall shear stress (τ_w) may be calculated from the equation:-

$$\tau_w = \rho \cdot C_\mu^{1/2} \cdot k_p \tag{10}$$

This enables the true velocity u_p to be calculated from u^+ using the conventional definition for the skin-friction velocity, as follows:-

$$u_p = u^+ \sqrt{\frac{\tau_w}{\rho}} \tag{11}$$

This treatment of the near-wall behaviour of the fluid flow does not tie the flow to the wall, since flow separation will occur wherever a velocity directed purely away from the wall is required to satisfy the equations of continuity and momentum conservation in a local region. In this case, the shear stress is zero in the equation above and the component of velocity parallel to the wall (u_p) will also be zero. The prediction of flow separation using this technique has been demonstrated in a number of works, for example Pai, Michelfelder and Spalding (1977). The wall stresses may be related to the mass-transfer coefficients through the Chilton-Colburn analogy between mass and momentum transfer, so that:-

$$Sh_x \cdot Sc^{1/3} = \frac{C_f}{2} \tag{12}$$

$$C_f = \frac{\tau_w}{\rho \cdot u^2/2} \tag{13}$$

where C_f is the skin friction coefficient.

EXPERIMENTAL

Mass-Transfer Coefficients

Mass-transfer coefficients have been measured by Kho *et al.* (1989) in a 2.55 m wide × 2.8 m tall × 2.3 m long industrial-type kiln at the School of Forestry, University of Canterbury, Christchurch, New Zealand. Local mass-transfer coefficients along the boards were determined using a slight modification of the naphthalene sublimation technique used by Danckwerts and Anolick (1962), Sørenson (1969) and Miller(1973).

The experiments involved the use of an aluminium slab of dimensions 640 mm × 100 mm × 20 mm, with a 100 mm × 98 mm × 2 mm recess milled at the centre of the board (Figure 3).

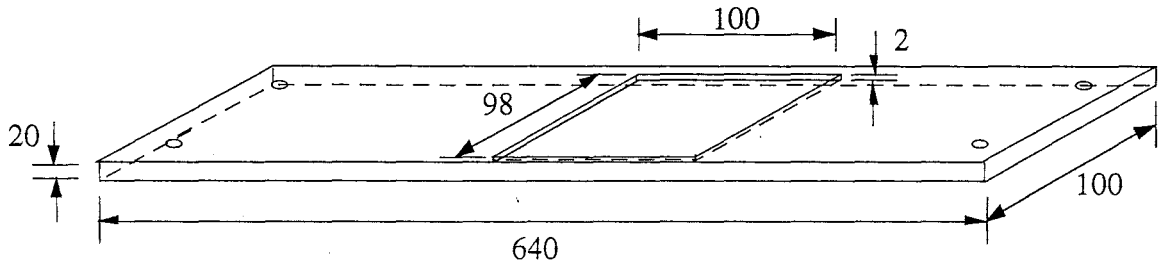

Figure 3 Isometric view of the test board.

Analytical-grade naphthalene was cast into this recess, and the surface of the casting smoothed until a visually smooth surface was obtained. The thickness of the casting was monitored using a Mitutoyo dial gauge with a resolution of ±0.005 mm, and changes in the thickness of naphthalene (Δb) over 90 or 120 minute time intervals (Δt) were converted into mass-transfer coefficients using the following equation:-

$$K = \frac{\rho_N.R.T}{M_N.P_{No}} \cdot \frac{\Delta b}{\Delta t} \qquad (14)$$

where ρ_N is the density of solid naphthalene, R is the universal gas constant, T is the absolute temperature, M_N is the molar mass of naphthalene and P_{No} is the vapour pressure of naphthalene at the subliming surface. The resolution of the dial gauge was 4% of the minimum thickness of naphthalene sublimed in any experiment, so the uncertainty in the measured mass-transfer coefficients is of this order.

After casting, the thickness of the test board was built up to the desired thickness by bolting 2 or 3 mm thick aluminium boards of a similar dimension to the underside of the test board. This test board was placed inside a box which was connected directly to the exhaust duct of the kiln to give once-through air flow (Figure 4). The box contained five sheets of medium-density fibreboard, each with dimensions 640 × 500 × 25 mm, except for the test layer which was recut to accommodate the test board. The layers were separated by two 25 × 25 mm stickers placed 600 mm apart. The box system allowed retrieval of the aluminium board in less than a minute. The rest of the kiln was stacked with dry timber boards using the same geometrical configuration. Therefore air was cycled through the stack until it was vented to atmosphere through the box containing the aluminium board.

Further details of the technique and the experimental equipment are given in Kho *et al.* (1989). Air velocities of 3 m s^{-1}, 5 m s^{-1} and 7 m s^{-1} between the boards were used giving Reynolds numbers based on the board spacing of over 5000. The temperature used in these tests was 41±0.5°C.

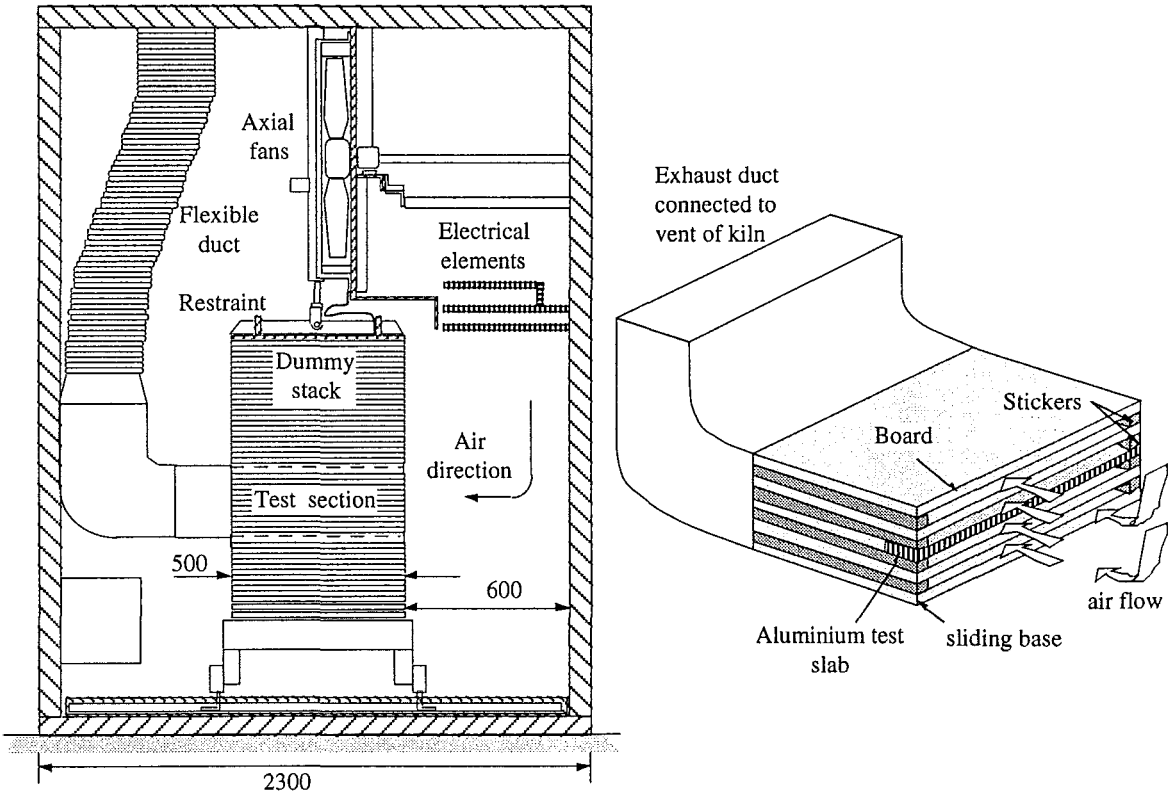

Figure 4 Side elevation of the kiln arrangements and an isometric view of the test section.

Wind tunnel

A low turbulence-intensity wind tunnel was used for the flow visualization measurements due to the difficulty in observing the floe patterns inside the timber kiln used for the measurements of the mass-transfer coefficients. The tunnel was 0.340 m high, 0.225 m wide and 3.85 m long, and incorporated a settling chamber 0.840 m high, 0.740 m wide and 0.500 m long to damp fluctuations from the Rootes blower used for the air supply. The settling chamber was followed by a bell-mouthed transition to a honeycomb 0.340 m high, 0.225 m wide and 0.150 m long, with channels 5 mm square to reduce the level of turbulence. The tunnel had clear Perspex sides to enable the flow patterns to be visualized and recorded. The turbulence intensity, as measured by a TSI hot-wire anemometer with a 10 μm platinum-rhodium wire, was between 5% and 15%. This range is somewhat lower than the levels recorded by Langrish *et al.* (1991) in the timber kiln used by Kho *et al.* (1989) which were from 16 - 23% (Table 1). Here, air velocities of 3 m s^{-1} and 5 m s^{-1} above the boards were used. In these wind-tunnel experiments, a single row of boards was used, but an important feature of the stacking arrangement in a timber kiln (gaps between adjacent boards in the streamwise direction) was retained.

Velocity between the boards ($m\ s^{-1}$)	Turbulence intensity in front of stack (%)	Mass-transfer coefficient from the flat-plate correlation ($m\ s^{-1}$)	Measured mass-transfer coefficient ($m\ s^{-1}$)	Enhancement of measured coefficient over correlation (%)
3	16	0.0047	0.0078	66
5	19	0.0071	0.0115	62
7	23	0.0092	0.0167	83

Table 1 The enhancement of the asymptotic values of the mass-transfer coefficients above the values from the flat-plate correlation for turbulent flow, together with the free-stream turbulence levels in the timber kiln.

The lighting arrangement is shown in Figure 5. This used top and bottom illumination. Slide projectors were used since they have high-intensity lamps. Recording the visualized flow patterns on film was difficult due to the low light levels. Black-and-white films (Ilford HP5) with a rating of 800 ASA was used with an exposure time of 1/60 s and a time between frames of 1 s. This exposure time was sufficiently short to capture the development of the flow pattern while giving an adequate light level.

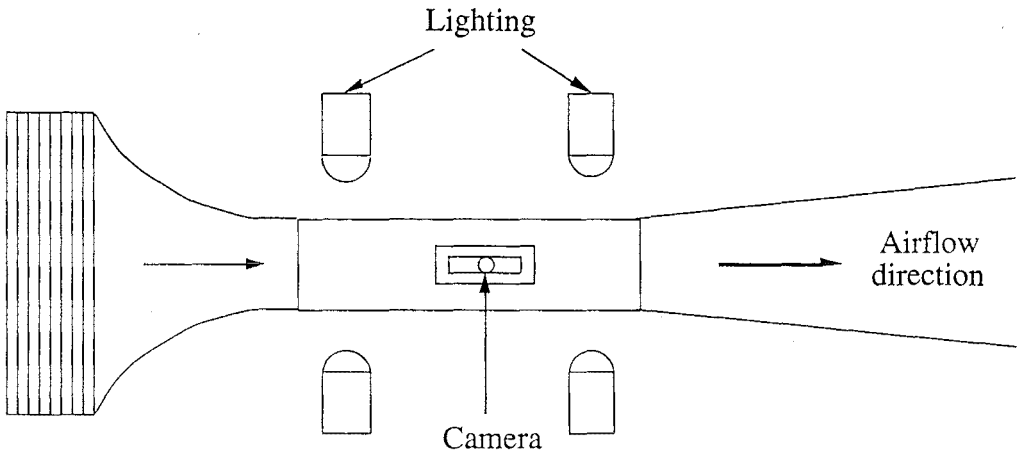

Figure 5 Schematic diagram of the lighting arrangement for flow visualization.

Smoke Generator

A simple smoke generator was constructed, as shown in Figure 6. This consisted of a 150 mm long glass tube of 40 mm diameter in which pieces of 'mosquito coil' were burnt to give a dense smoke. The air flowrate through the glass tube was controlled so that the velocity of the smoke jet which was injected into the wind tunnel could be maintained at the same velocity as the air in the tunnel. Isokinetic injection minimized the dispersion rate of the smoke trail. The smoke was injected into the wind tunnel using a 5 mm diameter copper tube as a compromise between achieving an adequate rate of smoke injection and minimizing the obstruction to the airflow.

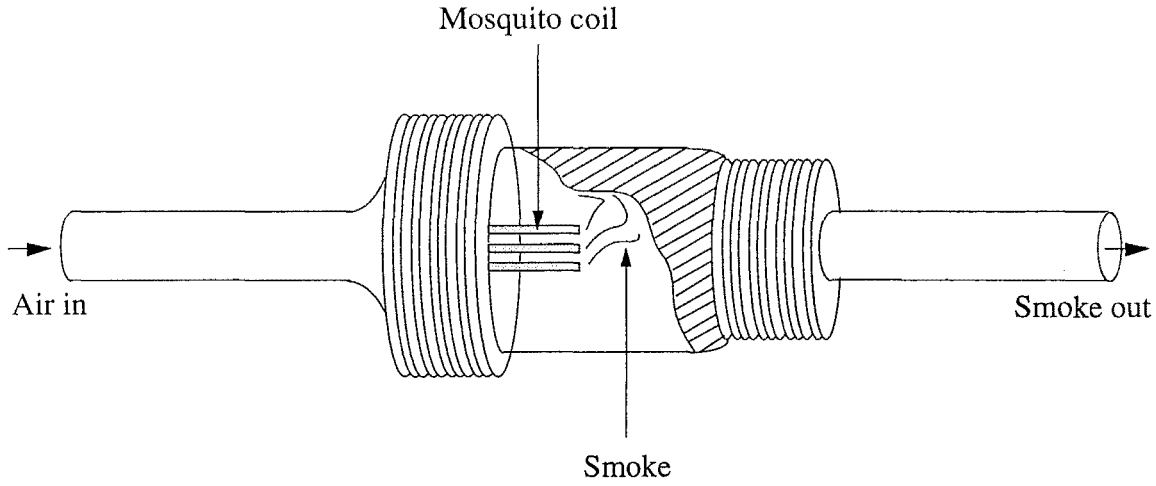

Figure 6 Sketch of the smoke generator.

RESULTS AND DISCUSSION

Flow Patterns

A sample set of photographs from the flow visualization work of Lee (1990) is displayed in Figure 7. This shows three consecutive and repeated motions of the airflow in the gap, involving the generation of eddies at the gap, outward movement of eddies from the gap and forward movement of deformed eddies along the board surface. In Figure 7(c), taken two seconds after Figure 7(a), the eddy which has been rejected from the gap in Figure 7(b) is considerably flattened and deformed in the downstream direction. This sequence of movements was repeated every 1-7 seconds, with the variation quoted (1-7 s) being from experiment to experiment. The reason for the variation in the experimentally-measured time period is unknown, since the experiments were carried out under closely-similar conditions, but may be due to the sensitivity of the vortex-shedding phenomenon under these conditions to very small (less than 0.2 mm) changes in alignment.

The flow in the gaps is predicted by our numerical simulation to be periodic with a period of almost exactly 2 seconds, which is within the range found by Lee (1990). The calculated period is not sensitive to the size of the time step used in discretizing equation (5), providing that the size of the time step is less than or equal to 0.1 s. Plots of the computed streamfunctions around the gaps are shown in Figure 8.

The predicted sequence of events is:-

1. There is a slow circulation in the gap. The streamlines outside the gap show no large effects due to the slow circulation.

2. The circulation in the gap speeds up. The streamlines drawn into the gap and push away from the leading edge of the board on the downstream side. The increasing speed of circulation is shown by the streamlines becoming more closely spaced, with one closed streamfunction contour in the gap in Figure 8(b), while there are two fully-closed streamfunction contours shown in Figure 8(d).

3. The circulation zone speeds up further, pushing the streamlines away from the gap. The streamlines are directed down at the following board.

4. Eventually the main body of the flow pushes the circulation zone back into the gap. The speed of the circulation zone slows down and we return to the original situation (slow circulation in the gap).

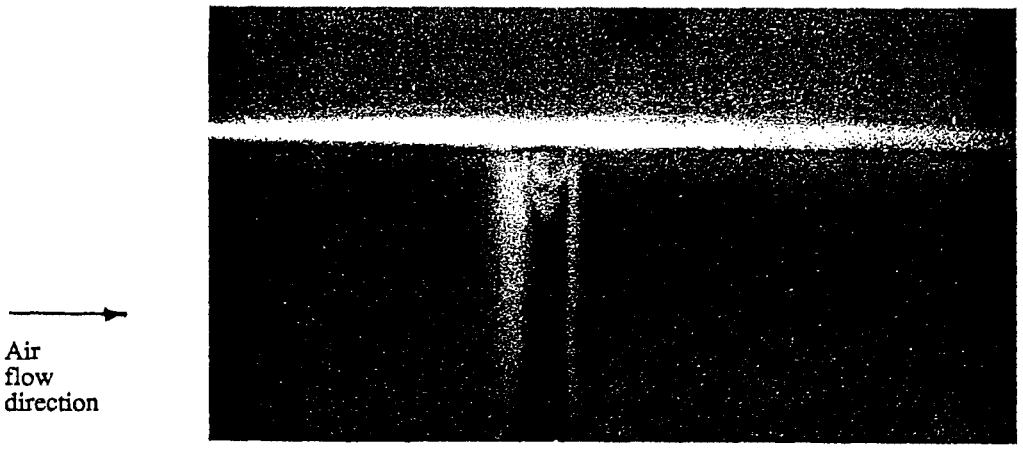

Gap 1 mm
(a) Generation of the eddies

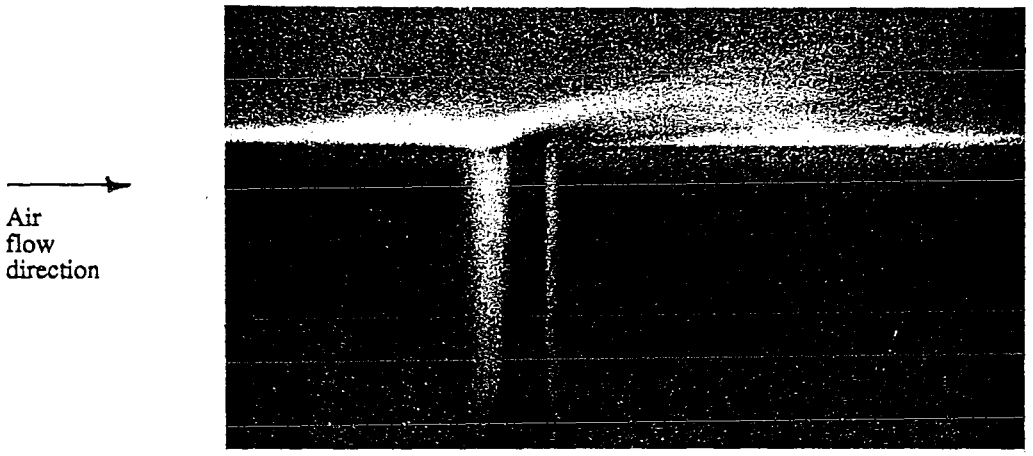

Gap 1 mm
(b) Outward motion of the eddies (1 second after (a))

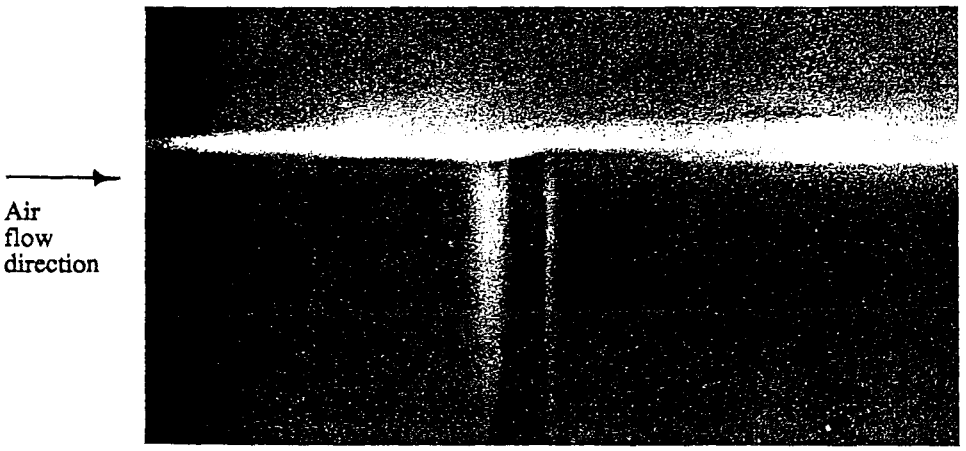

Gap 1 mm
(c) Forward motion of the deformed eddies (2 seconds after (a))

Figure 7 A typical set of photographs from the flow visualization experiments.

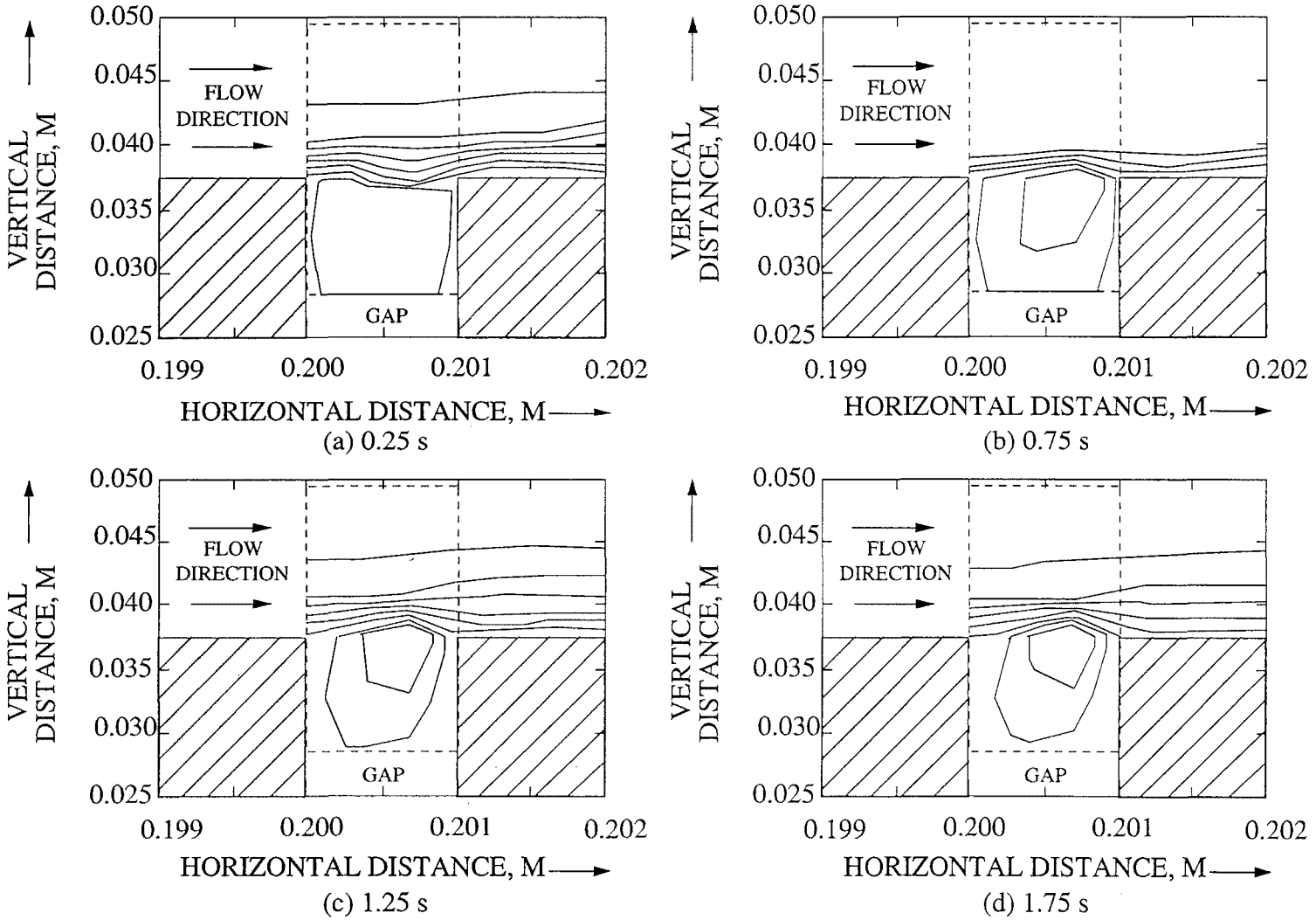

Figure 8 Streamfunctions plots around the gap between two boards, from the numerical simulation (distances are relative to the bottom left-hand corner of the grid in Figure 2)

Therefore, the generation and dissipation of eddies in the gaps is predicted, even though the results of the simulation do not show all the features observed experimentally such as the outward movement of the eddies from the gap and their movement along the board surface. However, a significant feature is the substantial amount of momentum exchange between the gaps and the bulk of the airflow. This momentum exchange is important in the context of the effect of surface roughness on mass transfer, which will be discussed in the following section.

Since the board thickness was 25 mm and the air velocity was over 1 m s^{-1}, a period for the oscillations of 1-7 s implies a frequency of under 1 Hz and a Strouhal number of under 0.025 for the oscillations in the gaps. This value is over an order of magnitude less than the Strouhal numbers for vortex shedding from isolated flat plates observed by Nakamura *et al.* (1991). The difference suggests that the proximity of the boards in the region of the gaps has increased the time scale of the flow in this region substantially compared with the situation for isolated flat plates.

Mass-Transfer Coefficients

Figures 9, 10 and 11 show comparisons (for velocities of 3, 5 and 7 m s^{-1} between the boards respectively) between the predictions of the numerical simulation for time-dependent flow and both the measured mass-transfer coefficients and theoretical correlations for mass transfer above flat plates. These measurements were performed in the timber kiln. The distance from the leading edge of the first board has been treated as the appropriate distance in equations (1) and (2). The predicted mass-transfer coefficients from the time-dependent simulation are time-averaged values, since the flow patterns and therefore the mass-transfer coefficients are predicted to vary with time. The contours of the predicted streamfunctions over the downstream board in Figure 8 show that the velocity over the boards changes during each cycle, causing variations in the mass-transfer coefficients. The mass-transfer coefficients were averaged over a much longer time period (200 s) than the period of the flow oscillations (2 s).

The close correspondence between the flow patterns in the timber kiln and those in the wind tunnel is suggested by the similarity between the mass-transfer coefficients measured over the array of boards in both pieces of equipment, as shown in Figure 12 for an air velocity of 5 m s^{-1} over the boards. The differences between the mass-transfer coefficients recorded in the wind tunnel and the kiln are not great, with the coefficients being greater in the kiln over boards two to four (from the start of the array) and greater in the wind tunnel over the first and last boards. This indicates that the flow patterns observed in the visualization study in the wind tunnel also occur in the timber kiln.

Langrish *et al.* (1991) have found that the numerical simulation assuming time-independent flow predicted the asymptotic values of the mass-transfer coefficients (far from the leading edges of the boards) within 15%, but underestimated the magnitudes of the enhancements near the leading edges considerably, as shown in Figures 9 to 11. The simulation, which incorporates time-dependent effects, is much more successful in predicting the enhancements in the mass-transfer coefficients at the leading edges than the simulation where the flow patterns were assumed to be independent of time, particularly over the last three boards. However, the predicted peak values are still only about half those observed although the asymptotic values of the mass-transfer coefficients are still predicted within 15%.

Explorations with the numerical simulation suggested that the predicted asymptotic values were larger than those over continuous flat plates due to the turbulence-generating effects of the leading edges of the boards. This is an important contribution of the numerical simulation, and the results are also consistent with those of Sparrow *et al.* (1982).

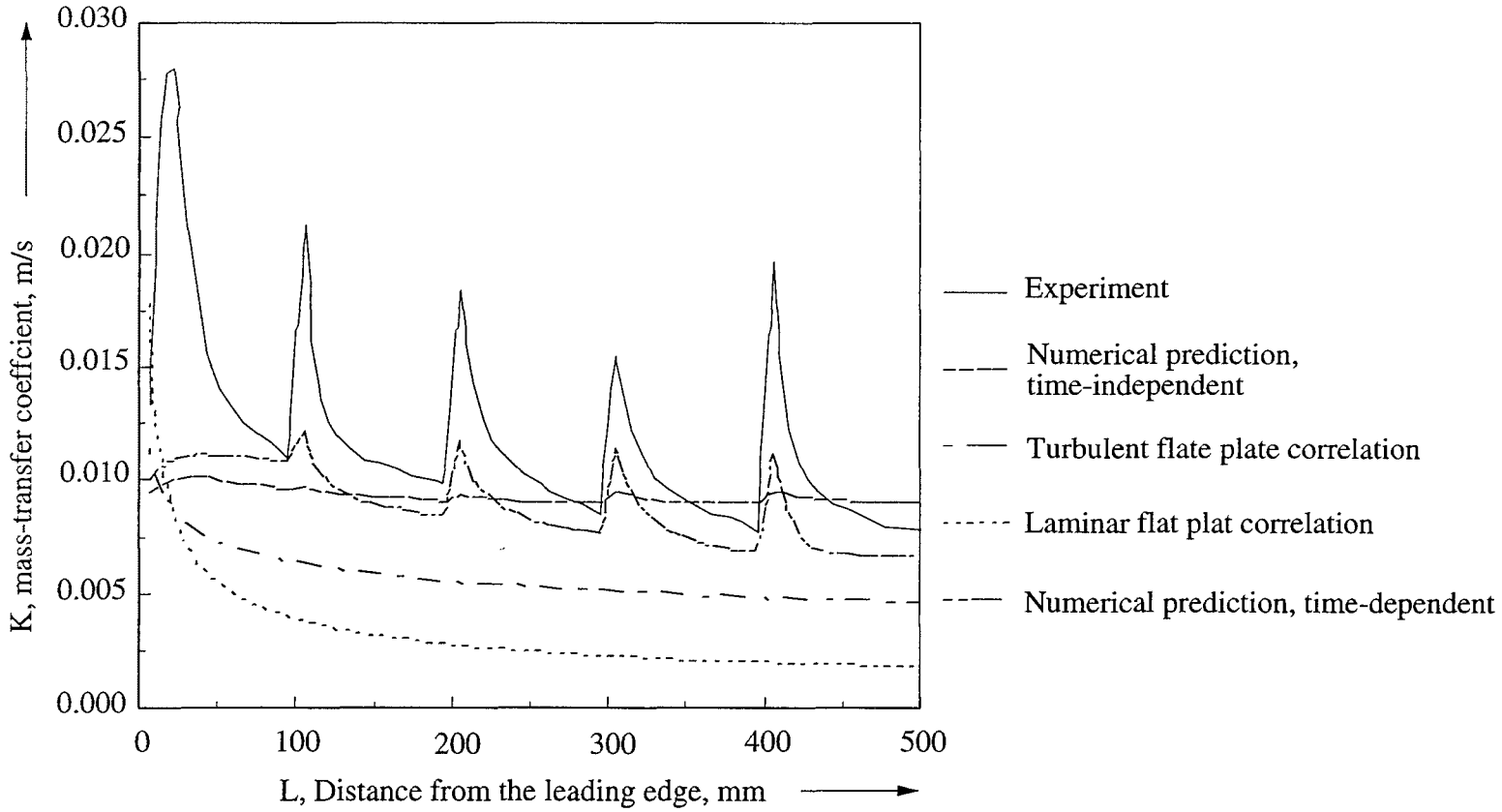

Figure 9 Comparison of the predictions of the numerical simulation, the experimental results and empirical correlations for an air velocity between boards of 3 m/s in the kiln

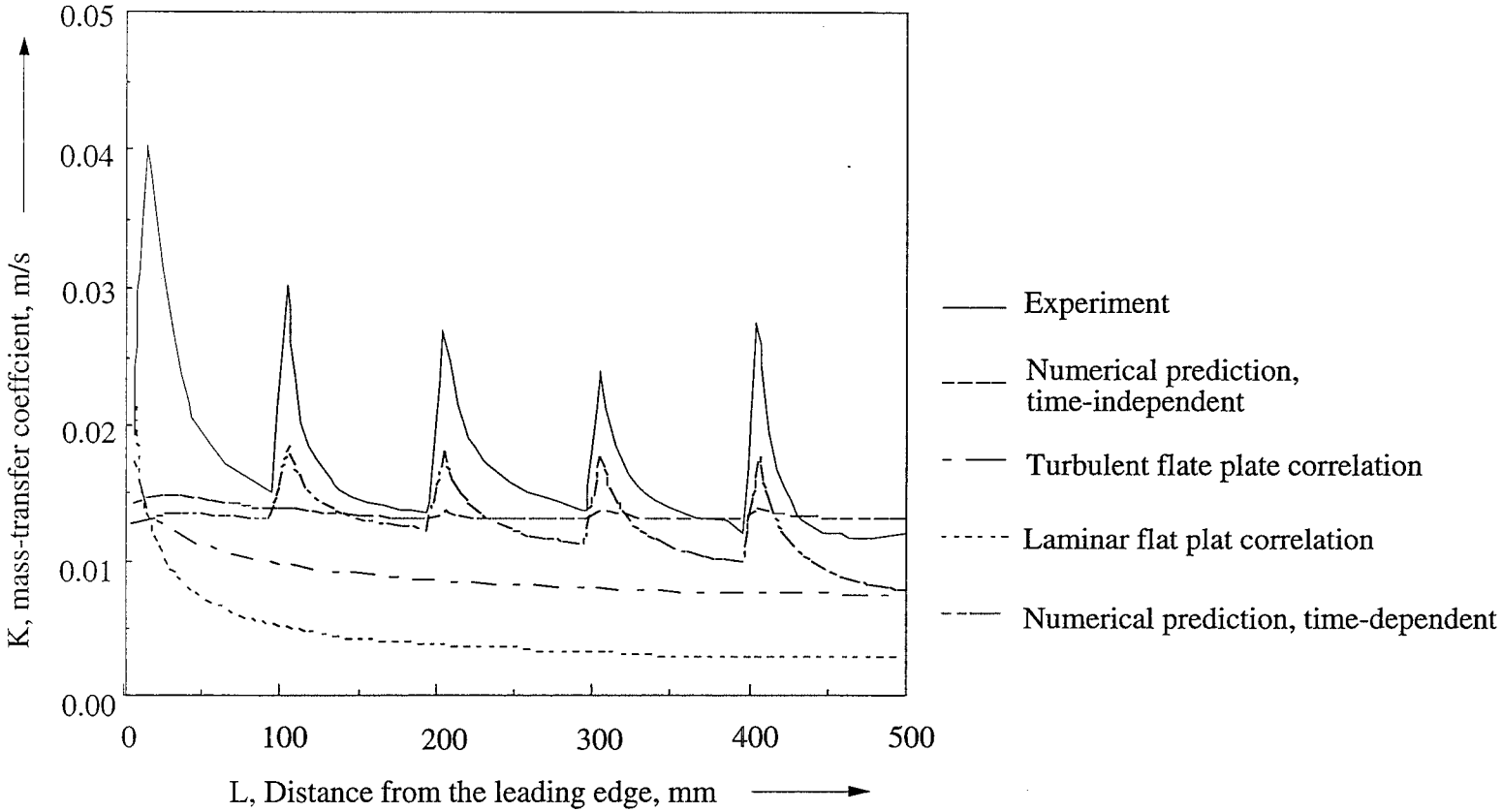

Figure 10 Comparison of the predictions of the numerical simulation, the experimental results and empirical correlations for an air velocity between boards of 5 m/s in the kiln

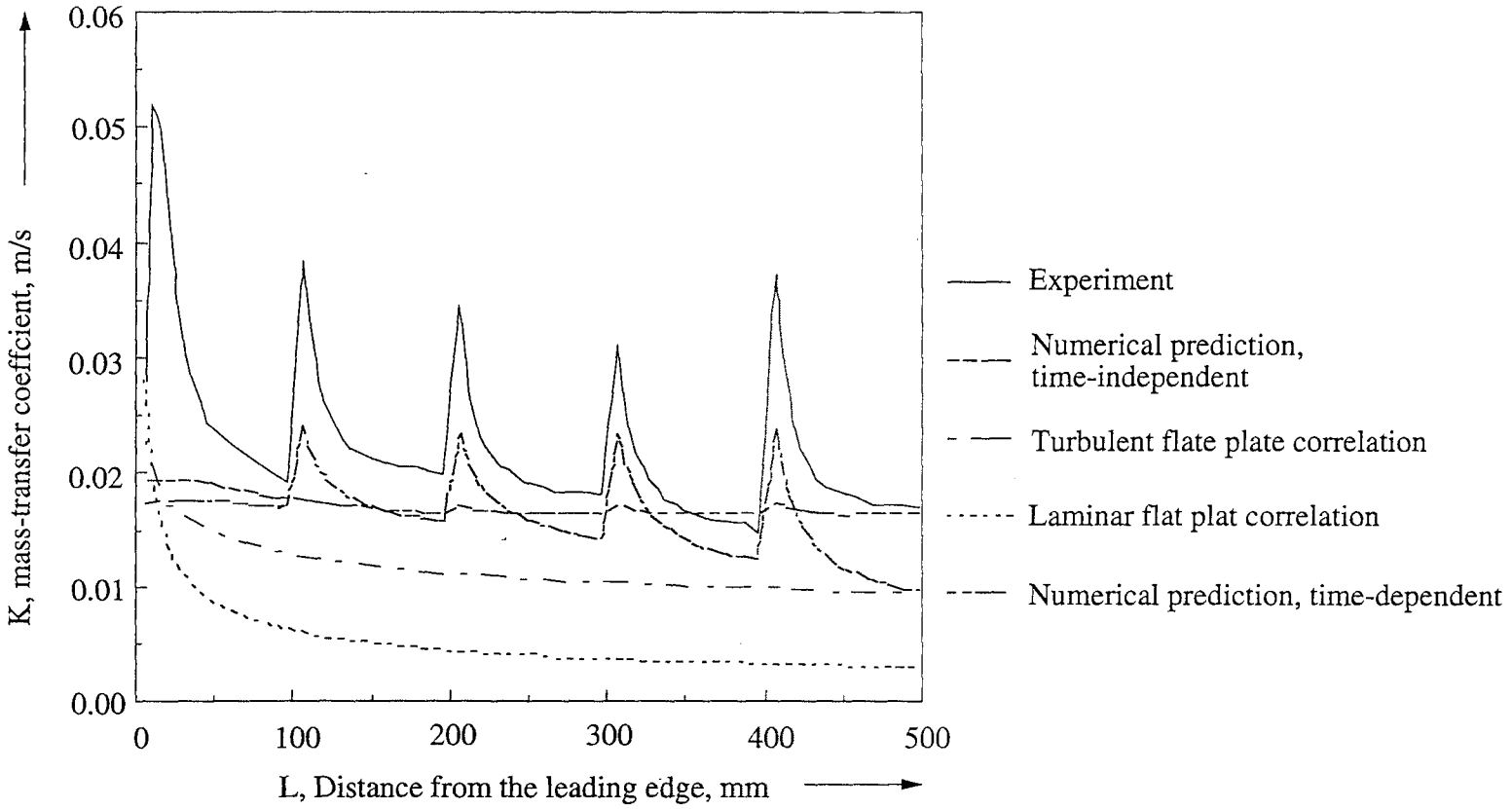

Figure 11 Comparison of the predictions of the numerical simulation, the experimental results and empirical correlations for an air velocity between boards of 7 m/s in the kiln

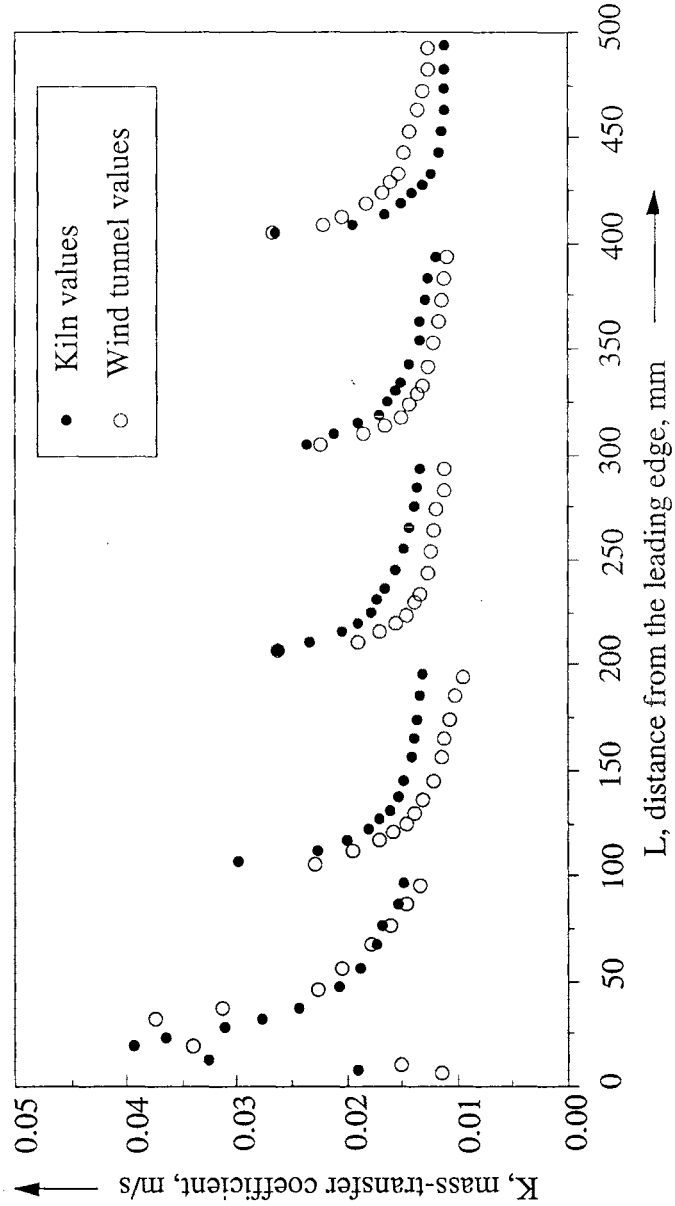

Figure 12 Comparison of the measured mass-transfer coefficients in the timber kiln and the wind tunnel for an air velocity above boards of 5 m/s

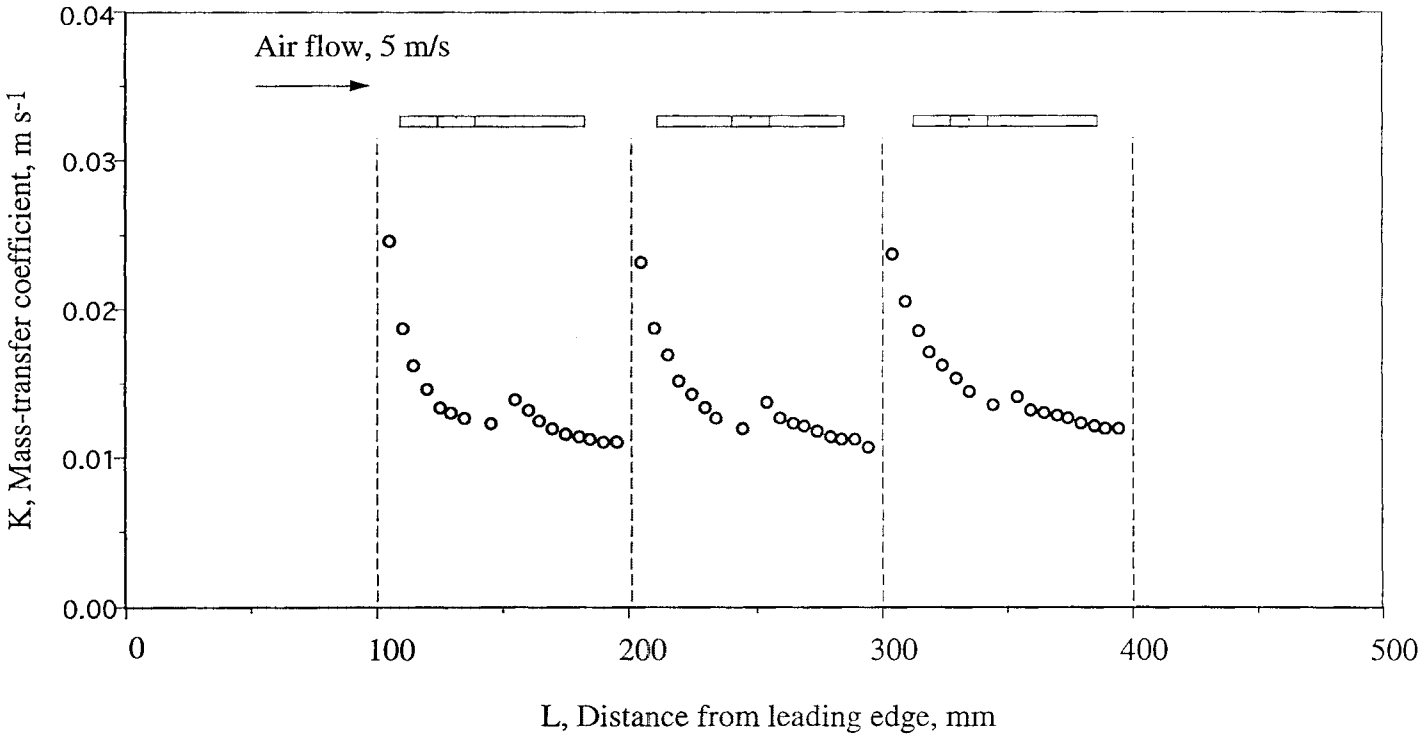

Figure 13 The effect of an interruption in the surface coating of naphthalene on the profile of the mass-transfer coefficients for an air velocity above the boards of 5 m/s in the wind tunnel

As shown in Table 1, the measured enhancement of the asymptotic mass-transfer coefficients over the values predicted by the flat-plate correlation for turbulent flow is 66% at a velocity of 3 m s^{-1} between the boards, 62% at a velocity of 5 m s^{-1} and 82% at a velocity of 7 m s^{-1}. These results are generally consistent with the experimental findings of Sugawara *et al.* (1988), who found that the heat-transfer coefficients levelled off at a value about 55% higher than those obtained for very small free-stream turbulence at turbulence levels above 7-8%, for two reasons. Firstly, the experimental uncertainty in the mass-transfer coefficients measured here was of the order of 4% (Langrish *et al.*, 1991). Secondly, there is some doubt that the enhancement in the heat-transfer coefficients reported by Sugawara *et al.* (1988) levels off above a turbulence intensity of 9%. In the region of low turbulence intensities where the heat-transfer coefficients do increase dramatically with turbulence level, their data points scatter around a single curve of best fit by enhancements of up to 5%, suggesting that this is the experimental uncertainty in their results. At turbulence intensities of more than 5%, they present data for only two turbulence intensities, 7.3% and 8.3%, where they found that the enhancements in the heat-transfer coefficients were the same. If the uncertainty in the enhancements at these turbulence intensities was the same as at lower levels, the assertion by Sugawara *et al.* (1988) that there is a plateau region must be opened to question: for a steadily increasing curve could be drawn through their data, and the enhancement of the heat-transfer coefficients would continue above turbulence intensities of 9%. The turbulence intensities in the plenum space of the kiln (about 100 mm from the stack entrance) were from 16% to 23%, so the enhancements that we have measured of above 55% are consistent with an increase in the transfer coefficients above a turbulence level of 9%. The results of Bayley and Turner (1971), who have found that the heat-transfer coefficients from a turbine blade doubled when the turbulence intensity was increased from 0.45 - 5.9%, illustrate that the enhancement of transfer coefficients with increasing turbulence intensity is very dependent on the flow geometry, as their results show a larger effect of turbulence intensity than those of Sugawara *et al.* (1988).

The reason for the large disagreement between numerical simulation and experiment over the first board may be that the wall model which we have used assumes that there is a uniform shear stress in the region between the near-wall grid point and the wall. In a rapidly developing boundary layer, such as that over the first two boards, this will not be true. Grid refinement is not an adequate answer in itself, as we need to account for the damping of turbulence near the wall in some way. In order to overcome this limitation, it would be necessary either to use a low Reynolds number turbulence model to account for the damping of the turbulence near the wall, or to use a better near-wall turbulence model, as investigated by Polat *et al.* (1990), which may give closer quantitative agreement. The values of the mass-transfer coefficients predicted by the numerical simulation are likely to be strongly affected by the choice of wall treatment. Also, the Reynolds number of the flow, based on the spacing between the board rows, is only just turbulent at velocities of 3 to 7 m s^{-1} between the boards, so the use of a high Reynolds number turbulence model is not strictly correct.

The effects of surface roughness on the mass-transfer coefficients have been estimated by making a depression in the surface coating of naphthalene and measuring the mass-transfer coefficients around the interruption in the flat casting. The naphthalene was melted with a hot edge to give an interruption in the casting 2 mm deep. For an air velocity over the boards in the wind tunnel of 5 m s^{-1}, the resulting effects of the interruption in the casting, as shown in Figure 13, are an order of magnitude less than those at the leading edge, suggesting that the effects of surface roughness are minor.

The effects of surface roughness can also be estimated by altering the values of the constants in the wall model of the numerical simulation to allow for the presence of wall roughness, using the procedure suggested by Jayatilleke (1969). He suggested that the effect of a roughness element of height y_r on the constant E in the universal velocity profile (equations 7 and 8) could be predicted by the equation:-

$$E = \frac{34.02}{y_r^+ + 3.305} \qquad (15)$$

where y_r^+ is the dimensionless roughness height, equal to $y_r \cdot \sqrt{\rho \cdot \tau_w / \mu}$. If we take a value for the effective roughness height of rough sawn timber of 0.5 mm and modify the wall constant E accordingly, the numerical simulation predicts that the mass-transfer coefficients will be changed by less than 5%.

This study also illustrates that the gap at the front of each board is deep enough for a circulation zone to form, allowing momentum exchange to occur between the gap and the bulk of the airflow. This creates the large enhancements in the mass-transfer coefficients at the leading edges. The 2 mm deep gaps in our roughness tests are not deep enough for circulation zones to form. No time-dependent momentum exchange occurs. This is a similar situation to the time-independent simulation reported in Langrish *et al.* (1991) which allowed no time-dependent momentum exchange and so predicted only small leading edge enhancements. Therefore these observations are consistent with our theoretical model.

CONCLUSIONS

For the case of in-line boards with gaps between them, we have predicted that the enhancement of the asymptotic values of the mass-transfer coefficients above those predicted by conventional flat-plate correlations is due to the effects of the gaps in generating additional turbulence throughout the array of boards. The enhancements at the leading edges of the boards are also predicted by the simulation to be a consequence of the time-dependent nature of the flow. Periodic oscillations in the flow patterns around the gaps with a period of 1-7 s were observed in the flow visualization study, in agreement with the period of 2 s predicted by this simulation. The Strouhal number for this flow oscillation is over an order of magnitude less than that for vortex shedding from an isolated flat plate. However, the enhancement in the mass-transfer coefficients at the leading edge of the first board in not predicted well, because the treatment of the flow near the wall requires improvement in the simulation.

ACKNOWLEDGMENTS

Thanks are due to Mr Paul Fuller of the School of Forestry for assistance with the mass-transfer measurements, Mr Ho Siang Lee of the Department of Chemical and Process Engineering for the flow visualization experiments and Mr Trevor Berry of that Department for the photograph.

REFERENCES

Bayley, F.J. and Turner, A.B. 1971. Transpiration Cooled Turbines, *Proc. Instn. Mech. Engrs. (London)*, **185**, 943 - 951.

Bird, R.B., Stewart, W.E. and Lightfoot, E.N. 1960. *Transport Phenomena*, p.158, J. Wiley, NY.

Danckwerts, P.V. and Anolick, C. 1962. Mass-Transfer From a Grid Packing to an Air Stream, *Trans. Instn. Chem. Engrs.*, **40**, 203 - 213.

Harrison, S.T.L. and Mackley, M. 1992. A pulsatile flow bioreactor, *Chem. Engng. Sci.*, **47(2)**, 490 - 493.

Jayatilleke, C.L.V. 1969. The influence of surface roughness on the resistance of a laminar sublayer to momentum and heat transfer, In U. Grigull and E. Hahne (eds), *Progress in Heat and Mass Transfer*, **1**, Pergamon Press, NY, 193 - 330.

Kho, P.C.S., Keey, R.B. and Walker, J.C.F. 1989. Effects of Minor Board Irregularities and Air Flows on the Drying Rate of Softwood Timber Boards in Kilns, *Proc. I.U.F.R.O. Wood Drying Symposium*, Seattle, Washington, U.S.A., 150 - 157.

Langrish, T.A.G., Kho, P.C.S., Keey, R.B. and Walker, J.C.F. 1991. Experimental measurement and numerical simulation of local mass-transfer coefficients in timber kilns, *Seventh Polish Drying Symposium*, Lodz, **Vol. 2**, 113 - 128. (Also accepted for publication in Drying Technology, 1992).

Launder, B.E. and Spalding, D.B. 1974. The Numerical Computation of Turbulent Flows, *Computer Methods in Applied Mechanics and Engineering*, **3**, 269 - 289.

Lee, H.S. 1990. Flow Visualisation on High Temperature Wood Drying, *B.E. (Chem. and Process) Report*, University of Canterbury, New Zealand, 67 p.

Luikov, A.V. 1966. *Heat and Mass Transfer in Capillary-Porous Bodies*, p. 284, Pergamon Press, Oxford.

Mackley, M. and Ni, X. 1991. Mixing and dispersion in a baffled tube for steady laminar and pulsatile flow, *Chem. Engng. Sci.*, **46(12)**, 3139 - 3151.

Miller, W.R. 1973. Mass-Transfer Within Arrays, *B.E. (Chem.) Report*, University of Canterbury, New Zealand, 22 p.

Nakamura, Y., Ohya, Y. and Tsuruta, H. 1991. Experiments on vortex shedding from flat plates with a square leading and trailing edges, *J. Fluid Mech.*, **222**, 437 - 447.

Patankar, S.V. 1980. *Numerical Heat Transfer and Fluid Flow*, Ch. 1 - 6, Hemisphere, NY.

Pai, B.R., Michelfelder, S. and Spalding, D.B. 1977. Prediction of furnace heat transfer with a three-dimensional mathematical model, *Int. J. Heat Mass Transfer*, **21**, 571 - 580.

Perré, P. and Moyne, C. 1991. Processes related to drying: Part II, Use of the same model to solve transfers both in saturated and unsaturated porous media, *Drying Technology*, **9(5)**, 1153 - 1179.

Polat, S., Mujumdar, A.S., van Heiningen, A.R.P. and Douglas, W.J.M. 1990. Effect of Near-Wall Modelling on Prediction of Impingement Heat Transfer, *Drying Technology*, **8(4)**, 705 - 730.

Ranz, W.E. and Dickson, P.F. 1965. Mass and Heat Transfer Rates for Large Gradients of Concentration and Temperature, *Ind. Eng. Chem. Fundamentals*, **4(3)**, 345 - 353.

Sørenson, A. 1969. Mass-Transfer Coefficients on Truncated Slabs, *Chem. Eng. Sci.*, **24**, 1445 - 1460.

Sparrow, E.M., Niethammer, J.E. and Chaboki, A. 1982. Heat Transfer and Pressure Drop Characteristics of Arrays of Rectangular Modules Encountered in Electronic Equipment, *Int. J. Heat Mass Transfer*, **25(7)**, 961 - 973.

Sugawara, S., Sato, T., Komatsu, H and Osaka, H. 1988. Effect of free-stream turbulence on flat plate heat transfer, *Int. J. Heat Mass Transfer*, **31(1)**, 5 - 12.

Welty, J.R., Wicks, C.E. and Wilson, R.E. 1969. *Fundamentals of Momentum, Heat and Mass Transfer*, p. 559, J. Wiley, NY.

NOTATION

Δb	thickness of naphthalene sublimed	m
c	chord	m
C_f	skin friction coefficient, equation (13)	-
C_μ	constant in turbulence model, equation (9)	-
D	diffusivity of the solute through air	$m^2\ s^{-1}$
E	constant in wall model, equation (8)	-
f	vortex-shedding frequency	s^{-1}
h	under-relaxation factor	-
I	turbulence intensity	%
k	turbulence kinetic energy per unit mass	$m^2\ s^{-2}$
k_p	turbulence kinetic energy per unit mass at the near-wall grid point	$m^2\ s^{-2}$
K	local mass-transfer coefficient	$m\ s^{-1}$
L	distance from the leading edge of the board	m
M_N	molar mass of naphthalene	$kg\ mol^{-1}$
P	static pressure	$N\ m^{-2}$
P_{No}	vapour pressure of naphthalene at the subliming surface	$N\ m^{-2}$
R	universal gas constant	$8.314\ J\ mol^{-1}\ K^{-1}$
S_ϕ	source term in equation (1)	-
t	time	s
Δt	time of sublimation	s
T	absolute temperature	K
u	horizontal component of velocity	$m\ s^{-1}$
u_p	velocity at the near-wall grid point	$m\ s^{-1}$
u'	root-mean-square of the fluctuating component of velocity	$m\ s^{-1}$
u^+	dimensionless velocity	-
v	vertical component of velocity	$m\ s^{-1}$
W	board thickness	m
x	horizontal distance	m
y	normal distance from wall	m
y_p	normal distance of the near-wall grid point from the wall	m
y_r	height of the roughness element	m
y_r^+	dimensionless height of the roughness element	-

Greek

ϕ	general variable, equation (1)	-
ϕ_{old}	value of ϕ from last iteration	-
ϕ_{new}	new value of ϕ, under-relaxed	-
ϕ^{*}_{new}	new value of ϕ produced without under-relaxation	-
ε	dissipation rate of turbulence kinetic energy	$m^2\ s^{-3}$
K	von Karman constant, equation (8)	-
μ	dynamic viscosity	$kg\ m^{-1}\ s^{-1}$
υ	kinematic viscosity	$m^2\ s^{-1}$
Γ_ϕ	transfer coefficient associated with phi, equation (1)	-
ρ	density	$kg\ m^{-3}$
ρ_N	density of solid naphthalene	$kg\ m^{-3}$
τ_w	wall shear stress	$N\ m^{-2}$

Dimensionless numbers

C_f	skin friction coefficient = $\tau_w/(\rho \cdot u^2/2)$
Re_x	local Reynolds number = $(x \cdot u)/\upsilon$
Sc	Schmidt number = υ/D
Sh_x	local Sherwood number = $(K \cdot x)/D$
St	Strouhal number = $f \cdot W/u$